THE ASSESSMENT OF CORROSION-DAMAGED CONCRETE STRUCTURES

by

MICHAEL PETER WEBSTER

BEng, MSc, DIC, CEng, MIStructE, MICE

A Thesis submitted to

The University of Birmingham

For the degree of

DOCTOR OF PHILOSOPHY

School of Civil Engineering,

University of Birmingham,

Birmingham, B15 2TT, UK.

July 2000

ABSTRACT

Data from existing research are linked together to produce an overview of the effects of chloride-induced corrosion on reinforced concrete structures. The effects of chloride-induced corrosion on the following mechanisms have been investigated:

(i) Cracking.
(ii) Bond strength.
(iii) Flexural strength.
(iv) Shear strength.
(v) Column behaviour.

Models have been developed to link material and structural aspects of deterioration. Despite the complexity of the behaviour, many of the models are modifications to existing procedures contained in UK codes. Material and structural models are integrated together in a spreadsheet for assessing the variation in load-carrying capacity with time.

Time to cracking and residual load-carrying capacity are found to be sensitive to small variations in key parameters such as the cover and the surface chloride level. Predictions from a spreadsheet model indicate that structures designed and built to BS 8110 should achieve their design life without the need for significant repair. The predictions also indicate that the UK Highways Agency was justified in making BD 57 more onerous than BS 5400.

With validation against further test data the procedures developed in this Thesis could form the basis for codes of practice for the assessment of corrosion-damaged concrete structures and the durability design of new concrete structures.

ACKNOWLEDGEMENTS

I would like to acknowledge the input made by my two supervisors, Professor Les Clark of the University of Birmingham and Professor George Somerville formerly of the British Cement Association. In particular, I would like to thank Professor Clark for helpful discussions and in-depth comments on the wide range of topics covered in this Thesis.

My colleague, at the British Cement Association, Dr Don Hobbs helped me with a variety of discussions on the material aspects of corrosion. For that and for proof-reading this Thesis I would like express my thanks.

Thanks are also due to two of my former colleagues Dr Tony Jones and Christina Doyle for proof-reading this Thesis and providing a variety of comments. Finally, thanks are due to my former colleague Serena Smith for typing much of this Thesis and for preparing many of the figures.

CONTENTS

Page

LIST OF FIGURES

LIST OF TABLES

NOTATION

a	=	$(D + 2d_0) / 2$ (inches)
A	=	concrete cross-sectional area (mm^2)
a	=	maximum aggregate size (mm)
A_1	=	a variable (function of the corrosion rate)
A_2	=	a variable (function of the corrosion rate)
A_c	=	area of concrete (mm^2)
Acorr	=	area of the of bar corroded (mm^2)
A_s	=	area of tension reinforcement (mm^2)
$A_{s.eff}$	=	effective area of the corroded tension reinforcement (mm^2)
$A_{s.nom}$	=	nominal area of the uncorroded tension reinforcement (mm^2)
A_{sl}	=	the area of effectively anchored additional longitudinal tensile reinforcement (mm^2)
A_{sc}	=	area of reinforcement in compression (mm^2)
A_{st}	=	area of tension reinforcement (mm^2)
A_{sv}	=	area of link reinforcement (mm^2)
A_{sw}	=	area of shear link reinforcement (mm^2)
a_v	=	shear span (mm)
b	=	$C + ((D + 2d_0) / 2)$ (inches)
b	=	width or effective width of the section (or flange) in the compression zone (mm)
b’	=	effective depth to the reinforcement taken perpendicular to the y-axis (mm)
B_R	=	bias ratio between the true and mean resistance of the member
b_w	=	width of the section (mm)
c	=	concrete cover to reinforcement (inches, mm)
c_h	=	horizontal concrete cover to reinforcement (mm)
c_v	=	vertical concrete cover to the tension reinforcement (mm)
c/D	=	cover to bar diameter ratio
c_0	=	constant relating to bond strength
C_i	=	the initial total chloride content in the concrete (i.e. from sea dredged aggregate or calcium chloride accelerator) (%)
corr	=	amount of corrosion (%)

C_s = the total chloride content at the surface (%)

$C_{x,t}$ = the total chloride content at depth, x, at time t (%)

D = reinforcement diameter (inches, mm)

d = effective depth of the tension reinforcement

d_0 = thickness of the pore band around the steel-concrete interface (inches)

d_a = maximum aggregate size (mm)

D_c = the chloride diffusion co-efficient (m^2/s)

d_s = thickness of rust required to cause tensile splitting stresses (inches)

d_v = shear depth = 0.9d (mm)

erfc = the error function complement (1 – erf)

$E_{c.eff}$ = effective elastic modulus of concrete = $E_c/(1+\phi)$ (kN/mm^2)

E_s = elastic modulus of steel reinforcement (kN/mm^2)

f() = a function

f'_c = concrete cylinder strength (N/mm^2)

f_b = bond strength (N/mm^2)

$f_{b.8110}$ = bond strength of the tension reinforcement calculated in accordance with BS 8110

$f_{b.corr}$ = corroded bond strength (N/mm^2)

$f_{b.link}$ = bond strength contributed by the link reinforcement (N/mm^2)

$f_{b.Tepfers}$ = bond strength calculated using the Tepfers formula (N/mm^2)

f_{bu} = ultimate bond stress (N/mm^2)

f_{ct} = concrete tensile strength (N/mm^2)

f_{ctr} = concrete modulus of rupture (N/mm^2)

f_{cu} = concrete cube strength (N/mm^2)

f_{st} = stress in tension reinforcement (N/mm^2)

f_{su} = ultimate shear stress of unreinforced concrete (N/mm^2)

f_t = tensile strength of the concrete (N/mm^2)

f_y = characteristic yield strength of reinforcement (N/mm^2)

f_{yv} = characteristic yield strength of the shear (N/mm^2)

f_{ywd} = characteristic yield strength of shear reinforcement (N/mm^2)

h’ = effective depth to the reinforcement taken perpendicular to the x-axis (mm)

i_{corr} = annual mean corrosion rate (mA/ft^2)

I	=	the second moment of area of the reinforcement (mm^4)
I_{corr}	=	corrosion rate ($\mu A/cm^2$)
I_{NA}	=	second moment of area of the cover concrete about the neutral axis for rust-induced loading (mm^4)
I_x	=	second moment of area of the cover concrete about the x-axis (mm^4)
I_y	=	second moment of area of the cover concrete about the y-axis (mm^4)
j_0	=	variable relating to the lever arm
j_r	=	rate of rust production (g/m^2s)
k	=	variable relating to restraint to compression reinforcement
k	=	variable relating to member depth and reinforcement curtailment
k_1	=	constant relating to the beam shear capacity
k_2	=	constant relating to the beam shear capacity
k_3	=	constant relating to the beam shear capacity
k_4	=	constant relating to the beam shear capacity
L	=	concrete cover to reinforcement (cm)
l	=	the effective length of the reinforcement (mm)
L_{crack}	=	length of crack (mm)
M	=	moment (kNm)
m	=	constant relating to the lever arm
M_r	=	mass of rust per unit length of bar (g/m)
M_{spall}	=	moment required to spall the cover concrete (Nm)
M_{st}	=	mass of steel consumed to produce Mr (g)
M_{ux}	=	moment capacity about the x-axis coexistent with N (kNm)
M_{uy}	=	moment capacity about the y-axis coexistent with N (kNm)
M_x	=	applied moment about the x-axis (kNm)
M_x’	=	increased moment about the x-axis (kNm)
M_y	=	applied moment about the y-axis (kNm)
M_y’	=	increased moment about the y-axis (kNm)
N	=	ultimate axial strength (kN)
N_{uz}	=	column squash load = $(0.67\ f_{cu} / \gamma_{mc})\ A_c + (f_y / \gamma_s)\ A_{sc}$ (kN)
P_{cr}	=	the critical buckling load (kN)

$P_{cr.pce}$ = pressure to induce cover cracking assuming a partly cracked elastic stress state (N/mm^2)

$P_{cr.plas}$ = pressure to induce cover cracking assuming a plastic stress state (N/mm^2)

P_r = applied pressure (N/mm^2)

Q = weight loss of bar per unit area (g/cm^2)

r = a constant

r_1 = internal cylinder radius – bar radius (mm)

r_2 = external cylinder radius (mm)

Rb = ratio of corroded to uncorroded bond strength

R_d = design resistance of the section being considered

R_{red} = reduced resistance (bending, shear, axial etc) of a deteriorated structure

s = bar spacing (cm)

s_v = spacing of the link reinforcement (mm)

s_x = spacing of cracks perpendicular to the longitudinal reinforcement $\approx d_v$ (mm)

t = the exposed time (years)

T = force in the reinforcing bar (kN)

t_{cor} = corrosion time (s)

V = shear force (kN)

v = shear stress = $V / b_w d$ (N/mm^2)

v_x = elastic shear stress acting in the x direction (N/mm^2)

$v_{x.rust}$ = elastic shear stress due to rust component acting in the x direction (N/mm^2)

v_y = elastic shear stress acting in the y direction (N/mm^2)

$v_{y.rust}$ = elastic shear stress due to rust component acting in the y direction (N/mm^2)

$v_{y.sw}$ = elastic shear stress due to concrete self-weight acting in the y direction (N/mm^2)

V_{arch} = shear strength contribution due to arch behaviour calculated using the Bazant and Kim formulae (kN)

V_{beam} = shear strength contribution due to beam shear calculated using the Bazant and Kim formulae (kN)

V_c = concrete component of the shear load-carrying capacity (kN)

$V_{c.corr}$ = shear load-carrying capacity in the corroded beam (kN)

V_{cg} = concrete contribution to shear resistance (kN)

V_{Fe}	=	volume of iron (Fe)
V_R	=	co-efficient of variation relating to the reliability level of the test and inspection data
V_{Rd1}	=	concrete contribution to the shear capacity (kN)
V_{Rd3}	=	total shear capacity (kN)
V_{rg}	=	shear resistance (kN)
V_{rust}	=	volume of rust product ($inch^3$)
V_s	=	ultimate shear force in the shear links (kN)
V_{sg}	=	shear link contribution to shear resistance (kN)
V_{spall}	=	shear force required to spall the cover concrete (N)
V_x	=	shear force acting in the x direction (N)
V_y	=	shear force acting in the y direction (N)
w	=	uniformly distributed self-weight (kN/m)
w	=	crack width (mm)
$w_{flex.spall}$	=	equivalent uniformly distributed load to be resisted by flexure (kN/m)
w_{rust}	=	equivalent uniformly distributed load capacity available to resist rust (kN/m)
$w_{shear.spall}$	=	equivalent uniformly distributed load to be resisted by shear (kN/m)
W_{st}	=	mass of steel corroded (lb/ft^2)
x	=	the depth below the exposed surface to the middle of the sample (m)
x	=	distance along the x-axis to the point where the stress is being checked (mm)
X	=	reduction in reinforcing bar radius (μm)
y	=	distance along the y-axis to the point where the stress is being checked (mm)
Z	=	section modulus (mm^3)
z	=	lever arm (mm)
ν	=	Poisson's ratio of concrete
α	=	ratio of the molecular weight of steel divided by the molecular weight of rust
α_n	=	a function of N / N_{uz}
α_R	=	deterioration factor obtained from the Condition Rating
β	=	tensile stress factor
β	=	a coefficient which is a function of N/bhf_{cu}

β_C = target value of the minimum acceptable safety level

δ_{cr} = bar radial loss required for corrosion-induced cracking (μm)

δ_{pp} = bar hole flexibility

δ_{pore} = bar radius loss accommodated with concrete pores surrounding the bar (μm)

δ_{spall} = bar radius loss corresponding to critical spalling load (μm)

δr = net radial expansion of the reinforcing bar required to cause cracking (μm)

δr_{cover} = expansion of the reinforcing bar restrained by the confining action of the concrete cover (μm)

δr_{free} = free expansion of the reinforcing bar, due to the rust growth, that would occur if the bar were not surrounded by concrete (μm)

δr_{free} = free radial expansion, due to the rust growth, that generates sufficient net radial expansion to crack the cover (μm)

δr_{pore} = radial expansion of rust that is accommodated within the pore structure of the concrete cover without inducing stress (μm)

δr_{rust} = radial expansion generated by the rust (μm)

δ_{rust} = mid-span deflection corresponding to critical spalling load (mm)

ε_1 = principal tensile strain

ε_t = circumferential strain at the bar-concrete interface

ε_{tmax} = maximum circumferential strain at the bar-concrete interface

ε_x = longitudinal strain

ϕ = angle between the line of action of the rust and the x-axis (°)

ϕ_{cr} = concrete creep co-efficient

γ_{mc} = partial safety factor for strength of concrete

γ_{ms} = the partial safety factor for reinforcement

γ_{mv} = the partial safety factor for shear

ν_c = Poisson's ratio of concrete

ν_s = Poisson's ratio of steel

θ = inclination of principal average stresses (crack inclination)

ρ = reinforcement ratio = A_s / bd

ρ_{fe} = density of iron (kg/m^3)

ρ_l = longitudinal reinforcement ratio (A_s / $b_w d$)

ρ_r = density of hydrated rust (g/cm^3)

ρ_{rust} = density of rust (kg/m^3)

ρ_{st} = density of steel (kg/m^3)

σ_{cp} = compressive stress induced by prestress (N/mm^2)

σ_{cr} = critical buckling stress (N/mm^2)

$\sigma_{flex.spall}$ = allowable flexural stress available to resist spalling stresses (N/mm^2)

$\sigma_{flex.sw}$ = flexural stress induced by self-weight (N/mm^2)

σ_s = stress in the reinforcement (N/mm^2)

$\sigma_{shear.spal}$ = allowable flexural stress available to resist spalling stresses (N/mm^2)

l

$\sigma_{shear.sw}$ = shear stress induced by self-weight (N/mm^2)

σ_{tmax} = tensile stress when the concrete cover cracks (kgf/cm^2)

τ_{Rd} = ultimate shear stress (N/mm^2)

ξ = variable to reflect size effects in shear

$\Delta\delta r$ = rate of radial bar reduction (μm/year)

$\Delta\delta r_{rust}$ = rate of increase in radial expansion of rust with time (μm/year)

ΔD = increase in bar diameter (cm)

Δ_{cr} = bar section loss required for corrosion-induced cracking (%)

Φ = resistance reduction factor based on the current condition of the structure

1 INTRODUCTION

1.1 Background

Reinforcement corrosion is the biggest durability problem facing the UK. In a recent press release, the Building Research Establishment[1] estimated the direct cost of reinforcement corrosion to the UK economy to be around £550M per year. In addition, there are the traffic delay and loss of use costs to add to this estimate. Hobbs[2] estimates that around 90% of these costs are due to chloride-induced reinforcement corrosion.

However, cost is only one issue. Safety is the prime issue. As the reinforcement corrodes there is the potential for cracking, spalling of concrete and reductions in reinforcement cross-section. This leads to two safety concerns:

(i) Falling of loose concrete onto pedestrians, vehicles, users etc.
(ii) Reductions in load-carrying capacity leading to collapse.

To date no reinforced concrete structures have collapsed in the UK due to reinforcement corrosion. However, this is not the case elsewhere. Yeung[3] has reported on reinforcement corrosion contributing to the collapse of several reinforced concrete canopy structures in Hong Kong.

In many cases of corrosion in reinforced concrete structures telltale signs of rust staining and cracking indicate that corrosion is proceeding. This implies that remedial action is required. However, resources are scarce, and it is not always possible to take remedial action straight away. In the case of the Midlands Links viaducts[4] the extent of corrosion was so great that the whole network could not be repaired in one go for reasons of cost, resources and disruption. This meant leaving corroded bridges for several years before they were repaired. To achieve this, knowledge of the likely safety levels within the bridges had to be estimated before they could be left for any period of time. The technology for assessing such situations has not been developed sufficiently and, as such, conservative decisions have had to be made based on the limited information available.

Sustainability is another important issue. One of the key components of sustainability is ensuring that structures fulfil their function for as long as required, even beyond their first use. In order to judge whether a structure is suitable for re-use or not an estimate is required of the remaining service life of that structure. The technology to do this is not available currently.

This Thesis is aimed at addressing such gaps in current knowledge.

1.2 Scope of the research

The main questions that need to be answered from a structural appraisal are:

(i) Is the structure safe?
(ii) Will it remain safe?
(iii) When is action required?
(iv) What action is required?

The procedures developed in this Thesis should allow engineers to address the first three points. The fourth point is beyond the scope of this Thesis.

There is much literature available on the individual aspects of corrosion. However, little is available on the process of assessing the whole life of a concrete structure.

In determining the current and future load-carrying capacity of a corroded concrete structure it is necessary to estimate the deterioration of the materials, determine the structural effects and then estimate the load-carrying capacity now and in the future. The practising engineer will typically rely on guidance documents and codes of practice. However, there are three principal omissions from these documents:

(i) No link is provided between the deterioration of the materials and that of structural performance.
(ii) No quantitative guidance is presented for deterioration with time.
(iii) No recognition is made of the fact that deteriorated structures may not behave the same

as new ones.

Without these, realistic assessment of the levels of safety within a structure over its whole life is not possible. In addition, no criteria are available to define minimum performance criteria. This leaves the assessing engineer with no choice but to make crude assumptions, which may or may not be conservative. As a result the engineer is not able to provide the structure's owner with a confident answer to the question: "How long will my structure last?". This is not a satisfactory situation.

The majority of research related to chloride-induced corrosion is aimed at gaining an understanding of one limited area of corrosion. Often, the output from this work is not used. The aim of this Thesis is to use the existing research and link together the various aspects to produce an overview of the effects of corrosion on reinforced concrete structures. No new tests have been undertaken. A qualitative understanding of the structural effects of corrosion is presented for various load-carrying mechanisms followed by modifications and extensions to existing code procedures to provide a quantitative means of assessing corrosion-damaged concrete structures. In doing so, the research crosses several disciplines.

By approaching the Thesis in this manner use can be made of the existing research by validating, extending and linking together existing research to produce new ideas and solutions. Areas where further research is required are also identified.

1.3 Scope of the Thesis

In Chapter 2 the literature relating to the components of the whole life behaviour of concrete affected by chloride-induced corrosion is reviewed. To ascertain the whole life performance of a reinforced concrete structure, every stage has to be investigated from first exposure to the environment to potential collapse. This implies that both material and structural aspects of whole life behaviour have to be considered. Corrosion mechanisms related to chloride environments are reviewed followed by the effects that corrosion has on structural integrity. The effects of corrosion on cracking, bond, bending, shear and column behaviour are considered in turn. Finally, current practice in the assessment of corrosion-damaged concrete structures is reviewed.

The current situation is summarised, and gaps in current knowledge are identified leading to recommendations for this research.

Chapter 3 contains an investigation into the effects of accelerated corrosion on the onset of cracking. Two models are presented for predicting the onset of cracking: a rigorous and a simplified one.

Chapter 4 contains an investigation into the effects of accelerated corrosion on the bond strength of reinforcing bars embedded in concrete. Recommendations are made for extending the bond rules in current UK codes of practice to allow for the effects of corrosion.

Chapter 5 contains an investigation into the effects of accelerated corrosion on the flexural strength of reinforced concrete members. Recommendations are made for modifying current UK codes of practice to permit the assessment of flexural strength when corrosion is present.

Chapter 6 contains an investigation into the effects of accelerated corrosion on the shear strength of reinforced concrete members. Three approaches to calculating shear strength are investigated, and recommendations are made for modifying current UK codes of practice to permit the assessment of shear strength when corrosion is present.

Chapter 7 contains an investigation into the effects of accelerated corrosion on the column (combined bending and axial compression) behaviour of reinforced concrete members. Recommendations are made for modifying current UK codes of practice to permit the assessment of column behaviour when corrosion is present.

The procedures developed in the previous chapters are used in Chapter 8 to investigate implications for the design and assessment of reinforced concrete structures in chloride environments. The provisions of UK codes of practice are investigated.

In Chapter 9 the conclusions drawn from this research are presented.

In Chapter 10 the recommendations resulting from this work are presented along with recommendations for further research.

In Appendix A the recommendations of Chapters 3, 4, 5, 6 and 7 are brought together as a set of procedures for predicting the whole life behaviour of reinforced concrete subject to chloride environments. Material and structural aspects are linked. The model is implemented in the spreadsheet *BEAMCOL_CORR*. A typical print out from this spreadsheet is included in Appendix B.

2 LITERATURE REVIEW

In order to make a judgement on safety of corroded concrete structures we need to have an appreciation of how concrete structures respond to corrosion. There are two components to this: firstly, to review the available test data from accelerated corrosion tests and, secondly, to interpret these data in relation to the behaviour of real structures and the requirements for producing procedures compatible with UK codes of practice. In this Chapter the first of these two components is addressed.

2.1 Corrosion mechanisms

Chloride ions penetrate the concrete and break down the protective layer around the reinforcement. The rate at which they penetrate the concrete is a function of the quality and quantity of the concrete surrounding the reinforcement and the internal and external environments. The time for the chloride ion level at the reinforcement to reach the critical level for the onset of corrosion is known as the *Initiation Period*.

Once the protective layer around the reinforcement has been removed corrosion can take place in the presence of moisture and oxygen. The corrosion products occupy more space than the original steel and, as such, can cause expansive stresses that can lead to cracking of the concrete cover and spalling. The cross-section of the reinforcement is also reduced. The time taken for corrosion to result in sufficient deterioration that remedial action is required is known as the *Propagation Period*.

The concept of Initiation and Propagation periods can be illustrated by Tuutti's[5] model shown in Figure 2-1. As detailed discussions of the processes are given in references 5, 6 and 7 only a summary is presented here.

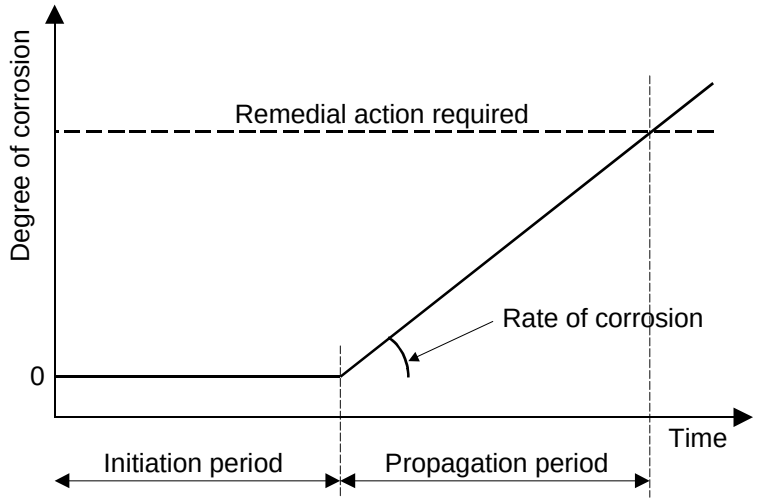

Figure 2-1: The corrosion process (Tuutti[5])

Metals corrode in acids, whilst they can be protected from corrosion by an alkaline environment. Concrete contains hydroxides particularly calcium hydroxide. In moist concrete the presence of calcium hydroxide creates an alkaline environment within the concrete of pH 12 to 13. This high alkalinity leads to a 'passive' oxide layer forming on the surface of the reinforcing steel. This passive layer prevents corrosion from occurring (beyond that that took place when the reinforcement was exposed to the atmosphere before inclusion in the concrete).

Once the passive layer has been broken down as a consequence of chloride ingress, the reinforcement can start to rust (corrode) if there is the right balance of moisture and oxygen. The process is an electrochemical one with reactions taking place in two zones with different electrochemical potential: anodes and cathodes. This is shown in Figure 2-2 where there will be a potential difference between the area of depassivated reinforcement and the passive area. As a result of this potential difference, a current will flow. Electrons will be transferred from the more negatively charged metal (anode) to the more positive one (cathode). Simultaneously, there will be a flow of electrons in the electrolyte (pore solution) from the cathode to neutralise the metal ions released at the anode. This will allow more metal ions to be released from the anode. The result is that the anode dissolves reducing the cross-section of the reinforcement.

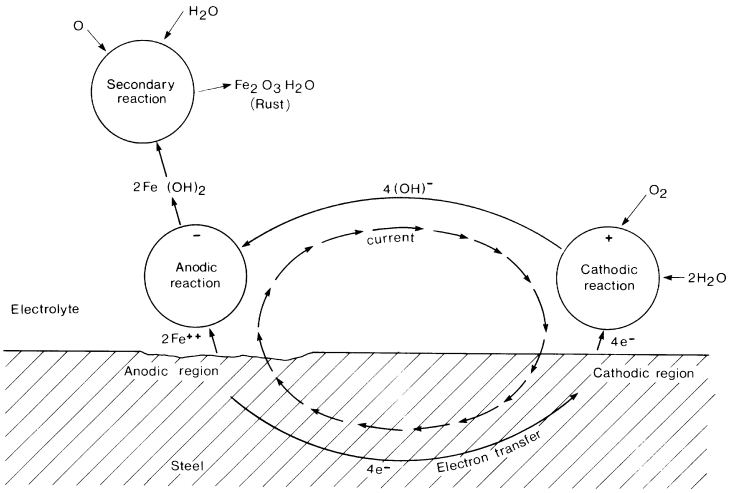

Figure 2-2: Anodic and cathodic reactions (Beeby[7])

It is important to note that both oxygen and water are required for the cathodic reaction. If the cathodic reaction is unable to take place then the electrons created in the anodic reaction cannot be consumed by the cathodic reaction. They must be consumed elsewhere on the steel surface to preserve electrical neutrality, as it is not possible for large amounts of electrical charge to build up at one place on the steel. The practical implications are that if the concrete is 'dry' corrosion will not proceed because there is insufficient moisture for the cathodic reaction (e.g. internal concrete). If the concrete is 'wet' then oxygen will have difficulty in penetrating the pore structure and corrosion will not proceed because there is insufficient oxygen for the cathodic reaction (e.g. submerged concrete). This suggests that there is an intermediate range of relative humidity at which corrosion can take place.

There are several ways to express the reactions; Figure 2-2 is one way. Ferrous hydroxide forms as the $2Fe^{++}$ ions at the anode combine with the hydroxide ($4(OH)^-$) ions flowing from the cathode. In the presence of oxygen and moisture, the ferrous hydroxide ($2Fe(OH)_2$) converts to ferric oxide ($Fe_2O_3H_2O$) i.e. rust.

The quantity of iron that reacts (rusts) is proportional to the corrosion current and time in accordance with Faraday's law. This law is used in many of the tests described in the following sections.

When unhydrated, ferric oxide (Fe_2O_3) is dense and has a volume of around twice that of the steel it replaces. When it becomes hydrated (takes in water) it swells and becomes porous. This swelling can lead to a volume increase of between two to four-fold at the steel-concrete interface. This gives the flaky red/brown rust on the reinforcing bar and can cause cracking (and spalling) of the cover concrete. Some of the rust will be accommodated in the concrete pore structure adjacent to the corroding bar. Corrosion is the loss of iron at the anode, whilst rust is the product formed at the anode.

The effects of various parameters on the corrosion process are summarised in Table 2-1.

Table 2-1: Parameters affecting the corrosion process

Parameter	*Effect*
Moisture[5, 6, 7]	Moisture is required initially for the cathodic reaction and then for rust formation at the anode. Without sufficient moisture, the rate of corrosion will be negligible.
Oxygen[5, 6, 7]	Oxygen is required initially for the cathodic reaction and then for rust formation at the anode. It is possible that chloride-induced corrosion will be controlled by oxygen availability as chlorides typically enter with moisture. With low levels of oxygen, the rate of corrosion will be negligible.
Resistivity[6]	The higher the resistivity, the lower the corrosion current will be. Resistivity increases with temperature, and decreases with increasing moisture content (RH).

2.2 Chloride-induced corrosion

Chloride ions can be present in concrete as a result of:

(i) The application of de-icing salts.
(ii) Exposure to a marine environment.
(iii) Exposure to airborne salt.
(iv) Inclusion within the concrete (in set accelerators or inadequately washed sea-dredged aggregates).

For options (i), (ii) and (iii) chloride ions can enter the concrete by a number of mechanisms, the main ones being:

(i) Diffusion.
(ii) Capillary suction under wetting and drying conditions.
(iii) Under a hydrostatic head.
(iv) Through cracks and defective joints.

Chlorides from external sources, e.g. marine exposure or exposure to de-icing salts, are the main concern, as witnessed from the deterioration in bridges, multi-storey car parks and marine structures. Based on a study of 200 concrete bridges, Wallbank[8] highlighted the main causes of corrosion as being:

(i) Low cover to reinforcement.
(ii) Inadequately compacted cover concrete.
(iii) Failure of bridge expansion joints.
(iv) Lapped bars restricting access for concrete.
(v) Cold joints at kickers.
(vi) Poorly designed mixes.

These indicate that the protection to the reinforcement assumed in design is not always achieved, and that design and construction issues are more significant than material ones.

The chloride ions attack the passive layer around the reinforcement. The depassivation mechanism for chlorides is somewhat different to that for carbonation. With carbonation, the passive layer is neutralised. With chlorides, the chloride ions attack the passive layer but there is no drop in pH. The exact mechanisms by which chlorides attack the passive film are not fully understood.

Broomfield[6] suggests that chlorides act as catalysts to corrosion when there is sufficient concentration at the reinforcement surface to break down the passive layer. The chloride ions are not consumed in the process. Theophilus[9] also indicates that chloride ions in solution reduce the ionic resistance of the concrete as an electrolyte.

For chlorides to affect the passive layer, their concentration must exceed a critical level in the pore solution. These chlorides in the pore solution are known as free chlorides. The critical level is expressed in terms of either a total chloride content (expressed as a percentage by mass of either the cement or the concrete) or the molar ratio of chloride to hydroxyl ions in the pore solution. Whilst the total chloride content is relatively easy to measure, and the molar concentration may appear more relevant, there are a number of complications[6, 9]. These include:

(i) The pore solution is not readily accessible for analysis.
(ii) Chlorides react with the cementitious components, in particular C_3A, to form insoluble compounds. Chlorides can be bound chemically (by aluminates) or physically (by absorption) on the pore walls.
(iii) Bound chlorides can become unbound by carbonation (and by sulphates).
(iv) Different cements contain different C_3A contents.
(v) Different cements contain different and alkali levels.
(vi) The critical chloride level will depend on the w/c ratio, as the hydroxyl ion concentration will decrease with increasing w/c ratio.
(vii) Corrosion can be suppressed if there is too much or too little moisture, or if oxygen is excluded, regardless of the chloride levels.

Chloride ions generally require moisture to transport them through the concrete. This leads to

high pore moisture contents that increase electrical conductivity, which enables the anode and cathode to function when separated. This is known as a macrocell[6]. Macrocells can lead to localised pitting corrosion where the section loss can be four to eight times that of homogeneous corrosion[5]. When considering the structural effects of corrosion, it is necessary to distinguish between general and local corrosion:

- *General corrosion* leads to a more uniform loss of reinforcement section, and is generally associated with carbonation and some chloride-induced corrosion. It results in longitudinal cracks along the length of the reinforcement due to rust growth.

- *Local corrosion* leads to a pitting form of corrosion, and the loss in cross-section can be around four to eight times that of general corrosion. It can occur when the oxygen supply is limited. Less rust product will be generated, and surface cracking may not result unless general corrosion is also present.

2.2.1 Initiation period

The initiation period in chloride affected concrete is usually expressed as the time taken for the chloride concentration to reach a critical level at the reinforcing bar. Unlike carbonation, there is no front that moves through the concrete but instead a concentration that gradually builds up with time, and varies with depth.

The transport mechanisms by which chlorides penetrate concrete will vary according to the exposure conditions. Concrete that remains wet for most of its life is likely to be subject to diffusion. Diffusion results in mass transfer of free ions in the pore solution from regions of higher concentration to regions of lower concentration[10]. Fick's 2nd law is often used to describe this.

Where concrete is subjected to a wetting and drying environment, i.e. multi-storey car parks and bridges, the first ten or twenty millimetres of concrete may not be saturated for long periods. When non-saturated concrete comes into contact with chlorides (in solution) the concrete will take up the solution by capillary suction[10]. Chlorides can penetrate the non-saturated areas

considerably faster than they can penetrate the deeper, saturated areas where diffusion is the main transport mechanism.

There are further complications when concrete is exposed to wetting and drying conditions[2]. The chlorides are likely to enter the concrete in solution. The chlorides are subsequently deposited in the pores during drying periods and are then available to go into solution during the next wetting cycle. The converse is also possible, where washout of the chlorides can occur when the concrete is exposed to rain or non-salt-laden vehicle spray.

Carbonation also has an effect on concrete subject to wetting and drying. The surface layers can carbonate during the drying periods, and this leads to two effects. Parrott[11] has found that carbonation can increase or decrease the permeability of surface layers depending on the type of cement used. Tuutti[5] has found that carbonated concrete does not have the same binding capacity as uncarbonated concrete. This implies that the ratio of free chlorides (in the pore solution) to total chlorides (in the concrete) will be higher in the carbonated surface zone than in the uncarbonated zones further in.

In the UK, the maximum allowable total chloride level is specified as being 0.4% by mass of cement for reinforced concrete[69]. This chloride level is often taken as the level at which corrosion begins, i.e. the end of the initiation period. However, Hobbs[2] has reviewed a variety of literature and suggests that this approach is unsatisfactory as there is no unique total (or free) chloride concentration that initiates corrosion. The critical threshold level is likely to be higher than 0.4%, as 0.4% is the maximum chloride content allowed in new concrete, and one would not expect a specification to allow concrete to contain a critical level of chlorides from day one.

From the preceding discussion it can be seen that chloride ingress is extremely complex and identifying the end of the initiation period is extremely difficult without making simplifying assumptions. For instance, observations can be made of when structures crack, corrosion rates can be measured and back-estimation of the initiation period can be made.
Some researchers[5, 6, 10, 2, 12] have made the assumption that chloride ingress can be approximated as a diffusion process and, as such, Fick's 2nd law can be used both to analyse data and make

future estimates. Solution of Fick's 2nd Law leads to the following expression:

$$C_{x,t} = C_i + (C_s - C_i)\left[erfc\left[\frac{x}{2\sqrt{D_c t}} \right] \right] \quad \text{… (2-1)}$$

where: $C_{x,t}$ = the total chloride content at depth, x, at time t (%)

C_i = the initial total chloride content in the concrete (i.e. from sea dredged aggregate or calcium chloride accelerator) (%)

C_s = the total chloride content at the surface (%)

x = the depth below the exposed surface to the middle of the sample (m)

D_c = the chloride diffusion co-efficient (m^2/s)

t = the exposed time (years)

erfc = the error function complement (1 – erf)

Fick's 2nd law is only strictly applicable to saturated homogenous materials, which concrete is not. This is particularly so in the cover region where, close to the surface large variations in cement content can occur and the concrete can be subject to a wetting and drying environment. The diffusion co-efficient, D_c, obtained from fitting Fick's 2nd law is thus termed an effective diffusion coefficient, D_{ce}. Whilst discrepancies from the measured data may occur near the exposed surface, the best-fit curve gives a reasonable fit to the measured data at greater depths where the reinforcement is likely to be. The accuracy of these predictions is likely to vary depending on the environment to which the concrete is subjected.

In order to establish representative values of D_{ce} and C_s for marine and de-icing salt exposure conditions, the Author undertook an extensive review of the published performance of real structures and concrete specimens subject to these environmental conditions in conjunction with Hobbs[2], and Hobbs and Matthews[12]. Chloride profiles measured in situ were used to calculate D_{ce} and C_s using the spreadsheet CHLORPRO[13]. Where the profiles were not given, the original researcher's values of D_{ce} and C_s were used.

The marine and de-icing salt exposure conditions that will typically be designed for are designated XS3 (tidal splash and spray zones) and XD3 (cyclic wet and dry) in BS EN 206[14]. The

de-icing salt exposure data are primarily taken from exposed vertical faces in situ bridge piers. Few data on multi-storey car parks (MSCP) were available. There the critical elements are horizontal and ponding will have an effect. The results for de-icing salt exposure may not be directly applicable to MSCP under normal exposure. Further data are required for MSCP.

Marine exposure

For Portland Cement (PC) concrete the Author, in conjunction with Hobbs and Matthews[12], has shown that the effective diffusion co-efficient can be related to the water/cement (w/c) ratio as shown in Figure 2-3.

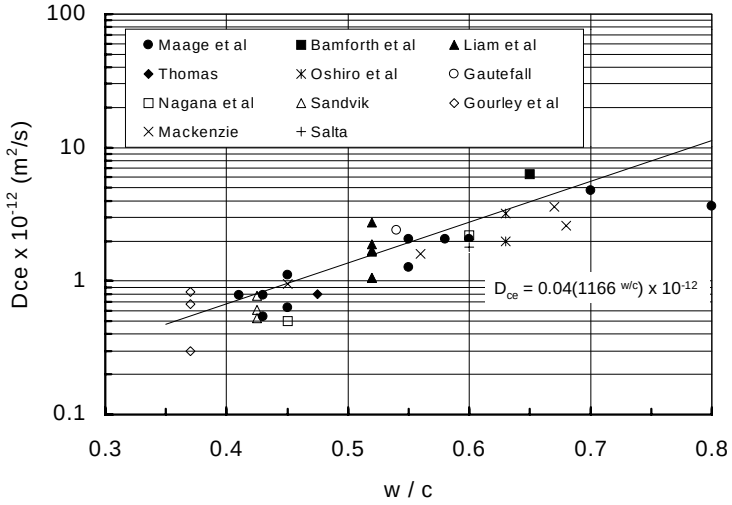

Figure 2-3: Relationship between effective diffusion coefficient, D_{ce}, for concrete and w/c for temperature corrected marine exposure XS3 (Hobbs and Matthews[12])

The data have been measured in a variety of locations around the world. Chemical reactions proceed faster at higher temperatures. To allow for this, the effective diffusion coefficients have been normalised to average UK marine temperatures using the Arrhenius function. The best-fit relationship is shown in Figure 2-3.

Figure 2-4 shows little variation in effective diffusion coefficient with time for PC concrete with w/c ratios appropriate for marine exposure. As such Hobbs and Matthews[12] suggest that a constant value of the effective diffusion co-efficient can be adopted over the whole life.

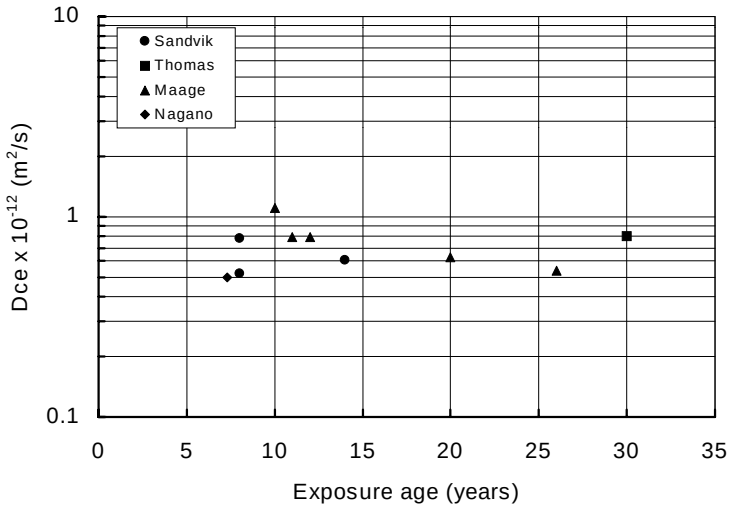

Figure 2-4: Relationship between effective diffusion coefficient, D_{ce}, for concrete and age of marine exposure XS3 for PC concrete with $0.45 \leq w/c \leq 0.5$ (Hobbs and Matthews[12])

Hobbs and Matthews[12] have plotted surface chloride concentration values to estimate their variation with time. These are shown in Figure 2-5. Whilst C_s is an artificial value that varies according to exposure and cement type, it does not appear to vary significantly with time. As such, they propose a representative C_s value of 0.4% by mass of concrete for PC concrete.

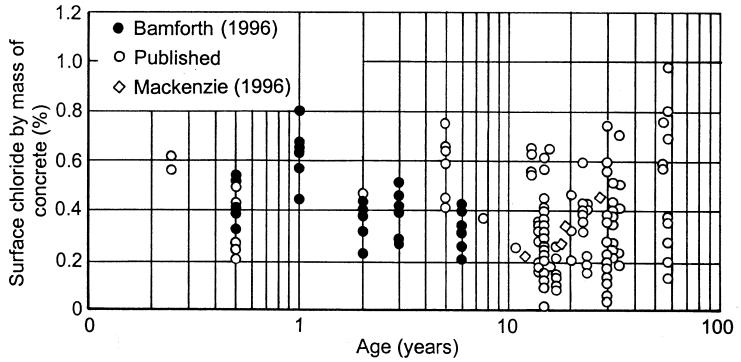

Figure 2-5: The variation in surface chloride content for concrete with age of marine exposure XS3 (Hobbs and Matthews[12])

De-icing salt exposure

The approach used for marine exposure has been repeated by the Author in conjunction with Hobbs and Matthews[12] for de-icing salt exposure. The relationship between D_{ce} and w/c ratio is

shown in Figure 2-6 along with the best-fit relationship.

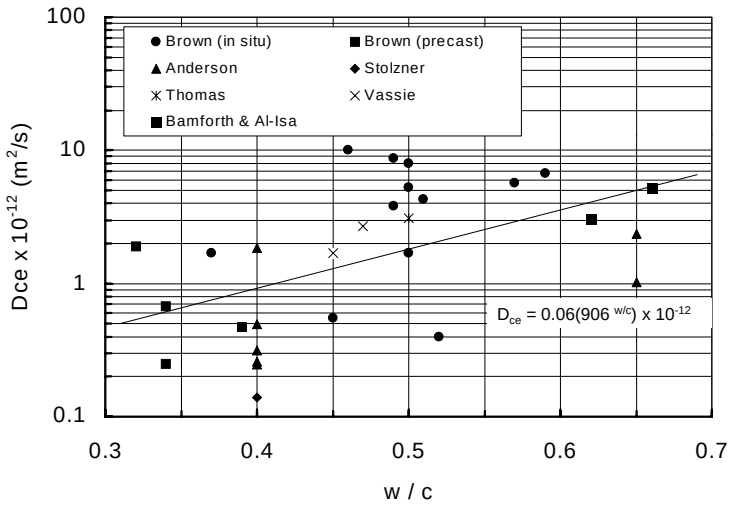

Figure 2-6: Relationship between effective diffusion coefficient, D_{ce}, for concrete and w/c ratio for de-icing salt exposure XD3 (Hobbs and Matthews[12])

It is interesting to note that there is considerably more scatter in the de-icing salt data than in the marine data. This could be due to the differences in exposure conditions. In a marine environment, the concrete is likely to be subject to moisture on a daily basis even if it is not in direct contact with the sea at all times, for instance in the splash zone. In a de-icing salt environment the concrete is only likely to be in contact with moisture after periods of rain. The concrete will spend long periods of the year where the surface is not in contact with moisture. This suggests that Fick's 2nd law is likely to be more appropriate for use with marine exposure.

It may be thought that the use of Fick's 2nd law is not appropriate for de-icing salt exposure. However, Fagerlund and Hedenblad[15] have shown that the internal moisture conditions within the concrete are not greatly affected by external variations in relative humidity beyond the first 10 to 20 mm from the surface (depending on the quality of the concrete). Whilst Fick's 2nd law may not be appropriate to these 10 to 20 mm of cover concrete, beyond that, and in the regions closer to the reinforcement, Fick's 2nd law can be used to give a reasonable estimate of the chloride content[12]. Hence, the concept of effective diffusion coefficient. Fick's 2nd law has to be viewed as a mechanism for obtaining an engineering answer rather than a theoretical explanation of the process of chloride ingress. By calibrating Fick's 2nd law against data from structures as proposed here the shortcomings of Fick's 2nd law can be overcome to an extent.

The relationship between surface chloride concentration and effective diffusion co-efficient is shown in Figure 2-7. The relationship is not an obvious one. However, Hobbs and Matthews[12] have proposed the C_s values given in Table 2-2.

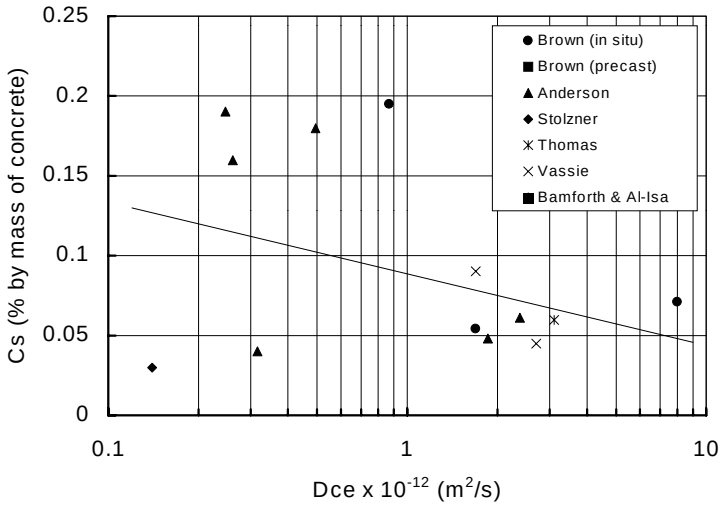

Figure 2-7: Relationship between effective diffusion coefficient, D_{ce}, and surface chloride level, C_s, for de-icing salt exposure XD3 (Hobbs and Matthews[12])

Hobbs and Matthews[12] have also deduced critical chloride levels for XS3 and XD3 exposure classes. These are given in Table 2-2.

Table 2-2: Values of C_s and C_{crit} for XS3 and XD3 exposure classes[12]

Exposure condition	C_s *(% by mass of concrete)*	C_{crit} *(% by mass of concrete)*
XS3 - Tidal, splash and spray zones	0.4	0.2
XD3 – Cyclic wet and dry	0.1*	0.06

* For D_{ce} values of $1x10^{-12}m^2/s$ or higher take C_s as 0.1%. For D_{ce} values less than $1x10^{-12}$ m^2/s increase C_s in accordance with Figure 2-7.

A summary of the parameters affecting the initiation period is given in Table 2-3.

Table 2-3: Parameters affecting chloride-induced corrosion - Initiation period

Parameter	*Effect*
Cement type[5]	The ability to bind chlorides into the cement matrix depends on the C_3A content of the cement. The greater C_3A content, the greater the binding capacity. Binding reduces the amount of free chlorides in the pores.
w/c[2, 12]	The lower the w/c ratio, the slower the ingress of chlorides will be. At lower w/c ratios, the pores will be smaller and are less likely to be interconnected.
Cl^-/OH^-[2, 5]	For chlorides to affect the passive layer, their concentration in the pore solution needs to exceed a critical level. This is expressed as a molar ratio of free chlorides to hydroxyl ions. It is extremely difficult to measure and thus cannot be regarded as a criterion for real structures.
Carbonation[5]	Carbonated concrete has a lower binding capacity than uncarbonated concrete. This implies that a higher proportion of the total chlorides is available in the pore solution as free chlorides.
Cover[5, 7, 2, 12]	Generally, the larger the cover is, the longer chlorides will take to reach the reinforcement.
Exposure[2]	There are three components to consider: amount of chlorides applied, frequency of wetting and drying and temperature. External chlorides come from two primary sources: de-icing salts and seawater. The application of the former will vary according to the number of applications (related to the number of days of cold weather).
Transport mechanisms[12]	Where the concrete is saturated for the majority of the time chloride ingress is primarily by diffusion. Where surface zones remain unsaturated for long periods chloride ingress can by capillary suction which is more rapid than diffusion. These unsaturated surface zones can also carbonate. Chlorides may enter in solution, but when the moisture evaporates from the surface zones, chlorides are deposited in the pores (ready to be washed in further during the next wetting cycle). In addition, there is the possibility of chlorides being washed-out from the surface zones.
Temperature[12]	As with most chemical reactions, chloride ingress progresses faster at higher

Parameter	*Effect*
Cracking[7]	temperatures. Cracks can allow chlorides to reach the reinforcement far quicker than they would do through uncracked concrete. However, for corrosion to take place at the anode (crack) the cathode must have access to oxygen and moisture. This implies that cracks transverse to the reinforcement are less significant than those that run along the length of the reinforcement.

2.2.2 Propagation period

The criteria for determining the end of the propagation period vary from first cracking to loss of load-carrying capacity. These criteria are dealt with in other sections of this Thesis. However, the common feature that determines the propagation period is the corrosion rate. This is dealt with in this section.

Chlorides generally enter the concrete in solution and, as such, there should be sufficient moisture present for corrosion to take place. The corrosion rate, and length of propagation period, is thus likely to be controlled by the ability of oxygen to reach the cathode. The rate of diffusion of oxygen through saturated concrete is low, and the cathodic reaction may have to rely on dissolved oxygen in the water. The presence of water will lower the electrical resistivity of the concrete increasing the corrosion current in the presence of oxygen. In addition, the chlorides reduce the electrical resistivity of the concrete. This increased conductivity enables a local anode to be serviced by a length of reinforcing bar acting as a cathode i.e. macrocell corrosion with local pitting.

Hobbs and Matthews[12] have reviewed the literature on structures built since the 1940's, and summarised the reported observations for concrete structures subject to marine and de-icing salt exposure. These indicate a wide range of performance depending very much on the w/c ratio. Those structures where the w/c is below 0.45 are showing little or no signs of deterioration. Those structures where cracking had occurred were used to make estimates of the propagation

period of around 15 to 20 years. Many studies on deteriorating structures will not have been reported in the public domain due to client confidentiality. This makes building a detailed database of observations difficult and, as such, generalisations regarding the length of the propagation period should be treated with caution.

In situ corrosion rates can now be measured using the linear polarisation technique with apparatus such as the GECOR 6[16]. The measured corrosion rates offer the possibility of being able to calculate the propagation period directly. However, the values measured in situ represent only a snapshot at one point in time and are not necessarily representative values. This is likely to be due to variations in temperature and moisture levels with time[17]. Guidance is required on sampling and conversion to representative values.

Andrade and Alonso[17] have collected a series of corrosion rate (I_{corr}) measurements with the GECOR 6 apparatus from a variety of Spanish structures where chloride-induced corrosion is occurring. These are shown in Figure 2-8 as a cumulative frequency plot. Unlike the diffusion coefficients the corrosion rates have not been corrected to reflect the difference in ambient temperature between UK and the country of origin[18].

Grantham et al[19] have measured in situ corrosion rates on four occasions in one year in a UK multi-storey car park. These data are also shown in Figure 2-8. Further data such as this opens the possibility of producing such curves for a variety of structures and exposure conditions. A characteristic (95%) corrosion rate can then be obtained and used in design and assessment. This would avoid the need for complex modelling and would offer relevance by basing rules on measurements from real structures.

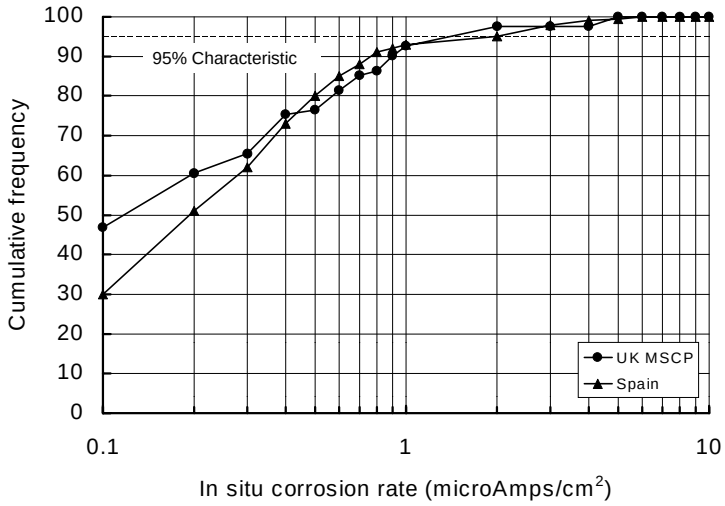

Figure 2-8: In situ chloride-induced corrosion rates measured in UK and Spanish structures[17,19]

Bamforth[20] has observed an exponential relationship between chloride content and corrosion rate in concrete blocks made with PC concrete and a high w/c ratio of 0.66, exposed to the sea at Folkestone. Bamforth has combined these results with the observations of Andrade et al[17] on threshold and maximum corrosion rates to define exponential relationships for the three marine exposure conditions: 'wet, rarely dry'; 'airborne sea water and cyclic wet/dry'; and 'tidal zone'. These relationships have potential as they recognise that corrosion will increase with increasing chloride content (and thus lower resistivity) and that corrosion rate will vary with exposure condition (presumably due to the varying ease of oxygen ingress under each condition). As data measured on real structures become available, these relationships can be calibrated and validated further.

Atkins et al[21] have proposed an inverse linear relationship between half-cell potential and corrosion rate. In the discussion that followed their presentation, it emerged that the relationship was derived from in situ measurements on similar elements in a bridge network. Andrade et al[17] have observed a similar trend in measurements on a variety of structures. However, whilst there is a general trend the scatter is too great to suggest that a general relationship is appropriate. It is likely that this relationship can only be applied to similar elements under similar exposure conditions.

A summary of the parameters affecting the corrosion rate, and thus the propagation period, is

given in Table 2-4.

Table 2-4: Parameters affecting chloride-induced corrosion - Propagation period

Parameter	*Effect*
Moisture[5, 7]	Moisture is required for both the cathodic reaction and the formation of rust at the anode. Conductivity is also increased by moisture.
Oxygen[5, 6, 7, 2]	Oxygen is required for both the cathodic reaction and the formation of rust at the anode. It is possible that the propagation period will be determined by the access of oxygen to the cathode. Moisture is unlikely to control as chlorides generally enter the concrete in solution. Higher moisture levels in the pores can block the ingress of oxygen.
Resistivity[5, 17]	Resistivity of the concrete will limit current flow between anode and cathode. Resistivity is primarily a function of the internal RH, higher RH leading to lower resistivity. Concrete containing chlorides will tend to have a higher RH as chlorides generally enter in solution.
Temperature[18]	As with most chemical reactions, corrosion progresses faster at higher temperatures. However, resistivity is likely to rise with increasing temperature and this may cancel out some or all of the potential increase for reinforcement embedded in concrete.
Corrosion product[5]	Chloride-induced corrosion can result in either general corrosion products or localised pitting. Localised pitting occurs where a length of cathode serves a local anode. The loss of reinforcement cross-section at a pit can be four to eight times that with general corrosion. It is not clear where and when pitting will occur rather than general corrosion.

2.3 Cracking

One of the potential results of reinforcement corrosion is cracking of the cover concrete. This occurs because the rust product occupies a greater volume than the original reinforcement. Several aspects of corrosion and cracking have been investigated in the past, namely:

(i) Under what conditions cracking occurs.
(ii) The influence of corrosion-induced cracking on structural performance.
(iii) The influence of design crack width limits on corrosion.
(iv) The influence of existing cracks on structural performance.

The first point will be considered in this section. The influence of corrosion-induced cracking on structural performance will be considered separately in each of the sections on bond, bending, shear and column behaviour. The third and fourth points are not considered in this Thesis, as they are primarily design issues.

2.3.1 Experimental

Andrade et al[22] tested four types of concrete block specimens each 150 by 150 by 380 mm containing 16 mm bars subject to accelerated corrosion. An applied current and 3% calcium chloride by weight of cement in the mix were used to accelerate corrosion. The time to first visible cracking and subsequent crack widths were recorded for each specimen. Assuming 100% current efficiency, Faraday's law was used to calculate the corresponding loss of reinforcement section. Details are given in Table 2-5.

Comparing specimens II, III and IV, increasing the cover from 20 to 30 mm (II to III) increased the radius loss required for cracking by 48%. Decreasing the applied current (corrosion rate) from 100 to 10 $\mu A/cm^2$ (II to IV) brought a 21% increase in radius loss required for cracking.

Table 2-5: Specimen details (Andrade et al[22])

Specimen No.	*Reinforcement*			*Applied current ($\mu A/cm^2$)*	*Radius loss at first crack (μm)*
	Diameter (mm)	*Position*	*Cover (mm)*		
I	16	Corner	20 top 30 side	100	18
II	16	Face centre	20	100	14
III	16	Face centre	30	100	21
IV	16	Face centre	20	10	17

The first visible crack could only be viewed with a magnifying glass. Its width was estimated to be less than 0.05 mm. The cracks were not observed to be continuous when they appeared. They generally appeared at the centre of the specimen first and then propagated to join and spread along the full length.

In specimens I, II and III a calculated section loss of 100 μm was found to give a crack width of around 0.3 to 0.4 mm. In specimen IV, a 50 μm loss gave a 0.3 mm crack width. Both Tuutti[5] and Parrott[11] have suggested that around 100 μm section loss is required to give cracking. The amount of section loss to give cracking is an important factor in service life calculations. Typical section losses in structures are in the region of 2 to 10 μm/year[23]. As such, limiting section losses of 20 to 100 μm could lead to five-fold differences in estimates or the propagation period.

It is possible that the section losses will actually be greater than the values estimated by Andrade et al[22]. They observed diffusion of the rust product into the pores of the surrounding concrete. This rust is unlikely to generate stress until the pores are filled. In addition, Andrade et al[22] assume 100% current efficiency in their calculation of section loss. This is unlikely to be correct, as the applied current is likely to cause a temperature rise in the reinforcement, and possibly also disperse into the concrete.

A section loss of 20 μm on a 16 mm bar only represents a loss of 0.5% in cross-section. This is unlikely to have any serious structural consequences on the basis of section loss alone. Particularly as BS 4449[24] allows manufacturing tolerances in mass of ±9%, ±6.5% and ±4.5% for

bars of 6 mm, 8 and 10 mm, and 12 mm and above respectively.

How much crack width is tolerable is another important question in determining the service life. If a crack in a structure cannot be seen by the naked eye, it is unlikely to be of much significance aesthetically. It is only when cracks reach around 0.3 mm wide that they become noticeable. This ties in with the suggestions of Tuutti[5] and Parrott[11] of 100 μm section loss being the limiting value.

Alonso et al[25] applied accelerated corrosion to a series of 27 concrete specimens 380 by 150 by 150 mm. Reinforcing bars of 3, 8, 10, 12 and 16 mm diameter were used either in the middle of a 150 by 150 mm face or a corner. Covers of 10, 15, 30, 50 and 70 mm were used. Water/cement ratios of 0.52, 0.60 and 0.65 were used giving concrete tensile strengths ranging from 2.4 to 3.9 N/mm^2. Accelerated corrosion was achieved by including 3% $CaCl_2$ by weight of cement in the mix and by applying currents of 3, 10 or 100 $\mu A/cm^2$. The corrosion-induced crack widths were measured at intervals from first cracking. At the end of the tests, the specimens were broken open and the amount of corrosion established from weight loss measurements. The amount of corrosion occurring at each of the crack widths was then extrapolated from the applied current and time assuming a uniform section loss that increased linearly with time.

The relationship between radius loss to cause first cracking and cover to bar diameter (c/D) ratio was found to be linear with a correlation coefficient of 0.92. Around 50 μm of radius loss was sufficient to induce cracking in the specimens where the bars had c/D ratios greater than 2. For those with c/D ratios of less than 2 only 15 to 30 μm was found to be necessary. The influence of cover on the increase in crack width with time was such that the rate of increase in crack width was significantly slower for those with covers in the range of 50 to 70 mm than for those specimens with covers less than 30 mm.

Alonso et al[25] found that the corrosion rate had an effect on the amount of corrosion required to induce cracking, with the corrosion rates of 3 and 100 $\mu A/cm^2$ requiring more corrosion to induce cracking than the corrosion rate of 10 $\mu A/cm^2$. This is in conflict with the observations of Andrade et al[22]. However, as Andrade et al did not measure their section losses, and there is little

difference between radius losses of 14 and 17 μm it is difficult to draw definitive conclusions from their data. Once cracking had been induced, larger amounts of corrosion were required to generate a given crack width at higher corrosion rates.

Those specimens with lower w/c ratios required less corrosion to initiate cracking. Alonso et al[25] interpret this as resulting from less void space being available to the corrosion product in concrete with lower w/c ratios. Similarly, they found in the 300 by 300 by 300 mm specimens used for bond tests (and described in Section 2.4) the top cast bars required more corrosion to induce a given crack width than bottom cast bars. Alonso et al felt that this was due to the extra void space being available around the top cast bars.

Cabrera[26] applied accelerated corrosion to seven 300 by 100 by 200 mm slabs. Each had three deformed bars of either 12, 16 or 20 mm diameter embedded in the bottom face. The slabs were stored at 35°C and 45% RH for 28 days before immersion in a 5% NaCl solution. After 31 days a potential of 3 volts was applied to accelerate corrosion. The variations in bar size and bottom and side cover are shown in Table 2-6. The observed crack patterns are given in Figure 2-9.

Table 2-6: Specimen variables (Cabrera[26])

Type	*Bar size (mm)*	*Bottom face*		*Side face*		*Spacing (mm)*
		Cover (mm)	*c/D*	*Cover (mm)*	*c/D*	
A-12	12	20	1.67	44	3.67	100
A-16	16	20	1.25	44	2.75	98
A-20	20	20	1.00	44	2.20	96
B-12	12	20	1.00	20	1.00	124
C-12	12	30	2.50	30	2.50	114
C-12T	12	30	2.50	30	2.50	114

Note: The type C-12T slab also had two 8 mm deformed bars underneath the three main bars to simulate the presence of transverse reinforcement.

In the initial stages of corrosion the cracks in the type A slabs were near vertical, reaching

downward to the bottom surface and propagating upwards but not reaching the top surface. By the final stage extra cracks had propagated to the bottom face giving forked cracking. No cracks propagated to the side faces, whose cover was twice that to the bottom face.

In the type B slab with equal bottom and side cover, two vertical and one horizontal crack were present in both initial and final stages. In the final stage, the vertical cracks had propagated upwards. No forked cracks were found towards the bottom face. This trend was repeated in the type C-12 slab. The cover was again equal on both the bottom and sides. The crack patterns seem to be a function of the ratio of side to bottom cover.

Two horizontal cracks were found propagating from the two outer bars to the side faces on the C-12T slab with transverse reinforcement. No vertical cracks were present. This shows the beneficial effects of having reinforcement intersecting the cracking plane.

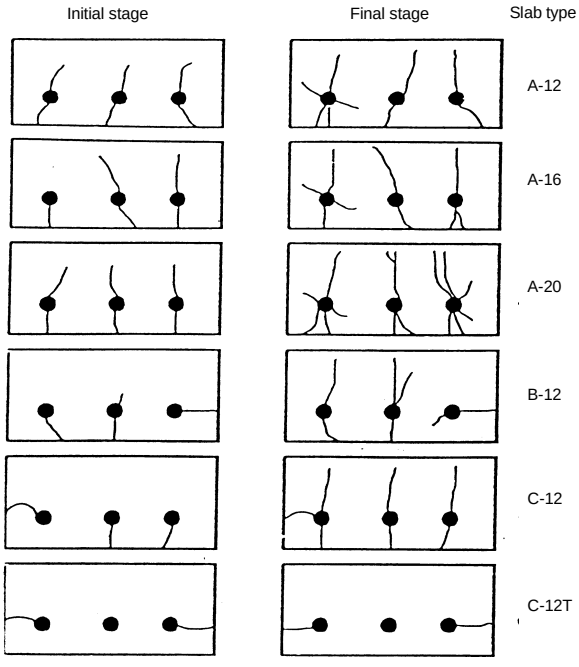

Figure 2-9: Observed crack patterns (Cabrera[26])

The increase in crack widths with increasing corrosion is shown in Figure 2-10. Faraday's law was used to calculate the amount of corrosion during the test. Weight loss measurements were taken at the end, and gave reasonable agreement with Faraday's law.

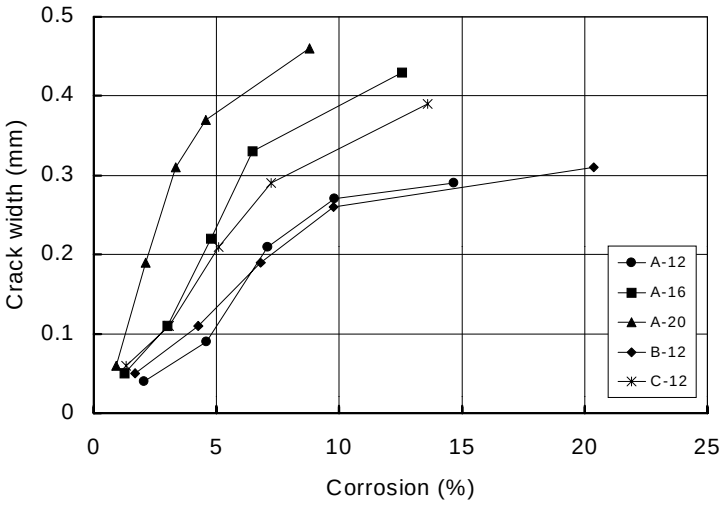

Figure 2-10: Relation of average crack width to corrosion (Cabrera[26])

Early on there appears to be a relationship between corrosion and crack width. This diminishes with increasing corrosion. It is possible that once the crack is established, the rust product has a transport path away from the bar and the induced stresses per unit of corrosion are less. This is important for engineers trying to relate section losses to observed crack widths.

Cabrera[26] also presents two equations for calculating corrosion-induced crack widths. These equations give reasonable agreement with Cabrera's test data in the early stages of corrosion, and then become less accurate. Cabrera presents these two equations with no background. As such, a critical review is not possible.

Liu[27] embarked on a long-term series of tests consisting of sixty specimens. Only four had cracked when the work was reported. Slab specimens were 1180 by 216 by 1180 mm whilst block specimens were 280 by 178 by 330 mm. The parameters investigated in the slab programme are given in Table 2-7.

Table 2-7: Variables investigated in slab tests (Liu[27])

Parameter	*Variables investigated*
Chlorides in mix (kg/m^3)	0.0, 0.36, 0.71, 1.42, 2.85, 5.69 and 7.2
Cover (mm)	25, 51 and 76
Bar diameter (mm)	16 and 19
Bar spacing (mm)	152 and 203
Exposure	Indoors (with periodic wetting) and outdoors

One of the key features of these tests is that the corrosion was accelerated by the use of cast in chlorides rather than an applied current. This should give a slower rate of corrosion, and thus results closer to those that would be obtained in practice. On the negative side, the free chlorides in the pore system are likely to be different with internal than external chlorides, as the internal chlorides have the opportunity to bind with the cement during hydration.

Details of the four specimens that have cracked to date are given in Table 2-8. The specimens were cored to measure the amount of corrosion that had taken place. Cracking was observed to meander along the line of the reinforcing bars.

Table 2-8: Cracking of slab and block specimens (Liu[27])

	Reinforcement				*Cracking*			
No.	*Diameter (mm)*	*Spacing (mm)*	*Cover (mm)*	*c/D*	*Time (years)*	*Wt loss (g/cm^2)*	*Percent (%)*	*Radius loss (mm)*
OA2859.6	16	203	51	3.2	1.84	0.0393	1.26	0.0502
OB3859.6	16	203	76	4.8	3.54	0.0601	1.93	0.0769
OE(F)18512.0	16	203	25	1.6	0.72	0.0298	0.96	0.0381
Block 9.6	12.7	-	51	4	2.38	0.0392	1.57	0.0501

The cover to bar diameter (c/D) ratio appears to be the most important parameter, with both time to cracking and percentage section loss at the time of cracking increasing with increasing c/D. The radius loss values followed the same trend with the c/D ratio for the 16 mm bars, but not for

the 12.7 mm bar. This suggests that the non-dimensional parameters of percentage corrosion and c/D may better describe the amount of corrosion to cause cracking. The radius loss at cracking varied from 38 to 77 μm. This is a little lower than the 100 μm value suggested by Parrott[11] and Tuutti[5], but is still of similar magnitude.

Morinaga[28] carried out a series of tests on hollow concrete cylinders. Applied oil pressure within the hollow simulated the expansive pressure generated by rust. The effects of bar diameter, cover thickness and concrete tensile strength were investigated. The failure pressure was found to increase with increasing tensile strength and cover. Increasing the cover for a given tensile strength was found to be more effective than increasing the tensile strength for a given cover. Morinaga derived the following relationship to predict when cracking would occur:

$$\sigma_{t\max} = f_t \left(\frac{r_2}{r_1} \right)^{0.85} \qquad \textbf{… (2-2)}$$

where: f_t = tensile strength of the concrete (kgf/cm^2)

r_1 = internal cylinder radius – bar radius (cm)

r_2 = external cylinder radius (cm)

σ_{tmax} = tensile stress when the concrete cover cracks (kgf/cm^2)

Following on from this, Morinaga also cast reinforcing bars within cylinders and subjected them to accelerated corrosion. 100 and 150 mm diameters cylinders 100 mm high were used with 0.5, 1 or 5% calcium chloride cast in. 9, 19 and 25 mm bars were embedded, and had potentials of 1.5, 3, 6 or 12 volts applied to them. The time to cracking varied from 10 to 2000 minutes.

The higher the chloride content, the higher the bar section loss was at cracking. This suggests that at higher corrosion rates more corrosion is required to crack the concrete cover than at lower corrosion rates. However, Alonso et al[25] and Saifullah and Clark[42] found that whilst the amount of corrosion to cause cracking did initially increase with increasing corrosion rate, beyond a certain corrosion rate the amount of corrosion required to cause cracking reduced. It is possible that these results are due to differences in corrosion product at higher corrosion rates where a

more liquid product can result. This highlights the effects of corrosion rate when interpreting laboratory and in situ data.

At higher concrete strengths (w/c = 0.4), less corrosion was required to crack the concrete with higher cover than with lower cover. This is somewhat different to what one would expect from the results of other researchers[35, 26, 27] where increasing cover to bar diameter ratios were found to be beneficial. At lower strengths (w/c = 0.7), similar corrosion was required to crack both the lower and higher covers. An explanation for the discrepancy with the results of other researchers may be the excessively high corrosion rates used by Morinaga[28].

2.3.2 Analytical

Bazant[29] undertook an analytical study of corrosion-induced cracking leading to an expression for time to corrosion-induced cracking.

Bazant assumed the rust product to be hydrated red rust, $Fe(OH)_3$. Assuming steady state corrosion occurs after depassivation, the bar diameter D increases by an amount ΔD. This volume increase is due to the conversion of steel (Fe) to hydrated rust $Fe(OH)_3$. One unit of mass of steel was taken to produce 0.523 units of $Fe(OH)_3$. The density of the $Fe(OH)_3$ was taken to be 25% of the steel. The mass of rust per unit length of bar, M_r is taken as:

$$M_r = s j_r t_{cor} \qquad \text{… (2-3)}$$

where: s = bar spacing (cm)

j_r = rate of rust production (g/m^2s)

t_{cor} = corrosion time (s)

The volume change due to conversion of Fe to Fe $(OH)_3$ is equated to the volume change due to increase in diameter as follows:

$$\frac{M_r}{\rho_r} - \frac{M_{st}}{\rho_{st}} = \frac{\pi\left((D+\Delta D)^2 - D^2\right)}{4} \qquad \text{… (2-4)}$$

where: M_{st} = mass of steel consumed to produce Mr (g)

ρ_{st} = density of steel (7.85 g/cm^3)

ρ_r = density of hydrated rust (ρ_{st}/4 g/cm^3)

D = original bar diameter (cm)

ΔD = increase in bar diameter (cm)

By combining and re-arranging the previous two equations and ignoring the term ΔD^2, it is possible to get equation

$$t_{cor} = \frac{\rho_{cor} D \Delta D}{s j_r} \quad \text{… (2-5)}$$

Where:

$$\rho_{cor} = \frac{\pi}{2\left(\frac{1}{\rho_r} - \frac{0.583}{\rho_{st}}\right)} \quad \text{… (2-6)}$$

In the derivation of this expression, the constant 0.583 was found to be 0.523 possibly indicating a typing error in the original paper. 0.523 is the ratio of the molecular weight of Fe to Fe $(OH)_3$, and is required to ensure that the two sides of the equation are compatible.

If the value of ΔD necessary to crack the concrete cover can be found, then t_{cor} can become time to cracking, t_{cr}, and the propagation period is defined. Bazant[29] considers the concrete cover to be an elastic material with pressure exerted on a circular hole. The pressure to crack a concrete member is suggested to be greater than that required to crack a thick walled cylinder but less than that required to crack an infinite medium. ΔD is given by:

$$\Delta D = P_r \delta_{pp} \quad \text{… (2-7)}$$

where: P_r = applied pressure

δ_{pp} = bar hole flexibility

Bazant[29] suggests that the bar hole flexibility be taken as the average of the thick-walled cylinder (δ^0_{pp}) and infinite (δ^1_{pp}) cases to give:

$$\delta_{pp} \approx \frac{\delta^0_{pp} + \delta^1_{pp}}{2} \quad \text{… (2-8)}$$

$$\delta^0_{pp} = \frac{D(1+\upsilon)}{E_{ef}} \quad \text{… (2-9)}$$

$$\delta^1_{pp} = \frac{D}{E_{ef}}\left[1+\upsilon+\frac{D^2}{2L(L+D)}\right] \quad \text{… (2-10)}$$

where: ν = Poisson's ratio of concrete

D = bar diameter (cm)

E_{ef} = effective elastic modulus of concrete

L = the cover (cm)

If a series of parallel bars are corroding, such as those in a slab, the ΔD of one bar is likely to be affected by the expansion of the adjacent bars on either side. To allow for this, Bazant[29] suggests that an extra term be added to give:

$$\delta^0_{pp} = \frac{D(1+\upsilon)}{E_{ef}} + \frac{D^3}{s^2 E_{ef}} \quad \text{… (2-11)}$$

and

$$\delta^1_{pp} = \frac{D}{E_{ef}}\left[1+\nu+\frac{D^2}{2L(L+D)}\right] + \frac{2D^3}{s^2 E_{ef}} \quad \text{… (2-12)}$$

Bazant[29] adds further refinement to allow for the potential of different failure modes depending on the ratio of bar spacing to cover. When the bar spacing is large (Bazant suggests $s > 6D$) the

cracking consists of two cracks propagating from the bar to the surface at 45° to one another. In this case, ΔD is given by:

$$\Delta D = \frac{2 f_t L \delta_{pp}}{D} \qquad \textbf{… (2-13)}$$

where: f_t = tensile strength of the concrete.

The other failure mode is caused by cracks propagating horizontally and joining up to give a plane of cracks. In this case, ΔD is given by:

$$\Delta D = f_t \left[\frac{s}{D} - 1 \right] \delta_{pp} \qquad \textbf{… (2-14)}$$

Bazant suggests that this case is likely to be critical when the cover is greater than 0.5 (s-D). That is, the horizontal cracks propagating from adjacent bars meet before vertical cracks propagate to the surface.

Unfortunately, Bazant[29] provides no comparison with field or experimental data to validate his theory. Liu[27] reported on work carried out by colleagues at Virginia Tech that suggested that Bazant's approach underestimated the time to cracking. No figures are given to show how close the results were. It is likely that Bazant's approach would underestimate the time to cracking, given that it considers the entire corrosion product to have the potential to induce stress. Several investigators[22, 25, 27] have found that the rust product diffuses into the concrete pore structure surrounding the bar. Stress is unlikely to be induced until the surrounding pores are full and the rust product has nowhere else to go. The time for the rust to fill the pores should thus be added to the times calculated by Bazant's approach.

Cady and Weyers[30] have used the Bazant[29] cracking model as part of a bridge management exercise. They studied 169 bridges in Pennsylvania, all built in the same year to the same specification. 50 mm cover was specified to the top steel in deck slabs. Within fifteen years, 20

of these bridges had been overlaid due to deterioration (cracking and spalling). This implies that the cracking would have started much earlier than the ten to fifteen years at which repairs were carried out. The observations of bridge structures reported by Hobbs and Matthews[12] suggest that the time to repair should have been considerably longer than this. It is the Author's opinion that these short times to repair have resulted from plastic settlement cracking and the absence of deck waterproofing.

Based on in situ chloride measurements, the average initiation period was estimated to be 4.7 years. The propagation period was estimated to be 2.3 years. Thus cracking was expected at around seven years. This seems compatible with the observations in the 20 bridges. The Bazant model may be expected to underestimate the time to cracking. When deterioration rates are high though, a large relative error only leads to a small absolute error in time to cracking. For lower deterioration rates, Bazant's model may not be as satisfactory if it predicts, say, 10 years instead of 25.

Liu[27] and Weyers[31] produced a model to accompany the experimental programme carried out by Liu[27]. The main advances of this model over that proposed by Bazant[29] are:

(i) Not all of the corrosion product is considered to induce stress in the concrete. An allowance is made for that product that fills the pores surrounding the bar or migrates away.
(ii) The rate of growth in rust product is taken as being inversely proportional to the thickness of rust already present. This recognises that the transport path to the bar surface is growing with increasing rust product.

Liu[27] assumes uniform corrosion, such that the critical amount of rust is made up of three components:

(i) An amount of rust to fill the space left behind by the corroded steel.
(ii) An amount of rust that fills the pore space adjacent to the bar without inducing any stress in the surrounding concrete.

(iii) An amount of rust that causes sufficient stress to crack the concrete cover.

This critical amount of rust to cause cracking, W_{crit}, is given by:

$$W_{crit} = \rho_{rust}\left(\pi(d_s + d_0)D + \frac{W_{st}}{\rho_{st}}\right) \quad \textbf{… (2-15)}$$

where: d_0 = thickness of the pore band around the steel-concrete interface (inches)

d_s = thickness of rust required to cause tensile splitting stresses (inches)

D = original bar diameter (inches)

W_{st} = mass of steel corroded (lb/ft^2)

ρ_{st} = density of steel (490 lb/ft^3)

ρ_r = density of hydrated rust (225 lb/ft^3)

An expression is proposed for the elastic stress distribution in a thick-walled cylinder. This is then equated to an expression for the plastic stress distribution in order to cancel out the pressure terms and derive an expression for d_s. This is not strictly correct, as the elastic and plastic stresses are only likely to be equal at one point, the steel concrete interface. Beyond this the elastic stress distribution reduces whilst the plastic stress remains constant. Substituting for d_s Liu proposed:

$$W_{crit} = \rho_{rust}\left(\left(\pi\left(\frac{Cf_t}{E_{ef}} + \left(\frac{a^2 + b^2}{a^2 - b^2} + \nu_c\right) + d_0\right)D + \frac{W_{st}}{\rho_{st}}\right)\right) \quad \textbf{… (2-16)}$$

where: a = $(D + 2d_0) / 2$ (inches)

b = $C + ((D + 2d_0) / 2)$ (inches)

f_t = concrete tensile strength (psi)

C = concrete cover to reinforcement (inches)

E_{ef} = effective elastic modulus of concrete $E_{ef} = E / (1 + \phi_{cr})$

ϕ_{cr} = concrete creep co-efficient

As the rust layer gets thicker, the distance to the bar surface is assumed to get larger and the

growth of rust production decreases. Liu gives the rate of rust production as:

$$\frac{dW_{rust}}{dt} = \frac{k_p}{W_{rust}} \quad \text{… (2-17)}$$

Where the factor, k_p, is given by:

$$k_p = \frac{2.59x10^{-6}\pi D i_{corr}}{\alpha} \quad \text{… (2-18)}$$

where: i_{corr} = annual mean corrosion rate (mA/ft^2)

α = ratio of the molecular weight of steel divided by the molecular weight of rust (0.523 for $Fe(OH)_3$ or 0.622 for $Fe(OH)_2$)

By integrating the differential equation, the time to cracking, t_{cr}, is given by:

$$t_{cr} = \frac{W_{crit}^2}{2k_p} \quad \text{… (2-19)}$$

Liu[27] and Weyers[31] give predicted times to cracking that bracket the observed values very closely. The higher value of α gave longer times to cracking as the density of $Fe(OH)_3$ is lower than that of $Fe(OH)_2$.

The Author has been unable to re-create either Liu's or Weyers' results. There are a number of possible explanations for this:

(i) Both Liu and Weyers give the value of d_0 as 12.5 μm. However, Liu states that the Imperial equivalent is 4.9×10^{-3} inches whilst Weyers suggests that it is 5×10^{-5} inches. In fact, 12.5 μm is 4.9×10^{-4} inches. Weyers[32] indicated that the value was based on experimental observations. Unfortunately, no details are given.

(ii) The constants in the equation for k_p do not agree. Liu gives a value of 2.56×10^{-6} for the

Imperial version, whilst Weyers gives a value of 0.098 for the metric version. These do not correspond to one another.

(iii) The units of k_p are not consistent with those required to give t_{cr}. It is likely that the anomaly lies in k_p as both t_{cr} and w_{crit} are more fundamental values (time and weight).

As such, it is difficult to verify the model quantitatively. Qualitatively, the model contains some important improvements on Bazant's model. These concepts should be used in any future model.

Morinaga[28] has developed a time to cracking model to accompany his cylinder tests. As with other researchers, the model is based on thick cylinder theory. However, Morinaga combines this theory with the empirical relationship derived from his tests on cylinders subject to oil pressure.

The circumferential strain is taken as a maximum at the bar-concrete interface, and is given by:

$$\varepsilon_{t\max} = \frac{P_{\max}}{E_t}\left(\frac{r_2^2 + r_1^2}{r_2^2 - r_1^2} + \nu\right) \quad \textbf{… (2-20)}$$

The corresponding stress at the bar-concrete interface is given by:

$$\sigma_{t\max} = P_{\max}\left(\frac{r_2^2 + r_1^2}{r_2^2 - r_1^2}\right) \quad \textbf{… (2-21)}$$

However, Morinaga[28] has derived an empirical relationship for σ_{tmax}, such that:

$$P_{\max}\left(\frac{r_2^2 + r_1^2}{r_2^2 - r_1^2}\right) = f_t\left(\frac{r_2}{r_1}\right)^{0.85} \quad \textbf{… (2-22)}$$

By substitution, and ignoring Poisson's ratio, the following is derived:

$$\varepsilon_{t\max} = \frac{f_t}{E_t}\left(\frac{r_2}{r_1}\right)^{0.85} \quad \textbf{… (2-23)}$$

where: f_t = tensile strength of the concrete (kgf/cm^2)

r_1 = internal cylinder radius – bar radius (cm)

r_2 = external cylinder radius (cm)

E_t = elastic modulus of concrete (kgf/cm^2)

ε_{tmax} = maximum circumferential strain at the bar-concrete interface

Morinaga[28] derived the strain at the bar-concrete interface based on rust growth as:

$$\varepsilon_t = \frac{Q(\alpha - 1)}{\rho r_1} \qquad \textbf{… (2-24)}$$

where: r_1 = internal cylinder radius – bar radius

Q = weight loss of bar per unit area

α = ratio of rust volume to steel volume

ε_t = circumferential strain at the bar-concrete interface

ρ = density of steel

By equating the two circumferential strains and expressing Q as a rate, q, in time, t, it is possible to derive the following expression for time to cracking, t_{cr}:

$$t_{cr} = \left(\frac{f_t}{E_t}\right)\frac{\rho}{(\alpha - 1)}\left(\frac{r_1}{q}\right)\left(\frac{r_2}{r_1}\right)^{0.85} \qquad \textbf{… (2-25)}$$

Morinaga[28] simplifies this expression for his test specimens and shows a good relationship with these specimens. Unfortunately, the method has yet to be validated against other test data. As with other analytical procedures this approach has considerable merits, but there are a number of points which need considering in any future use of the model:

(i) In real structures the time to cracking is likely to be considerably longer than the 10 to 2000 minutes observed in Morinaga's tests. An effective value of the elastic modulus

would have to be used to simulate the effects of creep.

(ii) The rate of corrosion growth is considered to be linear. This may be reasonable for such accelerated tests. However, Liu[27] has postulated that the corrosion rate decreases with increasing corrosion.

(iii) In the model all of the rust growth is assumed to contribute to stressing the concrete, whereas some of the rust is likely to be accommodated within the concrete pore structure.

2.3.3 Numerical

In an accompanying paper to Andrade et al[22], Molina et al[33] carried out non-linear finite element analyses of the four specimens. As it is not possible to model corrosion directly, it was modelled by combining two effects:

(i) A decrease in stiffness of the reinforcement. This was achieved by varying linearly the properties from those of steel to those of rust. Given the lack of experimental data, rust was assumed to have elastic properties similar to water based on the assumption that water is one of the main components of rust.

(ii) An increase in volume. This was achieved by imposing an initial strain on the elements to be corroded. The rust was assumed to occupy twice the volume of the virgin steel.

The analyses showed initial cracking at section losses of around 2 to 8 μm. The normal stress in the primary crack had reduced to zero at section losses of around 20 to 50 μm. This suggests that the crack is fully open by this stage. The calculated rate of deformation with increasing section loss is similar to that measured in the four specimens. However, the analytical and experimental values are out of phase with one another, with the analytical values overestimating deformation at a given section loss. It is possible that this is due to the rust product filling the surrounding concrete with significant deformation not occurring until the pores are full. It would seem that knowledge of the initial non-damaging amount of corrosion is required before estimates can be made of the time to cracking.

Chan et al[34] carried out a series of finite element analyses of the bond specimens tested by Saifullah[35]. Both uniform and non-uniform corrosion were simulated by prescribing nodal

displacements of the bond element surrounding the reinforcing bar.

Three phases were identified: internal cracking, external cracking and penetration. Internal cracking occurs first at the boundary of the bar, and was found to be independent of the cover. A radial expansion of 0.5 μm was required to initiate internal cracking in all cases although the induced stresses were marginally higher for higher c/D ratios (1.93 and 2.15 N/mm^2 for c/D = 0.5 and 1.5 respectively). External cracking is, as the name suggests, when cracks start appearing on the surface. This was found to be dependent on the c/D ratio. Radial expansions of 0.6 and 2 μm were required to crack the cover when c/D = 0.5 and 1.5 respectively. The penetration stage is when the internal and external cracks meet to penetrate the cover.

The compressive stresses between bar and concrete near the crack propagation points reach a peak at the external cracking stage, and then decrease. Chan et[34] al draw an analogy between this behaviour and that observed in Saifullah's[35] bond tests. The peak compressive stress corresponding to the formation of external cracks. The compressive stress is then reducing by the time penetration occurs. This corresponds to the point of visual cracking in the bond specimens where the residual bond strength has reduced from its peak value.

Bars in structures rarely corrode uniformly, usually the corrosion starts on the side where the chlorides enter. Chan et al[34] simulated this by applying radial expansion to one quadrant only. They found that around 80% of the uniform expansion was needed to crack the surface in this case. This suggests that for similar section losses, non-uniform corrosion product in the critical quadrant would crack the cover. This complicates any relationships that may exist between section loss and cracking.

Dagher and Kulendran[36] have developed a two-dimensional non-linear finite element model for studying the effects of corrosion on cracking. A radial expansion was applied to the nodes making up the bar element to simulate arbitrary shapes of corrosion product. No comparisons are made with experimental data. Dagher and Kulendran[36] acknowledge that the answers are sensitive to variations in both mesh size and strength criteria.

The model was applied to typical North American bridge decks. The results are presented for the section of a deck with two #6 (19.1 mm) bars at 6 inch (152.4 mm) centres with 2 inches (50.8 mm) of cover. Uniform expansion is applied to the bar giving first internal cracking at an expansion of 1.9 μm. The cracks then propagated both horizontally and vertically. At an expansion of 14 μm the horizontal cracks had met whilst the vertical cracks were still around 25 mm from the top surface. This suggests that cracks can propagate around 75 mm horizontally whilst in the same period, they only propagate 25 mm vertically. From a practical point of view, this implies the possibility of delamination before any vertical cracks appear on the surface. Bazant[29] identified that the bar hole flexibility requires modification when adjacent bars are corroding.

Similar results were found with bar spacings of 8 and 10 inch (203 and 254 mm). However, with the 10 inch bar spacing two cracks were predicted to propagate from each bar towards the top surface. This can happen in practice, and results in a cone of concrete being loosened over a length. The two cracks were predicted to propagate simultaneously, whilst the tests of Cabrera[26] show that one crack propagates first followed by the second one later.

Ueda et al[37] carried out non-linear finite element analyses on concrete sections containing either corner or internal bars (i.e. bars other than corner bars). Thirty-one positions of corner bar were investigated. The direction of crack propagation was found to be a function of location. For those bars near either the side or bottom cover, the cracks propagated towards the smaller of the covers. The volume expansion required to cause a fully penetrating crack was found to increase linearly with increasing cover. When the side and bottom covers became greater than the bar spacing, the cracks first propagated internally (horizontally) before a second crack propagated in the direction of the smaller of the side or bottom cover. The volume increase to cause a full, penetrating crack was found to increase linearly with bar spacing. Ueda et al only modelled the effect of a single bar without the contribution of adjacent corroding bars.

For the bars not in corners, Ueda et al[37] found that cracks propagated in either the horizontal or vertical directions depending on the smaller of bar spacing or bottom cover. Once the direction of cracking had been defined, the volume increase to cause fully penetrating cracking was related

linearly to the cover or bar spacing in the direction of the crack, independent of what was happening at right angles to the crack. Ueda et al[37] determined that the transition point between vertical and horizontal cracking occurred when the bottom cover to bar diameter ratio exceeded 0.65. The Author would have expected the transition to be a function of the ratio of bottom cover to bar spacing. However, Ueda et al claim that the relationship holds for most ratios of bottom cover to bar spacing. Perhaps if the effects of adjacent bars were modelled the conclusion may have been different.

Ueda et al[37] separated out the effects of different concrete properties. There was found to be little increase in the critical volume expansion with increasing concrete compressive strength. However, as the concrete compressive strength increases so does the tensile strength and elastic modulus. The effects of these were separated out to show an increase in the critical volume of expansion with increasing tensile strength whilst the critical volume decreased with increasing elastic modulus. The two effects together more or less cancel each other out to give the negligible effect of increasing compressive strength. In addition, it would also seem reasonable to consider the potential decrease in pore space with increasing strength. If there is less pore space for the rust to occupy then less rust is required to cause cracking.

2.3.4 Summary

The mechanisms of corrosion-induced cracking are summarised in Table 2-9.

Table 2-9: The effects of various parameters on corrosion-induced cracking

Parameter	*Effect on cracking*
Concrete tensile strength[28, 37]	The amount of bar expansion to cause cracking increases with increasing concrete tensile strength. However, increasing the tensile strength is not as effective as increasing the c/D ratio.
Concrete elastic modulus[37]	The amount of bar expansion to cause cracking increases with decreasing concrete elastic modulus.
c/D ratio[22, 25, 26, 27, 33, 35, 36, 37]	The amount of corrosion required to cause cracking increases linearly with increasing c/D ratio.
Section loss and crack width[22, 25, 26]	At lower levels of corrosion the crack width can be related to the section loss in each of the tests.
Corrosion rate[22, 25, 42]	At lower corrosion rates the amount of corrosion required to cause cracking was found to be larger than at higher corrosion rates. However, beyond a certain corrosion rate that trend reverses.
Concrete pore structure[22, 27, 33]	The measured amount of corrosion to cause cracking was found to be significantly higher than that predicted by analytical or numerical methods. Corrosion products were observed in the concrete pore structure surrounding the corroding bar. This could explain the discrepancy.
Corrosion of adjacent reinforcement[29, 36]	The corrosion of adjacent bars may produce a horizontal delamination plane depending on the relative size of the bar spacing and the cover.
Crack propagation[26, 29, 36, 37]	Cracks propagate first in the direction of the smaller cover for single bars. The second crack will either propagate to the same face or normal to the first crack depending on bar spacing and relative cover sizes. For multiple bars the cracks propagate first in the direction of either the smaller cover or the spacing between adjacent bars depending on the relative size of the two.

2.4 Bond strength

Design and assessment code rules are derived on the assumption that the strains in both concrete and reinforcement are the same, that is perfect bond exists between the two materials. If this is not the case then the structural element may not be able to mobilise its full load-carrying capacity. Any deterioration mechanism that reduces concrete tensile strength and/or induces cracking around reinforcement is likely to reduce the bond strength. Corrosion induces cracking and, as such, bond is likely to be affected.

Al-Sulaimani et al[38] carried out two sets of bond tests with deformed bars. Series I consisted of pullout tests on 150 mm concrete cubes with 10, 14 and 20 mm bars embedded centrally. Series III consisted of two-point loading tests on 150 by 150 by 1000 mm beams with one 12 mm bottom bar with an anchorage length of 144 mm. A constant current of 2 mA/cm^2 was used to corrode the main reinforcement. The results of Series I are shown in Figure 2-11.

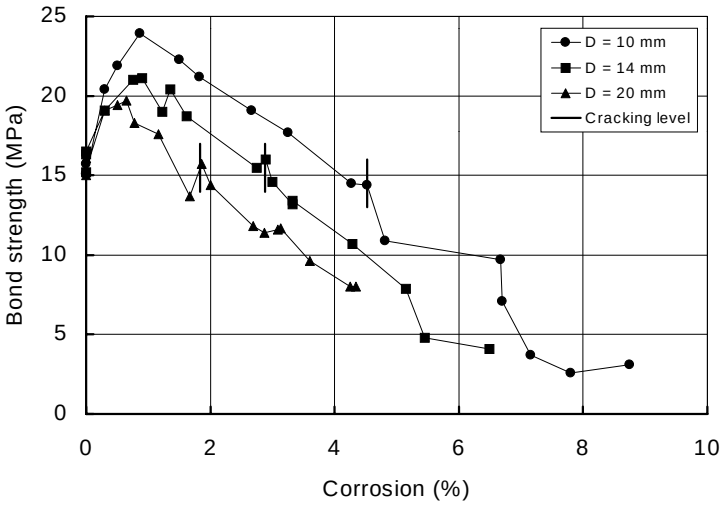

Figure 2-11: Relationship between corrosion and bond strength for deformed bars (Al-Sulaimani et al[38])

These results were categorised into four phases:

(i) Zero corrosion

(ii) Pre-cracking

(iii) Cracking

(iv) Post-cracking

The cracking referred to is visual cracking on the specimens. It is likely that fine internal cracks were present during the pre-cracking stage before surface cracks were visible.

During the first part of the pre-cracking phase the bond strength was observed to increase above that of the control specimens with increasing corrosion. Al-Sulaimani et al[38] explain this as being due to the increased confinement on the bars resulting from the expanding rust. Beyond this point, there was an approximately linear reduction in bond strength with increasing corrosion. At visual cracking, the bond strengths were around 95% of the control specimens.

Visual cracking was observed at corrosion values of 4.5%, 2.9% and 1.8% for the 10 mm, 14 mm and 20 mm bars respectively. The cover-to-bar diameter (c/D) ratios were 7.0, 4.9 and 3.25, thus highlighting the influence of the c/D ratio on time to cracking.

The c/D ratio appeared to be significant in all of the corroded specimens but not the control specimens. At similar percentages of corrosion, the 10 mm bars always had the highest bond strength followed by the 14 mm bars with the 20 mm bars having the lowest bond strengths. All three bar sizes had a similar gradient of bond strength reduction.

The influence of the c/D ratio on the bond strength of corroded specimens contradicts the results of uncorroded specimens. Reynolds[48] has shown that the bond strength of deformed bars increases with increasing c/D values until a c/D value of around 2.5. Beyond this there is little increase in bond strength as the mode of failure changes from a splitting mode to a pull-out mode. The c/D values (7.0, 4.9 and 3.25) used by Al-Sulaimani et al[38] in their tests are greater than 2.5 and also those typically found in practice. The main difference in corroded bond strengths appears to result from the differences in peak values achieved during the pre-cracking stage. Beyond that, all three bar sizes lose bond strength at a similar rate. This suggests that the differences in bond strength could be linked to the amount of corrosion required to generate the level of internal micro-cracking necessary to start the bond strength reducing from the peak. The higher the c/D ratio, the larger the amount of corrosion required to develop the internal micro cracking.

Observations of the specimens after testing revealed that the bar ribs had been degraded significantly whilst a heavy layer of corroded bar adhered to the concrete. This suggests that the mechanical interlock will be reduced whilst the frictional resistance is provided by a corrosion product on corrosion product surface.

For the series III beam tests, a similar increase in bond strength was found in the pre-cracking stage. When the longitudinal cracks appeared, there was a sharp reduction in the bond strength corresponding to a marked increase in end-slip. The bond strength then reduces very gradually in proportion to the percentage of corrosion. At the maximum level of corrosion, 4.5%, the bond strength is still above that of the control specimen and 1.5 times that required by the ACI code. Links are present, but not in contact with the main longitudinal bar under test. However, these links could explain why the bond strength is still above the control at 4.5% corrosion whereas in the pull-out tests the bond strength was around 50% to 90% of the control at 4.5% corrosion.

Almusallam et al[39] carried out a series of bond tests on 152 mm by 254 mm by 280 mm cantilever beam specimens. One 12 mm bar was placed in the centre of the smallest face with 64 mm cover (c/D = 5.33) to the top face. The central 102 mm of the bar was bonded to the concrete whilst the two outer zones subject to transverse pressure were unbonded. A constant current of 0.4 A (0.35 A/cm^2) was applied to the bar. This was an extremely high current, resulting in up to 80% corrosion.

As with Al-Sulaimani et al[38], the four phases of corrosion were observed. Pre-cracking was defined as being 0 to 4% corrosion. Cracking occurred at around 4-6% corrosion, and in excess of 6% corrosion was classified as post-cracking. Beyond around 6% corrosion, the failure mode changed to a continuous slippage.

The bond strength rose by about 15% in the pre-cracking phase and then dropped rapidly at cracking, reducing to 70% of the control value. Beyond 10% corrosion, up to 80% corrosion, the bond strength was near constant at around 15% of the control value. It is difficult to relate this behaviour to real structures, as there may have been considerable spalling well before the levels of corrosion achieved in these tests. Possibly, a limiting value of bond strength has been achieved representing the effects of friction and adhesion where the corroded bar is surrounded by

corrosion product.

The results during the pre-cracking phase show that despite a 25% loss of the rib profile due to corrosion, the bond strength is still around 15% greater than the control specimen. The appearance of cracking coincides with a 30% loss of rib section and around 5% increase in bond strength. Between 30 and 45% loss in rib section the bond strength reduces sharply to around 30% of the control. The crack width increases to 0.3 mm in this period whilst the corrosion increases from around 4 to 6%. This suggests that beyond the onset of cracking only a small amount of corrosion is necessary to reduce the bond strength significantly (by 70% in this case).

Cabrera and Ghoddoussi[40] carried out tests on deformed bars in both pullout specimens and beams. The pullout specimens were 150 mm cubes with a 12 mm bar embedded centrally (c/D = 5.75). The anchorage length was only 48 mm (4D) in order to ensure a slippage failure rather than concrete splitting or reinforcement yielding. There were two series of beam specimens, both 125 by 160 by 968 mm and subject to two-point loading. The embedment lengths corresponded to the shear spans of 384 and 190 mm. The anchorage lengths were debonded beyond the support centreline. In the series II specimens the two 12 mm bars were debonded for a length of 100 mm from the point load towards mid-span. 8 mm plain bars were provided at 40 mm centres over the shear span. A potential of 3 volts was applied to the 12 mm bars to accelerate corrosion. This is unusual as most researchers apply a current. The corrosion in the pullout specimens was determined by weight loss measurements. In the beam specimens corrosion was determined by Faraday's law. This is likely to be less accurate than physical measurements.

As with other investigators, in their pullout specimens Cabrera and Ghoddoussi[40] found an initial increase in bond strength followed by a subsequent reduction. In the specimens with Portland cement the maximum bond strength was reached at 4 days with a corrosion of 1.02%. By the next reading at 8 days (2.24% corrosion) a 0.2 mm wide longitudinal crack had been observed and the bond strength had dropped 10% from its peak down to the level of the control specimen. The reduction in bond strength was near linear, reaching 25% of the control at 12.6% corrosion. According to Cabrera and Ghoddoussi[40] all of the series I beams failed in flexure with the tension reinforcement yielding. The reduction in load (moment) capacity was found to be linearly

proportional to the corrosion of the tension reinforcement. This reduction was explained by the loss in reinforcement cross-section. This suggests that although there was no anchorage length beyond the support centreline and bond strength was being reduced due to corrosion and longitudinal cracking there was still sufficient bond to mobilise the yield strength of the reinforcement. End slip was noted once longitudinal corrosion cracking had occurred.

In the series II beams the ultimate failure load was found to remain more or less constant with increasing corrosion. The measured free-end slip did increase with increasing corrosion. The beams were intended to fail in bond slip. However, with a shear span to effective depth (a_v/d) ratio of 1.5 it is likely that the failure mechanism was crushing of the concrete due to the proximity of the load to the support. This could explain why the failure load remained constant whilst the corrosion increased.

Saifullah[35] and Clark and Saifullah[41] investigated the effects of accelerated corrosion on the bond strength of 8 mm ribbed and plain bars contained in the corners of concrete specimens 150 by 150 by 175 mm. A constant current of 0.5 mA/cm^2 was used for the main series of tests along with a 3.5% sodium chloride solution to accelerate corrosion. Cover-to-bar (c/D) ratios of 0.5, 1.0 and 2.0 were used. These are more typical of the values found in structures and are somewhat lower than those of other investigators. The bond test used by Clark and Saifullah had been shown by Chana[46] to give results that could be compared directly to those given in UK codes. In addition, the effects of bottom and top cast bars could be investigated.

Saifullah[35] has presented his data as a series of ratios of corroded to uncorroded (control) bond strength. The Author has converted these ratios back to the original bond strength values. In doing so, extra conclusions can be drawn over and above those contributed by the original investigator. In particular, it appears that both plain and ribbed bars have similar bond strengths at similar corrosion levels once cracking has occurred. This is shown in Figure 2-12 and Figure 2-13.

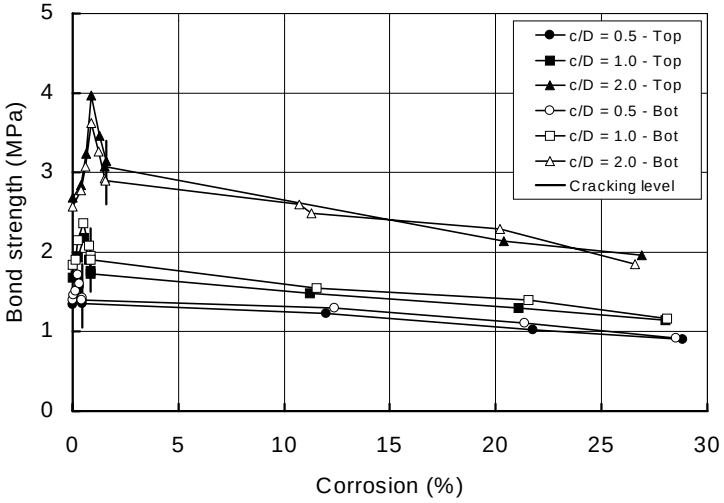

Figure 2-12: The relationship between bond strength and corrosion for plain bars (Saifullah[35])

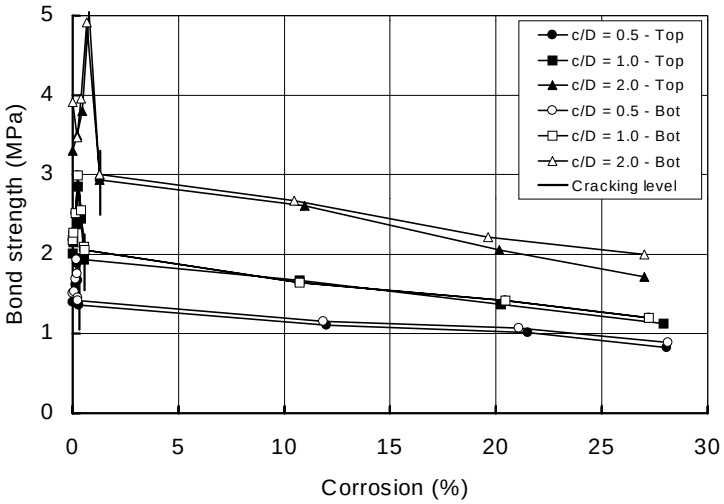

Figure 2-13: The relationship between bond strength and corrosion for ribbed bars (Saifullah[35])

The investigators[35, 41] observed the same four phases of behaviour as Al-Sulaimani et al[38]. Linear relationships were found in all phases. The main difference was that a sharp decrease in bond strength was observed from the peak value until cracking appeared. Once the specimens were in the post-cracking phase, the reduction in bond strength was much more gradual. At 25% corrosion the residual bond strength was around 70% of the control for plain bars and around 60% for ribbed bars.

Cracking was found to occur at higher levels of corrosion with plain bars than ribbed ones. This

could be due to stress concentrations resulting from corrosion on the ribs. At cracking, the plain bars still had a bond strength higher than the control whilst the ribbed bars had bond strengths marginally lower than the control. The ribbed bars then proceeded to deteriorate faster than the plain bars.

Whilst the c/D ratio was found to have little effect on the ratio of corroded to uncorroded bond strength, it had a significant effect on the absolute values of bond strength. The higher the c/D ratio, the higher bond strength was at all levels of corrosion.

As expected, the effect of casting position was found to be significant for the control specimens, with the bottom cast bars having higher bond strengths. Once corrosion had started, little difference could be found between the top and bottom cast bars. Thus, the bottom cast bars suffered proportionally larger reductions in bond strength due to corrosion.

Saifullah[35] and Saifullah and Clark[42] also investigated the effects of varying the accelerated corrosion rate on bond strength. Corrosion currents of 0.04, 0.09, 0.15, 0.25, 0.5, 1.0, 2.0, and 4.0 mA/cm^2 were investigated. The amount of corrosion to cause cracking increased initially up to 1.3% corrosion at a current of 0.15 mA/cm^2. It then decreased rapidly with increasing corrosion current until less than 0.2% corrosion was required to cause cracking at 4 mA/cm^2.

The bond strength was measured at the cracking stage, and the ratio of corroded to uncorroded bond strength was found to reach a peak value of around 1.2 at a current of 0.25 mA/cm^2. It then dropped to around 0.5 at a current of 4.0 mA/cm^2. Although the corroded specimens were at the cracking stage, the levels of corrosion were different. Bond strengths were also measured at corrosion levels of around 20%. The results again showed the same trend with a peak ratio of corroded to uncorroded bond strength of around 0.9 at 0.25 mA/cm^2 reducing to a ratio of around 0.3 at 4.0 mA/cm^2. Clark and Saifullah[41] have suggested the following reasons for their observations:

(i) Slower corrosion rates allow creep to relieve tensile stresses developed within the concrete.

(ii) Rust products can migrate into the concrete surrounding the bar.

(iii) Steel-concrete interface properties may change due to electrochemical polarisation.

(iv) Different rust products are produced at different corrosion rates. These products have different properties.

The differences between accelerated corrosion tests and corrosion rates observed in real structures (of 0.01 to 2 $\mu A/cm^2$ with 95% of structures with corroding reinforcement having corrosion rates less than 1 $\mu A/cm^2$) make interpretation of the test data in relation to real structures difficult. General trends have been observed. However, a view has to be taken on whether the same effects will be observed to the same extent in real structures.

Coronelli[43] has used the RILEM beam test to investigate the effects of corrosion on the bond strength of 14 mm deformed bars. The test comprises two beam halves 100 by 180 by 375 mm simply supported at one end and connected by a hinge at the other. Two-point loading is applied 75 mm either side of the hinge.

Three sets of specimens were tested: A, B and C. The 14 mm bar had covers of 43 mm (c/D = 3) and 28 mm (c/D = 2). 6 mm links were provided at 50 mm and 100 mm centres. 4 and 8 mm longitudinal bars were also present. The 14 mm bar was not in electrical contact with the other bars. The applied current was adjusted to give a section loss of around 10 μm/week.

In series A (c/D = 3, links at 50 mm centres and 8T8) all of the test bars failed by yielding in tension without any bond failures. In series B (c/D = 3, links at 100 mm centres and 4T8) longitudinal cracks were caused by corrosion. At 1.4% corrosion the bond strength fell to around 90% of the control. However, it then started increasing to around 95% at 2.8% corrosion and 1.05 at 4.2% corrosion. Series C (c/D = 2, links at 100 mm centres and 4T8) also showed increases in bond strength with increasing corrosion up to 8.4%. This time there was no initial drop in bond strength.

The specimens were investigated after testing. The corrosion product was found to either accumulate close to the reinforcement or flow into fine cracks (formed during corrosion) or

cavities (pores formed during casting). Corrosion products were found 20 to 30 mm from the bar.

It is difficult to explain the phenomenon observed in these tests. Coronelli suggests that the explanation is increased friction between the steel and concrete. The Author believes that the main factor is the beneficial influence of the link reinforcement restraining potential cracks. Tests by other investigators, such as Rodriguez et al[45], whilst not exhibiting increases in bond strength with corrosion, do show that bond strength can be maintained at the level of the control specimen by using links.

Lin[44] investigated the effects of accelerated corrosion on the bond strength of bars in beams lapped at mid-span. The beam sections were 76 by 152 by 1016 mm. A single #5 (6.25 mm) bar was used in the middle of the bottom face with 22 mm cover (c/D = 3.5). Eight series A beams had continuous bars whilst six series B beams had lapped bars. In the beam with lapped bars, the lapping bar was placed directly on top with no joggle giving a smaller effective depth. No links were provided in any beams. Series B beams will be discussed here whilst the series A beams will be discussed in the section on flexure.

The series B beams had laps of 100, 150 and 200 mm. One beam in each pair was corroded. The beams were stored back to back in seawater within a loading frame giving a single point load at mid-span. A current of 10 mA/cm^2 was applied to the #5 bar leading to longitudinal cracks in 7 to 7.5 days. There is an anomaly between the text and the tables given by Lin[44] in his paper. The text suggests a corrosion rate of 10 mA/cm^2 whilst Table 2 suggests a value of 0.1 mA/cm^2. Given the short time to cracking with a high c/D ratio, the Author's experience suggests that 10 mA/cm^2 is likely to be correct.

Whilst not stated explicitly, diagrams of the series A beams suggest that a single point load was used at mid-span to fail the beams. The failure load was seen to increase with increasing lap length for both control and corroded specimens. However, the residual failure load remained near constant at around 65% of the control. No description of the failure mechanism was given. However, sketches are provided for what are called beams 'A31' and 'A32'. Given that series A are numbered A1 to A8, whereas series B are numbered B11, B12, B21, B22, B31 and B32 it

is likely that the two sketches shown are beams B31 and B32. The control (B32) and the corroded beam (B31) both appeared to fail in shear. This makes the beams somewhat difficult to analyse, as mid-span laps are largely irrelevant to shear failure modes.

Rodriguez et al[45] have carried out a comprehensive set of tests on the effects of accelerated corrosion on 10 mm and 16 mm deformed bars using the corner bar test (Chana[46]). 300 by 300 by 300 mm cubes were used with 210 mm anchorage lengths. Cover-to-bar diameter ratios of 1.5 and 2.5 were investigated for specimens with two levels of link reinforcement. A current of 0.1 mA/cm^2 was applied to the longitudinal bars. The links were electrically isolated from the longitudinal bars. 3% $CaCl_2$ (by weight of cement) was added to the concrete mix to aid the corrosion process. Two corrosion periods were used to give what were referred to as level 1 (around 3%) and level 2 (around 8%) corrosion.

The interpretation of these tests is complicated by the fact that the concrete used for the control mixes was generally stronger than that used in the corroded mixes. However, Tepfers[47] relationship can be used for the bond strength of ribbed bars. This suggests that bond strength is directly proportional to the tensile strength of concrete. Thus any reduction from the control bond strength can be corrected to reflect initial differences in concrete strength.

Perhaps the most important point that comes out of this work is the importance of links in maintaining bond strength after corrosion. With level 1 corrosion and no links present the residual bond strength was 47% of the control. With two links it was 88% of the control, and with three links 90% of the control. With level 2 corrosion the differences were even more marked with residual bond strengths of 21%, 82% and 83% for zero, two and three links respectively. This suggests that whilst longitudinal cracks are present the links provide sufficient confinement and restraint to cracking that nearly full bond strength is maintained.

There seemed to be little difference in residual strength ratio between having two or three links present. In real structures, the longitudinal and link reinforcement would be in contact, and the links would tend to corrode first, as they are closer to the concrete surface. Links also tend to corrode at bends where they are in contact with longitudinal bars. As such, the influence of links

in real structures is unlikely to be as great as in these tests.

Whilst the bond strength in the bottom cast bars is higher than the top cast bars for the control specimens, the difference is negligible in the corroded specimens. This agrees with the findings of Saifullah[35]. The increase in c/D ratio was found to increase the residual bond strength but the ratio of residual to control decreased. The control specimens showed a 35% increase in bond strength with an increase in c/D from 1.5 to 2.5 whilst the corroded specimens showed an increase of only 15%. The residual bond strengths were 82% and 69% of the control for c/D values of 1.5 and 2.5 respectively.

Rodriguez et al[45] brought all of their findings together into a single empirical relationship based on the Tepfers[47] expression as modified by Reynolds[48] to include the contribution of links. The best fit to the test data is given by the following equation:

$$f_b = 0.6\left(0.5 + \frac{c}{D}\right) f_{ct}\left(1 - \beta X^{\mu}\right) + \frac{kA_s f_y}{sD} \qquad \textbf{… (2-26)}$$

Where:
- c = concrete cover (mm)
- f_b = bond strength (N/mm^2)
- f_t = tensile strength of the concrete (N/mm^2)
- f_y = tensile strength of the link reinforcement (N/mm^2)
- s = link spacing (mm)
- A_s = area of link reinforcement (mm^2)
- X = reduction in reinforcing bar radius (μm)
- β, μ, k = constants

This suggests that the effect of corrosion on the longitudinal bars can be described by a power relationship. Rodriguez et al[45] suggest that the link contribution is independent of the corrosion level in the longitudinal reinforcement, additive and varies linearly with the amount of links present. This conflicts with their experimental data where the link contribution was seen to be more effective at lower levels of corrosion and increasing the number of links from 2 to 3 made

little difference to the bond strength.

Rodriguez and Ortega[49] have carried out a series of beam tests to evaluate the effects of support reactions on the bond strength of reinforcement subject to accelerated corrosion. The beams were 150 by 200 by 1100 mm in section with a span of 900 mm. The main tension reinforcement consisted of two 12 mm ribbed bars with 18 mm cover (c/D = 1.5). 8 mm compression reinforcement was provided, as were 6 mm links in the shear span (three in type 41 beams and two in type 42 beams). The 12 mm bars were debonded on either side of the shear span by plastic sleeves in the anchorage zone beyond the support centreline, and by polystyrene void formers from the load towards mid-span. This was repeated at both supports giving two test zones. The shear span to depth (a_v/d) ratio was 0.85. 3% calcium chloride was added to the mix, and a current of 0.1 mA/cm^2 was applied to the two 12 mm bars. The link and compression reinforcement were electrically isolated from the two 12 mm bars.

The type 41 beams (with three links in the shear span) failed in shear followed by bond failure. There was considerable scatter in the results. The concrete used for the control specimens was nearly 50% stronger than that used for the corroded specimens. Taking this into account, it is difficult to detect any fundamental difference in the load-carrying capacity of the six specimens. This is not unexpected when such a short a_v/d ratio is used. One would expect a steep shear failure where the concrete strength dominates. The same failure mechanism was observed in the type 42 control beams. The three corroded beams failed by bond pullout according to Rodriguez and Ortega. However, when the differences in concrete strength are accounted for and the inherent scatter is considered it is, again, difficult to see any fundamental differences between the five specimens.

An interesting feature of the results is the strains in the 12 mm bars at maximum load. In the type 41 and 42 specimens the strains are 31 and 63% higher respectively in the control specimens than the corroded ones, whilst the failure loads are 22% and 37% higher respectively. This would seem to suggest that some slippage is occurring in the corroded bars, but that load-carrying capacity is being, more or less, maintained through the concrete.

It is difficult to separate out any effects that might occur due to support enhancement or bond strength from those which would occur due to shear enhancement over such a short shear span. An additional complication is the plastic debonding sleeve. Baldwin[50] has found that sleeves are not always fully effective, and load can be transmitted to the reinforcing bars.

Sakamoto and Iwasaki[51] have carried out a series of ASTM (C 234) pullout tests on 16 mm deformed and plain bars. The prime difference between their work and that of other investigators was that their specimens were not subject to an applied current to induce accelerated corrosion. Different levels of sodium chloride were, instead, added to the concrete mix and curing temperatures of 20°C and 50°C were used. This may give corrosion products and bond strengths that are more in line with those found in real structures. Unfortunately, the information presented is very sketchy and only qualitative conclusions can be drawn.

The sodium chloride has an unfortunate side effect in that it accelerates concrete strength gain. Sakamoto and Iwasaki[51] have compensated for this by normalising their bond strengths with respect to the compressive strength at the age of test. Bond strength is considered to be a function of tensile strength by Tepfers[47], and the square root of compressive strength by UK codes. Perhaps one of these should have been used to normalise the bond strengths, as using the compressive strength will over compensate.

Sakamoto and Iwasaki[51] also found the general trend observed by other researchers[35, 38, 39] of an initial increase in bond strength followed by a reduction for their deformed bars. However, the magnitude of the peak was not as substantial as that found by others. Possibly, this could be due to the slower corrosion rate. No, initial increase in bond strength was found for the plain bars, just a gradual decrease which conflicts with the observations of Saifullah[35].

Morinaga[28] has carried out bond tests on both laboratory specimens and samples from demolished structures. In the laboratory, Morinaga[28] cast 9, 19 and 25 mm round (plain) bars centrally in 100 and 150 mm diameter concrete cylinders. Potentials of 1.5, 3, 6 and 12 volts were applied to the specimens. 12 volts corresponded to the amount of corrosion required to cause cracking. The amount of corrosion was not measured. The same trend as observed by other researchers[35, 38, 39]

was found, with the initial increase in bond strength reaching a peak value and then reducing before visible cracking. Unfortunately, the tests did not carry on beyond the cracking stage. The results expressed as ratios of corroded to control (uncorroded) bond strength are given in Table 2-10.

Table 2-10: Ratios of corroded to uncorroded bond strength (Morinaga[28])

Bar diameter (mm)	*Cylinder diameter (mm)*	*c/D*	*Corroded / control bond strength*	
			Peak	*At cracking*
9	100	5.1	2.2	2.1
19	100	2.1	1.3	0.9
25	100	1.5	1.3	0.9
9	150	7.8	2.7	2.6
19	150	3.4	1.3	1.2
25	150	2.5	1.5	1.4

What distinguishes these results from those of other investigators in the size of the peak bond strength. The bars with c/D values of 2.5 or less had peak and cracking values compatible with those of other investigators[35, 38]. The exception was the 25 mm bars in the 150 mm cylinder which had higher peak and cracking values than the corresponding 19 mm bars. This contradicts both the 100 mm cylinder results and those of other investigators[35, 38].

Morinaga[28] also reported on tests carried out on precast concrete panels taken from a single storey office block. Despite being only nine years old, considerable corrosion, cracking and spalling had occurred. The chlorides had originated in sea dredged sand and seawater used in the mix. Panels 2000 by 1000 by 120 mm were taken for testing. The level of corrosion was classified on a scale of I to IV based on a qualitative description. Level IV corresponds to 'Loss of cross section can be observed by the naked eye'.

The bond strength of 9 mm round (plain) and 13 mm deformed bars exhibited different relationships with increasing corrosion. With plain bars, the peak is reached at level III corrosion,

and is around 165% of that at level I corrosion (just mill scale present). The bond strength tails off after level III, but is still around 30% higher than the level I value. The general trend is similar to that found by Saifullah[35], although the residual strength ratios are higher. Morinaga[28] does not say explicitly that the bars have cracked at level III corrosion. However, the behaviour of 851 specimens had been logged, and around 95% of those where cracking was visible were level IV corrosion. As such, there is a reasonable possibility that many of the level IV bars will be associated with a crack whilst the level III bars will not. This confirms the phenomenon observed elsewhere[35, 38] that the reduction in bond strength from the peak occurs before visible cracking. The increase up to the peak bond strength may be due to the increased frictional and adhesion resistance caused by the rust product. Considerable diffusion of the corrosion product into the surrounding concrete was reported at levels III and IV corrosion. This suggests that the plain bars would be sliding on an interface of corrosion product against corrosion product combined with an increased normal pressure due to rust growth.

The behaviour of the deformed bars was somewhat different from that observed in accelerated laboratory tests. There was no real peak like the plain bars. The bond strength dropped around 15% between level I and level II corrosion. It then remained more or less constant (commensurate with the scatter present) up to level IV corrosion where the reduction was around 20% from the level I bond strength. A possible explanation for the approximately constant bond strength was that the ribs were still intact. It would have been useful to have quantitative values of corrosion. For instance, at what corrosion level did the bond strength disappear completely due to cover spalling. This may well have shown that some of the high section losses achieved in the laboratory do not translate to real structures, as the cover would have spalled long before then.

Maslehuddin et al[52] investigated the effects of corrosion on the mechanical and bond properties of six bar types and sizes. 12, 16 and 32 mm hot-rolled deformed bars were investigated along with 8, 10 and 12 mm hot-rolled cold-straightened deformed bars. Each of the bars was exposed to the atmosphere on the West Coast of the Arabian Gulf for up to 16 months. Tensile tests on the bars and bond tests on the bars embedded in concrete were carried out periodically. The bond specimens were 150 mm cubes for the 8, 10, 12 and 16 mm bars and 200 mm cubes for the 32

mm bars. The bars were cast centrally giving c/D ratios of 8.9, 7, 5.8, 4.2 and 2.6 for the 8, 10, 12, 16 and 32 mm bars respectively. The embedment lengths were also varied to avoid yielding. 6 D was used for the 8, 10 and 12 mm bars, 3.5 D for the 16 mm bars and 2 D for the 32 mm bars. After 16 months exposure the average reduction in bar diameter was around 30 to 40 μm on all sizes. At 16 months residual bond strengths were measured of 75, 70, 75, 65, 100 and 105% respectively for the 8, 10, 12, 12, 16 and 32 mm bars. Given that all of the bars were ribbed and suffered similar losses of diameter (30 to 40 μm) it is possible that the reductions in bond strength are proportional to the reductions in rib profile. The larger bars have larger rib profiles, and losing 15 to 20 μm from the rib profile of a 32 mm diameter bar is unlikely to make too much difference. Losing a similar amount from the rib profile of smaller bars is likely to be more significant.

The effects of corrosion on the different phases of bond strength as observed in the tests reviewed in this section are summarised in Table 2-11.

Table 2-11: Effects of corrosion on the phases of bond strength

Phase	*Typical behaviour*
Uncorroded	Behaviour is as assumed in design codes.
Pre-cracking[35, 38, 39]	Expansive corrosion products are resisted by the surrounding concrete. The corrosion induces extra confinement to the bar. Light rusting on the bar surface increases the frictional resistance. The two together combine to increase the bond strength. This increase can typically be up to 1.5 times the uncorroded value.
Cracking[35, 38, 38, 39, 40]	When the first crack appears, much of the confinement is lost and there is a drop in bond strength from the pre-cracking peak. Plain bars appear to exhibit a larger drop than ribbed bars. Bond strengths in the region of 0.9 to 1.2 times the uncorroded strengths have been observed in tests.
Post-cracking[35, 38, 39, 40, 44, 45]	The bond strength has been observed to reduce with increasing corrosion. As the ribs of deformed bars deteriorate, there is little difference between them and plain bars. Some tests have shown the residual bond strength to be 0.15 times the uncorroded values at 8% corrosion. However, other tests have shown the residual to be 0.6 at 25% corrosion (but at a lower corrosion rate).

The effects of a number of parameters observed on the test specimens reviewed in this section are summarised in Table 2-12.

Table 2-12: Effects of various parameters on bond strength - corroded reinforcement

Parameter	*Effect on bond strength*
Cover to bar diameter (c/D) ratio[35, 38, 38, 39, 45]	An increase in c/D generally increases the time to cracking, and thus time to loss of bond strength. An increase in the c/D ratio appears to increase bond strength at lower levels of corrosion, but bond strengths begin to converge at higher levels corrosion.
Links[45]	Links appear to offer greater benefit to corroded members than uncorroded ones. In tests 70 to 80% of the uncorroded bond strength was maintained when corroded with links present compared to 20 to 30% when they were not.
Bar position[35, 45]	Once cracking has taken place, both top and bottom cast bars have similar bond strengths. That is, bottom cast bars suffer a greater proportional reduction in bond strength.
Concrete tensile strength[45]	The bond strength appears to increase with increasing tensile strength
Applied transverse stress[45, 40]	With the applied load so close to the support, the test set-up appeared to be a little too unrealistic to make a definitive judgement.
Corrosion rate[42]	Increasing the corrosion rate initially leads to increases in bond strength. Further increases in corrosion rate lead to reductions in bond strength for the same amount of corrosion.
Bar type[35, 38]	At first cracking, ribbed bars showed a smaller drop in bond strength than plain bars. Post-cracking, ribbed bars showed a larger drop. Ribbed bars appear to require less corrosion to cause cracking than plain bars.

2.5 Flexural strength

It is possible that corrosion may influence flexural strength in the following ways:

(i) Reduction in reinforcement cross-section.
(ii) Spalling of cover concrete.
(iii) Reductions in bond strength.
(iv) Reductions in ductility.

The first point is the easiest to investigate. The effects of the others will vary depending on the individual test regimes used.

Almusallam et al[53] tested simply supported one-way slabs 63.5 by 305 by 711 mm (610 mm span) reinforced with five 6 mm diameter deformed bars at 57 mm centres. The concrete was immersed in a few millimetres of 5% sodium chloride solution, and a constant current of 2A was applied to the five bars. A uniformly distributed load was applied to the slabs.

Almusallam et al[53] observed a small (<5%) increase in load-carrying capacity in the pre-cracking stage (1% corrosion). As soon as longitudinal corrosion cracking occurred (1.5% corrosion) the load-carrying capacity reduced by around 13%. At 13.9% corrosion, the load-carrying capacity was around 45% of the control. The reduction in load-carrying capacity appeared to follow a curve asymptotic to both corrosion and load-carrying capacity axes, with the loss in load-carrying capacity somewhat greater than the reduction in bar area. This is shown in Figure 2-14.

The non-linear variation in load-carrying capacity with increasing section loss suggests that other mechanisms are at work. The main suggestion that Almusallam et al[53] offer is reduction in bond strength. Descriptions of the failure mechanism would tend to support this. In the control specimens without longitudinal corrosion cracking, failure is by transverse flexural cracking. With increased deflection after the steel has yielded the flexural cracks propagate upward reducing the size of the compression zone leading to a secondary compression failure. With longitudinal corrosion cracking, the transverse flexural cracks tend to propagate upwards until they meet the longitudinal corrosion cracks. Ultimate failure then results due to a sudden

longitudinal splitting of the slab along the line of the corroded bars.

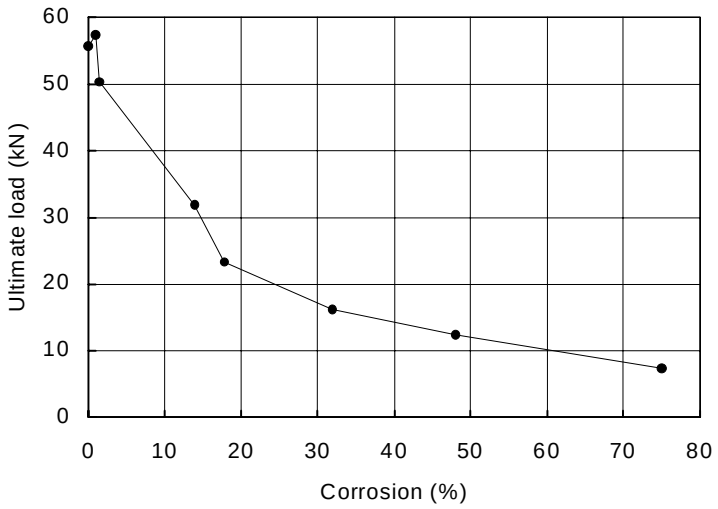

Figure 2-14: The variation in slab load-carrying capacity with corrosion (Almusallam et al[53])

The load-deflection curves provide an insight into effects of corrosion on member ductility. The control and pre-cracking slabs exhibited a distinct loss of stiffness after flexural cracks appeared and achieved deflections of around 16 to 17 mm before failure occurred. Half of this deflection occurred after flexural cracking. At 1.5% corrosion, a short length of gradient change due to a reduction in stiffness was observed followed by a plateau up to a deflection of around 13 mm when the slab failed. At 13.9% corrosion, there was no obvious loss of stiffness before the peak load was reached at a deflection of around 5 mm. Beyond that there was a rapid loss of load-carrying capacity. The result was similar at 17.8% corrosion where the peak load occurred at 4 mm deflection. At 32, 48 and 75% corrosion more of a plateau occurred, but these are unrealistically high levels of corrosion. The reduction in ductility and warning of failure would seem compatible with the descriptions of the failure mechanisms.

Huang and Yang[54] tested thirty-two simply supported beams 150 by 150 by 500 mm in section with single point loading. Two 12.7 mm reinforcing bars with 30 mm cover (c/D = 2.4) were corroded using an applied current of 50 mA/cm^2. No links or compression bars were used. Two sets of beams had 'middle surface cracks' induced in them. It is not clear from the paper where these were located or why and, as such, the results are not considered here.

The two sets without induced cracks both showed a small initial drop from the control and then a near-linear decrease in moment capacity with increasing corrosion. Unfortunately, the corrosion

is expressed as corrosion thickness in microns. This has been obtained by integrating the corrosion rate with time rather than by weight loss. By the time that the corrosion thickness has reached 8 μm around 75% loss in moment capacity is shown. Some investigators[5, 11] suggest that around 50 to 100 μm section loss is required just to crack the cover let alone cause any serious structural distress. It is possible that the extremely high applied current may be the cause of this loss in moment capacity. Mechanical damage and unusual rust product formation may occur at such corrosion rates. Many investigators use applied currents of 0.1 mA/cm^2, and even these are 100 times greater than most corrosion rates found in real structures.

Kawamura et al[55] tested two sets of simply supported beams. Maruyama and Shimomura[56] also present the same results. These consisted of a small series of beams 100 by 100 by 1200 mm, and a larger series 200 by 300 by 2800 mm.

The smaller series had one 13 mm ribbed bar placed in the centre of the tension face with 25.5 mm cover (c/D = 2). Links were provided in the shear span to prevent shear failure. A 3.1% sodium chloride solution was used as the mixing water, the beam was placed in a saline solution and current applied to the 13 mm bar. Unusually, the results are presented as failure loads for measured crack widths. Kawamura et al[55] suggest that the crack widths are proportional to the amount of corrosion that has taken place. However, Cabrera[26] has found that this is not always the case. Unfortunately, the corrosion data are not given. Despite stating that links were present, one set of data appears not to have links. Given that the two-point loading has a shear span to depth (a_v/d) ratio is 4; one would still expect a flexural failure in the control beams.

In the series with links corrosion appears to have virtually no effect on load-carrying capacity. When the crack width is 1 mm the residual load-carry ratio is 0.91, but with a 0.55 mm crack width it is 1.01. Allowing for the inherent scatter in these results it is difficult to discern any trends.

In the series without links, the failure mode for three of the beams is described as ‘diagonal tensile failure’, presumably this means shear. Even with these beams it is difficult to identify a trend as a 1 mm crack width gives a residual ratio of 0.85, whilst crack widths of 0.5 mm give

ratios of between 0.90 and 1.0.

The larger scale beams contained two 19 mm bars in the tension zone with cover of 40.5 mm (c/D = 2.1). Links and link hangers were provided. The links were electrically isolated from the two 19 mm bars. The 19 mm bars were lapped at mid-span. The link spacing at mid-span varied from 50 to 600 mm. Two-point loading was applied with an a_v/d ratio of 3.8. Longitudinal corrosion cracks appeared on the side faces, mainly where the laps were, as the cover was lower there. In some of the beams the crack widths were observed to decrease with decreasing link spacing.

The failure load and mode appear to be related to the amount of links in the lapped area at mid-span. The links appear to give a more ductile failure, and at higher loads. With links at 100 and 200 mm centres at mid-span, reductions in failure load get larger with increasing crack width (and presumably corrosion) but the load-displacement curves have plateaux indicating ductile behaviour. The beam with 600 mm link spacing at mid-span showed an abrupt loss in load-carrying capacity after peak load. Although the corrosion cracks were visible on the side faces, it is likely that some micro-cracks would have been heading towards the bottom face. This could potentially reduce the potential for dowel action leading to the bar pushing through the bottom cover.

Lee et al[57] carried out tests on 100 by 100 by 800 mm simply-supported beams in order to validate the non-linear finite element analysis model that they were developing. Two series of beams were tested. The singly reinforced series consisted of two 10 mm deformed bars in the bottom with a 10 mm cover (c/D = 1). The two bars were corroded by an applied current to give uniform corrosion. The doubly reinforced series consisted of two 10 mm deformed bars in each of the top and bottom zones with 4 mm links at 50 mm centres in the shear span. Corrosion was achieved by 'placing saltirized concrete up to the tension bars and then by cyclic wet-dry curing at a high temperature'. Two-point loading was applied to both series, giving an a_v/d ratio of 2.9. The corrosion rate is not given.

The load-deflection curves for the singly reinforced beams with 0, 2.7 and 7.9% corrosion showed ductile failures with long plateaux after the peak load was reached. The 0 and 2.7% corrosion

beams had similar stiffness and peak loads. The beam with 7.9% corrosion had a similar stiffness to the other two beams up to about one half on the peak load. Beyond that the stiffness was lower, and the peak load was about 10% lower than the other two beams.

Four levels of tension steel corrosion were achieved in the doubly reinforced beams: 0, 6.3, 9.0 and 14.0%. Again, ductile failures were achieved for all beams. The differences between the peak loads for the three corroded beams were negligible. All three achieved peak loads only marginally below that of the control. It is not possible to determine any differences in stiffness from the curves.

Lee et al[57] used constitutive laws for corroded reinforcement and the effects of corrosion on bond based on their experimental work to analyse their test beams and produced load-deformation curves that matched the experiments closely. Having validated their model, Lee et al[57] carried out two parametric studies. For the singly reinforced beam, they chose a corrosion of 25%. Such a level is likely to be unrealistically high for beams in practice. The two parameters that affected the load-deflection curve most were found to be the reinforcement yield stress and its elastic modulus. Changing the bond properties (stiffness and maximum bond stress) was found to have little effect for the unspecified changes made. The is probably reasonable provided that the reinforcement remains anchored at the supports.

The parametric study of the doubly reinforced beam was used to investigate the effects of general and pitting corrosion on load-deflection behaviour. Four levels of tension steel corrosion were considered: zero corrosion, 22% general corrosion, 45% pitting corrosion in the constant moment zone and 45% pitting in the shear span. All but the pitting corrosion in the constant moment zone exhibited ductile failure. Presumably reinforcement fracture is predicted in the constant moment zone leading to a brittle failure at a load 60% of that of the control beam. In this case the pitting corrosion in the shear span only reduces the peak load by about 10%. However, that may not always be the case. Here the shear span was large, and links were present and uncorroded. In practice, the links are also likely to be corroded.

Okada et al[58] subjected three sets of beams to accelerated corrosion. The cross-section of each was 100 by 200 mm. Two 13 mm deformed bars were provided top and bottom with covers of

20 mm (c/D = 1.54). One 13 mm deformed bar was provided in the centre of the section to act as a counter electrode. The reinforcement layout was symmetrical. Three lengths of beam were cast: 1600, 1400 and 1200 mm, corresponding to types 1, 2 and 3 respectively. Two-point loading was applied giving a_v/d ratios of 3.4, 2.9 and 2.3 respectively. All of the beams had 0.3% link reinforcement in the shear spans, corresponding to five, two and two 6 mm links respectively. After curing, a 3.1% NaCl solution was sprayed on all but the control beams until longitudinal cracks formed. Fine longitudinal cracks first appeared after 13 weeks of spraying. By 20 weeks cracks were easily visible on all of the sprayed beams. Okada et al[58] observed that most of the longitudinal cracks propagated from the junctions of the longitudinal bars with links. Three loading patterns were applied. Types 2 and 3 were related to seismic loading, and so will not be considered here as this Thesis is primarily concerned with UK practice where seismic loading is typically not considered. Type 1 loading consisted of a number of cycles of loading and unloading. The magnitude was increased until failure occurred. For all three types of beam, the load-carrying capacities of the corroded beams are significantly higher than those of the control beams. As the level of corrosion was not given, it is difficult to compare these results with those of other investigators. The ratios of corroded to control beams range from 1.27 to 1.45. In each case the failure mechanism was given as concrete compression failure. With such low levels of tension reinforcement a compression failure is unlikely. The crushing of the concrete in the compression zone is more likely to be a secondary effect occurring after the tension reinforcement has yielded.

Some confusion is caused by the lack of clarity in the presentation of the paper, the experimental technique and the incorrect notation used in places. It is likely that whilst a D13 counter electrode was used in the corroded beams, a D13 was not included at the centre of the control beams. This means that it is not possible to compare directly the corroded and control beams. Okada et al[57] attempt to get around this by comparing the ratios of measured to calculated load-carrying capacities. This has the inherent assumption that the errors associated with calculating corroded and control load-carrying capacities will be the same. Okada et al[57] do not state how their calculations were done. The Author calculated a load-carrying capacity for the control beams of around 60% of that given by Okada et al when using the information provided. This suggests that perhaps there is extra information such as bearing restraint in the test set up that is inducing extra

axial load and increasing the load-carrying capacity. Bearing restraint was present in the tests carried out by Rodriguez et al[45].

Rodriguez et al[45] applied accelerated corrosion to five sets of simply supported beams with cross-sections of 150 by 200 by 2300 mm. The details are given in Table 2-13. All of the reinforcement was corroded by including calcium chloride (3% by weight of cement) in the mixing water and by applying a current of 0.1 mA/cm^2. The amount of corrosion was determined by weight loss, whilst the pitting depths were measured.

Table 2-13: Details of test beams (Rodriguez et al[45])

Beams		*Concrete*		*Reinforcement*		
Type	*No*	*Type*	$f_{c\ (N/mm^2)}$	*Bottom*	*Top*	*Links*
11	2	Control	50	2T10	2T8	T6@170
	4	Corroded	34	2T10	2T8	T6@170
12	2	Control	48	4T12	2T8	T6@170
	4	Corroded	35	4T12	2T8	T6@170
13*	2	Control	52	2+2T12	2T8	T6@170
	4	Corroded	37	2+2T12	2T8	T6@170
21	2	Control	50	4T12	4T8	T6@170
	4	Corroded	35	4T12	4T8	T6@170
31	2	Control	49	4T12	4T8	T6@85
	4	Corroded	37	4T12	4T8	T6@85
5*#	2	Control	30	2+1T8	2T8	T6@100
	8	Corroded	35	2+1T8	2T8	T6@100

* Two of the tension bars continue past the support, the remainder are curtailed.

\# Four of the corroded beams had 80% of the service load applied during corrosion.

Two-point loading was applied giving an a_v/d ratio of 4.6. The support conditions corresponded to a pinned beam rather than a simply supported one. As a result, axial compression was induced in proportion to the applied load whereby $P_{axial} = 0.076\ P_{vertical}$. Thus the axial force provides

extra resistance to the applied load. The variation in ultimate load with increasing tension reinforcement corrosion is shown in Figure 2-15 for all of the beam series.

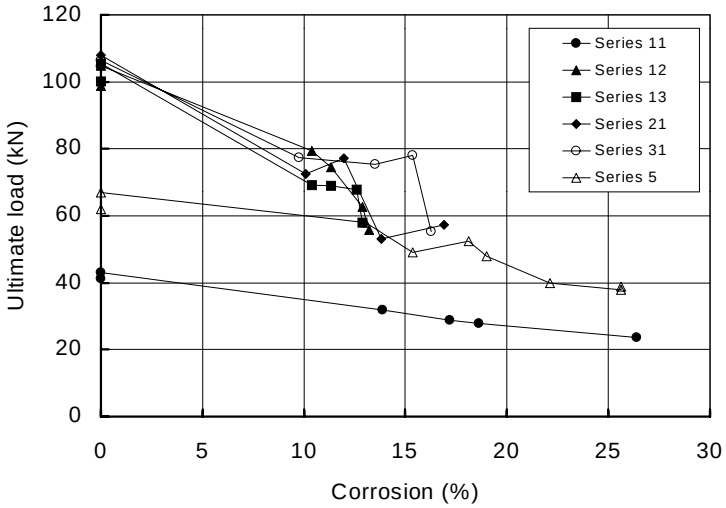

Figure 2-15: The variation in load-carrying capacity with tension reinforcement corrosion (Rodriguez et al[45])

All of the type 11 beams were observed to fail by yielding of the tension reinforcement. The corrosion on the type 11 beams ranged from 13.9 to 26.4% over four beams. The reduction in load-carrying capacity was observed to be linear from the control beam through to the most corroded one.

The control and least corroded (10.4%) type 12 beams (4T12) were judged by Rodriguez et al[45] to have failed by the concrete crushing in compression. This is highly unlikely given that only 1.8% tension reinforcement is present. The Author has carried out calculations for the control beams, and these indicate that the strains in the tension reinforcement are well in excess of the yield strains. It is more likely that a secondary compression failure occurred after the tension reinforcement yielded.

The remaining three corroded type 12 beams were observed to fail in shear. Given the high a_v/d ratio, this is likely to be due to reductions in both tension and link reinforcement area and a reduction in anchorage bond strength. In Figure 2-15 there is a distinct discontinuity where the two most corroded (12.9 and 13.2%) beams are, possibly indicating the change in failure mechanism.

The type 13 beams were identical to the type 12 beams except that two of the four tension bars were curtailed before the supports. The two control, and the two least corroded (10.4 and 11.3%) beams failed in a combination of shear and anchorage failure of the tension reinforcement. The two most corroded beams (12.6 and 12.8%) failed in shear. Rodriguez et al[45] put this down to pitting of the links reducing the shear capacity before any slip could occur in the tension reinforcement. The combined shear and anchorage failure was only observed in the type 13 beams. This suggests that the main parameter is the curtailment of half of the tension reinforcement. Given that the control specimens failed in this manner too, it may have implications for UK design codes. In these codes, 50% of the tension reinforcement can be curtailed before a simple support.

Type 21 beams were similar to the type 12 beams except for having twice the level of compression reinforcement. The load-carrying capacities and failure modes were near identical. 'Compression' failures occurred in the control beams whilst shear failures occurred in the corroded ones.

Type 31 beams had half the link spacing of type 21 beams. All of the beams except the most corroded were judged to have failed in 'compression'. The most corroded (16.3%) was judged by Rodriguez et al[45] to have failed in shear.

It can be seen from Figure 2-15 that in the cases of types 12, 13, 21 and 31, the change in failure mechanism was always signalled by a sharp drop in load-carrying capacity for little extra corrosion of the tension reinforcement.

The type 5 beams all failed in flexure. There was no apparent difference between those beams that were corroded under 80% of the service load and those that were corroded and then loaded. Rodriguez et al[45] observed spalling of the cover reinforcement to the compression reinforcement during failure. Cracking along the compression reinforcement was presumably exacerbated by the splitting forces due to the applied loading and the upward bowing movement of the compression reinforcement between adjacent links. This introduces the possibility of buckling of the compression reinforcement. Restraint is normally provided at points by links and between

the links by the cover. Cracking and spalling of the cover concrete removes the intermediate restraint. Corrosion of the links, particularly at the junction with the compression reinforcement, can reduce the restraint to both vertical movement and rotation.

Rodriguez et al[45] propose calculation methods based on EC2[59] and reduced section areas. They suggest two alternatives. One where the top and bottom cover is ignored, and another where the cover on all four faces is ignored. For the beams where bending failure dominated, these two cross-sections bracket the observed ultimate moments. For those where shear failure occurred, the cross-section with cover ignored on all four faces was found to underestimate most of the results by about 30%. Both the gross cross-section and the cross-section with top and bottom cover missing gave better results than the cross-section with cover missing on all four sides. None of the approaches suggested here addresses the fundamental behaviour of corroded members, and it is likely that further work is required.

Tachibana et al[60] tested a series of simply supported beams at varying levels of accelerated corrosion. The beams were 150 by 200 by 2000 mm with a span of 1500 mm. Two 16 mm deformed bars were used in the tension zone with 22 mm cover (c/D = 1.4). No links or compression reinforcement were provided. A current of 0.5 mA/cm^2 was applied to the two 16 mm bars for 3, 6, 10 and 15 days.

Tachibana et al[60] observed the same phenomenon as Rodriguez et al[45] of changing failure mode with increased corrosion. The control and 3-day corrosion beams were uncracked and both failed in flexure at similar loads. The 6, 10 and 15-day corrosion beams had corrosion-induced cracking. The 6-day beam failed in shear at 90% of the failure load of the control beams. The 10 and 15-day beams failed in a combination of bond and shear at 85 and 88% respectively of the control beams.

The control, 3 and 6-day beams had definite yield points followed by plateaux and ultimate loads. The 10 and 15-day specimens had no definite yield points, although there was a shallowing of the load-deflection curve at about half of the ultimate load, possibly indicating the onset of structural cracking. The sharp drop after peak load is of concern. It suggests that the mode of failure mode has changed from a ductile to a brittle one.

Tachibana et al[60] developed a non-linear finite element analysis model to investigate the problem further. Like Lee et al[57] they developed constitutive relationships from their experimental results. Both sets of investigators used bond element with properties based on experimental data. In this case, the bond element was modified to include the effects of corrosion for those elements in direct contact with the reinforcement, and to reflect the reduced frictional transfer of in-plane stress at longitudinal cracks. The effects of corrosive bursting stresses were simulated in the 2-D analysis by introducing vertical stresses in the zone of the corroding bar.

By varying the bond properties according to the test data, Tachibana et al[60] were unable to produce the load-deflection curve of the 15-day corrosion beam. The loads were considerably overestimated. Better agreement was obtained by introducing initial stresses to simulate corrosion stresses. These caused cracking along the reinforcement and so impeded shear transfer between the concrete and the bar thus simulating a reduction in bond. Impeding shear transfer between bar and concrete by using the bond element to simulate in-plane load transfer also gave reasonable results.

Ting and Nowak[61] developed a numerical procedure for assessing the effects of reinforcement area loss on the moment curvature relationship for arbitrary shapes of reinforced concrete sections. The method involved dividing a section into a series of horizontal strips and, for each curvature, applying strain compatibility to achieve equilibrium. Ting and Nowak[61] applied their model to a simply supported T-beam with corrosion in the outer layers of tension reinforcement (12 out of the 18 bars). Moment-curvature plots are given for 0, 20, 50 and 100% section loss of the outer bars. This shows the moment capacity getting smaller with increasing reduction in bar area. However, the ductility is increasing. The plateau beyond yield increases with increasing section loss. The ultimate failure, when the concrete crushes, occurs at greater curvatures, and thus deflections. The model presented is very simple and does not consider such points as bond reduction, cracking, spalling or fracture of the reinforcing bars. If these are taken into account, the experimental work of other investigators shows a reduction in ductility with increasing corrosion[53, 60, 63, 64].

Uomoto et al[62] tested simply supported beams under two-point loading. A 100 by 100 by 700 mm cross-section was used. 6, 10, 16 and 19 mm deformed bars with covers of 10 and 20 mm were used. No links or compression reinforcement were provided. 0, 0.5 and 3.3% sodium chloride contents were added to the mixing water. Some of the beams were loaded to give flexural cracking, and then a current of 167 mA was applied for 10 days. Unfortunately, the results of the whole series of experiments are not given, just an overview of trends.

Reinforcing bars were taken from the specimens after 10 days of corrosion. The 10 mm bars showed residual strengths of around 95, 93 and 90% for the 0, 0.5 and 3.3% NaCl addition levels respectively. A plot is given of beam tests with 10 mm deformed bars and 20 mm cover. The corroded specimens without induced flexural cracks showed residual load-carrying capacities of around 95, 92 and 66% for 0, 0.5 and 3.3% NaCl respectively. The beams with induced flexural cracks had residual load-carrying capacities of around 90, 81 and 76% for 0, 0.5 and 3.3% NaCl respectively. The descriptions given by Uomoto et al[62] indicate that whilst the control and 0% NaCl beams failed in flexure, the more corroded beams failed in a combination of shear and bond. This ties in with the findings of Tachibana et al[60].

Uomoto and Misra[63] tested two series of beams (A and B) and one series of columns. The series A beams are reported for a second time. They have already been reviewed as part of the paper by Uomoto et al[62]. The columns are discussed in section 2.7.

The series B beams were 100 by 200 by 2100 mm in section. Two 16 mm deformed bars were provided as tension reinforcement along with two 6 mm compression bars and 6 mm links at 170 mm centres. 1.25 kg/m^3 sodium chloride by weight of concrete was added to the mixing water. The beams were cured in moist air for 2 to 4 weeks. A current of 1 A was then applied to all bars for 7, 14 and 14 days, and gave 1.0, 1.2 and 1.4% corrosion respectively in the 16 mm bars. The beams were tested under two-point loading giving residual load-carrying capacities of 96, 92 and 83% of the control for 1.0, 1.2 and 1.4% corrosion respectively. The load-deflection curves show distinct yield and plateaux for the 0 and 1.0% corrosion beams. For the 1.2 and 1.4% corrosion beams the failure is abrupt with no plateau after the peak. The deflections at failure were around 12, 10.5, 9 and 8 mm respectively with increasing corrosion. Uomoto and

Misra[63] observed that failure of the corroded beams occurred in flexure coupled with spalling and buckling of the concrete in the compression zone.

The tests carried out by Lin[44] were primarily aimed at investigating the effects of corrosion on bond strength. As such, they are described in section 2.4. However, Lin's series A beams had one 16 mm bar with no splices. The cover was 17 mm (c/D = 1).

Those beams with an applied current of 5 mA/cm^2 had residual load-carrying capacities of 83.9, 94.0 and 87.7% of the control. Those with an applied current of 10 mA/cm^2 had ratios of 50.9, 43.4 and 36.6% of the control. Lin[44] expresses the load-carrying capacity in terms of moment capacity. However, the diagrams of failure mode indicate that whilst the 5 mA/cm^2 beams may have failed in flexure, the 10 mA/cm^2 beams have failed in a combination of shear and bond.

Lin's description of the test procedure suggests that beams were removed from the corrosion tank 'after the completion of the longitudinal crack'. Given that the beams corroded at a current of 10 mA/cm^2 first showed signs of cracking at 2 to 2.5 days (compared to 5.5 to 6 days for the 5 mA/cm^2 beams), it would seem reasonable to suggest that the longitudinal crack was complete earlier on the 10 mA/cm^2 beams than the 5 mA/cm^2 beams. Faraday's law indicates that the amount of corrosion is directly proportional to the product of corrosion rate and time. This would suggest that the 10 mA/cm^2 should have similar corrosion loss when both cracking forms and completes. With similar corrosion, the structural performance may also be expected to be similar. However, the 10 mA/cm^2 beams have a residual load of around 50% compared to 90% for the 5 mA/cm^2 beams, and failed by a different mechanism. Perhaps there is a corrosion rate effect. This has been identified by Clark and Saifullah[41] where they note that mechanical damage, different interface properties and different corrosion products can occur at higher accelerated corrosion rates. Both of the corrosion rates used by Lin[44] are extremely high. Rodriguez et al[45] preferred to corrode at 0.1 mA/cm^2, and even this is around one hundred times the highest rates found in real structures.

Daly[64] carried out 24 tests on simply supported beams to investigate bar type, cover and level of corrosion. The beams were 120 by 240 by 3000 mm with a span of 2600 mm. Two 12 mm

tension bars were provided with no link or compression reinforcement. Both plain and ribbed bars were tested with side and bottom covers of 12, 24 and 36 mm (c/D = 1, 2 and 3). A current of 0.22 mA/cm^2 was applied to the 12 mm bars. Corrosion was determined by weight loss. For the highest level of corrosion, the corrosion rate was doubled to 0.44 mA/cm^2. As one of the main aims was to investigate the effect of corrosion on bond and anchorage, a single point load was applied 1 m from the support (a_v/d = 4.5, 4.76 and 5.05). Details are given for the plain bar tests in Table 2-14 and the ribbed bar tests in Table 2-15.

The level 6 (see Note to Table 2-14) corrosion beams had residual strengths of 89, 93 and 78% respectively for c/D ratios of 1, 2 and 3. However, the failure mode had started to change. In the beams with c/D = 2 and 3 the mode was still flexure, but with some horizontal cracking suggesting bond failure. With the c/D = 1 one bar failed in bond whilst the other failed by fracture. However, the residual strength was still 89% of the control.

The level 9 corrosion actually had less corrosion than the level 2 corrosion beams, giving residual loads of 84, 91 and 102% of the control respectively for c/D ratios of 1, 2 and 3. With c/D = 1 the failure was flexure with horizontal cracking. With c/D = 2 the failure was by bond failure in both bars. This is not quite what would be expected given that c/D of 2 represents better bond conditions than c/D = 1 and 3% corrosion is somewhat smaller than 16%.

The load-deflection curves show distinct yield points and plateaux. However, those beams where the bars failed in bond or fracture had plateaux of about one third of the length of the other beams. The plateaux ended with sudden drops in loads. This seems to suggest that the beams did reach their yield strength with failure occurring before the ultimate strength could be reached.

Table 2-14: Flexural tests on corroded beams with plain bars (Daly[64])

Beam	*c/D*	a_v/d	*Corrosion (%)*	*Ultimate load (kN)*	*Corroded / control*	*Failure mode*
R12/0	1	4.5	0	27.4	1.00	Flexure
R12/3	1	4.5	0	28.4	1.04	Flexure
R12/6	1	4.5	22	24.4	0.89	1bar bond & 1 bar fracture
R12/9	1	4.5	16	22.9	0.84	Flexure with horiz. cracks
R24/0	2	4.76	0	27.6	1.00	Flexure
R24/3	2	4.76	2	27.3	0.99	Flexure
R24/6	2	4.76	4	25.7	0.93	Flexure with horiz. cracks
R24/9	2	4.76	3	25.1	0.91	2 bars bond
R36/0	3	5.05	0	25.1	1.00	Flexure
R36/3	3	5.05	2	25.5	1.02	Flexure
R36/6	3	5.05	22	19.5	0.78	Flexure with horiz. cracks
R36/9	3	5.05	0	25.6	1.02	Flexure

Note: Beam notation is bar type (R or T) / cover (12, 24 or 36) / corrosion level (0, 3, 6 or 9)

With the ribbed bars (see Table 2-15), level 3 corrosion had little effect. Residual strengths of 96, 96 and 99% (of the control) were recorded for c/D ratios of 1, 2 and 3 respectively. The beams with c/D = 1 and 2 failed in flexure, whilst flexure was accompanied by horizontal cracking when c/D = 3.

The level 6 corrosion beams had residual strengths of 76, 79 and 87% of the control. With c/D = 1 and 2 flexural failure was accompanied with horizontal cracking, whilst c/D = 3 gave bond failure in one bar. It is not clear why there should be a bond failure with c/D = 3 and not with c/D = 1. Both had full-length longitudinal corrosion cracks whilst the beam with c/D = 1 had 70% more corrosion.

The level 9 corrosion beams had residual strengths of 70, 70 and 69% of the control. With c/D = 1 and 2 both bars failed in bond. With c/D = 3, a flexural failure was achieved but both bars

fractured. A local loss of around 50% of the bar section was believed by Daly[64] to be responsible for this. Although the corrosion for the level 9 beams was, on average, less than that for the level 6 beams the failure load was lower. However, the applied corrosion rate was twice that of the level 6 beams. Daly[64] suggests that the differences in load-carrying capacity may be a corrosion rate effect.

Table 2-15: Flexural tests on corroded beams with ribbed bars (Daly[64])

Beam	*c/D*	a_v/d	*Corrosion (%)*	*Ultimate load (kN)*	*Corroded / control*	*Failure mode*
T12/0	1	4.5	0	38.9	1.00	Flexure
T12/3	1	4.5	2	37.5	0.96	Flexure
T12/6	1	4.5	22	29.6	0.76	Flexure with horiz. cracks
T12/9	1	4.5	15	27.1	0.70	2 bars bond
T24/0	2	4.76	0	37.8	1.00	Flexure
T24/3	2	4.76	1	36.1	0.96	Flexure
T24/6	2	4.76	14	30.0	0.79	Flexure with horiz. cracks
T24/9	2	4.76	18	26.4	0.70	2 bars bond
T36/0	3	5.05	0	33.3	1.00	Flexure
T36/3	3	5.05	1	32.9	0.99	Flexure with horiz. cracks
T36/6	3	5.05	13	28.9	0.87	1 bar bond
T36/9	3	5.05	11	23.0	0.69	Flexure & 2 bars fractured

All of the beams where flexural failure occurred had long plateaux after yield on the load-deflection curves. The point at which bond failure in two bars occurred determined whether there was to be a plateau or not. With the level 3 corrosion c/D = 1 beam a plateau of about one third of the length of the flexural failures was present before a sudden reduction in load. In contrast, the level 3 beam with c/D = 2 had a sudden reduction in load straight after the peak load had been reached. This illustrates that a warning of failure cannot be relied upon when bond failure occurs.

Daly carried out a series of calculations to compare the test beams with predictions obtained by using BD 44/90[65]. The only modification to the BD44/90 procedure was to use reduced areas of

reinforcement. This was found to give reasonable predictions for the control and level 3 corrosion beams, but overestimated the load-carrying capacities of many of the level 6 and 9 beams. This lack of conservatism is likely to be because the code only predicts flexural failure and does not recognise that corroded beams behave differently to sound ones. In particular, reductions in bond strength can cause premature failure before the flexural strength is reached.

The effects of accelerated corrosion on bending strength are summarised in Table 2-16.

Table 2-16: Effects of corrosion on flexure

Parameter	*Effect on flexural strength*
Loss of reinforcement cross-section[44, 45, 53, 57, 60, 62, 63, 64]	Approximately linear losses of flexural strength up to a limiting value where bond or shear become critical. The critical section loss will vary with individual details (i.e. the presence of links or not).
Longitudinal corrosion cracks[53, 57, 60, 62, 63, 64]	These only appear to influence load-carrying capacity when anchorage or bond become critical. When longitudinal cracks are in the bending region and bond or shear failure is prevented, bending capacity still appears to be controlled by reinforcement cross-section.
Reduction in length of plateau of load-deflection curve[53, 60, 63, 64]	Changes in failure mechanism from flexure to bond, fracture or shear leads to brittle failure mechanisms that exhibits little or no load-deflection plateaux.
Corrosion at laps[55]	Ductility of failure increases with decreasing link spacing. Abrupt failure at peak load is possible at large link spacing.
Link corrosion[45, 55, 56]	There is a possibility that members with corroded links will not achieve their full flexural capacity due to premature shear failure. Considerable link corrosion is required for this to happen.

2.6 Shear strength

Structural design codes are usually written such that compliant designs will fail in a ductile rather than brittle manner. That is with plenty of deflection and visual warning of impending failure. This implies that members are intended to fail in bending, which is ductile, rather than in shear, which is brittle. When the member deteriorates, the shear capacity may diminish at a faster rate than the flexural capacity leading to the possibility of a change in critical failure mechanism.

Many of the shear failures due to accelerated corrosion have arisen out of tests aimed at investigating the effects of corrosion on beams rather than the effects of corrosion on shear. These beams failed in flexure when little or no corrosion was present, but failed in shear at higher levels of corrosion. The beams observed to fail in shear fall into three categories:

(i) Singly reinforced beams with no link reinforcement, such as those tested by Lin[44], Tachibana et al[60], Uomoto et al[63] and Uomoto and Misra[63] and Daly[66].
(ii) Singly reinforced beams with link reinforcement, such as those tested by Daly[66].
(iii) Doubly reinforced beams with links, such as those tested by Rodriguez et al[45].

Considerably higher levels of corrosion are required to change the failure mode of beams with links than those beams without links. The beams with links also tend to maintain much of their peak load unlike the beams without links where the failure is somewhat more brittle. As many of these beams were not intended to fail in shear in the first place, it is difficult to make judgements on the effects of corrosion on shear. Daly[66], however, specifically investigated the effects of corrosion on shear strength.

Daly[66] tested 48 simply supported beams to investigate the effects of bar type (plain or ribbed), cover, links, shear span to effective depth ratio and corrosion level. The beams were 120 by 240 by 3000 mm with a span of 2600 mm. The main tension reinforcement was provided by four 12 mm bars with side and bottom covers of 12, 24 or 36 mm (c/D = 1, 2 or 3). Either plain or ribbed bars were used for the beams without links, whilst only deformed bars were used in the beams with links. Where used, the links were 6 mm plain bars at 140 mm centres. The applied corrosion current was 0.22 mA/cm^2. Electrical continuity was ensured such that all bars corroded.

The amount of corrosion was determined by weight loss measurement.

The results of the beams with plain bars are given in Table 2-17.

Table 2-17: Shear tests on corroded beams with plain bars and no links (Daly[66])

Beam	*c/D*	a_v/d	*Corrosion (%)*	*Ultimate load (kN)*	*Corroded / control*	*Failure mode*
RS12/0	1	3.1	0.0	39.5	1.00	Shear, anchorage cracking
RS12/1	1	3.1	1.4	65.7	1.66	Shear, horiz. cracks in span
RS12/3	1	3.1	12.7	57.5	1.46	Shear, horiz. cracks in span
RS12/4	1	3.1	31.2	45.3	1.15	Shear, anchorage disrupted
RS24/0	2	3.3	0.0	52.6	1.00	Shear, horiz. cracks in span
RS24/1	2	3.3	0.0	75.7	1.44	Shear, anchorage cracking
RS24/3	2	3.3	12.0	55.1	1.05	Shear, anchorage cracking
RS24/4	2	3.3	27.4	42.8	0.81	Shear, anchorage disrupted
RS36/0	3	3.5	0.0	45.8	1.00	Shear
RS36/1	3	3.5	0.0	47.2	1.03	Shear, anchorage cracking
RS36/3	3	3.5	5.9	53.2	1.16	Shear, horiz. cracks in span
RS36/4	3	3.5	24.7	46.7	1.02	Shear, anchorage disrupted

Note: Beam notation is bar type (RS) / cover (12, 24 or 36) / corrosion level (0, 1, 3 or 4)

At level 1 corrosion all of the beams were observed to have longitudinal cracking along a length of the test span before the load test. The 0.0% corrosion losses are presumably due to weighing accuracy as corrosion was observed to have caused cracking. All three specimens failed in shear with some horizontal cracking along the shear span of anchorage regions. The residual failure loads were 166, 144 and 103% of the control beams for c/D ratios of 1, 2 and 3 respectively. However, the control beam had an abnormally low ultimate load in comparison with the other control beams. This casts doubt on the validity of the control beam.

The level 3 corrosion resulted in failure in shear with residual loads of 146, 105 and 116% of the control for c/D ratios of 1, 2 and 3 respectively. The shear failure was accompanied by horizontal

cracking either in the shear span or the anchorage length. The level 4 corrosion resulted in failure in shear with disruption of the anchorage zones, giving residual loads of 115, 81 and 102% of the control.

The load-displacement curves for the plain bars with c/D = 1 showed brittle failures at deflections of 10 mm or less except for the beam with level 3 corrosion. It is not clear why a plateau should have carried on until a deflection in excess of 45 mm before failure. The c/D = 2 beams showed brittle failure at around 10 mm deflection. The c/D = 3 beams again showed failure at around 10 mm deflection. However, the load did not reduce to zero immediately but decreased on a slope of around one to one third of the loading slope. The unloading slope became shallower with increasing corrosion. This could possibly be due to increased bond performance at higher covers leading to a small amount of post-failure load-carrying capacity. Improvements in bond strength with increasing c/D ratios are not usually associated with plain bars. However, Saifullah[35] observed that once corrosion had taken place, the bond strength of plain bars was improved by increasing cover.

The performance of the beams with plain bars showed only one beam out of nine where the residual was less than the control despite some of the beams having corrosion of up to 31%. As stated earlier, Saifullah has shown that corrosion can improve the bond strength of plain bars. However, one would have expected the extensive cracking to cancel out any earlier increases due to improved friction. The only remaining explanation possible is the opposite; that the bond breakdown in the span was such that tied arch behaviour resulted. This would require the anchorage to develop sufficient strength to allow the tension reinforcement to act as a tie. The support reaction would provide an enhancement to the bond strength at the start of the anchorage zone. This may also explain the disruption of the anchorage observed in the level 4 corrosion beams as the anchorage would have to work harder to support a tied arch than a conventional beam.

The behaviour of the beams with deformed bars showed none of the dramatic increases in strength observed in the beams with plain bars. The results are given in Table 2-18.

Table 2-18: Shear tests on corroded beams with ribbed bars and no links (Daly[66])

Beam	*c/D*	a_v/d	*Corrosion (%)*	*Ultimate load (kN)*	*Corroded / control*	*Failure mode*
TS12/0	1	3.1	0.0	56.9	1.00	Shear, anchorage cracking
TS12/1	1	3.1	4.3	48.6	0.85	Shear
TS12/3	1	3.1	21.5	39.0	0.69	Shear, anchorage disrupted
TS12/4	1	3.1	21.5	45.8	0.80	Shear, horiz. cracks in span
TS24/0	2	3.3	0.0	53.5	1.00	Shear, horiz. cracks in span
TS24/1	2	3.3	4.5	51.6	0.96	Shear, anchorage cracking
TS24/3	2	3.3	14.4	50.0	0.93	Shear, horiz. cracks in span
TS24/4	2	3.3	21.5	46.2	0.86	Shear, anchorage cracking
TS36/0	3	3.5	0.0	47.9	1.00	Shear, horiz. cracks in span
TS36/1	3	3.5	3.8	51.2	1.07	Shear
TS36/3	3	3.5	14.1	49.7	1.04	Shear, anchorage cracking
TS36/4	3	3.5	17.9	48.7	1.02	Shear, anchorage cracking

Note: Beam notation is bar type (TS) / cover (12, 24 or 36) / corrosion level (0, 1, 3 or 4)

At level 1 corrosion the residual loads were 85, 96 and 107% of the control for c/D = 1, 2 and 3 respectively. The failure modes were observed by Daly[66] to be shear cracking. At level 3 corrosion the residual loads were 69, 93 and 104% of the control. Horizontal cracking in the shear span or anchorage zone accompanied the shear failures. At level 4 corrosion the residual loads were 80, 86 and 102% of the control. Again, horizontal cracking in the shear span or anchorage zone accompanied the shear failure. The load-deflection curves showed failure to occur at a deflection of around 8 mm. The unloading curve beyond the peak load had a slope of around one half of that of the loading curve.

Reductions in load-carrying capacity with increasing corrosion were observed in the beams with c/D = 1 and 2. However, the load-carrying capacity of the beam with c/D = 3 remains marginally above the control at all levels of corrosion suggesting that it is largely unaffected by corrosion. Given that the cover to both the bottom and side faces of the bars was reasonably high (36 mm),

this may have helped maintain the bond strength at a level where the forces necessary for a shear failure could be mobilised.

The beams with links were of the same section as the beams without links. 6 mm plain link bars were provided at 140 mm centres. Link hangers were not used in the compression zone. Three shear spans were tested: series A at 400 mm, series B at 650 mm and series C at 1000 mm. Two covers to the main bars were used, 24 and 36 mm (c/D = 2 and c/D = 3) giving 18 and 30 mm covers respectively to the links. All of the corroded specimens had corrosion cracks along most or all of the longitudinal reinforcement. The results are given in Table 2-19.

The series A beams were designed to fail in shear in the control beams although the margin between shear and flexural failure was small. Both control beams did fail in shear. At level 1 corrosion the beam with c/D = 2 failed in shear with a broken link and a residual strength 86% of the control. The c/D = 3 failed in flexure with some horizontal cracking and a residual strength 106% of the control. Although the average link corrosion was only 6.1%, the links tended to corrode more at the junction with the longitudinal bars, and this could explain the breakage. The failure modes remained the same for the level 2 and level 3 corrosion, with the beams with c/D = 2 failing in shear whilst the beams with c/D = 3 failed in flexure.

The series B beams had the same shear span as the beams without links. With the presence of links the controls were expected to fail in flexure. The beam with c/D = 3 did. However, the beam with c/D = 2 failed in shear. The levels 1 and 2 corrosion beams all failed in flexure. There was some crushing in the compression zone, presumably as a result of a secondary compression failure. The beams with c/D = 3 had some horizontal cracking accompanying the flexure at failure. At level 3 corrosion there was an unexpected failure in the beam with c/D = 2. Shear links were only provided in the shorter shear span as failure was expected there. A shear failure occurred in the long shear span where no links were present. The residual strength, 79% of the control specimen, cannot therefore be compared directly with the other three beams in the series. The beam with c/D = 3 followed the same pattern as the level 1 and 2 beams.

Table 2-19: Shear tests on corroded beams with ribbed bars and links (Daly[66])

Beam	a_v/d	*Corrosion (%)*		*Ultimate load (kN)*	*Corroded / control*	*Failure mode*
		Main	*Links*			
L24A/0	2.0	0.0	0.0	118.9	1.00	Shear
L24A/1	2.0	1.4	6.1	102.5	0.86	Shear & broken link
L24A/2	2.0	5.6	12.7	90.9	0.76	Shear & broken link
L24A/3	2.0	9.5	23.2	84.1	0.71	Shear & broken link
L36A/0	2.2	0.0	0.0	93.8	1.00	Shear
L36A/1	2.2	2.1	12.7	90.9	1.06	Flexure, horiz. cracks
L36A/2	2.2	6.4	15	87.1	1.00	Flexure, horiz. cracks
L36A/3	2.2	9.2	31.8	74.5	0.95	Flexure, horiz. cracks
L24B/0	3.3	0.0	0.0	70.1	1.00	Shear
L24B/1	3.3	2.1	12	70.7	0.97	Flexure
L24B/2	3.3	7.1	17.2	76.7	0.93	Flexure
L24B/3	3.3	11.2	23.6	63.7	0.79	Shear & bond in long span
L36B/0	3.5	0.0	0.0	105.4	1.00	Flexure
L36B/1	3.5	1.3	7.2	111.2	1.02	Flexure, horiz. cracks
L36B/2	3.5	5.6	12.4	105.6	0.95	Flexure, horiz. cracks
L36B/3	3.5	7.7	21	100.3	0.94	Flexure, horiz. cracks
L24C/0	5.1	0.0	0.0	79.3	1.00	Flexure
L24C/1	5.1	2.2	11.1	81.1	1.01	Flexure, horiz. cracks
L24C/2	5.1	5.9	22.8	75.2	1.09	Flexure
L24C/3	5.1	8.8	20	74.9	0.91	Shear & bond in long span
L36C/0	5.4	0.0	0.0	66.6	1.00	Flexure
L36C/1	5.4	1.4	8.8	60.4	0.91	Flexure, horiz. cracks
L36C/2	5.4	3.8	17.8	63.3	0.95	Flexure
L36C/3	5.4	9.9	20.2	58.3	0.88	Shear & bond in long span

Note: Beam notation is with links (L) / cover (12, 24 or 36 i.e. c/D = 1, 2 or 3) / corrosion level (0, 1, 2 or 3)

The series C beams had a shear span of 1000 mm. This was the same as the beams in the

accompanying flexural tests (Daly[64]). As such, all of the beams were expected to fail in flexure. The control, level 1 and level 2 corrosion beams did fail in flexure. However the two level 3 beams (c/D = 2 and c/D = 3) both failed in shear in the long shear span where no links were present combined with bond failure at the link termination.

Daly[66] used BD 44/95[73] to calculate both flexural and shear capacities for all 48 beams. Only the average weight loss was considered, giving reduced cross-section areas for tension and, where appropriate, link reinforcement. The effects of bond were not considered. Comparisons of the test and predicted load-carrying capacity are shown in Table 2-20.

Table 2-20: Comparison of test load—carrying capacity and predictions to BD 44/95 (Daly[64])

Test beams		*Ultimate test load / BD 44/95 prediction*	
		Mean	*Coefficient of variation (%)*
Plain bars – no links	Control	1.07	15.6
	Corroded	1.31	17.4
Ribbed bars – no links	Control	1.22	5.9
	Corroded	1.15	8.9
Plain & ribbed bars –	Control	1.14	12.3
no links	Corroded	1.23	15.4
Ribbed bars with links	Control	1.20	2.9
– flexure	Corroded	1.25	6.6
Ribbed bars with links	Control	1.21	4.5
– shear	Corroded	1.10	13.8
Ribbed bars with links	Control	1.21	3.5
– flexure & shear	Corroded	1.20	10.6

The mean value of test/BD 44 for the ribbed bars was 1.15, and remained at a similar level for all three levels of corrosion. The mean test / BD 44 value for the corroded plain bars was 1.31. However, the ratio decreased with increasing corrosion, being 1.47, 1.34 and 1.11 for corrosion levels 1, 3 and 4 respectively. This is of concern as it suggests that the BD 44 formulae do not

reflect the changing behaviour of corroded plain bars with increasing corrosion. The method may possibly be unsafe at higher levels of corrosion.

Combining together all of the control beams with links regardless of whether they failed in flexure or shear, the mean ratio of test to BD 44 predictions was 1.21 with a coefficient of variation of 3.5%. For the corroded beams, the mean test / BD 44 value was 1.20 with a coefficient of variation of 10.6%. Whilst there was more scatter in the corroded beams, the BD 44 flexure and shear expressions gave similar mean values for both control and corroded beams.

If the twelve corroded beams that failed in flexure are considered alone, the mean is 1.25. For the six beams that failed in shear the mean was 1.10. The shear mean was brought down by two ratios of 0.95 and 0.92. In both of these beams a link broke despite the average level of link corrosion only being 12.7 and 23.2% respectively. This highlights one of the difficulties in assessing corroded structures: that of assessing the variability in cross-section loss.

Provided that links are present, and remain effective, BD 44 seems to provide reasonably safe predictions to load-carrying capacity even if it does not describe adequately the structural mechanics.

The effects of corrosion on shear strength are summarised in Table 2-21.

Table 2-21: Effects of corrosion on shear strength

Parameter	*Effect on shear strength*
Loss of reinforcement cross-section[45, 66]	The loss of shear strength is not linear with the reduction in tension and link reinforcement area.
Longitudinal corrosion cracks[45, 66]	The presence of longitudinal corrosion cracks appears to influence load-carrying capacity when anchorage bond becomes critical.
Link corrosion[45, 66]	It is possible that members with corroded links will not achieve their full bending capacity despite being designed to fail in flexure. Considerable link corrosion is required for this to happen. A more ductile failure mechanism is apparent when links are present.
Bar type[66]	Beams with corroded plain bars (and no links) demonstrated a significant enhancement in load-carrying capacity over the uncorroded control beams. This was not evident with the beams with ribbed bars.
Failure mode – beams designed to fail in flexure[44, 45, 60, 62, 63, 66]	The failure mode can change from flexure to shear with increasing corrosion.
Failure mode – beams designed to fail in shear[66]	It appears that there may be the possibility of tied arch behaviour occurring due to reduction in bond strength in the beams with no links particularly when plain bars are used.
Cover to bar diameter ratio[66]	Increases in the c/D ratio appear to cancel out much of the potential reductions in shear strength due to corrosion. It is unclear whether the bottom or side cover is the significant factor.

2.7 Column behaviour

Uomoto and Misra[63] tested both beams and columns subject to accelerated corrosion. The beams are discussed in Sections 2.5 and 2.6. Ten columns were tested. Each was 100 by 100 mm in cross-section by 400 mm long. Four 10 mm deformed bars were used, one in each corner with 20 mm cover. 6 mm deformed links were provided at 75 mm centres. As cracking was reported over both main reinforcement and links, it is likely that they were in electrical contact. Two levels of sodium chloride (1.0 and 6.6 kg/m^3) were added to the mix water. Two corrosion currents were applied (45 and 180 mA) for either 2 or 10 days. The columns were cured for two to four weeks before the current was applied. No pre-loading was applied during the corrosion period.

An axial load was applied to the columns. The corroded columns were reported to fail after spalling of the cover concrete or buckling of the longitudinal reinforcement. Uomoto and Misra[63] observed few cracks forming during loading. The final cracks were observed to be shear cracks close to the loading plates. Given how stocky the column was, this is not too surprising. The remaining cover concrete was removed at the end of the test. This revealed that most of the reinforcement in the corroded columns had buckled. No details were given of the bars in the control columns.

This leads to a similar discussion to that for the compression bars in beams in flexure given in Section 2.5. If the longitudinal bars fail in buckling rather than yield in compression the failure is likely to be at a lower load. In sound columns that comply with modern codes, bars should yield in compression with a sizeable margin between yield and buckling. However, column bars typically buckle after the ultimate strength has been reached[67]. As such, it is important to establish what are pre and what are post-ultimate phenomena.

The two columns with least corrosion have residual load-carrying capacities of 88 and 98% of the control columns. The other six corroded columns have residuals ranging from 77 to 84% of the control. Four of those columns have residuals in the range of 79 to 80% of the control despite two of them having had four times greater corrosion current applied than the other two. The reductions in load-carrying capacity are larger than could be explained on the basis of reinforcement area lost alone. Descriptions of the failure mode also suggest spalling of cover

concrete. In addition, the load-carrying capacity appears to reach a limiting value. This suggests that beyond a certain point increasing corrosion makes little difference to the load-carrying capacity. Possibly, this point is where the load is primarily being carried by the concrete that remains after spalling.

Rodriguez et al[68] tested 24 columns to investigate the effects of accelerated corrosion on column behaviour. Three types of column 200 by 200 by 2000 mm with end stiffening were tested. Type 1 columns had four 8 mm ribbed bars as the main reinforcement with 6 mm ribbed links at 100 mm centres. Type 2 columns had four 16 mm main bars with 6 mm links at 150 mm centres. Type 3 columns had eight 12 mm main bars with 6 mm links at 150 mm centres. 3% sodium chloride (by weight of cement) was added to the mixing water, and a current of 0.1 mA/cm^2 was applied to all of the reinforcement in the 1200 mm central test section.

Rodriguez et al[68] tested the columns under axial load. There were considerable differences in the compressive strengths of the concrete used in the columns. In order to make meaningful comparisons the control column strengths were normalised to those of the corroded columns.

For the type 1 columns, the residual load-carrying capacity ranged from 64% of the control column at 15.4% corrosion in the main bars to 56% at 27.8% corrosion. A limiting residual strength of around 55% was reached for the three most corroded columns. Between one and three links were found to have broken. For the type 2 columns, the residual ranged from 58% of the control at 9.3% corrosion to 54% at 15.1% corrosion. Again, the limiting residual strength was about 55% of the control. Between one and four links had broken. The results were similar for the type 3 columns. With residuals ranging from 63% at 9.8% corrosion to 51% at 16.3% corrosion. Again, the limiting residual was about 55% of the control. Between one and four links had broken. This confirms the observations of Uomoto and Misra[63] that there is a limiting value of axial load-carrying capacity beyond which further corrosion has little effect. The results also confirmed that the loss in load-carrying capacity was far greater than could be explained by loss of reinforcement cross-section alone.

Rodriguez et al[68] measured the strains on each face. From this they were able to determine the

extra eccentricity generated by non-uniform corrosion. Mean values of 7.1 and 2.3 mm were obtained for the x and y axes respectively on the control columns. The corresponding values for the corroded columns were 13.4 and 7.1 mm. Eccentricities due to initial imperfections and geometry are included in codes. For instance, BS 8110[69] suggests that a minimum eccentricity of the smaller of 0.05 h or 20 mm be taken in calculating the applied moment. This would correspond to the eccentricities of the control columns. To this, a value equal to the difference between the corroded and control columns should be added. Rodriguez et al[45] take a conservative value of the 95% characteristic corroded eccentricity minus the 5% characteristic control eccentricity, giving additional eccentricities of 20.7 and 14.1 mm in x and y directions respectively. Assuming a symmetric section this gives a single additional eccentricity of around 25 mm.

Rodriguez et al[68] noticed the phenomenon of premature buckling of the corroded reinforcement observed by Uomoto and Misra[63]. Their suggestion for calculating the buckling load in the reinforcement is to use Euler's critical load expression with an effective length of 0.75 times the spacing between adjacent links (s_v). A pin-ended column has an effective length of 1.0 s_v whilst a fixed-ended one of 0.5 s_v. Presumably, the 0.75 s_v is a reasonable estimate to reflect a situation with increased rotation at corroded links.

Rodriguez et al[68] tried several methods for calculating the residual strength. They considered gross concrete sections with an allowance made for the buckling of bars as a result of loss of links. Reduced concrete sections corresponding to the concrete core with no cover were also tried. On axial load-moment (N-M) interaction diagrams the test results fell between the gross and reduced concrete sections. This suggests that more work is required to develop a suitable procedure for assessing corroded columns.

In addition to the points raised in the experimental results, there is the possibility of a column that was classified as stocky at the design stage being classified as slender after corrosion because of the reduction in cross-section leading to an increase in the effective length of the column.

To the best of the Author's knowledge, no test data are available in the public domain on the

effects of corrosion on combined flexural and axial behaviour.

The effects of corrosion on axial load-carrying capacity are summarised in Table 2-22.

Table 2-22: Effects of corrosion on axial load-carrying capacity

Parameter	*Effect on axial load-carrying capacity*
Loss of longitudinal reinforcement cross-section[68, 63]	Leads to a reduction in load-bearing area in both axial compression and buckling. In addition, the rust product leads to cracking along the line of the reinforcement followed by spalling.
Spalling of concrete[68, 63]	Spalling of the concrete cover from the corner bars has two effects: a reduction in confinement of the main compression reinforcement, and a reduction in the concrete cross-section available to resist the axial load.
Loss of link reinforcement cross-section[68, 63]	When the links corrode the lateral restraint to the main compression reinforcement is likely to be lost. This will increase the effective length of the main compression reinforcement leading to a possibility of the reinforcement failing in buckling before it fails in compression.

2.8 Current assessment practice

The primary aim of a structural assessment is to carry out sufficient investigation and calculation to prove whether or not the structure is safe i.e. the load-carrying capacity is greater than or equal to the applied load effects.

The codes and guidance documents that provide the engineer with the means to do this are reviewed here. The load-carrying capacity would, ideally, be evaluated for both the current and future states to assess the likely long-term effects of deterioration. However, current practice in most codes and guides is to evaluate the current state of a structure as if it were a new structure with, possibly, a few refinements to reflect deterioration.

The assessment of deteriorated concrete structures is a relatively new subject area that has yet to find its way from the laboratory into practice in a manner suitable for everyday use. Many countries have yet to realise the importance of assessment, and this is reflected in the scarcity of codes of practice from even the most wealthy and technologically advanced countries. Many of the documents reviewed here relate to bridge assessment. There are likely to be three main reasons for this. Firstly, governments tend to be the main owner of bridges and can insist on inspections and assessments as a statutory requirement. Secondly, the development of assessment codes is only economic if a large population of structures is affected (such as the national bridge stock). Thirdly, in the Northern Hemisphere the use of de-icing salts on concrete bridges is the main source of deterioration.

BS 8110 Part 1[69] is the main code for the design of concrete building structures in the UK. Part 2[70] is intended for special circumstances where greater depth of calculation is deemed necessary, and contains a section on Appraisal and testing. However, this is intended primarily for the construction phase. BS 8110 is not an assessment code. As there is no formal building assessment code in the UK it is commonly used for that task. This brings about three problems:

(i) Deterioration is not considered at all in BS 8110, and so engineers are left to make their own judgement.
(ii) Some of the design models do not necessarily translate into assessment models,

particularly for deteriorated structures[71].

(iii) Where BS 8110 is applied to buildings that were designed to other codes, it possible that the building will not comply with BS 8110. This is not a fault with either code, but merely a reflection of the fact that codes do change with advances in knowledge and technology. However, it does complicate the assessment process.

The Institution of Structural Engineers[72] has published a report on the Appraisal of existing structures. This can be used in conjunction with BS 8110[69] to improve the assessment procedure. A considerable amount of background information is provided on materials, forms of construction, testing and reducing safety factors without altering the overall reliability by eliminating some of the factors that were unknown at the design stage. The major omission is the treatment of the structural effects of deterioration.

In the UK, the assessment of existing bridges has been a requirement for many years. Traditionally, bridges have been assessed to see whether they complied with current design codes rather than the codes to which the bridges were designed. Current design codes tend to be more onerous than those to which the bridges were designed leading to many bridges failing to comply with current design codes whilst appearing to perform adequately in service. Because of this the UK Highways Agency published its own assessment code BD 44/90[65] (updated in 1995 to BD 44/95[73]) with an advice note BA 44/90[74] (updated in 1996 to BA 44/96). Simple amendments were made to the design code (BS 5400: Part 4[97]) to produce the assessment code. As such, much of the conservative nature of the design code is contained in the assessment code. The main drawback is that deterioration is not considered in BD 44/95, although it is addressed, to a degree, in other Highways Agency documents.

BD 21/97[75] is the loading standard to be used in conjunction with BD 44/95[73] when assessing bridges. BA 16/97[76] is the advice note that accompanies it. In addition to providing guidance on loading, a condition factor F_c is proposed in BD 21/97. The assessed load-carrying capacity is multiplied by F_c (which can take a value between 0 and 1). It allows the assessing engineer to reduce the resistance (bending, shear etc.) to allow for any deficiencies noted in the inspection that cannot be allowed for in the calculation procedures. This condition factor is determined on

the basis of engineering judgement. Thus a crude means of assessing the effects of deterioration is presented. However, the lack of guidance means that engineers have to make judgements, possibly beyond their experience, and uniformity of assessment is not possible.

Recognising that the corrosion of bridges due to chlorides (in de-icing salts) is the biggest problem facing UK bridges, the Highways Agency produced Advice Note BA 51/95[77] to provide guidance on the effects of corrosion on load-carrying capacity and safety. This is the first codified attempt at quantifying the structural effects of corrosion in the UK, and provides reduction factors that engineers can include in their calculations. Simple qualitative guidelines for assessing the structural effects of corrosion are provided. The main quantitative recommendation is that bond should be reduced by 30% when cracking has occurred.

A 15-year bridge rehabilitation programme for trunk road bridges in the UK was launched in 1987. A similar programme for local bridges was launched soon after. Under a new EU directive for international transport, 40 tonne lorries were to be allowed on UK roads from 1999. These three activities have meant that a large number of bridges have been inspected and assessed in recent years. As the rehabilitation programme progressed it became increasingly apparent that there were fundamental limitations in the current assessment rules[78]. These were leading to strengthening being proposed for bridges which had been carrying traffic with no apparent sign of distress for many years. It also led to situations where it was unclear what the actual level of safety in a bridge was particularly where deterioration was present. In order to prioritise bridge maintenance funds effectively and to be able to forecast the future needs of the bridge stock rationally, it was considered necessary to revise the existing assessment rules. This work has yet to be completed but progress was reported in July 1996[79] and June 1998[80].

The Highways Agency has proposed a five level assessment procedure in BA 79/98[81]. An outline of their proposals is presented in Table 2-23. The procedure will be a progressive one starting at level 1 and progressing up to level 5 depending on the importance of the bridge. A level 1 assessment is likely to be fairly crude and based on existing assessment codes. If a bridge is adequate at level 1 then it is likely to be safe. However, if it does not pass a level 1 assessment then there is the option to progress to a more sophisticated level 2 assessment. This process can

continue up to a level 5 assessment.

At the higher levels of assessment the emphasis is on a reliability approach such that inherent differences in robustness between bridges can be identified in order to achieve similar safety levels. However, little mention is made of deterioration, and reliability analysis is not always appropriate to the assessment of deteriorated structures, as the effects of deterioration are not necessarily random. Basing assessments on reduced cross-sections, and not recognising that some of the design code rules will not necessarily be appropriate to deteriorated structures could lead to problems[71].

Table 2-23: Highways Agency assessment procedure (BA 79/98[81])

Level	*Procedure*
1	Assessment using simple analysis and codified requirements and methods.
2	Assessment using more refined analysis.
3	Assessment using better estimates (bridge specific design values of load and resistance, using probabilistic estimates where possible).
4	Assessment using bridge specific target reliability.
5	Assessment using full-scale reliability analysis.

In January 1990 the Canadian Standards Association (CSA) published Supplement No.1 *Existing Bridge Evaluation*[82] to be used in conjunction with CAN/CSA-S6-88 *Design of Highway Bridges*[83]. The significance of this supplement is that it recognises assessment as being a completely different activity from design. It also recognises that the inherent safety levels varies between different members and structures depending on their robustness. The process is essentially a simplified reliability analysis. The impact of deterioration on the safety of structures is recognised. Unfortunately, the technology for evaluating deterioration was not available to the code writers.

For assessment, the design resistance, ϕR, is multiplied by an extra term, U. The purpose of U (a resistance adjustment factor) is to fine-tune the resistance factor given for design. The U value varies for the different resistances bending, shear, axial etc. due to the levels of reliability inherent

in each resistance mechanism. For example, the resistance of reinforced beams in bending is more uncertain at higher reinforcement levels than at lower levels. Likewise uncertainty increases when the level of shear links is less that the minimum. The U value is used to recognise the uncertainties that are overcome in design by following prescribed rules but are present in assessment because the structure does not necessarily comply with current design and detailing rules. The CSA supplement notes that adjustments have to be made to each of the factors R and U to reflect the effects of deterioration. A procedure is presented for the modification of U based on tests or engineering judgement. No guidance is given in modifying R.

CEB Bulletin 243[84] provides a means of assessing the reductions in load-carrying capacity on the basis of:

(i) Condition Rating.
(ii) Level of inspection.
(iii) Extent of deterioration.
(iv) Extent of maintenance.
(v) Required service life.
(vi) Method of determining resistance (load-carrying capacity).
(vii) Redundancy in structure.

The Bulletin is contradictory in that it says the method is applicable only to those structures where no visible deterioration is observed. However, the elements used in determining the resistance reduction factor cover severe deterioration which is likely to be highly visible.

The reduced resistance is given by:

$$R_{red} = \Phi R_d \qquad \textbf{… (2-27)}$$

where: R_{red} = reduced resistance (bending, shear, axial etc) of a deteriorated structure
Φ = resistance reduction factor based on the current condition of the structure
R_d = design resistance of the section being considered

The concept of a Φ value is common in US and Canadian codes where it typically represents the uncertainty associated with each type of resistance. In Bulletin 243, it is derived form the following expression:

$$\Phi = B_R \, e^{-\alpha_R \beta_C V_R} \qquad \text{… (2-28)}$$

where: B_R = bias ratio between the true and mean resistance of the member

V_R = co-efficient of variation relating to the reliability level of the test and inspection data

α_R = deterioration factor obtained from the Condition Rating

β_C = target value of the minimum acceptable safety level, two levels are foreseen: 3.5 for normal expected service life and 2.5 for a limited period (i.e. until the next bridge inspection)

The value of Φ can vary from around 0.5 for severely deteriorated structures with little redundancy that have not been inspected regularly or maintained properly, to more than 1.0 for redundant structures in good condition that have been inspected regularly and properly maintained.

CEB 243 provides a means of reducing the load-carrying capacity based on deterioration. It uses test and inspection data obtained from the structure. However, it does not recognise that some elements of deteriorated structures behave differently to new structures. For instance, the design code resistance formulae may not be appropriate for use with deteriorated structures. Such an approach also assumes that all load-carrying mechanisms will reduce by the same amount for the same observed level of deterioration. This has not been established in any tests.

All of the documents reviewed in this section are aimed at establishing the current state of a structure without any consideration given to the future performance. Little mention is made of deterioration mechanisms, and no attempt is made to tie in material deterioration to structural deterioration. In addition, no criteria are available to define minimum performance criteria. This leaves the assessing engineer with no choice but to make crude assumptions, which may or may

not be conservative. As a result it is not possible to provide the structure's owner with a confident answer to the question: "How long will my structure last?".

In most of these documents, reference is made to the use of 'specialist literature'. However, such 'specialist literature' is often not available in a readily usable format. As such, the engineer has little information to use in day-to-day work.

2.9 Conclusions and the need for research

There is much literature available on the individual aspects of corrosion. In particular, there is a great deal of experimental data. However, little is available on the process of assessing the load-carrying capacity of corroded concrete structures. In particular, little material is available on assessment over the whole life of a structure.

The practising engineer does not necessarily have access to all of the literature reviewed in this Thesis, and would normally rely on guidance documents and codes. However, there are four principal omissions from the guidance documents available currently:

(i) No link is provided between the deterioration of materials and that of structural performance.
(ii) No quantitative guidance is presented on deterioration with time.
(iii) No recognition is made of the possibility that deteriorated structures may not behave the same as structures without deterioration.
(iv) No criteria are available to define minimum performance levels.

Without these, realistic assessments of the levels of safety within a structure are not possible. This leaves the assessing engineer with no choice but to make crude assumptions, which may or may not be conservative. As a result the engineer is not able to provide the structure's owner with a confident answer to the main questions required of a structural appraisal, namely:

(i) Is the structure safe?
(ii) Will it remain safe?

(iii) When is action required?

(iv) What action is required?

Limit state codes such as BS 8110[69] or BD 44[73] are likely to be the base code for assessments in the UK as they represent the latest thinking in code rules, and engineers are likely to be familiar with them. Limit state codes are also more appropriate for assessment as it is the 'failure' load that is of interest.

There are three approaches to modifying these codes to account for the effects of corrosion on concrete structures:

(i) Leave the code unchanged, and reduce section areas.

This appears to be what the UK Highways Agency[79, 80] is proposing for bridge assessment. This has the problem that it does not recognise that the reduction in load-carrying capacity may not be directly related to the material deterioration.

(ii) Leave the code unchanged, and introduce a capacity reduction factor.

This is the approach taken in BD 21[75] and in CEB Bulletin 243[84]. Again, this has the problem that it does not recognise that the reduction in load-carrying capacity is not directly related to the material deterioration. In the case of BD 21, it also requires some inspired guesswork from the engineer.

(iii) Modify the code resistance formulae to reflect the behaviour of deteriorated structures.

This has been attempted, to an extent, by Rodriguez et al[45] for EC2[59]. Unfortunately, the results are based on one set of laboratory tests where accelerated corrosion was used.

Option (iii) is the preferred approach as it is more realistic and logical. However, it requires good quality data to be available to develop reliable resistance formulae. This route will not

be fully achievable until sufficient data are available in the public domain (perhaps not for 10 to 20 years). However, an interim step is required. This is where the work described in this Thesis is required to address the first three principal omissions in the current guidance documents and to provide a means to address the fourth.

The aim of this research is thus to gain sufficient understanding of the effects of corrosion on reinforced concrete structures such that tools may be developed to address the principal omissions. A qualitative understanding of the structural effects of corrosion has been presented in this Chapter. In further chapters modifications and extensions to existing code rules are presented to allow the structural effects of corrosion to be assessed quantitatively.

3 CRACKING

3.1 Introduction

From the review of previous research, the important parameters controlling the amount of corrosion to cause cracking of the concrete surrounding a reinforcing bar were found to be:

(i) Thickness of cover concrete.
(ii) Tensile strength of cover concrete.
(iii) Bar size.
(iv) Rust occupying a greater volume than the original steel.
(v) Amount of rust product accommodated within the pores of the surrounding concrete without inducing stresses in the concrete.

The first three points can be addressed by a mechanics model, whilst the last two require a physical model.

3.2 Bar expansion to cause cracking

Previous researchers have proposed several models. These include non-linear finite element analysis, elastic thick-walled cylinder analogy and an infinite elastic medium. The elastic solutions are used to determine the expansive pressure at which the tensile strength of the concrete is exceeded at the bar-concrete interface. This is the deemed to be the point of cracking.

Tepfers[47] has investigated the use of elastic, plastic and partly cracked thick-walled cylinder models to predict the load at which bars fail in a pullout (bond) test. Although Tepfers work is usually considered to be related to bond strength, what he is actually determining is the point when the cover cracks. Deformed bars will generate longitudinal and radial stresses in the concrete when they are subject to load. For typical bar covers ($c/D < 2.5$) the radial stresses will be critical, and determine when the cover cracks.

Tepfers[47] found that the elastic model gave the load at which the cracking was starting at the bar-

concrete interface whilst the partly cracked elastic model corresponded to the load where the crack went right through the concrete cover. Given that the concrete has some plastic deformation, the ultimate load may be higher than the load at which the cover cracked depending on the c/D ratio. The elastic case was found to grossly underestimate the cover cracking load. The partly cracked elastic case was found to give a lower bound to the cover cracking load whilst the plastic case gave an upper bound. Tepfers[47] suggests taking the average of the partly cracked elastic and plastic cases for a mean value, or the partly cracked case for a lower bound design value. The partly cracked case is the basis for the ultimate bond strengths given in BS 8110[69], BS 5400[97] and BD 44/95[73].

It is proposed that an analogy be drawn between the radial stresses generated by deformed bars loaded in tension and the radial stresses generated due to expansive rust products.

For the partly cracked case, Tepfers[47] gives the following formula for calculating the internal pressure for cracking:

$$P_{cr.pce} = 0.6\left(0.5 + \frac{c}{D}\right) f_{ct} \qquad \textbf{… (3-1)}$$

For the plastic case, Tepfers[47] gives:

$$P_{cr.plas} = 2\, f_{ct}\, \frac{c}{D} \qquad \textbf{… (3-2)}$$

where:

c	=	concrete cover to bar (mm)
f_{ct}	=	concrete tensile strength (N/mm^2)
D	=	bar diameter (mm)
$P_{cr.pce}$	=	pressure to induce cover cracking assuming a partly cracked elastic stress state (N/mm^2)
$P_{cr.plas}$	=	pressure to induce cover cracking assuming a plastic stress state (N/mm^2)

Tepfers[47] approach of taking the average P_{cr} seems to give reasonable results when compared with his tests, and so the same is proposed here, giving:

$$P_{cr} = \frac{P_{cr.pce} + P_{cr.plas}}{2} \quad \textbf{… (3-3)}$$

This can be expressed as:

$$P_{cr} = 0.3\left(0.5 + \frac{4.33c}{D}\right) f_{ct} \quad \textbf{… (3-4)}$$

There will be a net radial expansion, δr, of the reinforcing bar to cause this cracking pressure. This net expansion is comprised of two components as follows:

$$\delta r = \delta r_{free} - \delta r_{cover} \quad \textbf{… (3-5)}$$

where: δr = net radial expansion of the reinforcing bar required to cause cracking

δr_{free} = free expansion of the reinforcing bar, due to rust growth, that would occur if the bar were not surrounded by concrete

δr_{cover} = expansion of the reinforcing bar restrained by the confining action of the concrete cover

Assuming elastic behaviour, the approach of Timoshenko and Goodier[85] can be used to calculate the radial strains in the bar and concrete. The strains at the interface between the bar and concrete will be equal. Thus δr can be calculated using:

$$\delta r = \frac{P_{cr}(1+\nu_c)D}{2E_{c.eff}} \quad \textbf{… (3-6)}$$

The bar will have a radial restraining pressure of P_{cr} acting on it. If this pressure is removed, then the bar will expand outward by an amount δr_{cover}, which is given by:

$$\delta r_{cover} = \frac{P_{cr}(1-\nu_s)D}{2E_s} \quad \text{… (3-7)}$$

where: $E_{c.eff}$ = effective elastic modulus (N/mm^2) of concrete = $E_c/(1+\phi)$ in the longer term where ϕ is the creep co-efficient and is, typically, taken as 2

E_s = elastic modulus of steel (N/mm^2)

ν_c = Poisson's ratio of concrete

ν_s = Poisson's ratio of steel

δr_{free} is then calculated in order to give the amount of free radial expansion due to rust which would result if the restraint were not present.

The total amount of rust generated, δr_{rust}, on a bar has two components:

$$\delta r_{rust} = \delta r_{free} + \delta r_{pore} \quad \text{… (3-8)}$$

where: δr_{rust} = radial expansion generated by the rust

δr_{free} = free expansion of the reinforcing bar, due to rust growth, that would occur if the bar were not surrounded by concrete

δr_{pore} = radial expansion of rust that is accommodated within the pore structure of the concrete cover without inducing stress

The value of δr_{rust} can be calculated on the basis of bar section loss and conversion into rust product of a greater volume. Time to cracking, t_{cr}, can be determined from the following:

$$t_{cr} = \frac{\delta r_{rust}}{\Delta \delta r_{rust}} \quad \text{… (3-9)}$$

where: $\Delta \delta r_{rust}$ = rate of increase in radial expansion of rust with time

3.3 Rust-induced increase in bar volume

The two most common forms of rust are ferrous hydroxide $Fe(OH)_2$ and ferric hydroxide $Fe(OH)_3$. The ratios of the molecular weight of the two forms of rust to iron Fe, α, are 0.622 and 0.523 for $Fe(OH)_2$ and $Fe(OH)_3$ respectively. The density of Fe is 7850 kg/m^3, whilst Liu[27] estimates the density of rust products to be around 3600 kg/m^3. The volume of the rust products can thus be determined from:

$$\frac{V_{rust}}{V_{Fe}} = \frac{\rho_{Fe}}{\alpha \rho_{rust}} \qquad \textbf{… (3-10)}$$

where: V_{Fe} = volume of iron (Fe)

V_{rust} = volume of rust product

α = ratio of the molecular weight of rust to the molecular weight of Fe

ρ_{fe} = density of iron (Fe)

ρ_{rust} = density of rust

The ratio of the volume of rust product to iron is 3.51 for $Fe(OH)_2$ and 4.17 for $Fe(OH)_3$. Given the uncertainty of which rust product will result, Liu[27] suggests that an average value should be taken. Thus, the rust product will be assumed to have a volume 3.84 times that of iron.

The rate of loss of bar radius per year, $\Delta\delta r$, can be calculated by using Faraday's law to give:

$$\Delta\delta r = 11.6 I_{corr} \qquad \textbf{… (3-11)}$$

where: $\Delta\delta r$ = rate of radial bar reduction (μm/year)

I_{corr} = corrosion rate (μA/cm^2)

Noting that the radial expansions and reductions are particularly small in comparison to the bar diameter the bar can be assumed to be gaining 3.84 units of radius for every 1 unit it loses; i.e. a net gain of 2.84 units. Thus:

$$\Delta\delta r_{rust} = 2.84(11.6 I_{corr}) \quad \textbf{… (3-12)}$$

Hence, δr_{rust} can be calculated for a given time from equation 3-9.

3.4 Rust product accommodated within concrete pore structure

The major unknown in the theory presented in Sections 3.2 and 3.3 is the amount of rust that is accommodated within the concrete pore structure surrounding the bar, δr_{pore}. This is likely to be a function of both the porosity and permeability of the surrounding concrete which are, themselves, a function of a number of parameters including:

(i) w/c ratio.
(ii) Degree of compaction.
(iii) Degree of hydration of the cement.
(iv) Fluidity of the rust products.
(v) Presence of fine cracking around the bar.

These parameters are difficult to measure or assess, and are beyond the scope of this Thesis. However, an empirical approach can be taken to estimate the magnitude of δr_{pore}. If the theory developed in Sections 3.2 and 3.3 is applied to experimental results where the bar section loss has been measured at the time of cracking, then the potential radial expansion due to rust formation, δr_{rust} can be estimated. The radial expansion for cracking can also be estimated, and whatever radial expansion is in excess of that to cause cracking can be assumed to be the rust product accommodated within the concrete pore structure.

Fifty test result have been analysed to determine δr_{pore}. The results are shown in Table 3-1. The criterion for choosing the test specimens was that they should have had the weight loss measured at time of cracking. Not all of the necessary concrete parameters (f_{cu}, f_{ct} and E_c) were provided in every case. Estimates of the missing values were based on the information provided.

Table 3-1: Evaluation of the amount of rust accommodated within the concrete pore space

Researcher	*Specimen*	*c / D*	*Cracking*		*Estimated parameters*							
			Wt loss	*Radius loss*	δr_{rust}	*Pcr plastic*	*Pcr pce*	*Pcr*	δr	δr_{cov}	δr_{free}	δr_{pore}
			%	*μm*	*μm*	*MPa*	*MPa*	*MPa*	*μm*	*μm*	*μm*	*μm*
Liu[27]	OA2859.6	2.7	1.26	50	143	16.5	5.9	11.2	10	0.9	11	132
	OB3859.6	4.3	1.93	77	218	26.3	8.8	17.5	15	1.5	17	202
	OE18512.	1.1	0.96	38	108	7.2	3.2	5.2	4	0.4	5	103
	Block 9.6	3.5	1.57	50	142	21.4	7.3	14.3	10	1.0	11	131
Al-Sulaimani,	10-11	7.0	4.27	108	306	41.0	13.2	27.1	15	1.4	16	290
Kaleemullah,	10-12	7.0	4.52	114	325	41.0	13.2	27.1	15	1.4	16	308
Basunbul, and	10-13	7.0	4.81	122	346	41.0	13.2	27.1	15	1.4	16	329
Rasheeduzzafar[38]	14-10	4.9	2.75	97	275	28.5	9.4	18.9	15	1.4	16	259
	14-11	4.9	2.89	102	289	28.5	9.4	18.9	15	1.4	16	273
	14-12	4.9	3.00	106	300	28.5	9.4	18.9	15	1.4	16	284
	20-9	3.3	1.67	84	238	19.0	6.6	12.8	14	1.3	16	223
	20-10	3.3	1.86	93	265	19.0	6.6	12.8	14	1.3	16	250
	20-11	3.3	2.00	101	285	19.0	6.6	12.8	14	1.3	16	270
Clark &	I - Plain	0.5	0.47	9	27	2.8	1.7	2.3	1	0.1	1	26
Saifullah[41]	III - Plain	1.0	0.83	17	47	5.7	2.5	4.1	2	0.2	2	45
	V - Plain	2.0	1.59	32	91	11.3	4.2	7.8	3	0.3	4	87
	II – Rib	0.5	0.30	6	17	2.8	1.7	2.3	1	0.1	1	16
	IV – Rib	1.0	0.58	12	33	5.7	2.5	4.1	2	0.2	2	31
	VI – Rib	2.0	1.30	26	74	11.3	4.2	7.8	3	0.3	4	71
Alonso et al[25]	I-1	1.3	0.45	18	51	8.9	3.7	6.3	5	0.5	6	45
	I-2	1.3	0.37	15	42	8.9	3.7	6.3	5	0.5	6	37
	I-3	1.9	0.61	25	70	13.3	5.1	9.2	8	0.8	8	61
	I-4	1.3	0.45	18	51	8.9	3.7	6.3	5	0.5	6	46
	I-5	3.1	0.77	31	88	24.1	8.4	16.2	13	1.4	14	73
	I-6	3.1	1.27	51	145	24.1	8.4	16.2	13	1.4	14	131
	I-7	1.3	1.11	45	127	9.6	4.0	6.8	5	0.6	6	121
	I-8	1.9	0.75	30	85	14.4	5.5	9.9	8	0.8	9	76
	I-10	1.9	1.28	51	146	9.5	3.6	6.5	6	0.5	7	139
	I-11	6.3	1.79	36	102	42.9	13.9	28.4	12	1.2	13	89
	I-12	1.3	0.44	18	50	8.6	3.6	6.1	5	0.5	6	45
	I-13	1.3	0.66	27	76	8.3	3.5	5.9	5	0.5	5	70
	I-14	1.9	1.43	29	81	12.5	4.7	8.6	4	0.4	4	77

Researcher	*Specimen*	*c / D*	*Cracking*		*Estimated parameters*							
			Wt loss	*Radius loss*	δr_{rust}	*Pcr plastic*	*Pcr pce*	*Pcr*	δr	δr_{cov}	δr_{free}	δr_{pore}
			%	*μm*	*μm*	*MPa*	*MPa*	*MPa*	*μm*	*μm*	*μm*	*μm*
	I-15	1.3	1.01	20	57	8.3	3.5	5.9	2	0.2	3	55
	I-16	1.9	0.70	28	79	9.5	3.6	6.5	6	0.5	7	72
	I-17	6.3	3.50	71	201	42.9	13.9	28.4	12	1.2	13	188
	I-18	1.3	0.40	16	45	8.6	3.6	6.1	5	0.5	6	39
	I-19	1.3	0.48	19	55	8.4	3.5	6.0	5	0.5	6	49
	I-20	1.3	0.63	25	72	8.4	3.5	6.0	5	0.5	6	66
	I-21	3.1	0.87	35	100	21.0	7.3	14.2	12	1.2	13	86
	I-22	3.1	1.29	52	147	21.0	7.3	14.2	12	1.2	13	134
	I-23	5.0	2.72	69	195	35.4	11.7	23.5	12	1.2	13	181
	I-24	4.2	1.82	55	156	29.5	9.9	19.7	12	1.2	13	142
	I-25	1.9	0.96	39	110	9.9	3.8	6.8	6	0.6	7	103
	I-26	1.9	1.33	54	152	9.0	3.4	6.2	6	0.5	6	146
	I-27	1.2	0.37	23	66	5.8	2.5	4.2	6	0.5	7	60
Cabrera[26]	A-12	1.7	2.04	62	175	10.7	4.2	7.4	5	0.5	5	169
	A-16	1.3	1.27	51	145	8.0	3.4	5.7	5	0.5	5	139
	A-20	1.0	0.92	46	131	6.4	2.9	4.6	5	0.5	5	125
	B-12	1.7	1.70	51	145	10.7	4.2	7.4	5	0.5	5	140
	C-12	2.5	1.32	40	113	16.0	5.8	10.9	7	0.7	8	105
Average of all tests			1.47	48					Average of all tests			127
Average of where c/D ≤ 4			1.0	37					Average of tests c/D ≤ 4			97

There is considerable scatter in the estimates of δr_{pore}, although there does seem to be a general trend of increasing δr_{pore} with increasing cover to bar diameter (c/D) ratio as shown in Figure 3-1. The c/D ratios used in the tests extended up to c/D values of 7. The majority of structures tend to have c/D ratios of around 1 to 2 for the main bars, with value of around 2 to 4 for link bars. Those bars with c/D greater than 4 have been excluded from the average calculations in the bottom line of Table 3-1 leading to an average δr_{pore} of 97, say 100μm.

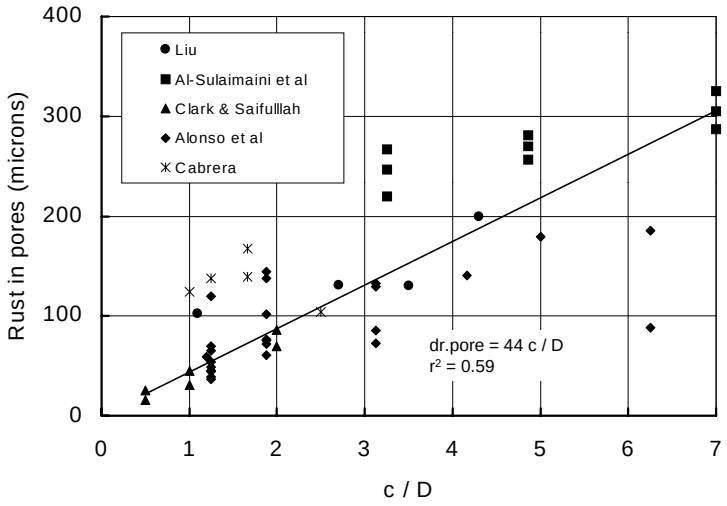

Figure 3-1: The relationship between δr_{pore} and cover to bar diameter ratio

There are two ways of approaching the estimation of δr_{pore} for design and assessment purposes. Either accept a blanket value of, say, 100μm or calculate a value based on the relationship between δr_{pore} and the c/D ratio. The former will overestimate the amount of corrosion required to crack the cover concrete for bars in the lower c/D ranges, and so the second approach appears to be more reasonable. Based on a linear regression analysis the best-fit relationship is:

$$\delta r_{pore} = 44\frac{c}{D}(\mu m) \qquad \text{… (3-13)}$$

Thus, the radial expansion due to corrosion necessary to cause cracking, δr_{rust}, is given by:

$$\delta r_{rust} = \frac{P_{cr}(1+\nu_c)D}{2E_{ef}} + \frac{P_{cr}(1-\nu_s)D}{2E_s} + 44\frac{c}{D} \qquad \text{… (3-14)}$$

where:

$$P_{cr} = 0.3\left(0.5 + \frac{4.33c}{D}\right)f_{ct} \qquad \text{… (3-15)}$$

The predictions from equation 3-14 have been divided by 2.84 to give the radius losses required to induce cracking. These are compared with the measured radius losses in Figure 3-2. Statistics

for the ratio of test/predicted radius losses are also given in Figure 3-2. Other than a few outliers, the predicted values appear satisfactory given the scatter and uncertainty present in such experiments.

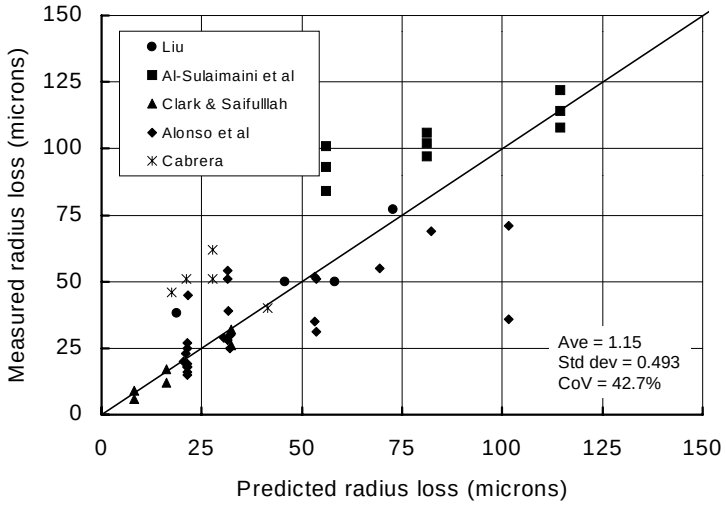

Figure 3-2: Comparison of measured and predicted radius loss to induce cracking

3.5 Simplified method of calculating the onset of cracking

Inspection of Table 3-1 shows that the radial expansion of the rust into the concrete pore structure is significantly greater than the radial expansion required to induce cracking stresses, and is the dominant parameter in determining the amount of rust to cause cracking. Inspection of Figure 3-1 shows that a reasonably linear relationship exists between δr_{pore} and the c/D ratio. Putting these two facts together, if there is a linear relationship between the dominant parameter and the c/D ratio, there is a reasonable chance that there will be such a relationship between the amount of rust to cause cracking and the c/D ratio. In Figure 3-3 the percentage weight loss is chosen to represent the amount of rust necessary to induce cracking. This is the parameter that an engineer is most likely to have from either weight loss or linear polarisation measurements.

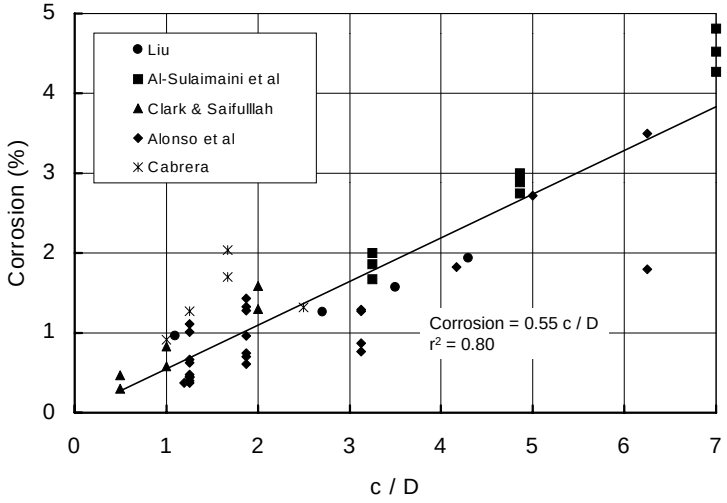

Figure 3-3: The relationship between bar weight loss due to corrosion and the c/D ratio

The linear relationship with the c/D ratio is even better than that for δr_{pore} ($r^2 = 0.80$ for percent weight loss compared to $r^2 = 0.59$ for δr_{pore}). This suggests that instead of using the procedure described in the previous sections, the following relationship can be used to calculate the amount of corrosion required to induce cracking:

$$\Delta_{cr} = 0.55\frac{c}{D} \qquad \text{… (3-16)}$$

where: Δ_{cr} = bar section loss required for corrosion-induced cracking (%)

Given the amount of scatter in the results and the variability and uncertainty associated with the input variables, undue sophistication is unlikely to be justified. A simple relationship is likely to prove just as effective, if not more so due to simplicity. Given the proximity of the constant to 0.5, it is suggested that the following version of the equation may be more convenient:

$$\Delta_{cr} = \frac{c}{2D}(\%) \qquad \text{… (3-17)}$$

Δ_{cr} can then be converted into the bar radius loss δ_{cr} as follows:

$$\delta_{cr} = \frac{D}{2} - \sqrt{\frac{D^2}{4}\left(1 - \frac{\Delta_{cr}}{100}\right)} = \frac{D}{2}\left[1 - \sqrt{1 - \frac{\Delta_{cr}}{100}}\right] \quad \textbf{… (3-18)}$$

If equation 3-18 is expanded as a binomial series (ignoring the third terms and beyond) and combined with equation 3-17, the following simplification is obtained:

$$\delta_{cr} \approx \frac{D\Delta_{cr}}{400} = \frac{c}{800} = 1.25c(\mu m) \quad \textbf{… (3-19)}$$

The time to cracking in years is then given by:

$$t_{cr} = \frac{1000\delta_{cr}}{11.6I_{corr}} \quad \textbf{… (3-20)}$$

where: c = concrete cover to bar (mm)

D = bar diameter (mm)

I_{corr} = corrosion rate ($\mu A/cm^2$)

δ_{cr} = bar radial loss required for corrosion-induced cracking (μm)

Δ_{cr} = bar section loss required for corrosion-induced cracking (%)

The section loss due to corrosion required to cause cracking is shown in Figure 3-4 for typical bar sizes and a selection of covers. Whilst the percentage section loss to induce cracking is unique for each bar diameter and cover, the corresponding radius loss is a function of the cover only. This implies that both 10 and 25 mm diameter bars with the same cover require the same radius loss to induce cracking. This would suggest that every 5 mm increase in cover requires around 6 μm extra radius loss to induce cracking.

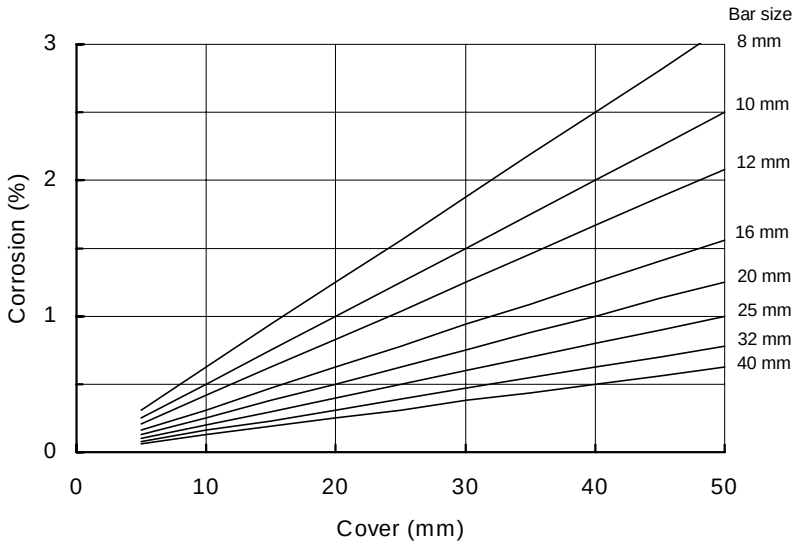

Figure 3-4: The predicted relationship between bar section loss required for corrosion-induced cracking and a range of covers and bar size

3.6 Spalling

Spalling occurs commonly in three forms:

(i) Spalling of a block of cover concrete to corner bars (Figure 3-5a).
(ii) Spalling of a wedge of cover concrete (Figure 3-5b and Figure 3-5d).
(iii) Delamination of a plane of concrete (Figure 3-5c and Figure 3-5e).

Each type of spalling occurs under different conditions related to bar spacing and cover. Each has its own geometry and criteria for failure.

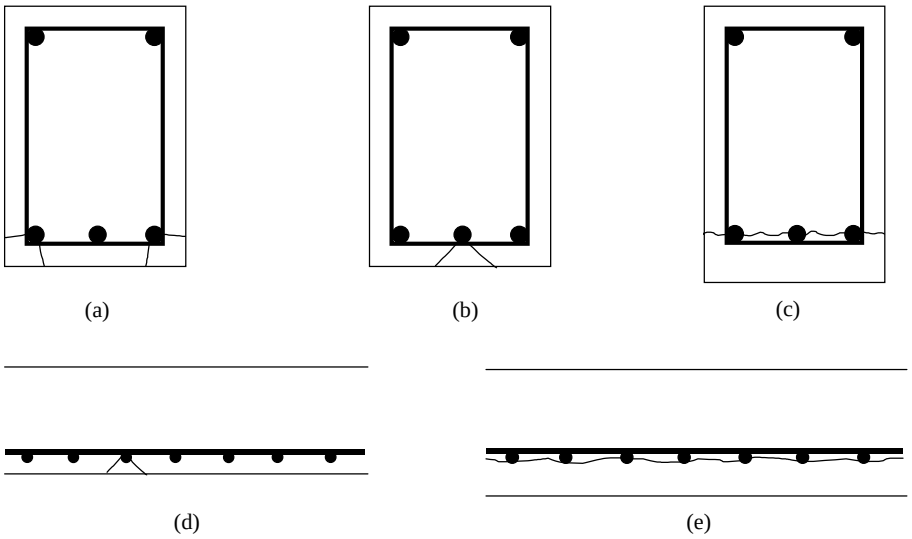

Figure 3-5: Types of spalling

A knowledge of when spalling is likely to occur would be valuable to engineers for two reasons:

(i) Avoidance of potential safety hazards due to spalled concrete falling onto passers-by.
(ii) As a visual means of assessing the amount of corrosion that has taken place to date.

The first point is an obvious safety concern. The second could provide a means of answering the questions that assessing engineers are regularly asked, such as: “My structure has cracked, has it corroded much and is it safe?”. In the previous section the amount of corrosion to cause cracking has been established. If the amount of corrosion to cause spalling can be established, in a structure that has cracked but not spalled the amount of corrosion can be bracketed between the cracking and spalling values.

Corner spalling (Figure 3-5(a)) is, in the Author’s opinion, the most common type of spalling and is addressed in this section, where a simple model is developed to predict the onset of corner spalling.

Corner spalling can only occur when two cracks propagate from the corroding bar to the exposed surface. When two cracks have occurred it is assumed that the cracked section of cover concrete is held in place by the concrete at either end. It is proposed that the cracked section of concrete can be idealised as a fixed-ended beam as shown in Figure 3-6, where the cover concrete is

assumed to be a rectangular beam.

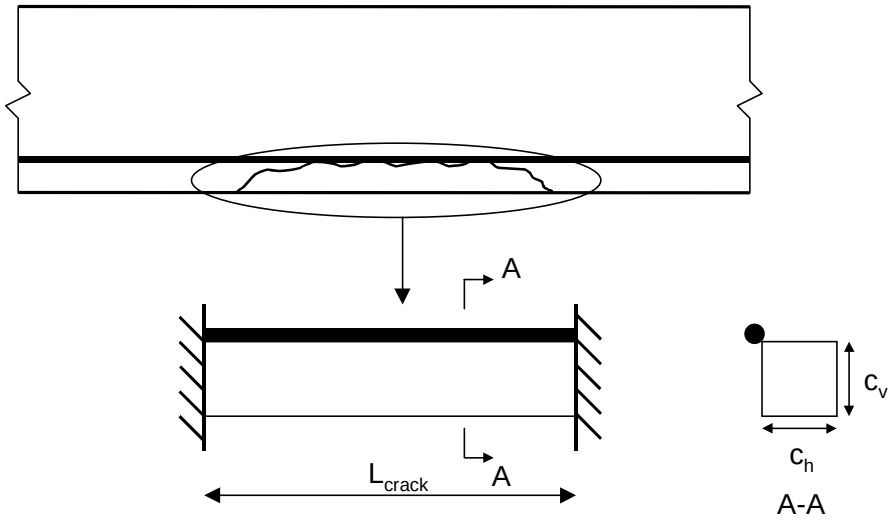

Figure 3-6: Idealisation of the spalling of cracked concrete cover to a corner bar

There will be two components of load acting on the cracked cover concrete: self-weight and the imposed deformation due to the radial expansion of the rust product. However, these two components will be bending about different axes as shown in Figure 3-7.

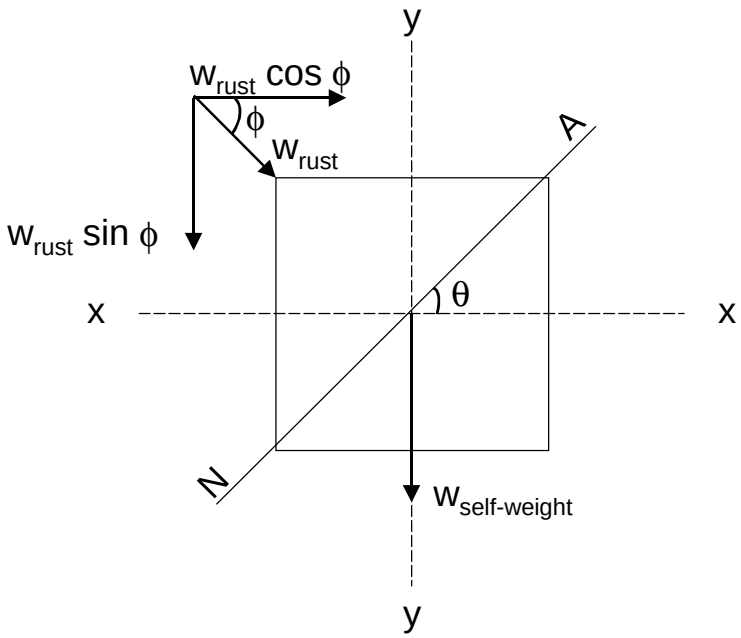

Figure 3-7: Components of bending in a section of cover concrete

The failure criterion of the cover concrete will be the lesser of the modulus of rupture or the

limiting shear stress at the supports. Raphael[86] obtained the following relationship between modulus of rupture and concrete cube strength from flexural tensile tests:

$$f_{ctr} = 0.437(0.8 f_{cu})^{2/3} \quad \textbf{… (3-21)}$$

Taylor[87] obtained the following relationship for the shear strength of unreinforced concrete from a series of tests:

$$f_{su} = 0.032 f_{cu} - 0.25 \quad \textbf{… (3-22)}$$

where: f_{ctr} = concrete modulus of rupture (N/mm^2)
f_{cu} = concrete cube strength (N/mm^2)
f_{su} = ultimate shear stress of unreinforced concrete (N/mm^2)

If the stresses induced by the self-weight of the cover concrete are calculated and subtracted from the allowable flexural stress the remaining stress capacity is available to resist the expansive forces generated by the rust.

Under self-weight the cover concrete will be bending about the x-axis as shown in Figure 3-7. For flexural failure, the maximum stress will occur in the top face at the support, and is given by:

$$\sigma_{flex.sw} = \frac{M}{Z} = \frac{\left[\frac{wL_{crack}^2}{12}\right]}{\left[\frac{c_h c_v^2}{6}\right]} = \frac{wL_{crack}^2}{2c_h c_v^2} \quad \textbf{… (3-23)}$$

where: c_h = horizontal cover to corroding bar
c_v = vertical cover to corroding bar
L_{crack} = length of crack
w = uniformly distributed self-weight

M	=	applied moment
Z	=	section modulus
$\sigma_{flex.sw}$	=	flexural stress induced by self-weight

The allowable flexural stress available to resist spalling is given by:

$$\sigma_{flex.spall} = f_{ctr} - \sigma_{flex.sw} \quad \text{… (3-24)}$$

The cover concrete will not be bending about its principal axes under the rust loading, but about a neutral axis (NA in Figure 3-7) inclined at an angle θ to the x-axis. The rust-induced load will be acting on the corner of the cover concrete at an angle ϕ to the x-axis. Assuming that the rust is exerting a uniform radial pressure, ϕ is taken as 45°. The rust product is assumed to be distributed along the crack according to a 4th power distribution such that the deflected profile of the cover concrete is compatible with the application of a uniformly distributed load.

The flexural stress induced in the cover concrete by the expansive rust products acting at an angle of ϕ and trying to spall concrete cover is given by:

$$\sigma_{flex.spall} = \frac{(M_{spall}\sin\phi)x}{I_y} + \frac{(M_{spall}\cos\phi)y}{I_x} \quad \text{… (3-25)}$$

Re-arranging, the moment induced by the expansive rust products is given by:

$$M_{spall} = \frac{\sigma_{flex.spall}}{\frac{x\sin\phi}{I_y} + \frac{y\cos\phi}{I_x}} \quad \text{… (3-26)}$$

For a built-in beam, M_{spall} is also given by:

$$M_{spall} = \frac{w_{flex.spall} L_{crack}^2}{12} \quad \text{… (3-27)}$$

Re-arranging, the maximum uniformly distributed load (udl) that the cover concrete can carry when bending is critical is given by:

$$w_{flex.spall} = \frac{12M_{spall}}{L_{crack}^2} \quad \textbf{… (3-28)}$$

where:

I_x	=	second moment of area of the cover concrete about the x-axis (mm^4)
I_y	=	second moment of area of the cover concrete about the y-axis (mm^4)
L_{crack}	=	length of the crack (mm)
M_{spall}	=	moment required to spall the cover concrete (Nmm)
$w_{flex.spall}$	=	equivalent udl (N/mm)
x	=	distance along the x-axis to the point where the stress is being checked (mm)
y	=	distance along the y-axis to the point where the stress is being checked (mm)
ϕ	=	angle between the line of action of the rust and the x-axis (45°)
$\sigma_{flex.spall}$	=	allowable flexural stress available to resist spalling stresses (N/mm^2)

The shear force acting on the cover concrete consists of two components: one in each of the x and y directions as follows:

$$V_x = V_{rust}\cos\phi \quad \textbf{… (3-29)}$$

$$V_y = V_{sw} + V_{rust}\sin\phi \quad \textbf{… (3-30)}$$

For a rectangular section the maximum elastic shear stress in each direction is 1.5 times the mean value such that:

$$v_x = \frac{1.5V_x}{c_h c_v} = v_{x.rust} \quad \textbf{… (3-31)}$$

$$v_y = \frac{1.5V_y}{c_h c_v} = v_{y.sw} + v_{y.rust} \quad \textbf{… (3-32)}$$

where:
- c_h = horizontal cover to corroding bar (mm)
- c_v = vertical cover to corroding bar (mm)
- v_x = elastic shear stress acting in the x direction (N/mm^2)
- $v_{x.rust}$ = elastic shear stress due to rust component acting in the x direction (N/mm^2)
- v_y = elastic shear stress acting in the y direction (N/mm^2)
- $v_{y.rust}$ = elastic shear stress due to rust component acting in the y direction (N/mm^2)
- $v_{y.sw}$ = elastic shear stress due to concrete self-weight acting in the y direction (N/mm^2)
- V_x = shear force acting in the x direction (N)
- V_y = shear force acting in the y direction (N)

The maximum shear stress is given by:

$$v_{\max} = \sqrt{v_x^2 + v_y^2} \quad \textbf{… (3-33)}$$

The limiting value of the shear stress is f_{su}, such that:

$$f_{su} = \sqrt{v_x^2 + v_y^2} \quad \textbf{… (3-34)}$$

Given that v_y comprises both self-weight and rust terms, the above expression can be given as:

$$f_{su} = \sqrt{v_{x.rust}^2 + (v_{y.sw} + v_{y.rust})^2} \quad \textbf{… (3-35)}$$

Squaring and expanding both sides, this gives:

$$f_{su}^2 = v_{x.rust}^2 + v_{y.sw}^2 + 2v_{y.sw}v_{y.rust} + v_{y.rust}^2 \quad \textbf{… (3-36)}$$

For the case considered here, ϕ is assumed to be equal to 45°. As a result, $\cos\phi = \sin\phi$, and thus $v_{x.rust} = v_{y.rust}$. Re-arranging and equating to zero:

$$2v_{x.rust}^2 + 2v_{y.sw}v_{x.rust} + (v_{y.sw}^2 - f_{su}^2) = 0 \quad \text{… (3-37)}$$

This can be solved as a quadratic equation to give $v_{x.rust}$. The resultant shear force, V_{spall}, is then given by:

$$V_{spall} = \frac{v_{x.rust}c_h c_v}{1.5\cos\phi} \quad \text{… (3-38)}$$

For a built-in beam, V_{spall} is also given by:

$$V_{spall} = \frac{w_{shear.spall}L_{crack}}{2} \quad \text{… (3-39)}$$

where: V_{spall} = shear force required to spall the cover concrete (N)

$w_{shear.spall}$ = equivalent udl (N/mm)

l

Re-arranging, the maximum udl that the cover concrete can carry when shear is critical is given by:

$$w_{shear.spall} = \frac{2V_{spall}}{L_{crack}} \quad \text{… (3-40)}$$

The critical udl, w_{spall}, which can be carried by the cover concrete, is the lesser of $w_{flex.spall}$ and $w_{shear.spall}$.

For compatibility the mid-span deflection of the cover concrete must be the same as the radial expansion of the bar. The radial stiffness of the expanding bar is likely to be considerably greater

than the flexural stiffness of the cover concrete and, as such, the effect of the relative stiffness can be ignored. Thus the radial expansion of the bar can be taken as the amount of rust generated, and is given by:

$$\delta_{spall} = \frac{w_{spall} L_{crack}^4}{384 E_{c.eff} I_{NA}} \quad \textbf{… (3-41)}$$

The second moment of area about an axis (in this case the neutral axis) can be calculated from the second moment of area about the principal axes, and is given by Case[88] as:

$$I_{NA} = I_x \cos^2\theta + I_y \sin^2\theta \quad \textbf{… (3-42)}$$

The angle of the neutral axis, θ, is given by:

$$\theta = \tan^{-1}\left[\frac{I_x \sin\phi}{I_y \cos\phi}\right] \quad \textbf{… (3-43)}$$

The amount of section loss to cause spalling, $dr_{spall,}$ is given by

$$dr_{spall} = \frac{1000\delta_{spall}}{2.84}(\mu m) \quad \textbf{… (3-44)}$$

However, it has been stated earlier in this Chapter that not all of the rust product induces stress, and an amount of rust product, δ_{pore}, is lost into the pores. As such, the radius loss to cause spalling is given by:

$$dr_{spall} = \frac{1000\delta_{spall} + \delta_{pore}}{2.84} = \frac{1000\delta_{spall} + \frac{44c}{D}}{2.84} \quad \textbf{… (3-45)}$$

where: c = the greater of the horizontal and vertical cover to bar (mm)

dr_{spall} = bar radius loss to cause spalling (μm)

D = bar diameter (mm)

E_{eff} = effective long-term elastic modulus of concrete (N/mm^2)

I_{NA} = second moment of area of the cover concrete about the neutral axis for rust-induced loading (mm^4)

w_{rust} = equivalent uniformly distributed load capacity available to resist rust (N/mm)

δ_{pore} = bar radius loss accommodated with concrete pores surrounding the bar (μm)

δ_{rust} = mid-span deflection corresponding to critical spalling load (μm)

δ_{spall} = bar radius loss corresponding to critical spalling load (μm)

This procedure has been implemented in a spreadsheet for a range of covers and crack lengths. Results are shown in Figure 3-8 for a C30 concrete with a 20 mm reinforcing bar. Flexure was found to be the critical failure mechanism in all cases. Figure 3-8 shows that less corrosion is required to spall covers with shorter crack lengths and greater thickness. It is likely that such cover concrete will be much more rigid, and the deflection at failure will be lower than their more flexible counterparts. Given that this process is deflection controlled, this is to be expected. It ties in with what is often observed in structures whereby most spalling is generally fairly small (a few hundred millimetres). This simple theory is, however, unable to take account of any horizontal splitting that may occur along the line of the reinforcing to accommodate the expansion. For smaller covers, the self-weight is predicted to dominate with longer crack lengths. This is shown in Figure 3-8 by the two lines for 10 mm cover.

The predicted radius losses required to induce cracking are also shown in Figure 3-8 for comparison purposes. For cracks up to 500 mm long there appears to be only a small difference in radius loss between that required for cracking and that required for spalling. Cabrera[26] has observed that the two cracks associated with a reinforcing bar do not reach the surface at the same time. However, it is unclear how much radius loss is required to induce the second crack. The radius loss between the first and second cracks would need to be added to the radius loss required to induce spalling to obtain a more realistic prediction of the time to spalling.

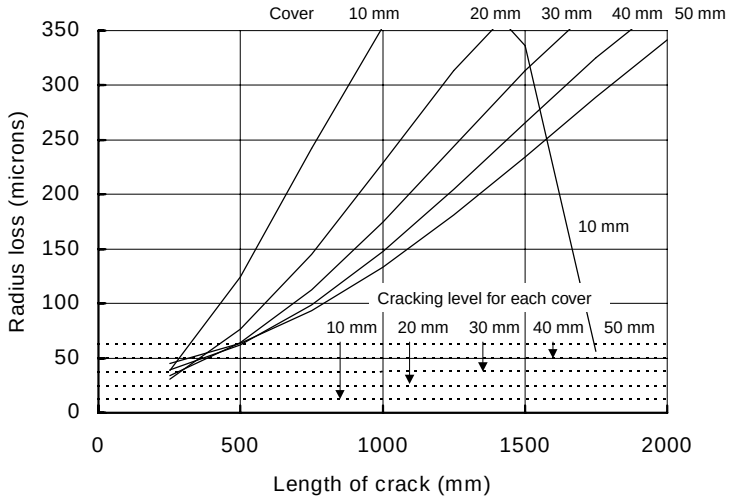

Figure 3-8: Predicted radius losses required to spall the cover concrete to a corner bar for various covers and crack lengths (C30 concrete and 20 mm reinforcing bar)

3.7 Conclusions

The following conclusions can be drawn from the work reported in this Chapter:

1. The amount of corrosion observed to cause cracking is substantially greater (typically an order of magnitude) than the amount of radial expansion theoretically required to induce cracking.

2. It is likely that the remainder of the rust product over and above that theoretically required to induce cracking will be accommodated in the concrete pore structure surrounding the bar.

3. A theory has been derived to estimate the amount of corrosion product that is accommodated within the pore structure.

4. The most significant variable in determining both the amount of corrosion product accommodated in the concrete pore structure and the amount of corrosion to cause cracking is the cover to bar diameter (c/D) ratio.

5. An estimate of the amount of corrosion required to cause cracking expressed as a percentage of the original bar area can be obtained by halving the c/D ratio.

6. A simplified theory can been derived to estimate the amount of corrosion required to cause the corner concrete to spall due to corrosion. The spalling theory indicated that corrosion over short lengths is more critical for spalling as the length of cover concrete is stiffer and will be able to absorb less rust-induced deflection.

7. The cracking and spalling theories can be used together to provide an estimate of the amount of in situ corrosion in concrete structures with corrosion-induced cracking.

4 BOND STRENGTH

4.1 Introduction

Design and assessment code rules are derived on the assumption that the strains in both concrete and reinforcement are the same, that is perfect bond exists between the two materials. However, corrosion can reduce the bond strength.

Checks on bond strength have been typically required in the following three situations:

i) *Anchorage lengths*: where reinforcement is curtailed.
ii) *Lap lengths*: where continuing bars are lapped.
iii) *Between adjacent flexural cracks*: where the reinforcement is required to transmit local bond forces between cracked areas.

Rules are given for the first two in BS 8110[69]. Checks on local bond have no longer been considered necessary in BS 8110[69] although they are still contained in BS 5400[97] and BD 44/95[73].

Bond is required for the main load-carrying mechanisms of bending, shear and axial load. These mechanisms do not require explicit checks in design provided that the code detailing clauses on anchorage lengths, lap lengths and minimum reinforcement levels are complied with. In the assessment of existing, and deteriorated, structures many of these clauses may not be complied with. In such cases, explicit checks on bond strength may well be required in order to calculate load-carrying capacities.

In this Chapter, the effects of corrosion on bond strength are considered in terms of how the clauses in BS 8110 could be modified to reflect the corroded behaviour.

4.2 Bond mechanisms

The two common types of reinforcement, plain and deformed bars, rely on different combinations of the bond mechanisms to carry load. Plain bars rely on friction and adhesion, whilst deformed

bars rely on friction, adhesion and mechanical interlock. Ribbed bars are the most commonly used deformed bars in current practice, and all of the literature on deformed bars reviewed in Section 2.4 related to ribbed bars. As such, the emphasis in this Thesis is put on ribbed bars. However, in the past other deformed bars such as square twisted deformed bars were used, and they may be found in the assessment of existing structures.

Plain bars tend to fail by the bar being pulled out through the concrete leaving little damage. Ribbed bars with low cover tend to fail as a result of longitudinal splitting cracks. If the cover is higher or links are present, a ribbed bar will pull out as a result of the ribs crushing the adjacent concrete. As one may expect, ribbed bars have higher bond strengths than plain bars of the same diameter.

In addition to the bar type effects, cover to bar diameter ratio, presence of links, lateral pressure, position in member, concrete tensile strength and bar embedment length all affect the bond strength as described in Table 4-1.

Table 4-1: Influence of various parameters on bond strength - uncorroded reinforcement

Parameter	*Effect on bond strength*	*Applicable to*	
		Plain	*Ribbed*
Cover to bar diameter (c/D) ratio[48]	The bond strength increases with increasing c/D ratio up to a limiting value of approximately 2.5, above which no enhancement occurs. At higher covers there is a tendency for bars to pull out rather than split the concrete.		✔
Links[48]	Links provide confinement to the concrete surrounding the longitudinal bar and intersect potential crack planes. As such, higher bond strengths can be achieved.		✔
Bar location[46]	Bars near the top of members tend to have lower bond strengths than bottom cast bars. The concrete surrounding top-cast bars is not as well compacted as that at the bottom of a member. In addition, plastic settlement can lead to reductions in bond strength.	✔	✔
Concrete tensile strength[48]	The bond strength increases with increasing tensile strength of the cover concrete for low c/D ratios.	✔	✔
Bar embedment length[50]	The further that the bar is embedded in concrete beyond the point at which it is required, the higher the bond forces which can be resisted (up to yield or slip).	✔	✔
Applied normal stress[89, 90]	Applied stress such as that at member supports provides a confining action and limits splitting cracking. This increases bond strength.	✔	✔
Dowel action	Dowel action, due to transmission of shear forces, is likely to increase the possibility of longitudinal splitting and thus reduce bond strength.	✔	✔

The influence of these individual parameters is not explicit in the BS 8110[69] approach to bond strength which is given by the following equation:

$$f_{bu} = \beta \sqrt{f_{cu}} \qquad \textbf{… (4-1)}$$

β takes different values depending on whether the reinforcement is plain, ribbed or fabric; and whether the bars are acting in tension or compression. In beams where the minimum level of links is not provided the bars have to be treated as plain bars irrespective of the type of bar used. The handbook[91] to BS 8110 gives the basis of the bond clauses as the work carried out by Reynolds[48] on laps in beams. The design formula for ribbed bars with no transverse shear reinforcement is based on the elastic partly cracked model of Tepfers[47], with the concrete tensile strength term expressed as a function of the compressive cube strength as follows:

$$f_{bu} = 0.2\,(0.5 + c/D)\sqrt{f_{cu}} \qquad \textbf{… (4-2)}$$

When nominal transverse (shear link) reinforcement is present, then an extra term, $0.2\sqrt{f_{cu}}$, is added to the basic equation to give:

$$f_{bu} = 0.2\,(0.5 + c/D)\sqrt{f_{cu}} + 0.2\sqrt{f_{cu}} \qquad \textbf{… (4-3)}$$

where: c = concrete cover to bar
D = bar diameter
f_{bu} = ultimate bond stress
f_{cu} = concrete cube strength

BS 8110[69] takes the default value of c/D as 1, and this gives the β value of 0.5 found in Table 3.26 of BS 8110. The previous three equations also contain a partial safety factor, γ_m, of 1.4. A reduction factor of 1.4 is proposed for top cast lapped bars where c/D is less than 2. BS 8110 ignores the beneficial effects of transverse compression at supports. However, simple supports may have a shorter anchorage length (12D) than is required in Table 3.26 of BS 8110. It is unclear

where this 12D requirement originates.

The ultimate bond strength has been calculated in accordance with BS 8110[69] for all of the test data on corroded bars collected in Section 2.4. The partial safety factor is set at 1.0 to allow comparisons. In Figure 4-1 the BS 8110 values are compared to the measured bond strengths obtained with corroded reinforcement.

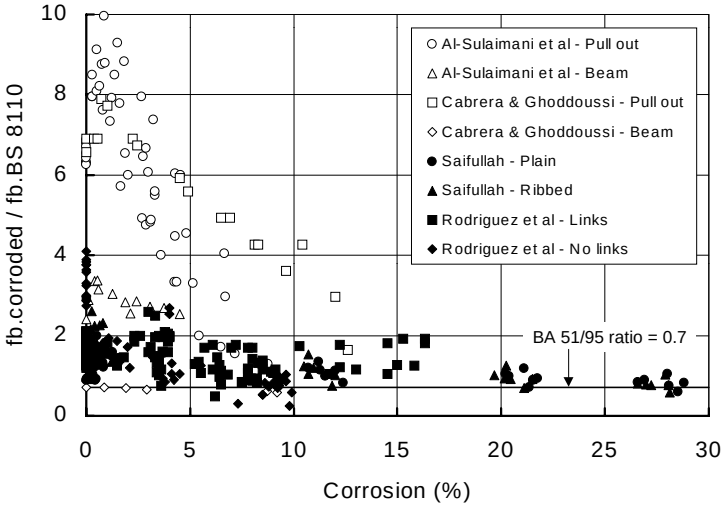

Figure 4-1: The effect of corrosion on the bond strength of reinforcing bars in comparison to the ultimate bond strength requirement of BS 8110 for all test data (reference numbers are given in Table 4-2)

It is interesting to note that the characteristic (5%) value of the ratio of corroded to BS 8110[69] bond strength considering all of the specimens is 0.74. Considering just the corroded specimens reported as cracked the characteristic value is 0.69. The value given in BA 51/95[77] for the ratio of corroded to BD 44[73] bond strength is 0.7 (BD 44 and BS 8110 both have the same approach to bond). This value was obtained at a time when considerably less data were available, and would thus appear to be validated to an extent by the additional data.

Many of the ratios in Figure 4-1 are well in excess of the ultimate bond strengths given in BS 8110. There are four potential reasons for this, and they need to be addressed when deriving modified procedures for use in BS 8110.

(i) A variety of different bond tests have been used, ranging from a bar embedded in the

centre of a cube to beam tests.

Whilst a variety of test procedures have been used in the past to obtain code values of bond strength, this Thesis is concerned with providing procedures for assessment based on current UK practice. In particular, the emphasis is on modifications to the procedures given in BS 8110[69]. Chana[46] has shown that the bond strengths obtained from his apparatus are compatible with those given in BS 8110. This apparatus simulates the segment of a beam adjacent to the support in a hogging region. Rodriguez et al[45] and Saifullah[35] have used similar apparatus.

(ii) Different corrosion rates have been used for the various tests.

This was discussed in Section 2.4. Saifullah and Clark[42] have highlighted the variations in bond strength with varying corrosion rate. Andrade et al[25] have also considered the effects of corrosion rate in relation to corrosion-induced cracking, and have made recommendations for the maximum accelerated corrosion rate (100 $\mu A/cm^2$) that can be used to give answers that are comparable with those obtained in real structures. This implies that those specimens with corrosion rates much above 100 $\mu A/cm^2$ should be viewed with a lower level of confidence.

(iii) The c/D ratio of many of the specimens was unrealistically high. The main longitudinal bars in structures tend to have c/D ratios in the range of 1 to 3, whereas some of the test specimens had c/D ratios of up to 7.

The specimens with unrealistic c/D ratios should be used qualitatively to gain an understanding of the effects of the c/D ratio, but not used quantitatively. The highest c/D ratios in structures are likely to be associated with shear links where values of up to 4 are possible. It is suggested that this is taken as an upper bound for the test results considered in the quantitative analysis.

(iv) Included in the test specimens are those in the pre-cracking stage where the corroded bond strength is higher than that in the corresponding uncorroded specimen.

In Section 2.4 a reduction in bond strength was found to occur only after cracking. As such, it

would seem reasonable to consider only those specimens where cracking was observed. Before cracking, the engineer is unlikely to be concerned about the effects of corrosion on bond strength.

The data concerning these four points are summarised in Table 4-2 for each of the researchers who presented quantitative information.

Table 4-2: Comparison of accelerated bond test procedures

Researchers	*Test method*	*Corrosion rate (mA/cm^2)*	*c / D ratios tested*	*Cracking recorded*
Al-Sulaimani et al[39]	Central bar pullout	2	3.25, 4.78 & 7.0	Yes
Al-Sulaimani et al[39]	Beam with two-point loading. Unclear where the anchorage length is measured from.	2	2.42	Yes
Cabrera and Ghoddoussi[40]	Central bar pullout	Unknown, but potential applied rather than current	5.75	Yes
Cabrera and Ghoddoussi[40]	Beam with two-point loading. Bar debonded past support.	Unknown, but potential applied rather than current	2.08	Yes
Rodriguez et al[45]	Corner bar pullout test (as used by Chana).	0.1	0.5, 1.0 & 2.0	Yes
Saifullah[35]	Corner bar pullout test (as used by Chana).	0.5	1.5	Yes

The series of tests carried out by Rodriguez et al[45] and Saifullah[35] address all four of the points made above, and are also the most comprehensive of those available as can be seen from the band near the bottom of Figure 4-1. Al-Sulaimani et al[39] have used a high corrosion rate and

unrealistic central bar pullout specimens. Their beam specimens are not described adequately for the data to be used with confidence. Cabrera and Ghoddoussi[40] have applied a potential rather than a current. This can have quite different effects on the corrosion (Andrade[92]). They have also used unrealistic pullout specimens. Their beams are debonded beyond the supports which is where the anchorage length would usually be required. This makes the tests difficult to interpret. Al-Sulaimani et al[39] do not state how they determined the amount of corrosion. Cabrera and Ghoddoussi[40] measured the amount of weight lost due to corrosion for the pullout specimens, but carried out calculations using Faraday's law to determine corrosion for the beam specimens. Saifullah[35] and Rodriguez et al[45] measured weight loss on all of their specimens. Andrade[92] has suggested that, based on her experience, only weight loss measurement gives satisfactory accuracy. Calculating weight loss on the basis of Faraday's law is too variable given the small amounts of corrosion involved.

It is thus proposed that only the test data of Rodriguez et al[45] and Saifullah[35] be used for the quantitative analyses. All of the available data will be used for the parametric (qualitative) analyses.

4.3 Parameter study

The key parameters describing the effect of corrosion on bond strength have been identified in Section 2.4, whilst the key parameters in the BS 8110[69] expression are identified in Section 4.2. The important parameters are thus considered to be:

(i) Cover to bar diameter (c/D) ratio
(ii) Concrete tensile strength
(iii) Amount of corrosion
(iv) Rate of corrosion

In addition, there are other parameters such as bar type and presence of links that will be dealt with in later sections of this Chapter.

The proposals in the following sections are intended to provide values for bond strength that can

be used in place of the values in Table 3.26 in BS 8110[69] when reinforcement corrosion is present. No bond tests have been carried out on corroded bars in compression and, as such, the proposals are only applicable to bars in tension. Only the post-cracking state is considered. Prior to this bond strength appears to be enhanced by corrosion and there should be little effect on safety.

(i) Cover to bar diameter (c/D) ratio

The effect of the c/D ratio on bond strength is shown in Figure 4-2. Whilst there is considerable scatter, there does appear to be a distinct trend of bond strength increasing with increasing c/D ratio.

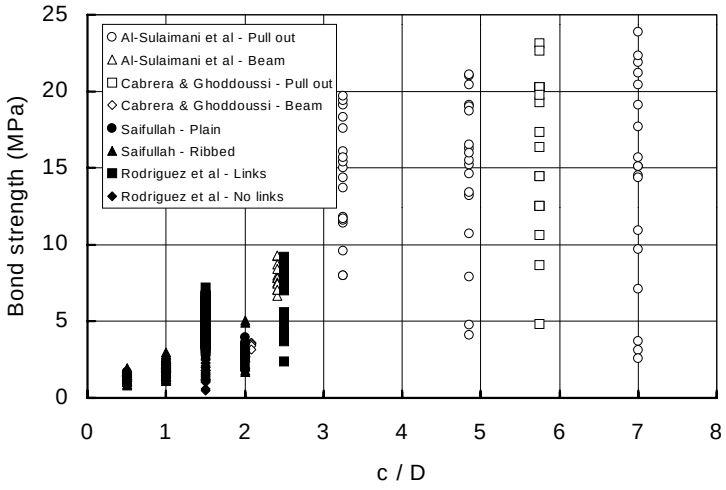

Figure 4-2: The effect of c/D ratio on the bond strength of corroded and non-corroded reinforcement bars

(ii) Concrete tensile strength

The effect of the concrete tensile strength on bond strength is shown in Figure 4-3. Whilst, again, there is considerable scatter, there does appear to be a trend of bond strength increasing with increasing tensile strength for the Rodriguez et al[45] and Saifullah[35] data.

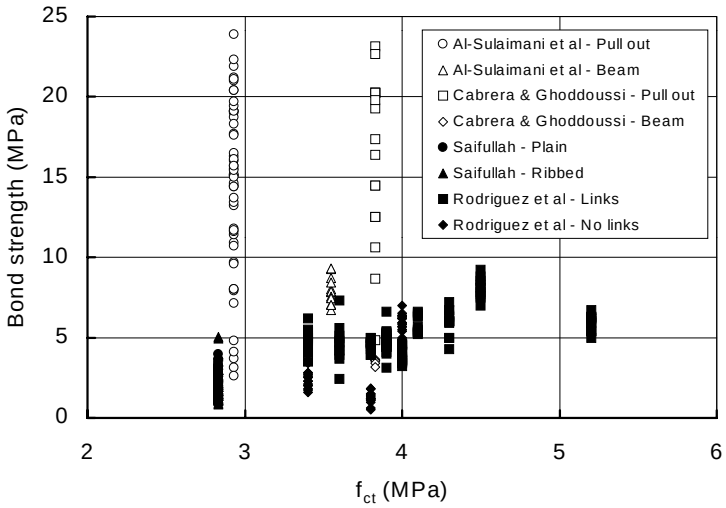

Figure 4-3: The effect of concrete tensile strength on the bond strength of corroded and non-corroded reinforcement bars

(iii) Amount of corrosion

The effect of the amount of corrosion on bond strength is shown in Figure 4-4. In addition to the scatter found in the previous two figures, there also appears to be two distinct groupings. The central bar pullout specimens of Al-Sulaimani et al[39] and Cabrera and Ghoddoussi[40] have considerably higher bond strengths than their accompanying beam tests, or the corner bar pullout tests of Rodriguez et al[45] and Saifullah[35]. It may well be that this is due to the high c/D ratios used in the central bar pullout specimens. However, both groupings show a distinct trend of bond strength decreasing with increasing corrosion.

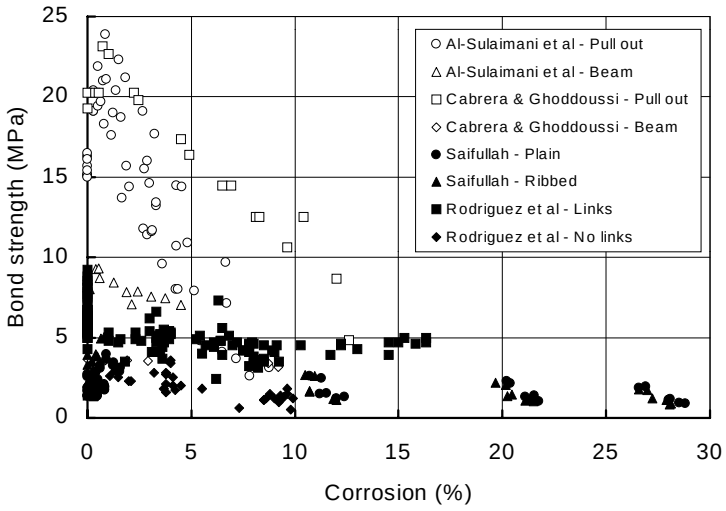

Figure 4-4: The effect of corrosion on the bond strength of reinforcement bars

(iv) Rate of corrosion

The variation in bond strength caused by accelerating the corrosion at different rates was discussed in Section 2.4. Saifullah and Clark[42] tested specimens at a variety of corrosion rates to determine the relative effects. As with other researchers, they found that the reduction in bond strength was linear once the specimen had cracked. This meant that specimens could be tested at around 5% and 20% section loss at various corrosion rates, and linear expressions could be derived for the ratio of corroded to uncorroded bond strength. The expression used is:

$$Rb = A_1 + A_2 corr \qquad \text{… (4-4)}$$

where: Rb = ratio of corroded to uncorroded bond strength

A_1 = a variable (function of the corrosion rate)

A_2 = a variable (function of the corrosion rate)

corr = amount of corrosion (%)

Saifullah tested his main set of specimens at 0.5 mA/cm^2 whilst Rodriguez et al tested theirs at 0.1 mA/cm^2. The values of A_1 and A_2 for a corrosion rate of 0.1 mA/cm^2 were found to be 1.112 and –0.024 respectively. The corresponding values for a corrosion rate of 0.5 mA/cm^2 were found to be 0.953 and –0.014. Values of Rb are shown in Figure 4-5 for the range of corrosion

levels used by Rodriguez et al[45] and Saifullah[35] in their tests.

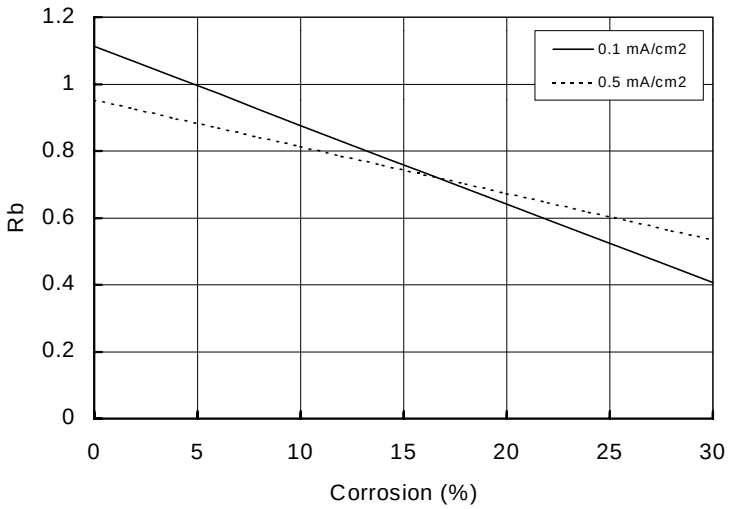

Figure 4-5: Possible variations in the ratios of corroded to uncorroded bond strength for corrosion rates used by Rodriguez et al[45] ($0.1mA/cm^2$) and Saifullah[35] ($0.5mA/cm^2$)

The decision has to be made as to whether the bond strengths should be normalised to a single reference corrosion rate for comparison purposes. Whilst there is divergence either side of 17% corrosion this has to be viewed in the light of the variability obtained in bond tests. Chana[46] recommends that at least three specimens be cast for ribbed bars (six for plain) to give confidence limits of ±20% for 95% probability. If the variability associated with the accelerated corrosion process is added to this, it would suggest that a high variability should be expected. In such a case the inherent variability in the test procedure is likely to be substantially larger than any differences caused by variations in the corrosion rates used by the two researchers. As such, it is concluded that the differences between the corrosion rates on Rb will be sufficiently small when comparing the data of Saifullah[35] and Rodriguez et al[45] that the differences can be ignored.

4.4 Ribbed bars without links

The background to BS 8110[69] discussed in Section 4.2 indicates that ribbed bars with links are treated as having two discrete components contributing to bond strength: a term for the ribbed bars alone plus a term for the links on their own. No interaction is considered. Ribbed bars are treated separately in this section, whilst the additional contribution of the links is dealt with in

section 4.5.

The parameters in Tepfers[47] expression, c/D ratio and tensile strength, are applicable both to the bond strength of uncorroded and corroded bars. As such, it is proposed to use Tepfers expression with a modification factor to allow for the influence of corrosion. In this way, continuity can be achieved with the expression behind the BS 8110 value of bond strength. An expression is sought such that:

$$f_b = f(corrosion)0.6\left(0.5 + \frac{c}{D}\right)f_{ct} \qquad \textbf{… (4-5)}$$

where: f_b = corroded bond strength (N/mm^2)

f(corrosion) = function of the amount of bar corroded

c/D = cover to bar diameter ratio

f_{ct} = concrete tensile strength (N/mm^2)

For convenience, the function f(corrosion) and the constant of 0.6 are combined together to give the variable, k, such that:

$$f_b = k\left(0.5 + \frac{c}{D}\right)f_{ct} \qquad \textbf{… (4-6)}$$

k was found to vary linearly with each of the four variables (percentage corrosion, radius loss, corroded area and percentage radius loss) that it was compared with. Linear regression analysis was applied to each of the four variables, and the following expression gave the best fit with a correlation coefficient, r^2, of 0.712:

$$k = 0.44 - 0.015Acorr \qquad \textbf{… (4-7)}$$

This expression is shown plotted in Figure 4-6.

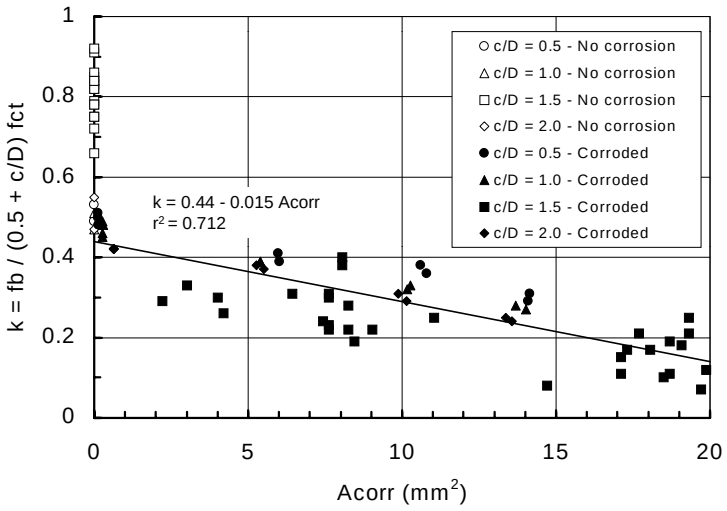

Figure 4-6: The relationship between Acorr and k for ribbed bars (c/D = 0.5, 1.0 and 2.0 from Saifullah[35]; c/D=1.5 from Rodriguez et al[45])

The expression for estimating bond strength is given below, and compared with the test data in Figure 4-7:

$$f_b = (0.44 - 0.015Acorr)\left(0.5 + \frac{c}{D}\right)f_{ct} \qquad \textbf{… (4-8)}$$

where: f_b = the corroded bond strength (N/mm^2)

Acorr = area of the of bar corroded (mm^2)

c/D = the cover to bar diameter ratio

f_{ct} = the concrete tensile strength (N/mm^2)

There is a tendency for some of the specimens tested by Rodriguez et al[45] to have lower bond strengths than those derived from the expression for corroded bond strength. However, when the lower bound expression for the bond strength (derived form the 5% characteristic) is used the estimates are much safer. This is shown in Figure 4-8 based on the following expression:

$$f_b = (0.31 - 0.015Acorr)\left(0.5 + \frac{c}{D}\right)f_{ct} \qquad \textbf{… (4-9)}$$

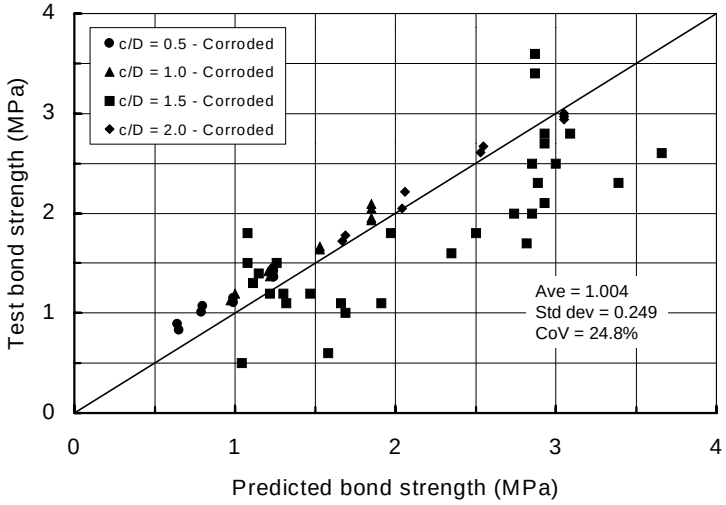

Figure 4-7: Comparison between predicted bond strength and test bond strengths for corroded ribbed bars with no links (c/D = 0.5, 1.0 and 2.0 from Saifullah[35]; c/D=1.5 from Rodriguez et al[45])

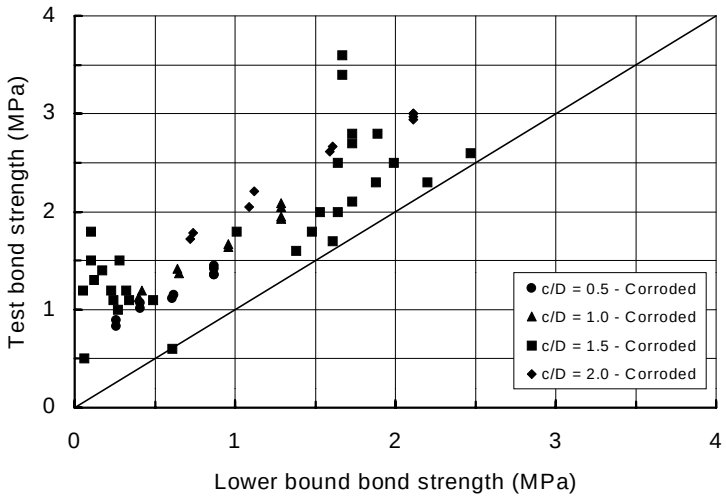

Figure 4-8: Comparison between predicted lower bound bond strength and test bond strength for corroded ribbed bars with no links (c/D = 0.5, 1.0 and 2.0 from Saifullah[35]; c/D=1.5 from Rodriguez et al[45])

The tendency for more of the predictions for the specimens tested by Rodriguez et al to be below the equality line in Figure 4-7 than for Saifullah's specimens could be due to the form of expression selected. Acorr represents the amount of bar area lost due to corrosion. It is likely that the ribs will corrode first. Different nominal diameters will have different rib areas and will

require different amounts of Acorr to corrode those rib areas. Perhaps a composite expression is required whereby the reduction in bond is related to a term for removal of the rib area plus a term relating to further corrosion necessary to reduce the bond resistance to zero. However, at least one other set of data with different bar diameters is required to check this hypothesis.

4.5 Ribbed bars with links

Tests by Rodriguez et al[45] indicate that links make a substantial contribution to the bond strength of corroded ribbed reinforcement. This is shown in Figure 4-9. When links are present, there is only a small reduction in bond strength below the uncorroded specimens. The contribution of links to the bond strength of corroded reinforcement is significantly more than the contribution to uncorroded reinforcement in this set of data.

As there is only one set of data with links, and the links were uncorroded, it is difficult to determine what level of link reinforcement is required to maintain bond strength. Another potential complication is that links have a tendency to corrode at corners where they are in contact with longitudinal reinforcement. Further bond tests are required with several levels of concrete strength and several levels of link corrosion.

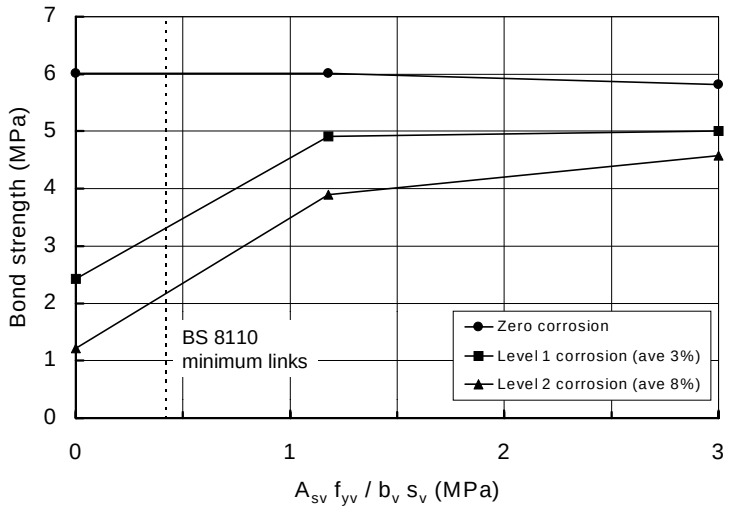

Figure 4-9: The effect of corrosion on the bond strength of ribbed reinforcing bars with links (Rodriguez et al[45])

In lieu of further data, it would seem reasonable to suggest that the following procedures are only valid when a minimum area of link reinforcement is present. When the area of link reinforcement is less than this minimum value, then the bars will have to be treated as ribbed bars without links. This is a similar principle to the rules in Table 3.26 of BS 8110[69] where ribbed bars with links less than the nominal level are treated as plain bars.

Two approaches are possible. Firstly, a conservative approach where the engineer is not able to ascertain how much link reinforcement is present, but feels confident that it is above the minimum level. The bond strength increases by an amount commensurate with the minimum level of links regardless of what level of links are present above the nominal. Secondly, an approach is required that takes into account the amount of link reinforcement present.

As Rodriguez et al[45] carried out their tests at one concrete strength, it is not clear whether the increase in bond strength should be $0.2\sqrt{f_{cu}}$, as used in BS 8110[69], or not. It is possible that links will restrict cracking locally around the corroding longitudinal reinforcement thus increasing the confinement of that reinforcement. Whilst the ribs are still present on the longitudinal reinforcement, it is possible to visualise that bond strength will be a function of the ribs shearing against the concrete (and thus the concrete tensile strength). When the ribs are corroded away, it is not so easy to visualise the mechanism, and perhaps the bond enhancement is more due to enhanced confinement of the corrosion product.

The data plotted in Figure 4-10 show that the increase in bond strength with increasing links is not linear. This makes it difficult to extrapolate the enhancement down to the level of minimum links. A curve has been drawn through the experimental data, and when the links correspond to the BS 8110 minimum ($(A_{sv}\ f_{yv}) / (b_v\ s_v) = 0.4$, BS 8110 Table 3.7) the bond enhancement is approximately 1 N/mm^2. This is likely to prove conservative for low levels of link corrosion. If data become available from bond tests with varying levels of corroding links, then this value should be reviewed.

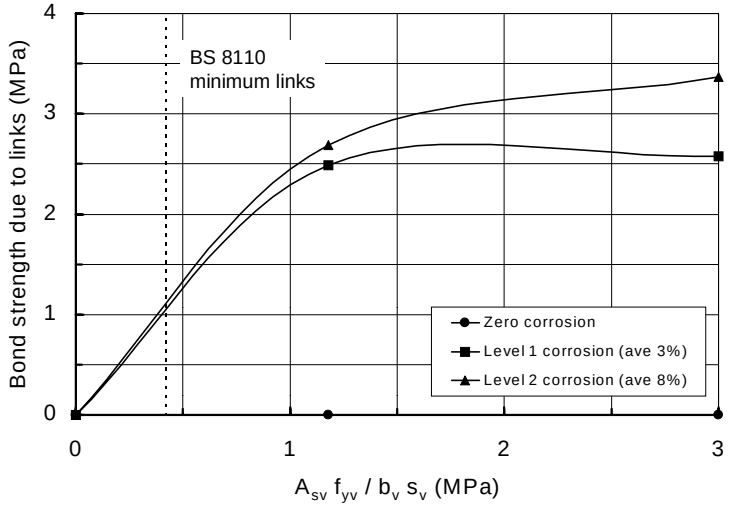

Figure 4-10: The enhancement of corroded bond strength due to the presence of links for varying levels of corrosion (Rodriguez et al[45])

Based on his measurements of the force in links at the ultimate bond strength, Reynolds[48] suggested that the bond strength of ribbed bars be enhanced by an amount $f_{b.link}$ given by:

$$f_{b.link} = \frac{22 A_{sv}}{s_v D} \qquad \textbf{… (4-10)}$$

where: $f_{b.link}$ = bond strength contributed by the link reinforcement (N/mm^2)
A_{sv} = area of link reinforcement (mm^2)
s_v = spacing of the link reinforcement (mm)
D = diameter of the longitudinal reinforcement confined by the links (mm)

The concrete and link component are thus treated as independent of one another. The constant 22 is a lower bound value corresponding to a stress in the links of 70 N/mm^2. Reynolds[48] measured higher stresses in the links at the ultimate load. However, the stress appeared to vary depending on the location of the links. Links within high shear zones (near supports) had much higher stresses in them than those in lower shear zones (near mid-span). Reynolds suggests that this increase in link stress was due to the opening of diagonal shear cracks near supports. In low shear zones, the links were only required to resist bond-splitting cracks. Given that the procedures given in BS 8110[69] are intended to be applicable to all situations, it seemed prudent

to select the lower bound value of 22. In BS 8110[69] the expression for link enhancement is then expressed as a function of $\sqrt{f_{cu}}$ (i.e. $0.2\sqrt{f_{cu}}$) for simplicity.

The longitudinal bar contribution to the bond strength was assumed to be given by the expression derived in Section 4.4. Combining this with Reynolds expression for the link contribution gives the following expression for the bond strength of corroded ribbed bars with links:

$$f_b = (0.44 - 0.015Acorr)\left(0.5 + \frac{c}{D}\right)f_{ct} + \frac{k_{link}A_{sv}}{s_v D} \qquad \textbf{… (4-11)}$$

The test data of Rodriguez et al[45] were analysed using linear regression analysis with no intercept, and k_{link} was found to be 75.1 with a correlation coefficient, r^2, of 0.781. Thus the bond strength of the corroded ribbed bars with links tested by Rodriguez et al[45] can be expressed as:

$$f_b = (0.44 - 0.015Acorr)\left(0.5 + \frac{c}{D}\right)f_{ct} + \frac{75A_{sv}}{s_v D} \qquad \textbf{… (4-12)}$$

A comparison of measured and predicted values is shown in Figure 4-11.

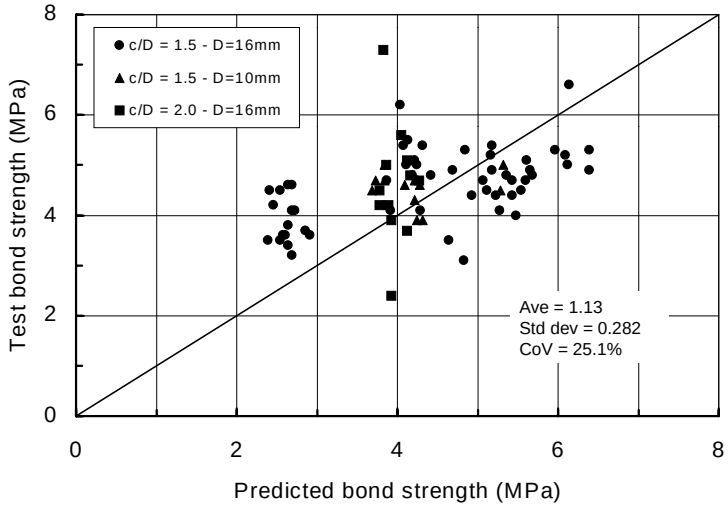

Figure 4-11: The comparison of test and predicted bond strength for corroded ribbed bars with uncorroded links (Rodriguez et al[45])

A lower bound relationship is required for assessment. In addition, further test data are required

to validate the value of k_{link} obtained here. As such, it may be prudent to use the bond enhancement of 1 N/mm^2 for all levels of link reinforcement above the minimum level. For the test data considered here this gives a similar answer to taking k_{link} as 22.

4.6 Plain bars

As only one set of experimental data is available, that of Saifullah[35], the following discussions should be viewed as indicative rather than definitive, and should be reviewed as more test data become available. As with the ribbed bars, only the post-cracking stage is considered.

In Section 2.4 it was noted that the bond strength and behaviour of the specimens with plain bars tested by Saifullah[35] were similar to those of the ribbed bars tested as part of the same programme. In addition, there is a distinct relationship with the c/D ratio shown in Figure 4-2. As such, it would seem reasonable to adopt the same approach as adopted for ribbed bars; i.e. modify the Tepfers[47] expression.

It is interesting to note that whilst the c/D ratio does not appear to be important for uncorroded plain bars, it is important when plain bars have corroded. This could be due to a combination of the uneven nature of the corrosion leading to a ribbed effect and the migration of the corrosion product into the surrounding concrete giving a composite material with enhanced bond characteristics as found by Williamson[93].

The relationship between the Tepfers model and the effects of corrosion on the bond strength of plain bars was determined using linear regression giving the following relationship between k and Acorr ($r^2 = 0.524$).

$$k = 0.45 - 0.011Acorr \qquad \textbf{… (4-13)}$$

The proposed best fit relationship for the bond strength of plain subject to corrosion is:

$$f_b = (0.45 - 0.011Acorr)\left(0.5 + \frac{c}{D}\right)f_{ct} \qquad \textbf{… (4-14)}$$

This is compared to the test data in Figure 4-12. It is very similar to the relationship for ribbed bars. However, the bond strength of plain bars appears to diminish at a slightly slower rate with increasing corrosion.

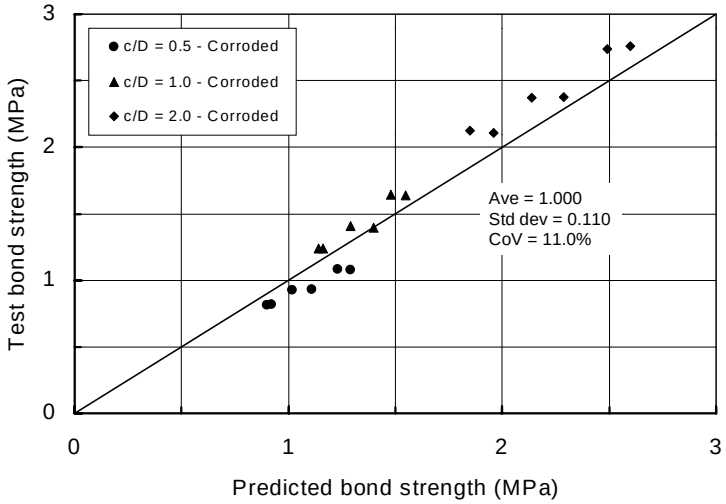

Figure 4-12: Comparison between predicted and test bond strength for the corroded plain bars tested by Saifullah[35]

Whilst a reasonable correlation is obtained, it is not possible to evaluate the effect of concrete tensile strength as only one tensile strength was used by Saifullah. The only parameter that is varying in the Tepfers expression is the c/D ratio. If the assumption that corroded plain bars behave in a similar manner to corroded ribbed bars is to be made, then the assumption must be made that the bond strength will vary with concrete tensile strength.

As with the ribbed bars, a lower bound expression for the corroded bond strength is derived to give a 95% characteristic value via the following expression:

$$f_b = (0.36 - 0.011Acorr)\left(0.5 + \frac{c}{D}\right)f_{ct} \qquad \textbf{… (4-15)}$$

This expression is compared to the test data in Figure 4-13. It gives higher predicted bond strengths than the corresponding lower bound expression for ribbed bars. It is likely that this is due to the greater scatter in the ribbed bar data being reflected in the lower bound expression.

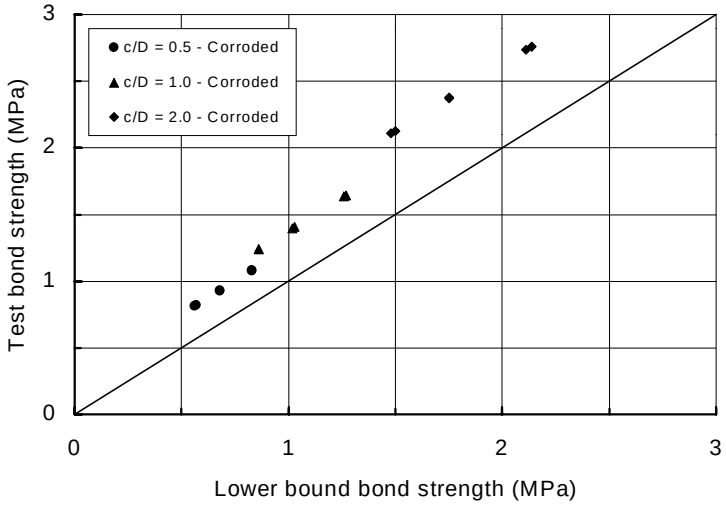

Figure 4-13: Comparison between lower bound and test bond strength for the corroded plain bars tested by Saifullah[35]

4.7 Integrating new bond rules into BS 8110

In design, anchorage bond is achieved by ensuring that a specified anchorage length is provided. However, in assessment the anchorage length provided will not necessarily be as large as that required in current design codes. Design codes provide safe and satisfactory solutions at the design stage. However, inherent conservatism in current design codes can result in perfectly adequate structures being condemned because they do not comply with them. This leads to two complications when assessing deteriorated structures:

(i) Even with no deterioration the anchorage bond would be considered inadequate if the anchorage length did not comply with current codes.

(ii) Corrosion can lead to reductions in bond strength.

The first point is beyond the scope of this Thesis. However, in the assessment of UK bridges inadequate anchorage lengths are a far bigger problem than bond reductions due to deterioration. The second point has been addressed in the previous sections of this Chapter.

Perhaps in the future bond should be considered as a subject in its own right to address a whole range of issues associated with both sound and deteriorated structures. Until such time as work

is undertaken to develop realistic bond rules for assessment, the engineer is left with no choice but to assume that the current code rules are satisfactory and use those as a basis for assessing corroded structures (with some modifications).

There are several problems with the bond rules given in UK codes that make conversion to assessment rules more difficult. These are given, along with potential solutions:

(i) There is no standard bond test on which the code bond values are based.

This prevents direct comparison with test carried out on corroded elements. However, bond strengths obtained from the corner bar pullout tests (Chana[46]) do correspond reasonably well with those given in UK codes.

(ii) The beneficial effects of increased cover to bar diameter (c/D) ratio are not considered in codes.

UK codes are calibrated on the basis of a c/D ratio of 1.0. This can result in over conservatism in sound structures, and the anomaly that corroded structures have a higher predicted bond strength than sound ones if the c/D ratio is considered for the deteriorated structure. The handbook[91] to BS 8110[69] indicates that the code rules are based on a version of Tepfers[47] partly cracked elastic solution. If the original expression behind BS 8110[69] is used rather than the simplified one (as included in BS 8110) then the beneficial effects of increased c/D ratios can be considered in sound structures.

(iii) The beneficial effects of transverse confinement due to support reactions are not considered explicitly in UK codes.

Implicitly this is considered, as the required anchorage length at simple supports is smaller than the value calculated from the general anchorage length rules. Whilst the general anchorage length rules are related to the grade of concrete, only a single value related to either bar diameter or effective depth is given for the simple support anchorage rules. As such, it is not possible to

establish a unique relationship between the general rules and those for simple supports.

(iv) The beneficial effects of transverse reinforcement are not addressed explicitly.

Tests have shown that the provision of transverse reinforcement can enhance the bond strength of ribbed bars. However, the UK codes only recognise two levels of enhancement: zero, when the level of transverse reinforcement is below the specified minimum and a value of $0.2\sqrt{f_{cu}}$ above this level. This implies that there are no benefits to be gained from levels of transverse reinforcement above the minimum. It also implies that the enhancement ceases to exist as soon as the level of transverse reinforcement is below the code minimum. Reductions below the minimum could be possible due to corrosion, or to existing structures that were designed to older codes that required less reinforcement. The cut-off level leads to a sudden drop in calculated load-carrying capacity that is unlikely to be realistic. In the absence of test data, there would appear to be little that can be done to rectify the situation currently.

(v) There is no consistent approach to incorporating experimental data into UK codes.

A consistent approach to incorporating experimental data is required. If the partial safety factors are set to unity in UK codes, then the formulae can be compared to the available test data. However, it is not always clear whether mean, characteristic or lower bound values have been used.

4.8 Conclusions

The following conclusions can be drawn from the work reported in this Chapter:

1. The ratio of corroded to code bond strength of 0.7 given in BA 51/95[77] corresponds to a lower bound (5% characteristic) to the available test data.

2. For the two sets of data considered for quantitative analysis the differences in bond strength due to differences in corrosion rates could be ignored due to the overall level of variability of the results.

3. The corroded bond strength increases with increasing c/D ratio.

4. The corroded bond strength increases with increasing concrete tensile strength.

5. The corroded bond strength of ribbed bars without links can be related to the Tepfers[47] bond strength by using a variable that is a function of the area of steel lost due to corrosion. This gives the best fit to the test data.

6. The corroded bond strength of ribbed bars is enhanced due to the presence of links. The enhancement appears to be more significant at lower levels of link reinforcement.

7. A bond enhancement of 1.0 N/mm^2 has been extrapolated from the test data for the point where the minimum amount of links, as specified in BS 8110, is present.

8. A more rigorous means of assessing the bond enhancement due to links is proposed. The proposal requires further data to validate it, in particular data with varying amounts of link corrosion.

9. Due to the lack of test data it is not possible to make recommendations for assessing the bond strength of ribbed bars with links when the level of link reinforcement is less than the minimum amount required in BS 8110.

10. The corroded bond strengths of ribbed and plain bars are similar.

5 FLEXURAL STRENGTH

5.1 Introduction

Flexure is typically critical at mid-span, and at the supports of continuous members. It will dictate how much tension (and compression) reinforcement is included in a member. Corrosion-induced reductions in tension (and compression) reinforcement could reduce the flexural load-carrying capacity of a member.

5.2 Flexural mechanisms

In order to produce a ductile member with plenty of warning of failure, a combination of tension and compression reinforcement is required which permits extensive cracking and deflection before failure. This is achieved in codes such as BS 8110[69] by ensuring that members are under-reinforced. That is, the reinforcement yields in tension before the concrete crushes in compression. Over-reinforced members fail by crushing of the concrete before yielding of the tension reinforcement. This gives little warning of failure, is not ductile and should be avoided. Compliance with code clauses limits the amount of reinforcement and the size of the concrete compression zone such that compliant designs are under-reinforced.

In order to illustrate the concepts, a singly reinforced section is considered. Re-arranging the formulae in Section 3.4.4.4 of BS 8110[69] such that the moment capacity is the subject rather than reinforcement area, we get:

$$M = (f_y / \gamma_{ms}) A_s z \qquad \text{… (5-1)}$$

and

$$z = \left[1 - \frac{0.75 (f_y / \gamma_{ms}) A_s}{(f_{cu} / \gamma_{mc}) bd}\right] d \qquad \text{… (5-2)}$$

where: A_s = area of tension reinforcement (mm^2)

b = width or effective width of the section (or flange) in the compression zone (mm)

d = effective depth of the tension reinforcement (mm)

f_{cu} = characteristic compressive cube strength of concrete (N/mm^2)

f_y = characteristic strength of reinforcement (N/mm^2)

z = the lever arm between the compression and tension zones (mm)

γ_{mc} = partial safety factor for strength of concrete

γ_{ms} = partial safety factor for strength of reinforcement

The equation for bending resistance is essentially the force in the tension reinforcement multiplied by the lever arm between the centroid of the steel and concrete forces. For doubly reinforced members, flanged members and members of general shape, the same principles of equating tension and compression forces to ensure equilibrium, and summing their moments applies. However, the approach is a little more complex and a strain compatibility method may need to be applied. Such an approach has been implemented in the spreadsheet *BEAMCOL_CORR* included in Appendix B.

The starting point is to consider the physical behaviour of reinforced concrete beams with corroded reinforcement, both in laboratory specimens and real structures. It is important to note that despite the link reinforcement corroding, vertical cracking is not always evident. The links will, because of their relatively small size, have higher cover to bar diameter (c/D) ratios than the main bars. In Section 3 it was found that the corrosion to cause cracking was directly proportional to the c/D ratio. Hence, it is not unreasonable for the concrete cover to the links to be uncracked whilst the cover to the longitudinal reinforcement is cracked. Cracking along the longitudinal reinforcement was observed in many of the tests carried out by Rodriguez et al[45] and Daly[64]. However, no spalling of the cover concrete was reported.

The physical parameters that may be affected by corrosion are listed in Table 5-1. If corrosion of the reinforcement in the compression zone has caused cracking, spalling may follow either due to the expansive rust product or lateral expansion of the compression reinforcement forcing the concrete cover off. This will partially reduce the breadth of concrete available in the

compression zone. Rodriguez et al[45] suggest that this loss should be considered in any calculations. However, it is likely that this will have little effect on the flexural load-carrying capacity of under-reinforced members as the load-carrying capacity is primarily controlled by the tension reinforcement. The reinforcement area will reduce due to corrosion. This reduction can vary considerably depending on whether pitting corrosion is present or not. The effective depth to the reinforcement, d, is unlikely to be affected unless most of the cover in the compression zone is lost. The concrete strength is unlikely to be affected.

Table 5-1: Effects of corrosion on flexural strength parameters

Parameter	*Effects of corrosion*
b	Possibly reduced in compression zone due to spalling at corners.
d	As uncorroded unless majority of cover in compression zone is lost.
A_s	Reduced cross-section.
f_y	As non-corroded.

5.3 Singly-reinforced members

Whilst the tests of several researchers are reviewed in Section 2.5, only Rodriguez et al[45] and Daly[64] provide sufficient data to undertake the detailed calculations necessary to develop an assessment method. Rodriguez et al[45] used compression reinforcement in their tests whilst Daly[64, 66] did not. The tests without compression reinforcement give an indication of whether flexural load-carrying capacity in singly reinforced members decreases in proportion to the amount of corrosion in the tension reinforcement. The ratio of test to predicted load-carrying capacity is shown in Figure 5-1 for both those beams tested as part of the flexural series[64, 66], and those beams tested as part of the shear series[66] but which actually failed in flexure. The relevant statistics are given in Table 5-2.

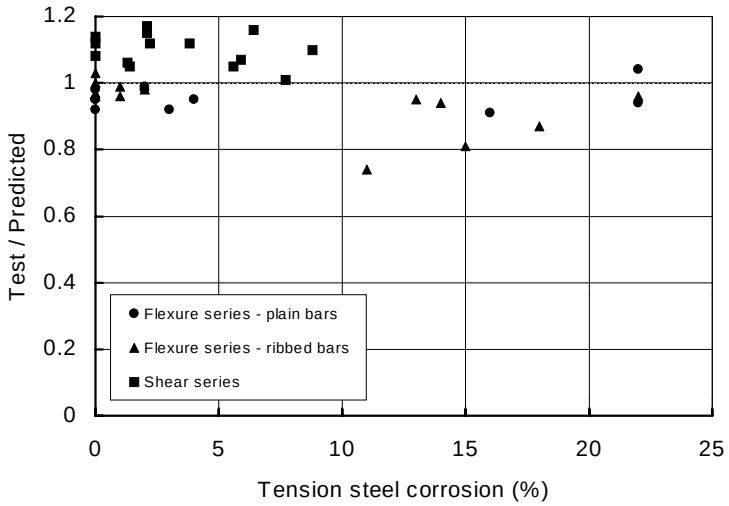

Figure 5-1: The ratio of test/predicted load-carrying capacity for singly-reinforced beams with varying amounts of corrosion and failing in flexure (Daly[64, 66])

Table 5-2: Comparison of the ratio of test/predicted flexural load-carrying capacity for uncorroded and corroded beams (Daly[64, 66])

Series	*Test / Predicted flexural load-carrying capacity*					
	Uncorroded beams			*Corroded beams*		
	Mean	*Standard deviation*	*Coeff. Variation*	*Mean*	*Standard deviation*	*Coeff. variation*
Flexure series – plain bars	0.952	0.031	3.3%	0.963	0.040	4.2%
Flexure series - ribbed bars	0.997	0.032	3.2%	0.913	0.086	9.4%
Shear series - failing in flexure	1.152	0.033	2.9%	1.154	0.078	6.8%

If the proposal of reducing the area of reinforcement for singly reinforced beams were a reasonable one, then one would expect the mean test to predicted load-carrying capacities for the corroded beams to be the same as that for the uncorroded beams. Inspection of Table 5-2 suggests that this is the case for the flexure series plain bars and the shear series. There is, however, a little more scatter in the test/predicted ratios for the corroded beams. This is to be

expected due to the uncertainties in the accelerated corrosion process, and in measuring the amount of corrosion induced.

The mean test/predicted ratios for the flexure series beams with ribbed bars was a little lower for the corroded beams suggesting that the load-carrying capacity is being over-estimated. Closer examination of the results indicates that of the three beams with the highest level of corrosion one failed due to fracture of both bars whilst the other two failed due to bond failure of both bars. Neither of these failure modes could be predicted by a flexural analysis. The fracture suggests a much higher local corrosion than the average value measured after the test. The ratios of test/predicted ratios for these three beams were 0.74, 0.81 and 0.87 respectively. If these three ratios are excluded, the statistics for Table 5-2 become mean = 0.966, standard deviation = 0.018 and coefficient of variation = 1.9%. These statistics are compatible with those of the control beams.

It seems reasonable to conclude that for the beams analysed here the flexural load-carrying capacity of singly-reinforced corroded beams can be estimated by reducing the area of reinforcement alone provided that premature failure due to bar fracture or bond does not occur.

5.4 Members with reinforcement in the compression zone

The term “members with reinforcement in the compression zone” is used in this section in preference to the term “doubly reinforced members”. The test beams investigated by Rodriguez et al[45] contained reinforcement in the compression zone whose primary function was as link hangers rather that to balance the extra force generated by increasing the tension reinforcement. This is likely to be typical of many members in practice. The proposals made later in this section are relevant to both those members where the compression reinforcement is included for buildability and those where it is included for increasing structural capacity.

Rodriguez et al[45] suggest that when the cover has spalled in the compression zone, the possibility of the compression reinforcement buckling rather than yielding should be considered. It is unlikely that this will reduce the load-carrying capacity by a significant amount as the amount of tension reinforcement controls the load-carrying capacity. However, with the dual reductions in

compression capacity resulting from a reduced concrete area and reduced compression reinforcement capacity the depth to the neutral axis will need to increase to balance the force available in the tension reinforcement. The section will need to be checked to ensure that the tension reinforcement still yields before the concrete crushes.

Rodriguez et al[45] suggest that the buckling load could be estimated by considering the compression reinforcement as a strut, and using the Euler equation:

$$P_{cr} = \frac{\pi^2 EI}{l^2} \qquad \textbf{… (5-3)}$$

where: E = the elastic modulus of the reinforcement (kN/mm^2)

I = the second moment of area of the reinforcement = $\pi D^4 / 64$ (mm^4)

l = the effective length of the reinforcement (mm)

P_{cr} = the critical buckling load (kN)

The effective length of the strut will vary according to the end fixity. If the length between adjacent links is considered, before corrosion and spalling the compression reinforcement is restrained by the cover concrete between the links and by the links themselves at the intersection with the compression reinforcement. When the cover concrete spalls, one element of the restraint is lost. When both link and compression reinforcement corrode, the restraint at the intersection is also reduced. A possibility is to consider the compression reinforcement as acting as a pin-ended strut. This implies an effective length of 1.0 times the actual length, and corresponds with the proposals made by Rodriguez et al[45].

Tassios[94] suggests three possible buckling modes for reinforcement after spalling (Table 5-3). The two local buckling modes are likely to be most appropriate to the compression zone of a beam. Tassios treats uncorroded reinforcement as being a pin-ended strut between adjacent links. This implies that corrosion is unlikely to make the effective length longer unless one or more links is unable to provide sufficient restraint to the outward movement of the compression reinforcement.

Table 5-3: Effective length of reinforcement for various buckling modes after spalling (Tassios[94])

Buckling mode	*Description*	*Effective length*
Global	Buckling over a considerable length. The buckling force is mobilised by reinforcement between adjacent links.	0.5 s_v
Local	Buckling between groups of links. Between group spacing greater than within group spacing.	1.0 s_v
Local	Buckling between first and third link, with second link providing insufficient restraint.	1.5 s_v

Note: s_v is the larger of the distance between adjacent links or adjacent groups of links.

The critical buckling stress for compression reinforcement can thus be given as:

$$\sigma_{cr} = \frac{\pi^2 E D^2}{16(ks_v)^2} \qquad \textbf{… (5-4)}$$

where: E = elastic modulus of the reinforcement (N/mm^2)

D = diameter of the compression reinforcement after corrosion (mm)

k = 1.0 when sufficient restraint is provided

= 1.5 when sufficient restraint is provided at first and third links, but less than effective restraint is provided at the second link

= 2.0 when sufficient restraint is provided at first and third links, but no restraint is provided at the second link

s_v = spacing between adjacent link reinforcement (mm)

σ_{cr} = critical buckling stress (N/mm^2)

In order to test the hypothesis that spalling in the compression zone needs to be considered, the beams tested by Rodriguez et al[45] have been analysed in two ways:

(i) Ignoring the effects of spalling of the cover concrete surrounding the compression reinforcement.

(ii) Including the effects of spalling of the cover concrete surrounding the compression reinforcement. These are loss of concrete section and the possibility of the compression reinforcement buckling.

The two sections are shown in Figure 5-2.

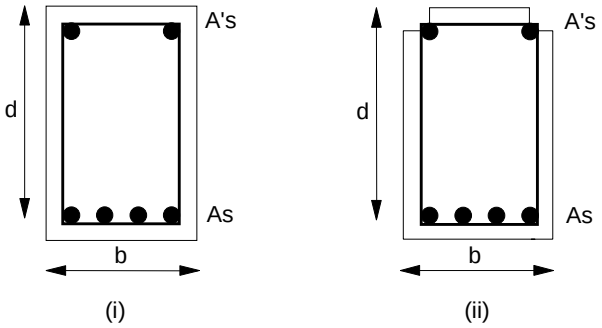

Figure 5-2: Sections used to analyse test specimens (i) Ignoring spalling in the compression zone; (ii) Considering spalling in the compression zone

The test/predicted ratios are plotted in Figure 5-3 and Figure 5-4 together with the relevant statistics.

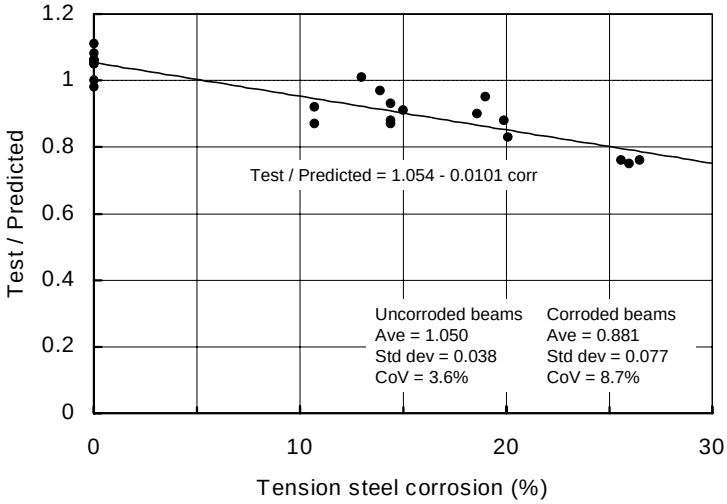

Figure 5-3: The variation in the ratio of test/predicted flexural load-carrying capacity with

corrosion for beams with reinforcement in the compression zone and ignoring the effects of spalling

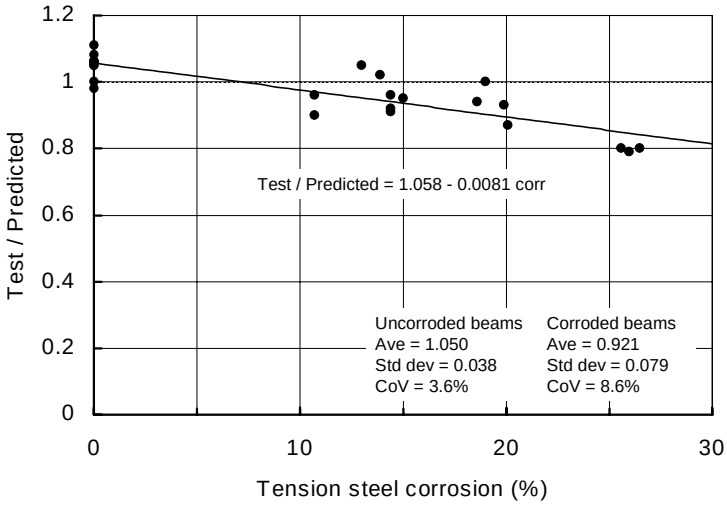

Figure 5-4: The variation in the ratio of test/predicted flexural load-carrying capacity with corrosion for beams with reinforcement in the compression zone and including the effects of spalling

In only one of beams was the reinforcement in the compression zone predicted to buckle. The bars in the compression zone were 8 mm diameter, and the link spacing was 170 mm in many of the beams. This gives a predicted buckling stress of 273 N/mm^2 for the uncorroded bar. The yield stress was measured as 615 N/mm^2. As such, one would expect any of these bars with spalled cover to buckle before they yielded. However, the beams were not designed as doubly reinforced, and the compression zones were predicted to be small. As such, the compression bars were only short distances from the neutral axis, and unlikely to reach a stress near yield (or buckling).

Ignoring the effects of cover spalling does not appear to offer a satisfactory solution, as the mean of the test/predicted flexural load-carrying capacity of the corroded beams appears to be somewhat lower than that of the uncorroded beams. By including the effects of cover spalling, the mean test/predicted load-carrying capacity of the corroded beams becomes closer to that of the uncorroded beams.

A distinct trend can be seen in both Figure 5-3 and Figure 5-4 of the ratio of test/predicted flexural load-carrying capacity decreasing with increasing corrosion in the tension reinforcement. This implies that the predictions are becoming less conservative as the amount of corrosion increases. There are only three parameters that can vary in Table 5-1, and two of those (b and A_s) have been considered here. That only leaves the yield strength, f_y.

Andrade et al[23] have applied accelerated corrosion to 12 mm diameter ribbed bars similar to those used by Rodriguez et al[45]. The variations in yield strength with corrosion were measured, and are shown plotted in Figure 5-5.

The reinforcement shows an apparent reduction in yield strength with increasing corrosion. It is interesting to note that the gradient of the regression line is close to the gradient of the regression line in Figure 5-4 for the beams where spalling was considered, and similar to that in Figure 5-3 for the beams where spalling was ignored. This suggests that the reduction in test/predicted flexural load-carrying capacity ratio with increasing corrosion can be explained by the decrease in yield strength with increasing corrosion. The analyses were repeated with this reduction in yield strength taken into account. The results are plotted in Figure 5-6 and Figure 5-7 together with the relevant statistics.

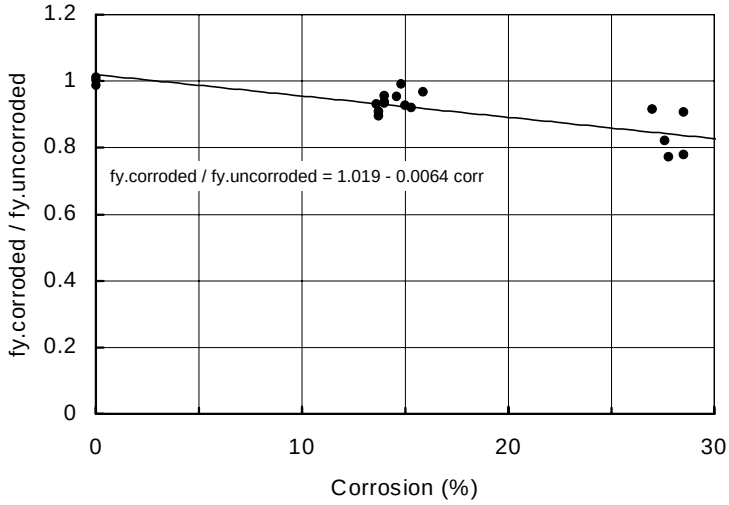

Figure 5-5: The variation in the ratio of corroded to uncorroded yield strength of 12 mm ribbed bars subject to accelerated corrosion (Andrade et al[23])

Whilst it would seem that the reduction in yield strength has to be considered to obtain satisfactory predictions of flexural load-carrying capacity, the reason for this phenomenon has to be established. Clark[95] suggests that there is no fundamental metallurgical reason for the yield strength to decrease with increasing corrosion. A possible explanation could lie in the test procedures used. Rodriguez et al[45] report differences between average and maximum amount of corrosion that suggest that significant pitting corrosion has occurred during the accelerated corrosion process. This apparent reduction in yield strength could be due to the bar failing at the point with maximum corrosion (and minimum cross-section), with this minimum cross-section being smaller than the average cross-section. The gradients in Figure 5-3 and Figure 5-4 would suggest that the larger the corrosion the bigger the difference between the maximum and average corrosion.

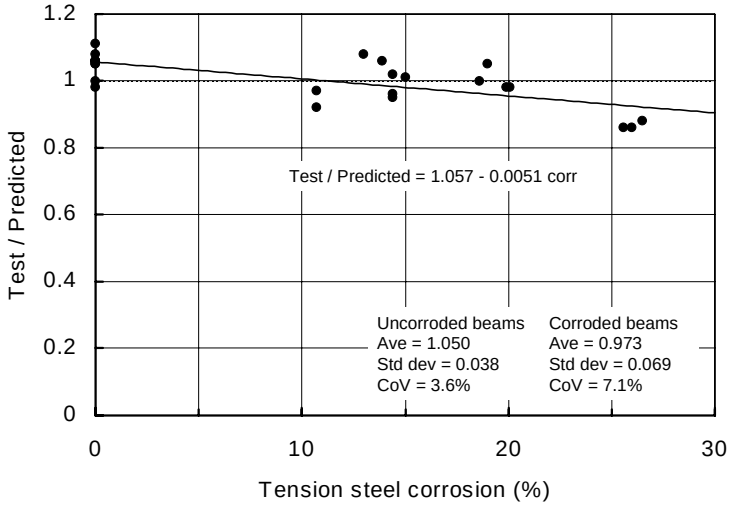

Figure 5-6: The variation in the ratio of test/predicted flexural load-carrying capacity with corrosion for beams with reinforcement in the compression zone, ignoring the effects of spalling and allowing for the apparent reduction in yield strength

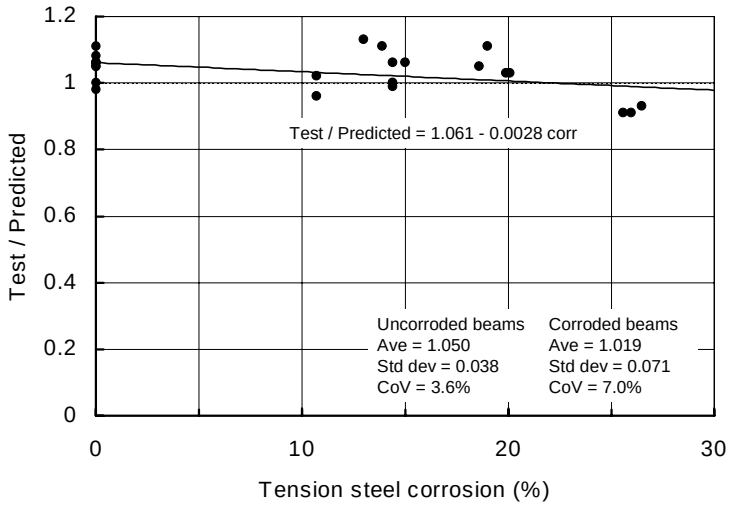

Figure 5-7: The variation in the ratio of test/predicted flexural load-carrying capacity with corrosion for beams with reinforcement in the compression zone, including the effects of spalling and allowing for the apparent reduction in yield strength

Reductions in the ratio of test/predicted flexural load-carrying capacity were not evident in the flexural series – plain bars and shear series beams tested by Daly[64, 66]. A slight increase was observed. However, Daly reports that the corrosion was largely general rather than pitting corrosion. This implies that there would be a much smaller difference between the maximum and average amount of corrosion. The flexure series – ribbed bars appeared to show a similar reduction to that observed by Rodriguez et al[45]. However, the reduction cannot be attributed to ribbed bars alone as the shear series beams also contained ribbed bars.

Review of the available literature suggests that this phenomenon has also been observed by Lee et al[57], Morinaga[28], Saifullah[35] and Du[96] in yield tests on reinforcement subject to accelerated corrosion. Although the phenomenon was observed in these cases, no explanation is given.

This phenomenon would seem to be applicable to all scenarios where an estimate of the remaining reinforcement area is made on the basis of average weight loss measurements. This suggests that either the maximum section loss should be measured in the critical areas, or a relationship should be developed to relate the maximum likely corrosion to the average. The former approach is likely to be impractical, as removing reinforcement from critical zones is highly undesirable. The latter approach is feasible, but would require large amounts of data to

establish a valid statistical relationship.

Based on Figure 5-6 and Figure 5-7 it would seem reasonable to conclude that the effects of the concrete cover spalling along the lines of the compression reinforcement should be considered when cracking is present. Whilst the cover to the compression reinforcement may not be spalled at the start of the test, the presence of cracking is likely to lead to spalling in the later stages of the test. The maximum load is reached during these later stages, when the cover is no longer contributing to the load-carrying capacity. The modifications required to assess the flexural load-carrying capacity of corroded beams with reinforcement in the compression zone are summarised in Table 5-4.

Table 5-4: Proposed modifications to allow calculation of the flexural load-carrying capacity of corroded beams with reinforcement in the compression zone

Property	*Modifications*
b	If cracking is present in the concrete cover along the lines of the compression reinforcement, reduce b to allow for spalling of the cover.
d	Use the uncorroded value, unless the majority of the cover to the compression reinforcement is spalled. In which case measure d from the outer face of the link reinforcement.
A_s	Base on measurements of cross-section loss. If only an average measurement of corrosion is available, this should be corrected to allow for the difference between the average and maximum corrosion. Further data are required to establish a general relationship.
f_y	For tension reinforcement use the uncorroded value. If cracking is present in the concrete cover along the lines of the compression reinforcement, calculate the Euler buckling load and take the smaller of that or the uncorroded yield stress.

5.5 Ductility

As discussed in Section 5.2 ductility is essential in concrete elements to provide a warning of collapse. Ductility is also required to allow redistribution of forces from highly stressed areas to less highly stressed ones. A typical example of the need for ductility is the requirement for plastic rotation at the support of a continuous member. Non-ductile failures can occur if:

(i) The concrete crushes in the compression zone before the tension reinforcement yields.
(ii) The tension reinforcement fractures before any significant signs of distress are visible.
(iii) An anchorage bond failure occurs before a member reaches its flexural load-carrying capacity.
(iv) A shear failure occurs before a member reaches its flexural load-carrying capacity.

The first two points are addressed in the following sections, whilst the third and fourth are dealt with in Chapter 6.

5.5.1 Corrosion in the compression zone

In the previous section it was concluded that the potential effects of spalling around the compression reinforcement had to be considered to give reliable predictions of the flexural load-carrying capacity. These effects are:

(i) Reduction of the amount of concrete available in the compression zone.
(ii) Potential failure of the compression reinforcement by buckling before the yield strength can be reached.

A parameter study has indicated that it is likely that these two effects will not reduce the flexural load-carrying capacity significantly, as the main parameter is the tension reinforcement. However, the depth to the neutral axis has to increase to mobilise sufficient compressive force to balance the force in the tension reinforcement. In the extreme case, this could lead to the concrete crushing in compression before the reinforcement yields in tension. This type of failure is undesirable as its lack of ductility gives little warning of failure. However, calculations should

indicate that such a failure is likely.

5.5.2 Reinforcement fracture

If a significant amount of the area of a reinforcing bar is lost due to, say, pitting corrosion there is a possibility that the bar will fracture rather than yield. To avoid premature fracture with little warning, minimum levels of ductility are specified in codes and standards for reinforcement. These minimum levels are usually expressed in terms of elongation at the maximum load (ε_u) and the ratio of ultimate to yield strength (f_{ult}/f_y). The BS EN 10080[24] criteria for the two common reinforcement ductility grades are given in Table 5-5. EC2[59] allows High ductility grade reinforcement to be used in all circumstances whilst Normal ductility grade is not permitted in situations where plastic analysis or moment redistribution in excess of 15% are used.

Table 5-5: Ductility requirements for reinforcement in BS EN 10080[24]

Reinforcement ductility grade	*Elongation at maximum load*	*Ultimate / yield strength*
Normal	2.5%	1.05
High	5%	1.08

The effect of accelerated corrosion on the ductility properties of 12 mm ribbed reinforcement was investigated by Andrade et al[23]. The results are shown plotted in Figure 5-8 for ε_u and Figure 5-9 for f_{ult}/f_y. The general trends appear to be that elongation decreases with increasing corrosion whilst the ratio f_{ult}/f_y may increase. However, the amount of scatter in the f_{ult}/f_y results makes it difficult to propose a relationship.

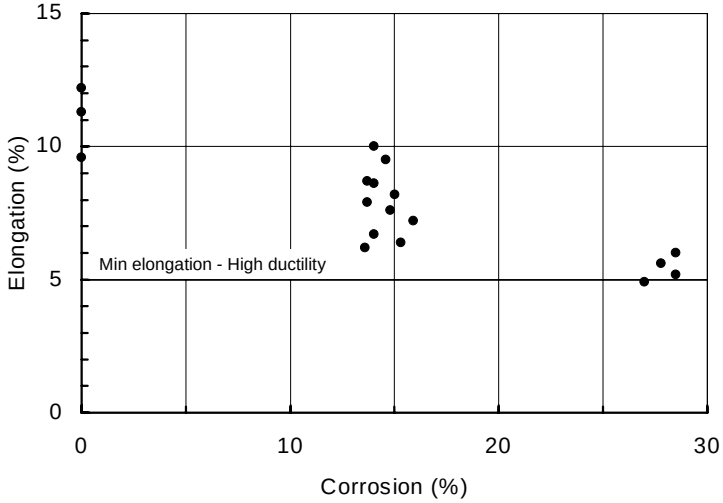

Figure 5-8: The effects of accelerated corrosion on the elongation at maximum load of 12 mm diameter ribbed bars (Andrade et al[23])

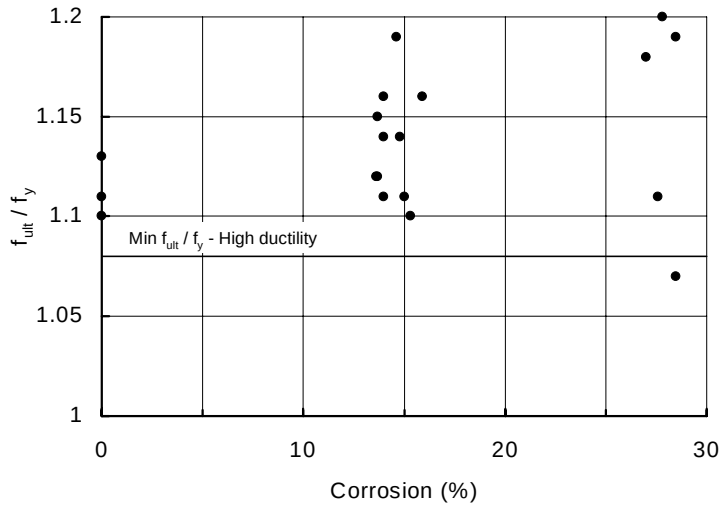

Figure 5-9: The effects of accelerated corrosion on the ratio f_{ult}/f_y of 12 mm diameter ribbed bars (Andrade et al[23])

The reinforcement tested by Andrade et al[23] had ductility properties well in excess of those required for the High ductility reinforcement grade in BS EN 10080[24]. At around 30% corrosion the elongation was becoming borderline for the High ductility grade. For other reinforcement with a lower initial elongation there is the possibility that corrosion may cause the elongation to fall below that required for High, or even Normal, ductility reinforcement. This implies that limitations may be required on the use of plastic analysis and the amount of redistribution allowed

when corrosion has occurred. Further test data are required to evaluate when any limitations should be applied.

Premature failure by fracture of reinforcement bars is likely to occur if the strain is such that the ultimate strength of the corroded bar is reached before the bar can yield. The difference between the yield and ultimate strength would provide a margin against this type of failure in uncorroded bars. However, corrosion can erode this margin. It can also reduce the elongation, such that the ultimate strength is reached at a lower strain. Du[96] has carried out a series of ductility tests on bars subject to accelerated corrosion, and has found that corrosion in excess of 10% is of concern. General relationships are required to evaluate what reductions in ε_u and f_{ult} / f_y are likely to be induced by corrosion.

5.6 Conclusions

The following conclusions can be drawn from the work reported in this Chapter:

1. The flexural load-carrying capacity of singly-reinforced corroded beams can be estimated by reducing the area of reinforcement alone (to allow for corrosion including pitting) provided that premature failure due to bar fracture or a change in failure mechanism does not occur.

2. When pitting corrosion was present the ratio of maximum to average corrosion was found to increase with increasing corrosion. This manifested itself as an apparent reduction in the reinforcement yield stress. Using the average corrosion (measured during the test) leads to overestimates of the load-carrying capacity.

3. Some beams can fail prematurely due to bar fracture, bond or shear. Checks are required to ascertain which is the critical mechanism for each member.

4. Corrosion can reduce both the elongation at maximum load and the ratio of yield to ultimate strength of the reinforcement. These reductions can lead to premature fracture of the bar before yield is reached. There are no general relationships for ascertaining the

reduction due to corrosion in either the elongation at maximum load or the ratio of ultimate to yield strength of a bar.

5. When reinforcement in the compression zone corrodes, a better fit to the experimental data is achieved by considering the effects of spalling concrete within the compression zone. Ignoring the effects of spalling leads to an overestimate of the flexural load-carrying capacity.

6. A procedure is presented for assessing the effects of corrosion on the buckling of reinforcement loaded in compression. This should also prove useful for the assessment of column behaviour (see Chapter 7).

6 SHEAR STRENGTH

6.1 Introduction

Corrosion can modify the failure mode by reducing the shear load-carrying capacity faster than it reduces the flexural load-carrying capacity. There are a two reasons for this:

(i) By necessity, shear links have lower covers than flexural reinforcement and will start to corrode first.

(ii) Shear is more sensitive to reductions in anchorage bond of the tension reinforcement at supports.

Concrete and shear reinforcement components of shear strength have been separated out in most shear design methods with the interaction between them being ignored. Whilst the models with separate components give good correlation with test data, there appears to be little physical meaning to them. If we contrast shear with flexure, it would not be unreasonable to suggest that the number of design methods is inversely proportional to the understanding of the phenomenon. Flexure is reasonably well understood and a simple rational approach can be used. Shear, on the other hand, still remains somewhat of a mystery with engineers being provided with a variety of empirical rules. This has proved satisfactory for design, where code detailing rules can be complied with to ensure that empirical rules are used within their limitations. In the assessment of existing structures, it is not always possible to comply with the specified detailing rules. This implies that whilst a structure may still be capable of carrying the required load, it has failed its assessment in accordance with the code. This is also the case for corroded structures where problems are arising which are outside the areas that have been researched and codified. The objectives of this Chapter are to provide a qualitative understanding of the performance of corrosion damaged concrete beams failing in shear and to propose modifications to the empirical equations used in BS 8110[69].

6.2 Shear mechanisms

In this Section current UK shear design methods are reviewed and the implications for corroded structures are established. Although this review is based on the UK building code BS 8110[69], the findings are also applicable to the UK bridge codes for design (BS 5400[97]) and assessment (BD 44/95[73]). They are all based on the same basic theory, although there is a lack of consistency in applying that theory.

The UK code method is based on a 45° truss with the concrete and the shear link reinforcement carrying the shear force between them. The main advancement from the rules contained in pre Limit state codes was the move away from the traditional Mörsch truss analogy where shear was carried by the shear links alone. It has been shown in tests[98] that the shear capacity of members with link reinforcement was larger than could be explained by 45° truss action alone. Hence, a concrete term was added to the shear link term to cater for this. Whilst the approach is still empirical, reasonable correlation with test results has been obtained[98]. This approach is used for both beam shear and punching shear.

The basic equation given in BS 8110, BS 5400 and BD 44/95 for shear resistance of reinforced concrete members with links is similar. The version used in BS 8110 is as follows:

$$V = V_c + V_s \qquad \textbf{… (6-1)}$$

In its entirety, this becomes:

$$V = \left[\frac{0.79}{\gamma_{mv}}\right]\left[\frac{400}{d}\right]^{1/4}\left[\frac{100\,A_s}{b_w d}\right]^{1/3}\left[\frac{f_{cu}}{25}\right]^{1/3} b_w d + \left[\frac{f_{yv}}{\gamma_{ms}}\right]\frac{A_{sv} d}{s_v} \qquad \textbf{… (6-2)}$$

where: A_s = area of effectively anchored longitudinal tensile reinforcement (mm^2)

A_{sv} = cross-sectional area of all the legs of the links (mm^2)

b_w = width of the section (mm)

d = effective depth to the tension reinforcement (mm)

f_{cu} = characteristic concrete cube strength (N/mm^2)
f_y = characteristic strength of the reinforcement (N/mm^2)
f_{yv} = characteristic strength of the shear reinforcement (N/mm^2)
s_v = spacing of the links along the member (mm)
V_c = ultimate shear force in the concrete (N)
V_s = ultimate shear force in the shear links (N)
V = shear force due to ultimate loads at the point considered (N)
γ_{ms} = the partial safety factor for reinforcement
γ_{mv} = the partial safety factor for shear

The term before the addition sign represents V_c, and was derived empirically. It gives the concrete contribution to shear when no shear links are present. It represents the contributions of:

(i) Concrete compression zone.
(ii) Longitudinal tensile reinforcement.
(iii) Aggregate interlock.
(iv) Size effect (shallow members can carry proportionally higher shear loads than deep ones).

Work carried out by Taylor[99] indicates that the relative contributions to the term V_c are as given in Table 6-1.

Table 6-1: Relative contributions to V_c (after Taylor[99])

Component	*Contribution to V_c (%)*
Concrete compression zone	20 to 40
Dowel action	15 to 25
Aggregate interlock	30 to 50

The second term of equation 6-2 represents V_s and is based on the load carried by vertical members in a 45° truss. The amount of longitudinal reinforcement (as required in BS 5400[97] and BD 44/95[73]) is also calculated from this 45° truss using the following equation:

$$A_{sl} \geq \frac{V}{2(f_y / \gamma_{ms})} \quad \textbf{… (6-3)}$$

where: A_{sl} = the area of effectively anchored additional longitudinal tensile reinforcement (mm^2)

BS 8110[69] does not contain this check on longitudinal tension reinforcement. For the assessment of deteriorated structures, it is suggested that this term should be included as the amount of effectively anchored longitudinal tension reinforcement may be limited by bond deterioration.

There are also a variety of limitations on the individual parameters that make up the equation 6-2. These relate to limiting stresses, required anchorage lengths, minimum link area, maximum link spacing, shear enhancement, member depth and safety factors and are given in the relevant Codes of Practice. As discussed in Chapter 4 the anchorage length and minimum link area criteria have implications for the assessment of corroded structures.

6.3 Shear strength of corroded members with ribbed reinforcement

The increase in shear load-carrying capacity with increasing corrosion for the beams containing plain bars described in Section 6.4 indicates that conventional code expressions for shear will provide neither an understanding of the phenomenon or satisfactory estimates of the load-carrying capacity. As such, beams with plain and ribbed bars are treated separately.

6.3.1 Members with no shear links

Only one set of test data (Daly[66]) is available for corroded members containing ribbed bars with no links where there is sufficient information to analyse the results. The test results for these members are shown in Figure 6-1 complete with regression lines. It is interesting to note the beneficial effects of increasing the cover to bar diameter (c/D) ratio. The increase in bond strength with increasing c/D was noted in Chapter 4. It would appear that the same phenomenon is apparent with shear strength as well.

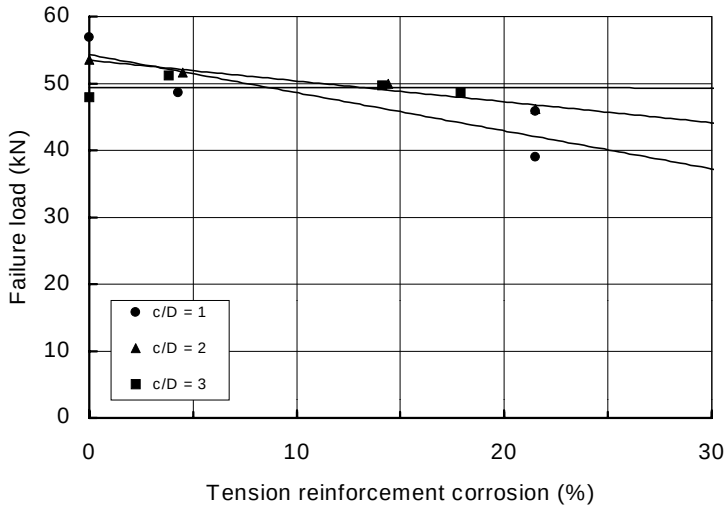

Figure 6-1: The variation in load-carrying capacity with corrosion for beams failing in shear (Daly[66])

The anchorage bond force that can be generated in a bar is a product of the anchorage length, bar perimeter and bond stress. The term A_s used to calculate V_c is referred to as the effective area of longitudinal reinforcement. BD 44/95[73] contains a procedure for calculating the effective area of reinforcement when the anchorage length provided is less than that required. The BD 44/95 method reduces the effective area of reinforcement in proportion to the square of the ratio of anchorage length provided to that required. Clark et al[100] have shown that this relationship underestimates shear strength, and have proposed that the square term be removed. A similar approach should be possible for calculating the effective area of reinforcement when the bar diameter and bond stress are less than that required by BS 8110[69].

The beams tested by Daly[66] are nominally identical. Assuming that there is no change in failure mechanism, for each c/D ratio the only parameter that varies in the expression for V_c (equation 6-2) is A_s. Using equation 6-2, the shear strength of the corroded beams is related to the control by the following expression:

$$\frac{V_{c.corr}}{V_c} = \frac{\left[\frac{100A_{s.eff}}{bd}\right]^{1/3}}{\left[\frac{100A_s}{bd}\right]^{1/3}} \qquad \text{… (6-4)}$$

This simplifies to:

$$A_{s.eff} = \left[\frac{V_{c.corr}}{V_c} A_s^{1/3} \right]^3 \quad \text{… (6-5)}$$

where: A_s = effective area of tension reinforcement in the uncorroded beam (mm^2)

$A_{s.eff}$ = effective area of tension reinforcement in the corroded beam (mm^2)

b = breadth of the beam (mm)

d = effective depth to the tension reinforcement (mm)

V_c = shear load-carrying capacity in the control (uncorroded) beam (kN)

$V_{c.corr}$ = shear load-carrying capacity in the corroded beam (kN)

The effective areas of tension reinforcement calculated using this approach are given in Table 6-2 along with effective corrosion levels implied by the ratio of effective to nominal areas of reinforcement.

The effective reinforcement areas for the TS12 (c/D = 1) and the TS24 (c/D = 2) beams are lower than the measured reinforcement areas. This implies that there are additional parameters determining the effective area of reinforcement. Given that the anchorage length provided in the beams was 150 mm compared to the 144 mm required in BS 8110[69], this implies that the reduction in effective area is a function of the decrease in bar diameter and bond stress. As indicated in Table 6-3 the composite effect on V_c is unlikely to be straightforward. The reinforcement contributes to two components of V_c. The aggregate interlock may possibly be affected in proportion to the loss in bar area whilst dowel action is possibly affected by the presence of cracking. This raises the following fundamental questions:

(i) How much is each component of V_c affected?

(ii) What are the effects of the interaction of the components of V_c?

(iii) How do we know that the empirical formulae are valid over a range of corrosion losses?

Table 6-2: Effective areas of tension reinforcement

Beam	*V (kN)*	*Reinforcement area*		*Reinforcement corrosion*	
		Measured (mm^2)	*Effective (mm^2)*	*Measured (%)*	*Effective (%)*
TS12/0	56.9	452	452	0	0
TS12/1	48.6	433	282	4.3	37.7
TS12/2	39	355	146	21.5	67.8
TS12/3	45.8	355	236	21.5	47.8
TS24/0	53.5	452	452	0	0
TS24/1	51.6	432	406	4.5	10.3
TS24/2	50	387	369	14.4	18.4
TS24/3	46.2	355	291	21.5	35.6
TS36/0	47.9	452	452	0	0
TS36/1	51.2	435	552	3.8	-22.1
TS36/2	49.7	388	505	14.1	-11.7
TS36/3	48.7	371	475	17.9	-5.1

Table 6-3: Possible effects of corrosion on the V_c component of shear

Component	*Possible effects of corrosion*
Concrete compression	Width of compression zone may be partially reduced by spalling if the compression reinforcement has corroded significantly.
Dowel action	Possible reduction due to loss of reinforcement cross-section and presence of longitudinal cracks (or spalling at later stage).
Aggregate interlock	Possible reduction due to reduction in tensile reinforcement restraining opening of shear crack.

If the approach adopted were to be similar to that for flexure, reduced values of A_s and b would be used. As there is a lack of physical meaning to the $V_c + V_s$ approach simple reductions may not be valid. A safe answer may be produced, however it may not. This suggests that

consideration of the physical processes is required.

Chana[101, 102] has investigated the shear failure of beams with no shear reinforcement by using a high speed tape recorder to record strains in the dowel, diagonal and compression zones up to and beyond the peak load. Using a slow playback speed, he was able to determine the following failure mechanism:

(i) As the beam is loaded flexural cracks appear on the tension face at intervals along the span.
(ii) The flexural cracks lead to a decrease in stiffness and thus an increase in deflection.
(iii) The flexural cracks extend upwards and start to become inclined due to the shear stresses induced.
(iv) As the load is increased the diagonal cracks open increasing the tensile stresses in the concrete at the reinforcement level due to dowel action.
(v) This leads to splitting cracks along the line of the reinforcement due to dowel action.
(vi) Restraint between the two beam segments is reduced leading to further opening of both the diagonal and dowel cracks.

This description suggests that failure is initiated by the appearance of the dowel splitting cracks. It also suggests that dowel action and aggregate interlock are dependent on one another. Dowel action is required to keep the beam segments together such that shear forces can be transmitted across the diagonal crack by aggregate interlock. Chana measured dowel forces that corresponded to around 15 to 40% of the shear failure load with a mean of 29%. This is higher than the values measured by Taylor[99]. However, Taylor was only able to carry out measurements up to about 90% of the failure load whereas Chana was able to record up to failure. Chana[101, 102] and Taylor[103] both found that failure in beams without shear links was instigated by the tensile splitting at the reinforcement level without yielding of the longitudinal reinforcement.

These tests suggest that dowel action is of vital importance to beams with no shear links. Based on Chana's description of the failure mechanism, the corrosion cracks along the line of the reinforcement would appear to be pre-empting the dowel splitting and offering the possibility of

failure at a lower load. This does not appear to have happened, with only small reductions in load-carrying capacity when c/D = 1 or 2 and little or no reduction when c/D = 3. There must be another explanation, possibly the tied-arch mechanism described in Section 6.4 for beams with plain bars. However, there are none of the increases in load-carrying capacity at lower corrosion levels. This suggests that the load-carrying mechanism is different to that for beams with plain bars particularly at lower corrosion levels. Without further tests on corroded beams, it is not clear exactly what the difference is and, as such, an empirical approach will have to be adopted. Because of their nature, empirical formulae are difficult to adapt with confidence. This is particularly the case when only one set of experimental data is available and is complicated by the need to cater for the effects of corrosion. However, there is little choice but to take this route.

It was suggested earlier in this section that $A_{s.eff}$ is likely to be a function of the bond strength. This is confirmed by Figure 6-2. The corroded bond strength is expressed as a ratio of the BS 8110[69] bond strength for uncorroded bars rather than the Tepfers bond strength. This is to maintain compatibility with BS 8110.

Figure 6-3 shows that $A_{s.eff}$ varies with tension reinforcement corrosion. It is also apparent from Figure 6-3 that the c/D ratio is a significant variable.

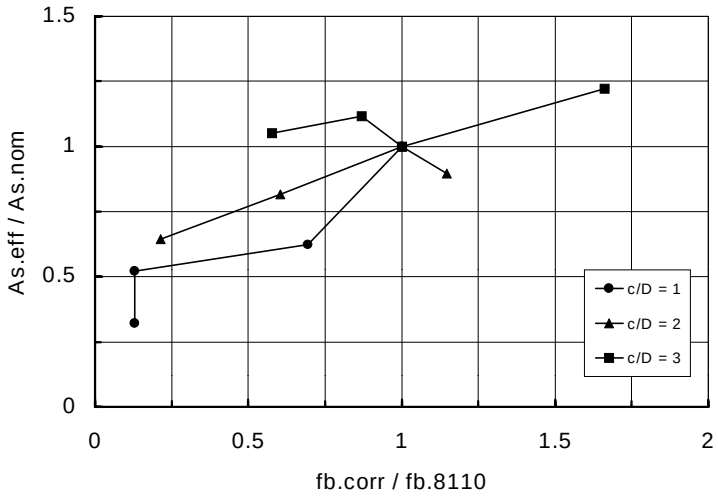

Figure 6-2: The variation in $A_{s.eff}/A_{s.nom}$ with the ratio $f_{b.corr}/f_{b.8110}$

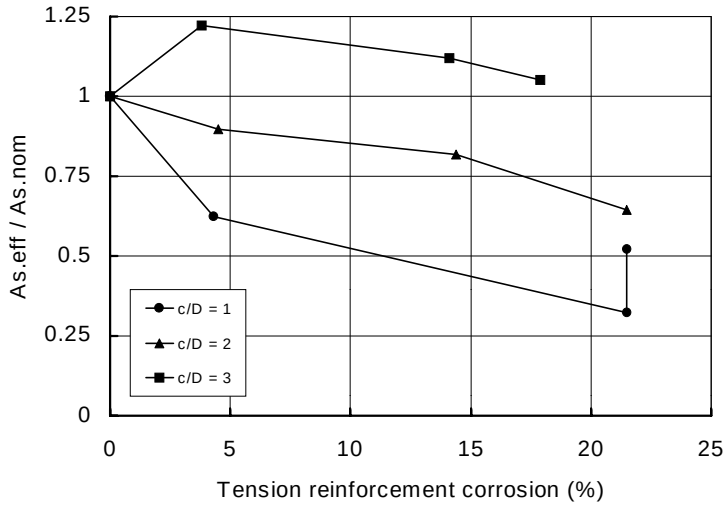

Figure 6-3: The variation in $A_{s.eff}/A_{s.nom}$ with tension reinforcement corrosion

Whilst it is apparent that the c/D ratio is a primary variable in determining $A_{s.eff}$, the test beams considered had the same c/D ratio both on the side and the bottom faces. It is not obvious which of the ratios should be used in the more general case where these two ratios will differ. For dowel action, Taylor[103] found in his tests that the failure load increased with increasing width of the horizontal failure plane. The effect of the bottom cover was negligible. As all of the beams were of the same width with the same bar sizes, the only potential reduction in the horizontal failure plane is due to corrosion-induced cracking. The length of corrosion-induced cracking across the beam width would increase with increasing c/D ratio assuming that the cover between the bar and the side face of the beam had cracked. This implies that dowel action would reduce with increasing c/D ratio. This is contrary to the failure loads that were observed to benefit from increasing c/D ratio. This implies that the vertical c/D ratio is the variable to be used. The potential loss of horizontal failure plane due to corrosion-induced cracking also raises the question as to whether dowel action is a feature in corroded beams with no shear reinforcement. Photographs of the failure mode indicate that the horizontal splitting associated with dowel action was present and thus the corrosion cracking along the line of the reinforcement was not as detrimental as initially thought.

Three variables were considered in deriving an expression for the effective area of tension reinforcement: tension reinforcement corrosion, c/D ratio and corroded bond strength. The formulae developed in Section 4.4 were used with a partial safety factor of one to estimate

corroded bond strength. Non-dimensional terms were used to allow the form of the expressions to remain applicable when applied to future test data. Both c/D and the ratio $f_{b.corr}/f_{b.8110}$ were found to make statistically significant contributions to the relationship. The tension reinforcement corrosion was not found to be significant and has been excluded as a primary variable. The tension reinforcement corrosion is included explicitly in the expression for corroded bond strength, as are the c/D ratio and the concrete tensile strength. The data and predictions of effective area are given in Table 6-4.

The following equation was obtained from linear regression analysis (correlation coefficient, r^2, is 0.845):

$$\frac{A_{s.eff}}{A_{s.nom}} = 0.796\left[\frac{c}{D}\right]^{0.293}\left[\frac{f_{b.corr}}{f_{b.8110}}\right]^{0.307} \quad \textbf{… (6-6)}$$

For assessment purposes, it is proposed that the equation be simplified to:

$$\frac{A_{s.eff}}{A_{s.nom}} = 0.8\left[\frac{c}{D}\right]^{0.3}\left[\frac{f_{b.corr}}{f_{b.8110}}\right]^{0.3} \quad \textbf{… (6-7)}$$

where:
- $A_{s.eff}$ = effective area of the corroded tension reinforcement (mm^2)
- $A_{s.nom}$ = nominal area of the uncorroded tension reinforcement (mm^2)
- c = vertical cover to the tension reinforcement (mm)
- D = nominal diameter of the uncorroded tension reinforcement (mm)
- $f_{b.corr}$ = corroded bond strength of the tension reinforcement (N/mm^2)
- $f_{b.8110}$ = bond strength of the tension reinforcement calculated in accordance with BS 8110 (N/mm^2)

Table 6-4: Comparison of test and predicted values of $A_{s.eff}$

Beam	*c/D*	*Corr. (%)*	$f_{b.corr}$ *(MPa)*	$f_{b.8110}$ *(MPa)*	$f_{b.corr}$ / $f_{b.8110}$	$A_{s.eff}$ / $A_{s.nom}$ *Test*	*Predicted*	*Test / Predicted*
TS12/0	1	0.0	na	2.69	1.00	1.00	0.80	1.25
TS12/1	1	4.3	1.87	2.69	0.70	0.62	0.72	0.87
TS12/2	1	21.5	0.35	2.69	0.13	0.32	0.43	0.74
TS12/3	1	21.5	0.35	2.69	0.13	0.52	0.43	1.20
TS24/0	2	0.0	na	2.69	1.00	1.00	0.99	1.02
TS24/1	2	4.5	3.09	2.69	1.15	0.90	1.03	0.87
TS24/2	2	14.4	1.63	2.69	0.61	0.82	0.85	0.96
TS24/3	2	21.5	0.58	2.69	0.22	0.64	0.62	1.04
TS36/0	3	0.0	na	2.69	1.00	1.00	1.11	0.90
TS36/1	3	3.8	4.46	2.69	1.66	1.22	1.30	0.94
TS36/2	3	14.1	2.34	2.69	0.87	1.12	1.07	1.05
TS36/3	3	17.9	1.55	2.69	0.58	1.05	0.94	1.11

The test and predicted values of the ratio $A_{s.eff}/A_{s.nom}$ are shown in Figure 6-4. Although $A_{s.eff}/A_{s.nom}$ values in excess of one have been derived from the test data, it is proposed to limit the ratio to 1.0 until further test data become available to confirm this phenomenon.

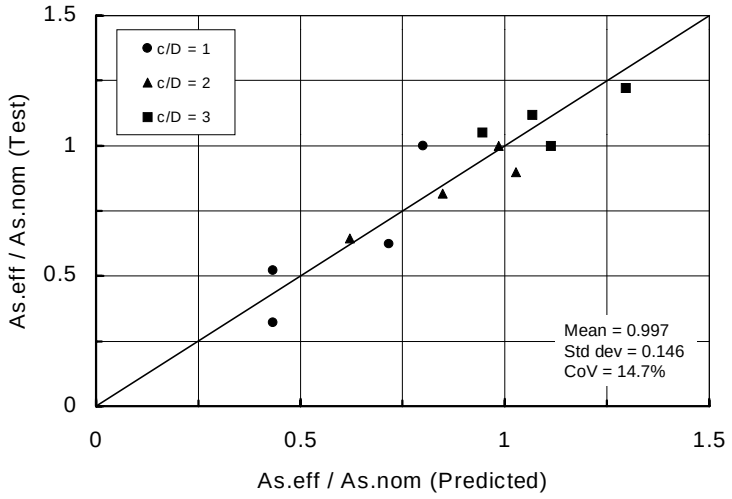

Figure 6-4: Comparison of test and predicted ratios of $A_{s.eff}/A_{s.nom}$

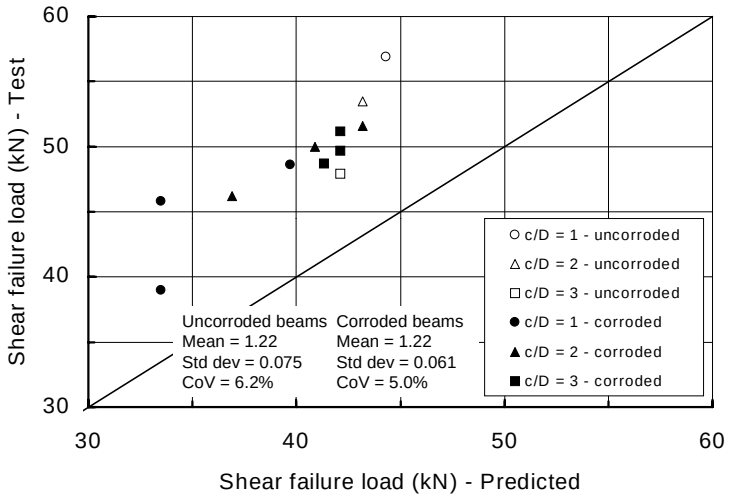

Figure 6-5: Comparisons of test and predicted shear load-carrying capacities

The test and predicted (using $A_{s.eff}$ values in the BS 8110 approach) values of the shear load-carrying capacity are shown in Figure 6-5 and are compared with other codes in Table 6-5. Whilst the predicted values are on the conservative side, the ratios of test/predicted shear strength for the corroded beams are compatible with those for the uncorroded beams. This suggests that the predictions are satisfactory.

The V_c term is also used in the BS 8110 expressions for punching shear strength. To the best of the Author's knowledge, there are no test data on slabs subject to corrosion and failing in punching shear. In the absence of such data no judgement can be made on the suitability of the proposed method for calculating V_c for assessing the punching shear strength of corroded slabs.

Comparisons with two other codes are also considered. EC 2[59] is selected primarily because it is likely to become the main code for concrete structures in the UK within the next ten years. Canadian Standards Association CSA A23.3[104] is selected because its procedures are based on the Modified Compression Field Theory. BS 8110 is used with the modifications proposed earlier in this section whilst the EC 2 and A23.3 procedures are those given in the codes with no modifications other than using reduced reinforcement areas.

In EC 2 the V_c term is known as V_{Rd1}, and is given by the following expression:

$$V_{Rd1} = \left(\tau_{Rd} k(1.2 + 40\rho_l) + 0.15\sigma_{cp}\right) b_w d \qquad \textbf{… (6-8)}$$

where: b_w = width of the member (mm)

d = effective depth to the tension reinforcement (mm)

k = variable relating to member depth and reinforcement curtailment

V_{Rd1} = ultimate shear force capacity due to the concrete and the tension reinforcement (N)

ρ_l = longitudinal reinforcement ratio (A_s / $b_w d$)

σ_{cp} = compressive stress induced by prestress (N/mm^2)

τ_{Rd} = ultimate shear stress (N/mm^2)

Several versions of the Modified Compression Field Theory[105] (MCFT) are available to achieve moment, shear and axial equilibrium. The versions vary in complexity however, all require iterative solutions to be used. The Author has adopted the solution known as the General method[106]. This was found to converge to the most stable and reliable answers. It is used in the Canadian Standard CSA A23.3[104] and is similar to the method described by Collins et al[106] and Adebar and Collins[107]. Ignoring the terms for prestressed concrete, the solution to the General method is as follows:

$$V_{cg} = 1.3\beta\sqrt{f_c'}\,b_w d_v \qquad \textbf{… (6-9)}$$

$$\beta = \frac{0.33\cot\theta}{1+\sqrt{500\varepsilon_1}} \le \frac{0.18}{0.3+\frac{24w}{a+16}} \qquad \textbf{… (6-10)}$$

$$\theta = \tan^{-1}\left[\frac{0.55+\frac{44\varepsilon_1 s_x}{(a+16)\sin\theta}}{1+\sqrt{500\varepsilon_1}}\right] \qquad \textbf{… (6-11)}$$

$$\varepsilon_1 = \varepsilon_x(1+\cot^2\theta) + 0.002\left(1-\sqrt{1-\frac{0.33\cot^2\theta(0.8+170\varepsilon_1)}{\sqrt{f_c'}(1+\sqrt{500\varepsilon_1})}}\right)\cot^2\theta \qquad \textbf{… (6-12)}$$

where:
- a = maximum aggregate size (mm)
- b_w = web width (mm)
- d = effective depth to the tension reinforcement (mm)
- d_v = shear depth = 0.9d (mm)
- f'_c = concrete compressive cylinder strength (N/mm^2)
- s_x = spacing of cracks perpendicular to the longitudinal reinforcement $\approx d_v$ (mm)
- V_c = concrete contribution to shear resistance (N)
- g
- w = width of shear crack (mm)
- β = tensile stress factor
- ε_1 = principal tensile strain
- ε_x = longitudinal strain
- θ = inclination of principal average stresses (crack inclination)

CSA A23.3 considers the co-existent effects of moment, shear and axial force. As such, co-existent moments are calculated at the base of the shear crack for each of the beams analysed here.

Comparisons of the predictions made using the different methods are shown in Table 6-5. There are two issues to consider in comparing the results: the mean test/predicted ratios, and the similarity between the test/predicted ratios for the control and corroded beams. The first gives an indication of how good the predictions are. The second indicates whether all of the significant differences between the control and corroded beams have been catered for. The modified BS 8110 approach gives identical mean values (1.22), and the coefficient of variation of the corroded beams (4.98%) is actually less than that of the control beams (6.16%). The reduction in the coefficient of variation suggests that the effects of corrosion have been addressed in the modifications such that any deviation of the predictions from the test values is due to the original BS 8110 shear model. This suggests that whilst there is inherent conservatism in the modified BS 8110 approach, it is the same degree of conservatism as intended in BS 8110 for uncorroded beams.

The predictions using EC 2 produce the best mean ratios for both the control and the corroded beams with mean test/predicted values of 1.03 and 0.99 respectively. The coefficient of variation was 5.56% for the control beams and 8.32% for the corroded beams. The fall in mean value coupled with the increase in the coefficient of variation suggests that perhaps some minor modifications are required to the EC 2 procedures to incorporate the effects of corrosion.

The predictions using the modified compression field theory as incorporated in A23.3 produce mean test/predicted ratios of 1.28 and 1.20 respectively for the control and the corroded beams. The coefficient of variation is 4.47% for the control beams and 13.19% for the corroded beams. The fall in mean value coupled with the increase in the coefficient of variation suggests that perhaps some modifications are required to the A23.3 procedures to incorporate the effects of corrosion.

Both the EC 2 and A23.3 procedures gave some unconservative predictions that were as much as 25% greater than the test values. All of the modified BS 8110 predictions were conservative.

Table 6-5: Comparison of BS 8110, EC2 and CSA A23.3 procedures for calculating the shear strength of corroded beams with no shear links

Beam	*Corrosion (%)*	*Vtest (kN)*	*BS 8110 (mod)*		*EC2*		*CSA A23.3*	
			Vpred (kN)	*Vtest / Vpred*	*Vpred (kN)*	*Vtest / Vpred*	*Vpred (kN)*	*Vtest / Vpred*
TS12/0	0.0	56.9	44.3	1.28	52.8	1.08	43.2	1.32
TS12/1	4.3	48.6	39.7	1.23	51.9	0.94	44.5	1.09
TS12/2	21.5	39.0	33.5	1.16	48.5	0.80	44.2	0.88
TS12/3	21.5	45.8	33.5	1.37	48.5	0.94	42.2	1.09
TS24/0	0.0	53.5	43.2	1.24	51.3	1.04	41.1	1.30
TS24/1	4.5	51.6	43.2	1.19	50.4	1.02	40.9	1.26
TS24/2	14.4	50.0	40.9	1.22	48.5	1.03	39.5	1.27
TS24/3	21.5	46.2	36.9	1.25	47.1	0.98	39.2	1.18
TS36/0	0.0	47.9	42.1	1.14	49.6	0.97	39.5	1.21
TS36/1	3.8	51.2	42.1	1.22	49.1	1.04	38.1	1.34
TS36/2	14.1	49.7	42.1	1.18	47.0	1.06	36.6	1.36
TS36/3	17.9	48.7	41.3	1.18	46.3	1.05	36.2	1.35
Control beams			Mean	1.22	Mean	1.03	Mean	1.28
			St. dev.	0.123	St. dev.	0.075	St. dev.	0.057
			C.o.V.	6.16%	C.o.V.	5.56%	C.o.V.	4.47%
Corroded beams			Mean	1.22	Mean	0.99	Mean	1.20
			St. dev.	0.061	St. dev.	0.082	St. dev.	0.158
			C.o.V.	4.98%	C.o.V.	8.32%	C.o.V.	13.19%
All beams			Mean	1.22	Mean	1.00	Mean	1.22
			St. dev.	0.075	St. dev.	0.061	St. dev.	0.141
			C.o.V.	4.99%	C.o.V.	7.68%	C.o.V.	11.59%

6.3.2 Members with shear reinforcement

There are two sets of test data that provide sufficient information for a quantitative assessment to be carried out, that of Daly[66] and that of Rodriguez et al[45]. Several of Daly's beams failed in flexure, and will be excluded from analyses in this section. Rodriguez et al designed their control beams to fail in flexure. It was only at higher levels of corrosion that the beams started failing in shear.

Deterioration affects strength in a variety of ways. If shear links are corroded, this may not necessarily mean that there will be a substantial reduction in shear strength. Codes generally ignore the interaction between the shear reinforcement and longitudinal reinforcement. As the shear reinforcement reduces, the longitudinal reinforcement will have to work harder to maintain equilibrium. This is recognised in the variable strut method used in EC2[59] and in the Modified Compression Field Theory[105] used in Canadian codes[104]. However, BS 8110[69] and the EC2 standard method assume a constant truss angle of 45°.

Chana[101] has found in his tests that the dowel action is enhanced by the presence of links provided that they are not widely spaced. Kani[112], Leonhardt and Walther[110], and Swamy et al[111] found that tied arch action only occurred in the absence of links. Presumably this was due to an enhancement of bond strength and dowel action when links are present. In Section 4.5 it was shown that bond strength is enhanced by the presence of links. These points suggest that the behaviour in shear of beams with links is likely to be different from those without.

The approach in BS 8110[69] and EC 2[59] is to use the same V_c term for beams with and without shear reinforcement and add an extra term when shear reinforcement is present. In this section the V_c was determined in the way described in Section 6.3.1.

As with the members with no shear reinforcement considered in Section 6.3.1 the shear methods in EC2[59] and CSA A23.3[104] were compared with those calculated in accordance with the modified BS 8110[69] procedures.

EC2 has two methods for calculating the shear strength of members with shear reinforcement:

the standard method, and the variable strut method. The standard method follows the traditional $V_c + V_s$ approach adopted by BS 8110. The variable strut method has no V_c term just a V_s term based on the shear links. A truss is assumed to consist of the shear links, tension reinforcement and a concrete strut. The angle of the strut is allowed to vary within certain limits. The main advantage of the method is that the strut angle can be varied to reduce the amount of shear links required in the designed member. Beeby et al[108] showed that the applied shear force would need to be greater than $3V_c$ for any reductions in shear links to be possible. Corroded members tend to have low residual areas of shear links with much of the shear resistance resulting from the V_c term. To lose the V_c term in favour of an enhanced but still small V_s term would be excessively conservative for assessment. The variable strut method as proposed for design is thus judged to be inappropriate for use in the assessment of corroded structures. An alternative plastic theory such as the upper bound solution given by Nielsen[109] would be required for assessment.

Only the standard method, given by the following expression, will be considered in this Thesis:

$$V_{Rd3} = V_{Rd1} + V_{wd} = \left(\tau_{Rd} k(1.2 + 40\rho_l) + 0.15\sigma_{cp}\right) b_w d + \frac{A_{sw} 0.9 d f_{ywd}}{s} \qquad \textbf{… (6-13)}$$

where:
- A_{sw} = area of shear link reinforcement (mm^2)
- b_w = width of the member (mm)
- d = effective depth to the tension reinforcement (mm)
- f_{ywd} = yield strength of shear links (N/mm^2)
- k = variable relating to depth and curtailment
- s = link spacing (mm)
- V_{Rd1} = concrete contribution to the shear capacity (N)
- V_{Rd3} = total shear capacity (N)
- V_{wd} = shear link contribution to the shear capacity (N)
- σ_{cp} = compressive stress induced by prestress (N/mm^2)
- τ_{Rd} = ultimate shear stress (N/mm^2)

The MCFT procedures for the General method (ignoring the prestress terms) are given below. At first, the method may appear to be a $V_c + V_s$ approach. However, there is interaction between

the V_c and V_s terms via the variable strut angle θ.

$$V_{rg} = V_{cg} + V_{sg} = 1.3\beta\sqrt{f_c'}\,b_w d_v + \frac{A_v f_y d_v \cot\theta}{s} \quad \textbf{… (6-14)}$$

$$\beta = \frac{0.33\cot\theta}{1+\sqrt{500\varepsilon_1}} \le \frac{0.18}{0.3+\frac{24w}{a+16}} \quad \textbf{… (6-15)}$$

$$\varepsilon_1 = \varepsilon_x + \left[\varepsilon_x + 0.002\left(1-\sqrt{1-\frac{v}{f_c'}(\tan\theta+\cot\theta)(0.8+170\varepsilon_1)}\right)\right]\cot^2\theta \quad \textbf{… (6-16)}$$

$$\varepsilon_x = \frac{M_u/d_v + 0.5N_u + 0.5V_u\cot\theta}{E_s A_s} \quad \textbf{… (6-17)}$$

where:

A_v	=	area of shear links (mm^2)
a	=	maximum aggregate size (mm)
b_w	=	web breadth (mm)
d	=	effective depth to the tension reinforcement (mm)
d_v	=	shear depth = 0.9d (mm)
f'_c	=	concrete cylinder strength (N/mm^2)
f_y	=	reinforcement yield strength (N/mm^2)
s	=	shear link spacing (mm)
V_c	=	concrete contribution to shear resistance (N)
g		
V_{rg}	=	shear resistance (N)
V_{sg}	=	shear link contribution to shear resistance (N)
v	=	shear stress = $V / b_w d$ (N/mm^2)
w	=	crack width (mm)
β	=	tensile stress factor
ε_1	=	principal tensile strain

ε_x = longitudinal strain

Tabular values of β and θ are provided in CSA A23.3[104]. These values are optimised to give the minimum amount of shear links in design. As corroded structures are likely to have small link areas, the optimisation is appropriate for assessment.

The comparisons are shown in Table 6-6. BS 8110[69] is used with the modifications presented earlier in Section 6.3.1, whilst the EC 2[59] and A23.3[104] procedures are used with no modifications.

The modified BS 8110[69] approach gives mean test/predicted values of 1.01 for the control beams and 1.06 for the corroded beams. However, much of this difference in mean values could be due to beams 131 and 132 (both are uncorroded) where all three methods appear to substantially overestimate the load-carrying capacity. The coefficient of variation of the corroded beams (15.2%) is actually less than that of the control beams (18.1%). Ignoring beams 131 and 132, the mean and coefficient of variation of the control beams are 1.13 and 8.1% respectively. This suggests that the predictions for the corroded beams are less conservative than those for the uncorroded beams.

The predictions using EC 2[59] give mean test/predicted values of 1.04 and 0.92 for the control and the corroded beams respectively. The coefficient of variation does fall from 32.3% for the control beams to 19.3% for the corroded beams. Ignoring beams 131 and 132, the mean and coefficient of variation of the control beams are 1.25 and 18.0% respectively. The size of the coefficient of variation and the significant drop in the mean suggest that modifications are required to the EC 2 procedures to incorporate the effects of corrosion.

Table 6-6: Comparison of BS 8110, EC 2 and CSA A23.3 procedures for calculating the shear strength of corroded beams with shear links

Beam	*Corrosion*		*Test*	*BS 8110*		*EC 2*		*A23.3*	
	Tens (%)	*Link (%)*	V_{test} *(kN)*	V_{pred} *(kN)*	V_{test} / V_{pred}	V_{pred} *(kN)*	V_{test} / V_{pred}	V_{pred} *(kN)*	V_{test} / V_{pred}
L24A/0	0.0	0.0	118.9	98.6	1.21	83.1	1.43	38.9	1.52
L24A/1	1.4	6.1	102.5	95.5	1.07	80.5	1.27	37.9	1.31
L24A/2	5.6	12.7	90.9	91.9	0.99	77.3	1.18	37.6	1.19
L24A/3	9.5	23.2	84.1	86.6	0.97	72.6	1.16	37.4	1.17
L24B/0	0.0	0.0	93.8	90.8	1.03	94.1	1.00	42.0	1.17
L36A/0	0.0	0.0	105.4	91.3	1.15	79.2	1.33	39.0	1.44
123	12.3	78.2	74.6	65.2	1.14	80.6	0.93	43.6	1.32
124	15.4	86.6	55.8	64.2	0.87	77.0	0.72	42.1	0.94
125	15.1	93.8	62.7	64.4	0.97	74.9	0.84	42.9	1.15
131	0.0	0.0	100.2	125.8	0.80	144.2	0.70	42.8	0.78
132	0.0	0.0	105.6	125.8	0.84	144.2	0.73	42.8	0.83
134	12.0	69.8	69.2	54.0	1.28	73.9	0.94	43.5	1.10
133	11.0	73.3	69.0	51.8	1.33	72.1	0.96	43.5	1.12
136	13.5	86.6	58.1	51.2	1.14	66.8	0.87	43.6	1.03
135	13.8	93.8	67.7	51.3	1.32	64.6	1.05	43.7	1.25
215	10.7	66.0	77.2	67.5	1.14	88.7	0.87	43.5	1.21
216	11.6	82.6	72.4	65.8	1.10	82.0	0.88	43.6	1.29
213	14.1	86.6	53.1	64.0	0.83	79.5	0.67	41.9	0.87
214	15.4	97.2	57.4	62.0	0.93	75.5	0.76	42.7	1.03
315	16.9	97.2	55.4	62.5	0.89	76.3	0.73	42.4	0.96
				Mean	1.01	Mean	1.04	Mean	1.15
			Control beams	S. dev.	0.182	S. dev	0.335	S. dev	0.339
				C.o.V.	18.1%	C.o.V.	32.3%	C.o.V.	29.6%
				Mean	1.06	Mean	0.92	Mean	1.13
			Corroded beams	S. dev	0.162	S. dev	0.178	S. dev	0.140
				C.o.V.	15.2%	C.o.V.	19.3%	C.o.V.	12.4%
				Mean	1.05	Mean	0.95	Mean	1.13
			All beams	S. dev	0.141	S. dev	0.223	S. dev	0.197
				C.o.V.	15.6%	C.o.V.	23.4%	C.o.V.	17.4%

Note: L series beams were tested by Daly[66], others were tested by Rodriguez et al[45].

The predictions using the modified compression field theory as incorporated in A23.3[104] give mean test/predicted values of 1.15 and 1.13 for the control and the corroded beams respectively. The coefficient of variation falls from 29.6% for the control beams to 12.4% for the corroded beams. Ignoring beams 131 and 132, the mean and coefficient of variation of the control beams are 1.38 and 13.3% respectively. The predicted values suggest that A23.3 gives satisfactory prediction of the effects of corrosion without modifications. This method seems to perform better for corroded beams when links are present than when they are not.

There appeared to be greater variability in the predictions when shear links were present. This could be due to variations in the amount of corrosion in different locations on a link. Links tend to corrode preferentially at the corner bends where they are in contact with the longitudinal bars. However, as links resist shear forces across diagonal cracks, they are perhaps not always required to resist shear forces in the corners. Hence, average and maximum corrosion measurements may not always be relevant unless the corrosion is reasonably uniform or the measurements are taken in the relevant location.

BS 8110 indicates that below a minimum link level of $A_{sv}\ f_{yv}/b\ s_v = 0.4$ the link reinforcement does not contribute to the shear resistance. All of the corroded beams tested by Rodriguez et al[45] had less shear reinforcement than this minimum level. As such the BS 8110 predictions are based on the V_c component alone. The EC 2 and A23.3 predictions have included the link contribution. Inspection of Table 6-6 shows that the effects of ignoring the links in the BS 8110 method are inconclusive, with a similar number of over and underestimates of the test load being made. However, the EC 2 standard method appears to overestimate the test load in most cases for the beams tested by Rodriguez et al[45] but not for those tested by Daly[66]. This suggests that the minimum level of links should be used with the EC 2 approach. The situation is confused further when the predictions from the A23.3 method are considered. The predicted loads were consistently smaller than the test loads for both the beams tested by Daly and those tested by Rodriguez et al for all but three corroded beams. This could be due to the fact that the strut angle is allowed to move to reflect the reducing amount of links.

6.4 Shear strength of corroded members with plain bars

Only the data obtained by Daly[66] are available for quantitative analysis. Considerable increases in shear load-carrying capacity after corrosion are shown in Figure 6-6. The beams with cover to bar diameter (c/D) ratios of 1 and 2 exhibited a more significant increase in shear load-carrying capacity at low corrosion levels than those with c/D =3. This is contrary to what would, initially, be expected as the bars with the higher c/D ratio would be expected to exhibit smaller reductions of bond strength.

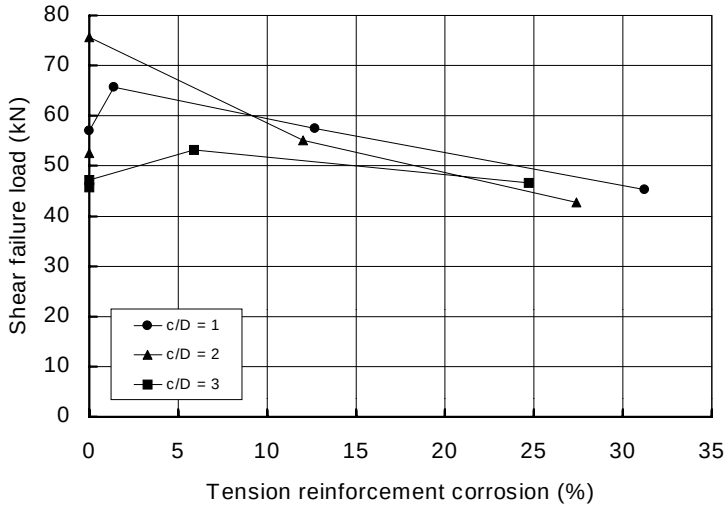

Figure 6-6: The variation in shear load-carrying capacity with corrosion for beams with plain bars

The phenomenon of beams reinforced with plain bars achieving higher shear load-carrying capacities than similar beams with ribbed bars is well known[110, 111, 112]. This increase is attributed to the lower bond strength of the plain bars in comparison to the ribbed bars. Provided that the anchorages remain intact tied arch behaviour can occur.

The beam flexural shear capacity relies on bond strength to transfer forces in the tension reinforcement into the concrete. As the bond strength diminishes the potential for force transfer between steel and concrete also diminishes until plane sections no longer remain plane. At this point the concrete and reinforcement are behaving independently of one another. The beam will either fail or find an alternative method of carrying the load. The alternative load-carrying mechanism in this case is likely to be the tied arch, as illustrated in Figure 6-7. Tied arch

behaviour relies on bond at the end anchorages. Even if the anchorage zones have undergone similar corrosion to the span sections, the anchorage bond strength is likely to be enhanced due to the presence of transverse compression from the support reaction.

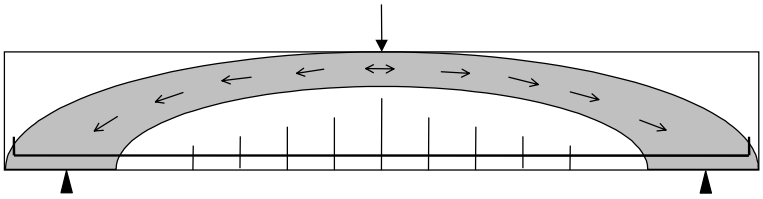

Figure 6-7: Tied arch action

Descriptions of the beams[66] prior to testing indicate corrosion cracking along the line of the reinforcement. This implies that there would have been a reduction in bond strength. Whilst disruption is reported at the anchorages there were no reports of anchorage failures.

Cairns[113] tested a range of beams in which the reinforcement was exposed for repair over various lengths. The anticipated failure mode was in shear. However, those beams where a bar was debonded over the majority of the length gave higher failure loads than predicted using the BS 8110[69] expressions for shear. In his discussion Cairns suggests that the observed phenomenon may be similar to that proposed by Lorentsen[114]. Lorentsen suggested that:

$$V = \frac{dM}{dx} = \frac{d(A_{st} f_{st} z)}{dx} = \frac{d(A_{st} f_{st})}{dx} z + A_{st} f_{st} \frac{dz}{dx} \qquad \text{… (6-18)}$$

where: A_{st} = area of tension reinforcement

d = effective depth to the tension reinforcement

f_{st} = stress in tension reinforcement

M = moment

V = shear force

z = lever arm

The first term of the final expression represents the contribution of the beam flexural shear capacity whilst the second term represents the arch action. There are two extremes to this expression. In an elastic beam the lever arm would remain constant, and the second term would be zero. In a tied arch the bond between the reinforcement and the concrete would be zero along the length of the beam and, as such, the stress in the reinforcement would be constant making the first term zero. The situation found in corroded beams is likely to be somewhere between the two extremes. The bond between the reinforcement and the concrete will have been reduced by corrosion but not to the extent that there is a complete breakdown over the whole length of the beam between supports. The loss of bond is likely to vary along the length of a beam due to variations in both corrosion and loading. The relative contributions of the arch and beam terms will thus vary. It could be possible that as the beam shear term reduces due to the reduction in bond the arch term could increase to replace or even exceed the beam shear term. The components are illustrated in Figure 6-8.

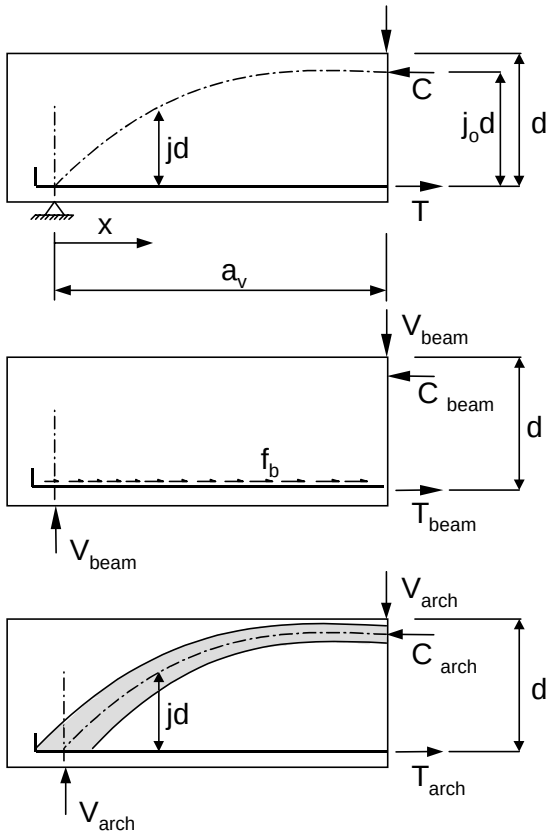

Figure 6-8: The beam shear and arch components of shear resistance

Considering the beam shear capacity term:

$$\frac{dA_{st} f_{st}}{dx} = \frac{dT}{dx} \qquad \textbf{… (6-19)}$$

This represents the change in tensile force along the length of the bar. That is the bond force per unit length transmitted between the steel and concrete. Bazant and Kim[115] have developed a theory for combined beam and arch behaviour. They express the beam shear term as:

$$\frac{dT}{dx} = c_0(\pi \Sigma D f_b) \qquad \textbf{… (6-20)}$$

where:
- c_0 = constant relating to bond strength
- D = bar diameter
- f_b = bond strength
- f_c = concrete compressive cylinder strength
- T = force in the reinforcing bar
- x = distance along the beam

If the cross-section remains constant whilst the amount of reinforcement, ρ, varies then D will be proportional to √ρ. The bond stress is proportional to the concrete tensile strength which, itself, is roughly proportional to the square root of the concrete compressive strength. Thus:

$$V_{beam} = k_1 \sqrt{\rho} \sqrt{f_c} b(j_0 d) \qquad \textbf{… (6-21)}$$

where:
- b = breadth of the section (mm)
- d = effective depth to the tension reinforcement (mm)
- f_c = concrete compressive cylinder strength (N/mm^2)
- j_0 = variable relating to the lever arm
- k_1 = a constant relating to the beam shear capacity

V_{beam} = beam shear component (N)

ρ = reinforcement ratio = A_{st} / bd

Bazant and Kim[115] have derived an empirical relationship, based on elastic theory, between the lever arm (see Figure 6-8) and the reinforcement ratio such that:

$$j_0 = k_2 \rho^{-m} \quad \text{… (6-22)}$$

Therefore:

$$V_{beam} = k_3 \rho^{0.5-m} f_c^{0.5} bd \quad \text{… (6-23)}$$

where: j_0 = a variable relating to the lever arm

k_2, k_3 = constants relating to the beam shear capacity

m = constant relating to the lever arm

Bazant and Kim[115] have also derived an empirical expression for the arch shear term, V_{arch}. The variation in lever arm (see Figure 6-8) is assumed to be related to the shear span by the following expression:

$$jd = j_0 d \left(\frac{x}{a_v} \right)^r \quad \text{… (6-24)}$$

where: a_v = shear span (mm)

r = a constant

x = position along the beam (mm)

When differentiated, this becomes:

$$\frac{d(jd)}{dx} = j_0 d \frac{r}{a_v} \left(\frac{x}{a_v} \right)^{r-1} \quad \text{… (6-25)}$$

By taking T = σ_s ρ b d, V_{arch} is given by:

$$V_{arch} = j_0 d \frac{r}{a_v}\left(\frac{x}{a_v}\right)^{r-1} \sigma_s \rho b d^2 \qquad \textbf{… (6-26)}$$

where: σ_s = stress in the reinforcement (N/mm^2)

The critical section is taken as being at a distance d from the support (i.e. x = d). Taking σ_s as constant along the debonded length, and introducing the expression for j_0, V_{arch} simplifies to:

$$V_{arch} = k_4 \frac{\rho^{1-m}}{(a_v/d)^r} bd \qquad \textbf{… (6-27)}$$

where: k_4 = a constant relating to the beam shear capacity

Both the beam and arch terms were amended by Bazant and Kim[115] to reflect the implications of size effect by introducing a multiplier, ξ, as follows:

$$\xi = \frac{1}{\sqrt{1+\frac{d}{25 d_a}}} \qquad \textbf{… (6-28)}$$

where: d = effective depth to the tension reinforcement
d_a = maximum aggregate size
ξ = variable to reflect size effects in shear

By carrying out non-linear regression on 296 test beams, Bazant and Kim[115] derived the following empirical expression for shear strength:

$$V = 0.83\xi\rho^{0.333} f_c^{0.5} bd + 206.9\xi\rho^{0.833}\left(\frac{a_v}{d}\right)^{-2.5} bd \qquad \textbf{… (6-29)}$$

Ideally, the first term would have been expressed in terms of bond strength such that the effects of a reduction in bond strength could have been included and the constants modified to suit. However, the term has been calibrated in terms of steel ratio and concrete compressive strength. Given the scarcity of shear test with corroded plain bars, re-calibration of Bazant and Kim's expression is not feasible. The expression will be used in the form given in equation 6-29.

The V_{beam} term is essentially a bond strength term. It is suggested that once a threshold bond strength has been reached and the reinforcement is no longer fully bonded V_{beam} will reduce in direct proportion to the reduction in bond strength. In the case of the beams tested here, the V_{arch} term will attempt to rise to compensate for the reduction in V_{beam}.

The threshold bond strength beyond which bond strength begins to break down is difficult to ascertain. An alternative approach is to consider the corroded bond strength as a proportion of the uncorroded bond strength. However, there are several ways of calculating the uncorroded bond strength including BS 8110[69] and Tepfers[47]. As the c/D ratio has little effect on the bond strength of uncorroded plain bars the Tepfers procedure is not applicable, and the BS 8110 approach will have to be used. Using the BS 8110 bond strengths may lead to the anomaly of lightly corroded bars with a high c/D ratio having a higher estimated bond strength than uncorroded bars. A possible solution is to limit the ratio $f_b/f_{b.8110}$ to one. The empirical approach proposed can be expressed as follows:

$$V = \left(\frac{f_{b.corr}}{f_{b.8110}} \right) V_{beam} + f\left(\frac{f_{b.corr}}{f_{b.8110}} \right) V_{arch} \qquad \textbf{… (6-30)}$$

where: f() = a function (to be determined)

$f_{b.corr}$ = corroded bond strength (N/mm^2)

$f_{b.8110}$ = uncorroded bond strength calculated using the BS 8110 formula (N/mm^2)

V_{beam} = shear strength contribution due to beam shear calculated using the Bazant and Kim formulae (N)

V_{arch} = shear strength contribution due to arch behaviour calculated using the Bazant and Kim formulae (N)

The form of the function for modifying V_{arch} can be determined by assuming that the V_{beam} term is appropriate for use with the beams tested by Daly[64]. The reduced V_{beam} term is then subtracted from the shear strength measured during the tests to give the contribution of V_{arch}.

The V_{arch} component can be seen from Figure 6-9 to be related linearly to the reduction in bond strength, with a correlation coefficient, r^2, of 0.81. Figure 6-9 is indicative of how the V_{arch} component varies from 40% of the test load-carrying capacity when fully bonded ($f_{b.corr}/f_{b.8110}$ = 1) to 100% of the capacity when bond is estimated to have broken down ($f_{b.corr}/f_{b.8110}$ = 0). A more useful relationship for assessment is that between the reduction in bond strength and the ratio of the arch component in the corroded member to the arch component derived by Bazant and Kim[115] (V_{arch} / V_{Bazant}). This is shown plotted in Figure 6-10.

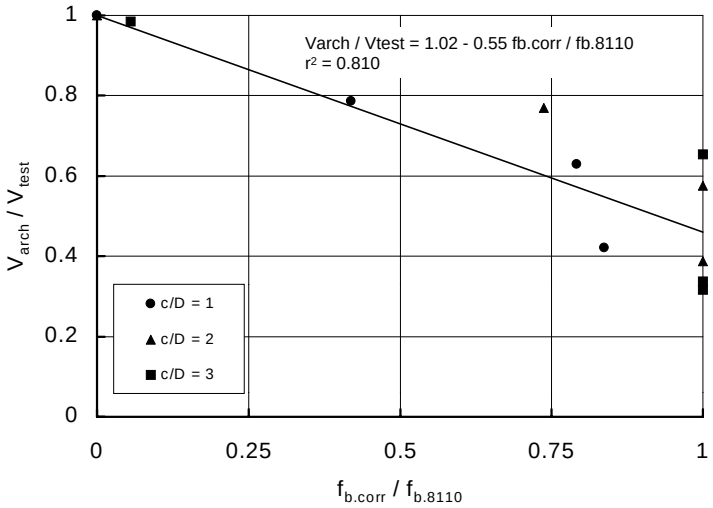

Figure 6-9: Variation in the ratio V_{arch}/V_{test} with the ratio $f_{b.corr}$ / $f_{b.8110}$

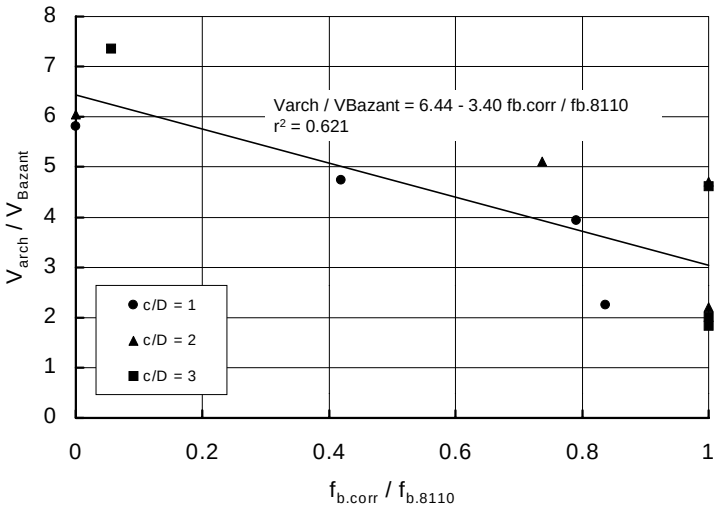

Figure 6-10: Variation in the ratio V_{arch} / V_{Bazant} with the ratio $f_{b.corr}$ / $f_{b.8110}$

The proposed relationship for simply supported beams with corroded plain reinforcement failing in shear (as tested by Daly[66]) is:

$$V = \left(\frac{f_{b.corr}}{f_{b.8110}} \right) V_{beam} + \left(6.44 - 3.40 \left(\frac{f_{b.corr}}{f_{b.8110}} \right) \right) V_{arch} \quad \textbf{… (6-31)}$$

where:

$$V_{beam} = 0.83 \xi \rho^{0.333} f_c^{0.5} bd \quad \textbf{… (6-32)}$$

$$V_{arch} = 206.9 \xi \rho^{0.833} \left(\frac{a_v}{d} \right)^{-2.5} bd \quad \textbf{… (6-33)}$$

The predicted shear load-carrying capacities are compared with the test values in Figure 6-11. The predicted values appear to be reasonable. Unfortunately, the generality of this expression cannot be proved as the tests were only carried out at one a_v / d ratio. Further tests are required to validate this expression.

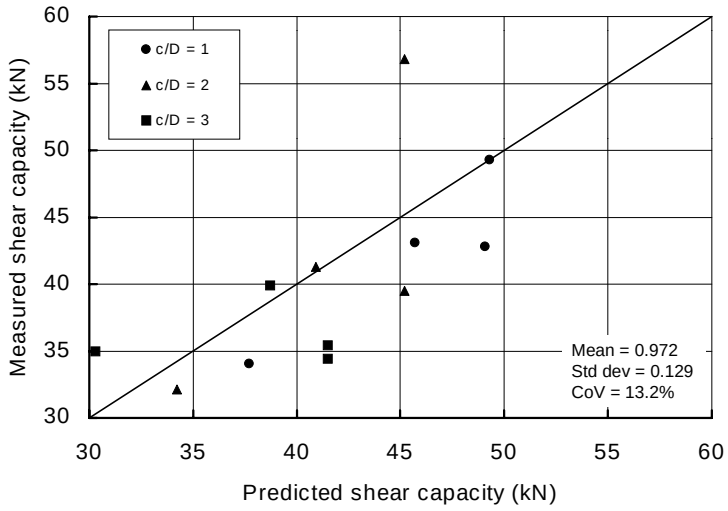

Figure 6-11: Comparison of measured and predicted shear load-carrying capacity for the beams tested by Daly[66] and containing corroded plain reinforcement

In the case of laboratory specimens the failure load is known. The load-carrying capacity can be apportioned between beam and arch behaviour for each beam specimen. This could then be related to the level of corrosion obtained and the beam and load geometry. In real structures the loading is not as simple as a single point load, the beams are often continuous, the reinforcement may be lapped and corrosion is typically localised rather than over the full length. Whilst the composite tied arch approach developed here is useful for a qualitative understanding of the behaviour of corroded beams in shear, it is unlikely to prove practical or reliable for use in practice.

Given the empirical nature of the proposed approach, it is difficult to tell when the failure mode will be dominated by a tied arch mechanism as opposed to a beam mechanism. This has implications for the anchorage forces that need to be developed. In a tied arch, the full yield strength of the bars may need to be developed. In beam shear, the tension reinforcement tends not to yield[102] but slip must be avoided to prevent premature shear failure. This brings the implication that sufficient anchorage should be provided to allow the reinforcement to yield. If this is not provided then anchorage bond will be a limiting criterion. BS 8110[69] currently requires an anchorage length of 12 bar diameters to be provided beyond the support centreline at simple supports. It is not clear where this requirement originated or what the range of its validity is.

6.5 Conclusions

The following conclusions can be drawn from the work reported in this Chapter:

1. The empirical nature of the BS 8110 procedures for calculating shear strength makes it difficult to identify where and how modifications are required to reflect the effects of corrosion.

2. The behaviour of beams with plain and ribbed bars without links appears to be different, with significant increases in shear load-carrying capacity over that of the uncorroded beams occurring in the beams with corroded plain bars.

3. Dowel action would be expected to reduce in corroded members with no links. However, any loss in dowel action appears to be offset by a change in failure mechanism.

4. The cover to bar diameter (c/D) ratio appears to have a significant beneficial effect in determining the shear load-carrying capacity once corrosion has occurred.

5. The effects of corrosion can be incorporated in the empirical shear rules of BS 8110 by calculating an effective area of tension reinforcement, and using this area to calculate the V_c component of shear resistance. The primary variables in the formula for effective area of tension reinforcement are c/D ratio and the ratio of corroded to BS 8110 bond strength.

6. The V_c component (calculated using the expression for the effective area of tension reinforcement) also appears to be appropriate for use with members containing links.

7. Due to the absence of test data, it is not possible to make a judgement on the suitability of the V_c component for use in calculating the punching shear capacity of a corroded slab.

8. Shear links have beneficial effects on both the bond and shear strength of corroded members. However, links are prone to significant corrosion due to their location.

9. It is not possible to ascertain whether shear links contribute to the shear resistance of corroded members when the proportion of links is considerably below the minimum level specified in BS 8110.

10. BS 8110 with the modifications proposed in this Chapter gives similar means and coefficients of variation for the test/predicted shear load-carrying capacities of both control and corroded beams. This suggests that for the beams considered here the effects of corrosion are catered for in the proposed modifications.

11. BS 8110 with the modifications proposed in this Chapter gives conservative predictions in the majority of cases.

12. EC 2 without any modifications gives the best mean test/predicted shear load-carrying capacity ratios for beams without links. It does so at the expense of a high coefficient of variation. When links are included, EC 2 tends to overestimate the shear capacity of corroded beams. This suggests that modifications are necessary to incorporate the effects of corrosion into the EC 2 procedures.

13. The Modified Compression Field Theory as implemented in CSA A23.3 gives adequate predictions for members with and without links. It appears better able to cope with a low level of link reinforcement. However, it may require some modifications to reduce the variability of the predictions when no links are present.

14. The increase in shear load-carrying capacity in beams with corroded plain bars has been explained using a model of tied arch behaviour that occurs in the presence of low bond strength. A numerical procedure is presented, but needs validation against further test data.

7 COLUMN BEHAVIOUR

The last of the key load-carrying mechanisms addressed in this Thesis is axial load-carrying capacity or, as it is referred to here, column behaviour. The term column behaviour is used to acknowledge that axial load on its own is not common in real structures. It usually occurs in conjunction with applied bending moments.

7.1 Column mechanisms

BS 8110[69] sub-divides columns according to three criteria: bracing, slenderness, and the bending to which they are subjected. The classification system is shown in Table 7-1

Table 7-1: BS 8110 classification system for columns

Criteria	*Categories*
Bracing	(i) Braced
	(ii) Unbraced
Slenderness	(i) Slender
	(ii) Stocky
Applied moment	(i) Primarily axial load with nominal moments.
	(ii) Significant moments bent about one axis only.
	(iii) Significant moments bent about two axes.

Only one set of data is available, that of Rodriguez et al[68], that contains sufficient data to allow a quantitative analysis to be undertaken. Although these columns are axially loaded, nominal moments are present due to a combination of the non-uniformity of the corrosion, imperfections in the casting and testing regime and, at later stages, spalling.

Test data are only available for the effects of accelerated corrosion on stocky columns subject to an axial load combined with eccentricity-induced moments. However, where appropriate, these test data are used to assess procedures for columns subject to applied moments.

7.2 Columns subject to axial load and nominal moments

BS 8110[69] gives the axial load-carrying capacity of short columns subject primarily to axial loads as:

$$N = \frac{0.67 f_{cu} A_c}{\gamma_{mc}} + \frac{f_y A_{sc}}{\gamma_{ms}} \qquad \textbf{… (7-1)}$$

where: A_c = area of concrete (mm^2)

A_{sc} = area of reinforcement in compression (mm^2)

f_{cu} = concrete compressive cube strength (N/mm^2)

f_y = reinforcement yield stress (N/mm^2)

N = ultimate axial strength (N)

γ_m = partial safety factor for concrete

γ_s = partial safety factor for reinforcement

When nominal moments are present BS 8110[69] reduces the axial capacity to 90% of this value. This approach has been applied to the columns of Rodriguez et al[68]. The corroded area of reinforcement has been used along with three different areas of concrete:

(i) Gross area – as cast.

(ii) With the corner concrete spalled – as considered for bending in Chapter 5.

(iii) With all of the cover concrete spalled – as observed by Rodriguez et al[68] in their column tests.

These sections are illustrated in Figure 7-1.

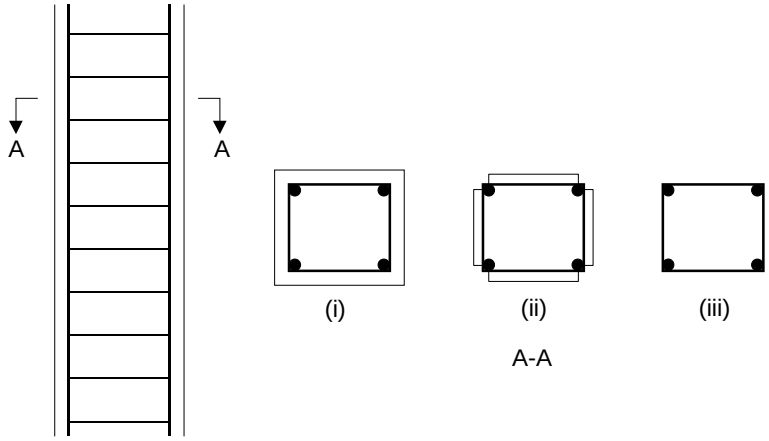

Figure 7-1: Various cross-sections used for the analysis of concrete columns with corroded reinforcement

Details of the uncorroded cross-sections tested by Rodriguez et al[68] are shown in Figure 7-2.

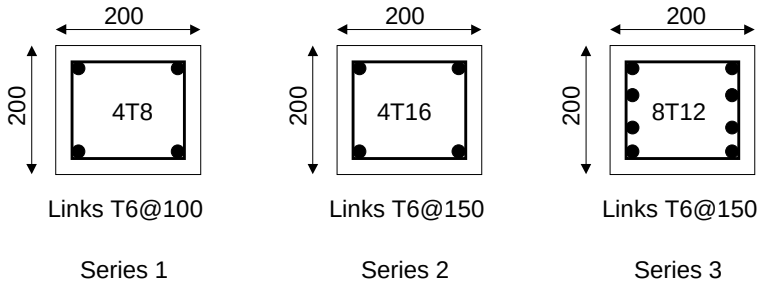

Figure 7-2: Cross-sections of the columns tested by Rodriguez et al[68]

The results are shown in Table 7-2 (as individual concrete and reinforcement components of axial capacity) and Figure 7-3 (as composite concrete plus reinforcement axial capacities). It can be seen that the best estimate of axial load-carrying capacity is obtained by ignoring the whole of the cover zone outside the links. The mean and coefficient of variation of the ratios of test to predicted loads for the corroded columns are 1.06 and 10.5% respectively.

Table 7-2: Contribution of concrete and reinforcement components to the load-carrying capacity of columns with corroded reinforcement

Column	*fcu* (N/mm^2)	*Compression bars*		*Axial load (kN)*	*Axial load-carrying capacity (kN)*			
		Provided	*Corrosion (%)*		*Gross concrete*	*Corners spalled*	*All cover spalled*	*Reinforcement*
11	35	4T8	0.0	1300	849	na	na	107
12	35	4T8	0.0	1320	849	na	na	107
14	45	4T8	14.9	993	1080	1042	695	91
13	45	4T8	15.4	990	1080	1042	695	91
15	44	4T8	18.6	947	1053	1016	677	87
16	44	4T8	20.8	828	1053	1016	677	85
17	45	4T8	24.3	822	1080	1042	695	81
18	45	4T8	27.8	862	1080	1042	695	77
21	40	4T16	0.0	1680	948	na	na	421
22	40	4T16	0.0	1702	948	na	na	421
24	45	4T16	9.0	1040	1055	1033	689	383
23	45	4T16	9.3	1080	1055	1033	689	382
25	43	4T16	10.9	1091	1016	996	664	375
26	43	4T16	11.2	1135	1016	996	664	374
27	46	4T16	14.9	973	1081	1059	706	358
28	46	4T16	15.1	997	1081	1059	706	357
31	41	8T12	0.0	1728	955	na	na	448
32	41	8T12	0.0	1673	955	na	na	448
33	45	8T12	9.8	1274	1070	1051	700	404
34	45	8T12	11.0	1178	1070	1051	700	399
36	52	8T12	12.6	1174	1214	1192	795	392
35	52	8T12	12.9	1203	1214	1192	795	390
37	51	8T12	16.3	1038	1196	1175	783	375
38	51	8T12	17.8	1170	1196	1175	783	368

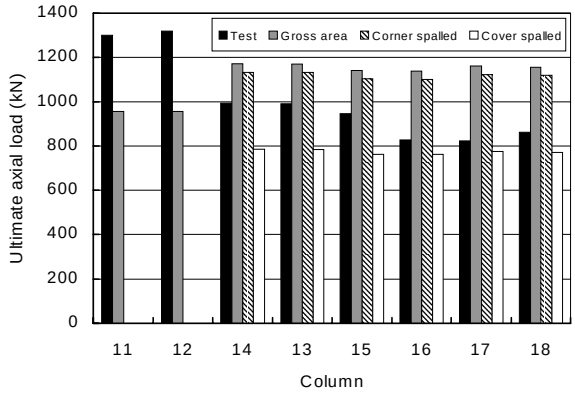

(a) Series 1

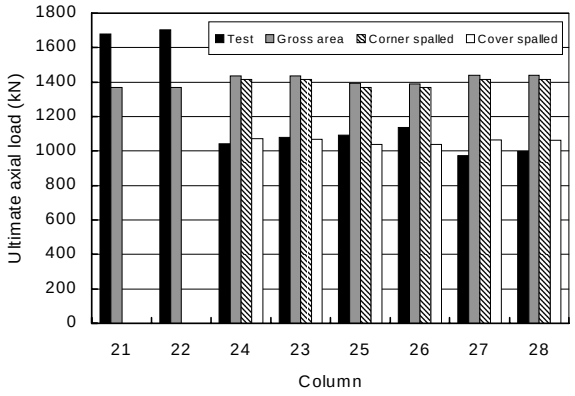

(b) Series 2

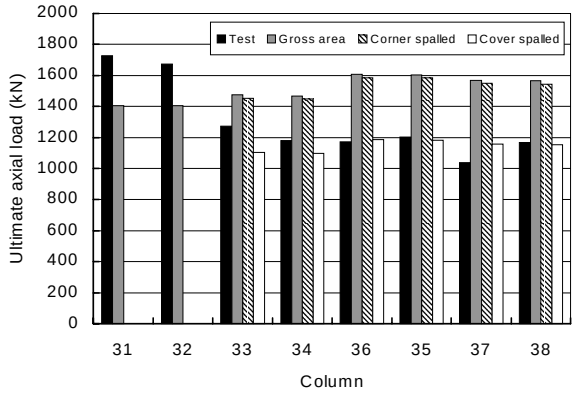

(c) Series 3

Figure 7-3: Comparison of axial load-carrying capacity of corroded columns calculated using three different areas of concrete

Breaking of between one and four links was observed by Rodriguez et al[68] after the tests. Bars were also observed, after the tests, to have buckled. This suggests that this phenomenon should be considered in the calculation of the axial load carried by the reinforcement. The loss of one link leads to predictions of premature buckling in the main bars. However, allowing for premature buckling using the procedures proposed in Section 5.4 leads to assumptions of negligible capacity in the reinforcement. Inspection of Table 7-2 indicates that this is not the case. A possible explanation for this is given by a combination of the load-strain curves presented by Rodriguez et al[68] and the fact that the observations were made after the test. The load-strain curves show reductions in load-carrying capacity after the peak load. It could be in this period after the peak load that the links start breaking and the bars start buckling to give the appearance observed at the end of the test. This is in contrast to the spalling of the cover concrete which is

observed at loads below the peak, and so should be included in any calculations. The estimates of load-carrying capacity indicate that the main compression bars appear to be sufficiently contained within the concrete after delamination of the cover to achieve their ultimate strength.

An interesting feature of this analysis is the substantial underestimate of the axial load-carrying capacity of the uncorroded columns. This suggests that either: the BS 8110[69] procedure is conservative, the 0.67 factor in equation 7-1 is not appropriate to the test arrangement used by Rodriguez et al[68] or that the moments generated during the tests were negligible rather than nominal. The interaction diagram approach used in Section 7.3 does, however, give reasonable predictions for the control columns.

7.3 Columns subject to axial load and moments about one axis

No tests have been carried out on corroded columns subject to significant moments. The moments used in this section are based on measurements by Rodriguez et al[68] of the applied axial load and the eccentricity induced by the test regime and spalling. The eccentricities were calculated by Rodriguez et al from displacement readings taken on all four faces at mid-height. The eccentricities and moments are given in Table 7-3.

The assessment of columns is typically based on moment-axial load interaction diagrams. The procedures derived in Chapter 5 have been applied to generate M-N curves for each of the three series of columns. In Section 7.1 it was found that a concrete cross-section with no concrete outside the links was the most appropriate cross-section for assessing corroded columns, and that approach is also used here. Three analyses have been conducted in order to bracket the likely conditions found in the experiments:

(i) Section as cast.
(ii) Section with no concrete outside the links without any reinforcement corrosion.
(iii) Section with no concrete outside the links and reinforcement corrosion corresponding to the average of the corroded columns in each series.

Table 7-3: Eccentricities and their corresponding moments induced during accelerated corrosion tests for the concrete columns tested by Rodriguez et al[68]

Column No	*N (kN)*	e_x *(mm)*	e_y *(mm)*	M_x *(kNm)*	M_y *(kNm)*
11	1300	4.9	8.8	6.4	11.4
12	1320	9.4	1.1	12.4	1.5
14	993	2.8	10.7	2.8	10.6
13	990	13.6	8.1	13.5	8.0
15	947	13.4	8.1	12.7	7.7
16	828	9.4	20.5	7.8	17.0
17	822	24.2	5.4	19.9	4.4
18	862	7.8	10.6	6.7	9.1
21	1680	8.2	2.3	13.8	3.9
22	1702	2.1	5.4	3.6	9.2
24	1040	22.2	15.6	23.1	16.2
23	1080	20.5	14.1	22.1	15.2
25	1091	13.8	16.4	15.1	17.9
26	1135	1.4	7.4	1.6	8.4
27	973	3.2	4.6	3.1	4.5
28	997	1.9	5.5	1.9	5.5
31	1728	1.2	5.2	2.1	9.0
32	1673	2.1	5.4	3.5	9.0
33	1274	10	7.9	12.7	10.1
34	1178	7.8	11.3	9.2	13.3
36	1174	9.2	20.9	10.8	24.5
35	1203	4	2	4.8	2.4
37	1038	4.8	4.6	5.0	4.8
38	1170	21.1	4	24.7	4.7

The results of these analyses are shown in Figure 7-4. As the Series 1 and 2 columns were

symmetric, the moment capacities about both the x and y axes were assumed to be the same. Hence, the moments about both axes are included on the one interaction diagram. The Series 3 columns had different reinforcement arrangements about the two axes. Hence, two interaction diagrams are necessary, one for bending about each axis.

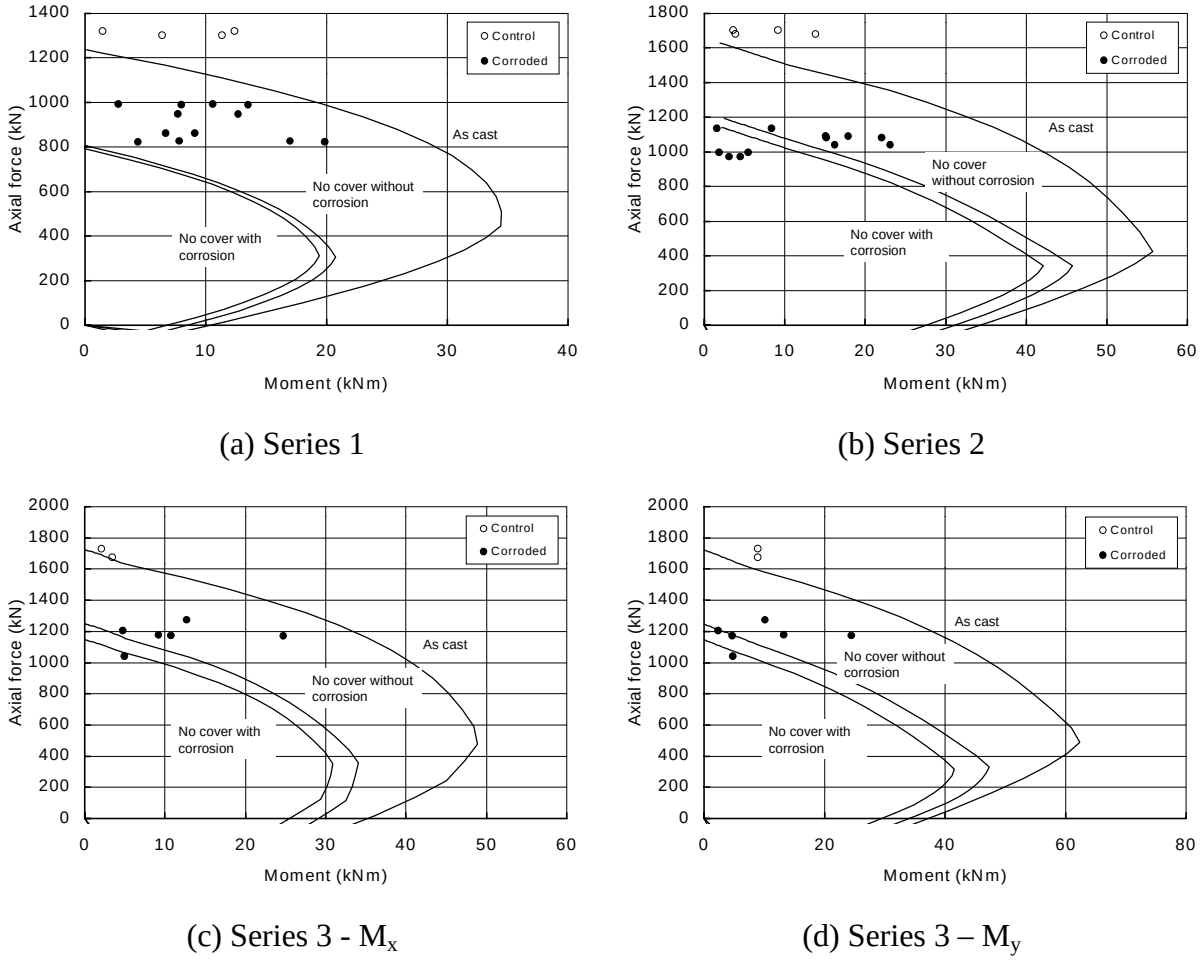

(a) Series 1

(b) Series 2

(c) Series 3 - M_x

(d) Series 3 – M_y

Figure 7-4: Moment-axial force interaction diagrams for corroded columns treated as bending about one axis

In the interaction diagrams for the Series 1 and 3 columns all bar two of the results are in the failure region. The two results inside the failure line are only marginally so. For the series 2 columns, five results are inside the failure line at low moments. This is not as serious as it may appear. BS 8110 requires a minimum eccentricity (the smaller of h/20 or 20 mm) be applied to all columns. Applying the minimum eccentricity would have resulted in larger moments than

resulted from the test eccentricities. This would have moved the results into the failure region. Treating the columns as subject to biaxial bending would also have a similar result.

7.4 Columns subject to axial load and moments about two axes

The BS 8110[69] approach to biaxial bending in symmetrically reinforced columns is to increase the moment about one axis and then to design for that increased moment using the approach for columns bent about one axis. Either the moment about the x or the y-axis is enhanced depending on the relative magnitude of the two moments. The enhanced moments are calculated using the following equations:

When:

$$\frac{M_x}{h'} \geq \frac{M_y}{b'} \qquad \text{… (7-2)}$$

$$M_x' = M_x + \beta \frac{h'}{b'} M_y \qquad \text{… (7-3)}$$

and when:

$$\frac{M_x}{h'} < \frac{M_y}{b'} \qquad \text{… (7-4)}$$

$$M_y' = M_y + \beta \frac{b'}{h'} M_x \qquad \text{… (7-5)}$$

where: b’ = effective depth to the reinforcement taken perpendicular to the y-axis (mm)

h’ = effective depth to the reinforcement taken perpendicular to the x-axis (mm)

M_x = applied moment about the x-axis (kNm)

M_x ’ = increased moment about the x-axis (kNm)

M_y = applied moment about the y-axis (kNm)

M_y = increased moment about the y-axis (kNm)

,

β = a coefficient which is a function of N/bhf_{cu}

Deterioration is not necessarily symmetric, and there is a possibility that the effects of corrosion may not be fully catered for by the BS 8110 approach. BS 5400[97] and BD 44/95[73] both use the method developed for CP 110[116], the forerunner to BS 8110. This method is based on comparing the applied moment about each axis to the corresponding moment capacity as follows:

$$\left(\frac{M_x}{M_{ux}}\right)^{\alpha_n} + \left(\frac{M_y}{M_{uy}}\right)^{\alpha_n} \leq 1 \qquad \textbf{… (7-6)}$$

where: M_x = applied moment about the x-axis (kNm)

M_{ux} = moment capacity about the x-axis coexistent with N (kNm)

M_y = applied moment about the y-axis (kNm)

M_{uy} = moment capacity about the y-axis coexistent with N (kNm)

N = applied axial load (kN)

N_{uz} = column squash load = $(0.67\ f_{cu} / \gamma_{mc})\ A_c + (f_y / \gamma_s)\ A_{sc}$ (kN)

α_n = a function of N / N_{uz}

This expression appears more logical for the assessment of corrosion-damaged concrete columns as it allows the moment applied about an axis to be compared explicitly with the moment capacity about that axis. Whilst this method is not as accurate as a three dimensional interaction diagram, Beeby[117] has shown that it gives a close fit to the interaction diagram solution for all but the lowest applied axial loads in which case it is conservative. Beeby also showed that the increased moment method gave similar answers to the BS 5400 and BD 44/95 approach. Hence, there is little to choose between the models in terms of end result.

As with the two preceding sections, the only data available are those of Rodriguez et al[68]. The moments used in this section are those given in Table 7-3. For the data of Rodriguez et al,

inequality 7-6 was found to be unsatisfactory. In most of the columns the moment capacity was predicted to be zero or negligible at the ultimate axial load leading to values of the inequality well in excess of 1.0. In real structures this is unlikely to be the case. The BS 8110 increased moment approach was used instead, and the results are shown in Figure 7-5. The results appear to be satisfactory for all bar two of the Series 2 columns which are marginally inside the failure line.

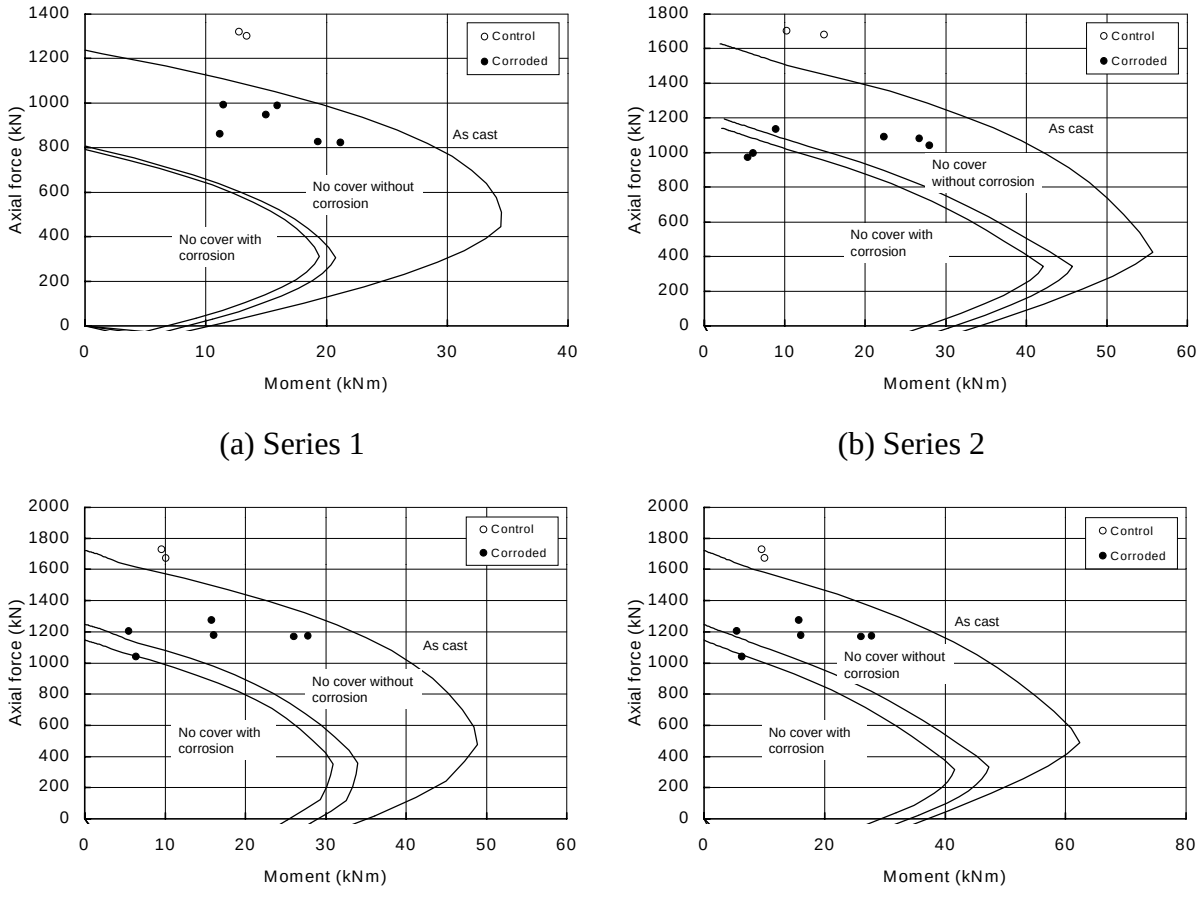

(a) Series 1

(b) Series 2

(c) Series 3 - M_x

(d) Series 3 - M_y

Figure 7-5: Moment-axial force interaction diagram for corroded columns treated as bending about two axes

Further test data are required for columns where the axial load is not so predominant.

7.5 Conclusions

The following conclusions can be drawn from the work reported in this Chapter:

1. The whole of the cover region outside the links should be ignored in calculating the axial load-carrying capacity of columns with corroded reinforcement.

2. Breaking of links and buckling of the compression reinforcement appears to be a post-failure phenomenon and, as such, should be ignored in strength calculations unless broken links are observed before loading is applied.

3. The methods developed for flexural and axial load-carrying capacity can be used together to create M-N interaction diagrams which predict adequately the failure of corrosion-damaged concrete columns subject to moments about one axis.

4. The BS 8110 method of using an increased moment about one axis to represent the effects of biaxial bending gives adequate predictions when used with the M-N interaction diagram for corrosion-damaged concrete columns.

8 IMPLICATIONS FOR THE DESIGN AND ASSESSMENT OF CONCRETE STRUCTURES

8.1 Introduction

In this Chapter, the assessment models developed in the previous chapters are used to assess the sensitivity of reinforced concrete structures subject to chloride-induced corrosion. Durability, detailing and maintenance related parameters are considered in order to obtain an indication of what the most significant parameters are. The resulting implications are discussed for both the design and assessment of concrete structures.

The models developed in the previous sections have been implemented in the spreadsheet *BEAMCOL_CORR*. The assessment procedures are summarised in Appendix A, and a print out from the spreadsheet is included in Appendix B.

For the purposes of this study, a simply supported reinforced concrete beam designed to resist the *Very severe* environment of BS 8110[69] has been used. Where appropriate, the durability options in BS 5400[97] and BD 57[118] are also considered. The beam and default parameters are shown in Figure 8-1. De-icing salt exposure is assumed.

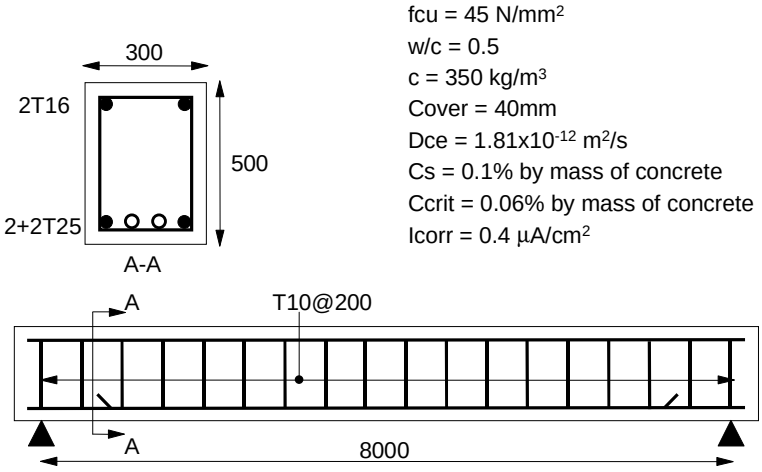

Figure 8-1: Reinforced concrete beam with default parameters

BS 8110[69] allows three different options for *Very severe* exposure: C40 with 50 mm cover, C45

with 40 mm cover and C50 with 30 mm of cover. As this beam has been designed for a parametric study the middle option has been selected. The effective diffusion coefficient (D_{ce}), surface chloride level (C_s) and critical chloride threshold level (C_{crit}) for de-icing salt exposure are based on the work of Hobbs and Matthews[12]. These are mean values that have been derived from observations and measurements of real structures. Based on these observations Hobbs and Matthews suggest that a typical propagation period (time between onset of corrosion and sufficient cracking to warrant repair) for de-icing salt exposure is around 25 years. In their work this implied that it will take around 25 years for a bar section to experience a loss of 100 μm, giving a corrosion rate of around 4 μm per year. Using Faraday's law and rounding to one significant figure a section loss of 4 μm per year corresponds to a corrosion rate (I_{corr}) of 0.4 μA/cm^2. This corrosion rate is assumed to be applicable to the *Very severe* exposure condition in BS 8110. Andrade and Alonso[17] suggest that typical pitting factors correspond to section losses of around four to eight times the losses due to general corrosion. A value of six will thus be assumed here. Two of the four T25 bars are curtailed before the support as permitted in BS 8110 clause 3.12.10.2 and are hence not available to resist shear at the support. The values shown in Figure 8-1 are referred to as the default values. In the parametric study variations around these default values are considered.

In addition to the assumptions inherent in the default values, other key assumptions in the analyses carried out in this Chapter are:

(i) All of the bars are assumed to corrode at the same rate, and in their most critical locations.
(ii) Significant spalling does not occur.
(iii) The link reinforcement remains anchored sufficiently.
(iv) The beam is loaded with a uniformly distributed load.
(v) The beam behaves in accordance with the procedures developed in the previous chapters (as summarised in Appendix A).

Figure 8-2 shows estimated reductions in load-carrying capacity with time for the beam with the default parameters. There are several events that occur during the life of a corroding beam that lead to reductions in load-carrying capacity. These are annotated in Figure 8-2.

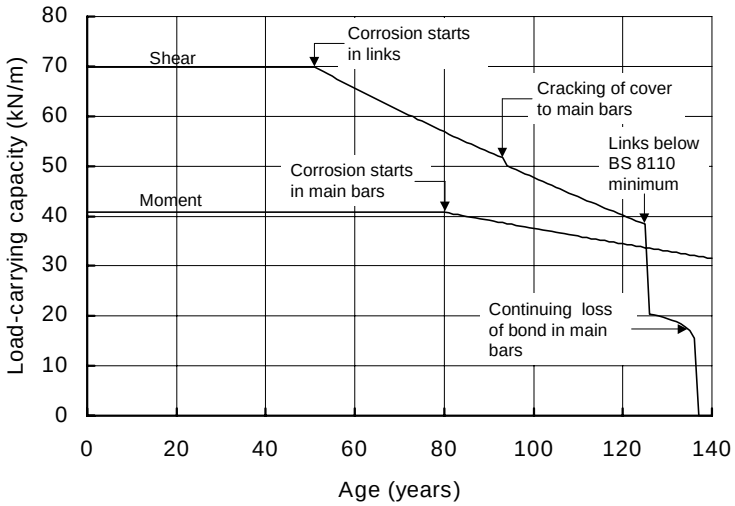

Figure 8-2: Reductions in load-carrying capacity for the default beam

It should be noted that the implied accuracy of the results presented here is not justified. The technology has not yet been validated sufficiently due to the lack of data from both laboratory experiments and real structures. For example, cracking due to corrosion predicted at 62 years does not imply that a crack will suddenly materialise at 62 years. The results should be viewed as estimates that are compatible with the current level of knowledge. As with any results, engineering judgement has to be applied in assessing their significance. The results are, however, useful as a means of comparing the relative impact of different scenarios.

8.2 Concrete durability parameters

There are two parameters that are commonly used to determine the nominal end of the service life: cracking of the cover concrete, and the reduction in residual load-carrying capacity. These criteria are considered here.

Time to cracking is often considered to be the point at which repair is necessary for aesthetic reasons, the risk of spalling or reductions in load-carrying capacity. The analysis of various laboratory studies carried out in Chapter 3 indicated that first cracking occurs at a percentage section loss corresponding to approximately half the c/D ratio. This is not necessarily the point at which repairs would be carried out, as the crack would be barely visible. However, it is the point from which bond strength is assumed to reduce. The point of first cracking is used in the

following parametric studies as a means of comparing different scenarios.

The amount of cracking corresponding to a section loss of 100μm has been assumed by a number of researchers[5, 11, 12] as the point where the crack is noticeable and may, at some time, develop into a spall. This value should perhaps be viewed as the point at which repair is required. The consequences of using section loss as a limiting criterion are discussed later in this Chapter.

If there has been a deterioration problem, then some loss of load-carrying capacity may be evident with time. The ratio of corroded to control load-carrying capacity is considered in order to give an indication of the possible reduction in load-carrying capacity with time. The reduction of load-carrying capacity is considered at 50, 75, 100 and 125 years. 75 and 125 years are considered in order to give an indication of the factor of safety at 50 and 100 years respectively. The residual load-carrying capacity is defined as the ratio of the corroded capacity ($w_{corroded}$) to the non-corroded capacity ($w_{control}$).

In the following analyses, each of the parameters w/c, cover, C_s, C_{crit}, I_{corr} and pitting factor are varied in turn. This gives an indication of the relative importance of each parameter. The results are given in Sections 8.2.1 to 8.2.6. In real life, there would be many more parameters varying about the default values selected here. This has been addressed in Section 8.2.7 by considering the interactions resulting from varying the four main parameters either side of the default values.

8.2.1 Concrete grade and w/c ratio

The results of varying the concrete grade are given in terms of time to cracking and residual load-carrying capacity in Table 8-1. The default value is shown boxed.

The concrete grade primarily determines the time to the onset of corrosion (the initiation period). Increasing the concrete grade also has a secondary effect of increasing the load-carrying capacity. However, many of the load-carrying mechanisms in beams are dependent primarily on the reinforcement or the concrete tensile strength. Hence any increase in load-carrying capacity is proportionally smaller than the increase in concrete grade.
A decrease of one grade can cut approximately 25% off the time to cracking, whilst a decrease

of two grades can lead to a decrease of approximately 40% in time to cracking and, ultimately, repair. The grade as supplied to site is generally greater than the nominal grade specified, as the concrete supplier adds a margin to ensure that the nominal grade is met. However, Bungey and Millard[119] have shown that there are inherent variations in strength grade within members due to placing and compaction, particularly in vertical members. Poor compaction and honeycombing may be equivalent to several reductions in grade.

Indicative service lives are not given in BS 8110[69]. However, Hobbs and Matthews[12] assume that the service life of structures designed to BS 8110 is intended to be around 50 years. With the cover to the links not cracking until around 62 years and no reductions in the load-carrying capacity at 75 years, the default values would appear to provide an adequate factor of safety on achieving a service life of 50 years. However, reduction of one grade indicates that the concrete surrounding the links will start to crack at 47 years, whilst there is a 7% reduction in load-carrying capacity at 75 years. Such a structure may be borderline in achieving a 50-year design life.

Table 8-1: The effects of variations in concrete grade on time to cracking and residual load-carrying capacity

Concrete			*Time to cracking (years)*		$w_{corroded} / w_{control}$			
w/c	f_{cu} *N/mm²*	*C kg/m³*	*Links*	*T25*	*50 years*	*75 years*	*100 years*	*125 years*
0.4	55	425	112	172	1.00	1.00	1.00	1.00
0.45	50	400	83	126	1.00	1.00	1.00	0.95
0.5	45	350	62	94	1.00	1.00	0.92	0.83
0.55	40	325	47	71	1.00	0.93	0.84	0.00
0.6	35	300	37	54	0.96	0.87	0.78	0.00
0.65	30	275	29	42	0.92	0.83	0.00	0.00
0.7	25	250	24	34	0.90	0.81	0.00	0.00

At 100 and 125 years the reductions in load-carrying capacity are predicted to be 8 and 17% respectively for the default values. Whilst this may not be a problem for most building structures, it will be for bridges. The design life for bridges is given as 120 years in BS 5400 and as 100

years in the Eurocodes. BS 5400[97] provides two durability options. In BD 57[118] the UK Highways Agency has decided to specify more onerous durability options than BS 5400 for those members not precast in a factory. The times to cracking and residual strength are given in Table 8-2 for BS 5400 and BD 57 durability options.

Table 8-2: The effects of variations in concrete grade and cover on time to cracking and residual load-carrying capacity for the beam designed to BS 5400 and BD 57

Durability options	*Concrete*			*Time to cracking (years)*		$w_{corroded} / w_{control}$	
	w/c	f_{cu} *N/mm²*	*Cover mm*	*Links*	*T25*	*100 years*	*125 years*
BS 5440 – 1	0.55	40	50	71	98	0.93	0.84
BS 5440 – 2	0.45	50	40	83	126	1.00	0.95
BD 57	0.45	50	50	126	178	1.00	1.00

With the first of the two BS 5400 options time to cracking and reductions in load-carrying capacity are predicted before the end of the 120 year design life. With the second option, minor reductions in load-carrying capacity are predicted along with cracking along the line of the links before 120 years. The second option is likely to prove better then the first.

The BD 57 option is predicted to escape any cracking or reductions in load-carrying capacity within the 120 year design life. On this basis, the decision of the Highways Agency to make BD 57 more onerous than BS 5400 for some concrete would appear to be justified.

8.2.2 Cover to reinforcement

The results of varying the reinforcement cover are given in terms of time to cracking and residual load-carrying capacity in Table 8-3. The default value is shown boxed.

The concrete cover to the reinforcement primarily determines the time to the onset of corrosion by providing a barrier to the ingress of chlorides, and the time to cracking by providing greater resistance to the expansive rust forces. Increasing the cover also has secondary effects of

increasing some load-carrying mechanisms whilst reducing others. The bond strength increases with increasing c/D ratio, whilst flexural and shear strength decrease due to the decrease in lever arm.

Table 8-3: The effects of variations in reinforcement cover on time to cracking and residual load-carrying capacity

Cover to links mm	*Time to cracking (years)*		$w_{corroded} / w_{control}$			
	Links	*T25*	*50 years*	*75 years*	*100 years*	*125 years*
10	6	18	0.85	0.76	0.00	0.00
15	11	27	0.88	0.79	0.00	0.00
20	18	37	0.92	0.82	0.00	0.00
25	27	49	0.96	0.86	0.00	0.00
30	37	62	1.00	0.91	0.81	0.00
35	49	77	1.00	0.96	0.86	0.00
40	62	94	1.00	1.00	0.92	0.83
45	77	112	1.00	1.00	0.99	0.89
50	94	132	1.00	1.00	1.00	0.96
55	112	153	1.00	1.00	1.00	1.00
60	132	176	1.00	1.00	1.00	1.00
65	153	200	1.00	1.00	1.00	1.00
70	176	227	1.00	1.00	1.00	1.00
75	201	254	1.00	1.00	1.00	1.00

The cover specified in BS 8110[69], and used as the default here is the nominal cover. BS 8110 allows the minimum cover to be up to 5 mm less than the nominal. A decrease of only 5mm cover to the reinforcement can cut approximately 15% to 20% off of the time to cracking, whilst a decrease of 10mm can lead to a 30% to 35% decrease in time to cracking (and, ultimately, repair). Such magnitudes of cover variation are well within those reported by Clark et al[120]. In the case of the beam considered in this Chapter the minimum cover of 35 mm appears to be adequate, with the cracking over the links at 49 years and a 4% reduction in load-carrying capacity at 75 years. Any further reductions may result in a structure being borderline in

achieving a 50-year design life without the need for significant repair.

8.2.3 Surface chloride level

The results of varying the surface chloride level, C_s, are given in terms of time to cracking and residual load-carrying capacity in Table 8-4. The default value is shown boxed.

The surface chloride level primarily determines the time to the onset of corrosion. It gives an indication of the aggressivity of the environment. The higher the surface chloride level is, the more aggressive the environment is.

Relatively small variations in the surface chloride level of, say, 0.025% can lead to approximately 20 years reduction in time to cracking and a 2% reduction in load-carrying capacity at 50 years. Such reductions may result in a structure being borderline in achieving a 50-year design life without the need for repair. This magnitude of variation may be possible if a movement joint or waterproofing fails and salt water leaks through exposing the concrete to a more severe environment. However, it should be noted that C_s values result from a solution to Fick's law, and are not measured directly. This makes it difficult to ascertain the effect of a leak unless C_s values can be determined from chloride measurements taken from similar concrete with some concrete subject to leaks and others exposed normally.

Table 8-4: The effects of variations in surface chloride level on time to cracking and residual load-carrying capacity

Cs % by mass of concrete	*Time to cracking years*		$w_{corroded} / w_{control}$			
	Links	*T25*	*50 years*	*75 years*	*100 years*	*125 years*
0.05	205	316	1.00	1.00	1.00	1.00
0.075	230	355	1.00	1.00	1.00	1.00
0.1	62	94	1.00	1.00	0.92	0.83
0.125	39	58	0.98	0.88	0.79	0.00
0.15	31	45	0.93	0.83	0.00	0.00
0.175	27	38	0.90	0.81	0.00	0.00
0.2	24	34	0.89	0.79	0.00	0.00

8.2.4 Critical chloride threshold

The results of varying the critical chloride level, C_{crit}, are given in terms of time to cracking and residual load-carrying capacity in Table 8-5. The default value is shown boxed.

The critical chloride level determines the time to the onset of corrosion. It is the level beyond which corrosion is judged to have begun. The lower the critical chloride level the earlier corrosion will start. It is not a parameter that engineers have much control over, and there is no unique value (see Section 2.2.1). However, a value has to be assumed for calculation purposes, and the sensitivity of the result to the assumed value of C_{crit} has to be considered.

Relatively small variations in the critical chloride level of, say, 0.01% can lead to reductions of around 20 years in time to cracking. Reductions in load-carrying capacity at 50 years require more substantial variations. Such reductions may result in a structure being borderline in achieving a 50-year design life without the need for repair.

Table 8-5: The effects of variations in critical chloride level on time to cracking and residual load-carrying capacity

C_{crit} *% by mass of concrete*	*Time to cracking (years)*		$w_{corroded} / w_{control}$			
	Links	*T25*	*50 years*	*75 years*	*100 years*	*125 years*
0.01	16	22	0.84	0.75	0.00	0.00
0.02	19	27	0.86	0.77	0.00	0.00
0.03	24	34	0.89	0.79	0.00	0.00
0.04	31	45	0.93	0.83	0.00	0.00
0.05	42	62	0.99	0.90	0.80	0.00
0.06	62	94	1.00	1.00	0.92	0.83
0.07	106	162	1.00	1.00	1.00	1.00
0.08	230	355	1.00	1.00	1.00	1.00

8.2.5 Corrosion rate

The results of varying the corrosion rate, I_{corr}, are given in terms of time to cracking and residual load-carrying capacity in Table 8-6. The default value is shown boxed.

The other parameters considered so far influence the initiation period up to the corrosion commencing, hence they have a larger part to play in the earlier life of a structure. Once corrosion commences, the corrosion rate can vary several orders of magnitude within the same structure. The corrosion rate is also likely to be a function of environment, grade and cover, and is thus linked to the other parameters. However, the technology is not available to establish what the relationship is between these parameters.

Variations in I_{corr} of 0.1 $\mu A/cm^2$ lead to approximately 2 years difference in time to cracking. It is only at I_{corr} values of three times the default that significant reductions in load-carrying capacity start to occur at 75 years. It would appear that the significance of variations in the corrosion rate is dependent on the relative lengths of the initiation period and the required service life. If a substantial period of the service life is required once corrosion has started, the corrosion rate will

have a significant role in whether that service life is achieved or not. For structures designed and built to the BS 8110 *Very severe* exposure condition and maintained such that the environment is compatible with the design, variations in the corrosion rate should have little influence on whether the 50-year design life is achieved.

Table 8-6: The effects of variations in corrosion rate on time to cracking and residual load-carrying capacity

I_{corr} $\mu A/cm^2$	*Time to cracking (years)*		$w_{corroded} / w_{control}$			
	Links	*T25*	*50 years*	*75 years*	*100 years*	*125 years*
0.01	488	625	1.00	1.00	1.00	1.00
0.1	95	134	1.00	1.00	0.98	0.96
0.25	69	102	1.00	1.00	0.95	0.89
0.4	62	94	1.00	1.00	0.92	0.83
0.5	60	91	1.00	1.00	0.90	0.37
0.75	57	87	1.00	1.00	0.54	0.00
1	56	85	1.00	1.00	0.49	0.00
1.25	55	84	1.00	0.64	0.00	0.00
1.5	54	84	1.00	0.64	0.00	0.00
1.75	54	83	1.00	0.64	0.00	0.00
2	53	83	1.00	0.64	0.00	0.00
2.5	53	82	1.00	0.64	0.00	0.00
5	52	81	1.00	0.64	0.00	0.00
10	52	81	1.00	0.64	0.00	0.00

8.2.6 Pitting factor

The results of varying the pitting factor are given in terms of time to cracking and residual load-carrying capacity in Table 8-7. The default value is shown boxed.

The pitting factor determines how much bar section will be lost for a given corrosion rate. The tensile strength of the longitudinal reinforcement resisting flexure and the link reinforcement

resisting shear are assumed to be related to the pitted bar diameter, whereas the bond and shear strength of the longitudinal reinforcement are assumed to be related to the average section loss. It is not a parameter that engineers have much control over. However, a value has to be assumed for calculation purposes, and the sensitivity of the result to the assumed value of pitting factor has to be considered.

Variations in the pitting factor have no effect on the time to cracking as this is dependent on an average amount of corrosion along the length of a bar. As with the corrosion rate, it would appear that the significance of variations in the pitting factor is dependent on the relative lengths of the initiation period and the required service life.

Table 8-7: The effects of variations in pitting factor on time to cracking and residual load-carrying capacity

Pitting factor	*Time to cracking (years)*		$w_{corroded} / w_{control}$			
	Links	*T25*	*50 years*	*75 years*	*100 years*	*125 years*
1	62	94	1.00	1.00	0.99	0.97
2	62	94	1.00	1.00	0.97	0.94
3	62	94	1.00	1.00	0.96	0.91
4	62	94	1.00	1.00	0.95	0.88
5	62	94	1.00	1.00	0.94	0.86
6	62	94	1.00	1.00	0.92	0.83
7	62	94	1.00	1.00	0.91	0.51
8	62	94	1.00	1.00	0.90	0.51
9	62	94	1.00	1.00	0.88	0.51
10	62	94	1.00	1.00	0.58	0.51

8.2.7 Interaction between the key parameters

The results of varying the concrete grade, cover, surface chloride level and corrosion rate are given in terms of times to initiation and cracking, and residual load-carrying capacity in Table

8-8. The variations are taken one step on either side of the default values to give an indication of the relative importance of the four parameters.

For the initiation period the parameters can be ranked in the following order of descending significance:

(i) Surface chloride level – variations led to a near five-fold variation in the initiation period.
(ii) Cover - variations led to a three-fold variation in the initiation period.
(iii) Concrete grade – variations led to a two-fold variation in the initiation period.
(iv) Corrosion rate – not applicable.

The significance of the variables will vary depending on the size of variation considered. However, the surface chloride level appears to be the most significant parameter in this case. This is at odds with what the Author[121] found when considering the relationship between quality and whole life costing. Because of the way that whole life costing works, the earlier that a cost occurs the larger the discounted cost is at present day values. Very low values of cover resulting from problems in design and construction can lead to repair being required very early. Hence, cover was considered to be the most significant parameter within the range of values considered.

When considering the interaction effects on the residual load-carrying capacity the conclusions vary depending on the age considered. At 50 and 75 years the conclusions are similar to those for the time to cracking. However, at 100 and 150 years the corrosion rate appears to be the most significant parameter. This confirms the conclusions reached in Section 8.2.5.

It has been demonstrated that provided the default values are achieved, there should be no unplanned maintenance or remedial works. Chloride-induced corrosion appears to be sensitive to deviations from the default values. If there are deviations from the default values then there is an increased chance of unplanned maintenance and remedial work with the associated cost and disruption to users of the structure. This highlights the importance of "getting it right first time". That is, achieving good design and construction practice with the right materials, achieving the required cover and ensuring that the concrete is compacted. In addition, the environment should

be controlled such that there is no increase in severity of the exposure.

Table 8-8: The effects of interaction of key concrete durability parameters on the times to initiation and cracking, and residual load-carrying capacity

		Cs		*Links*		*Main*		$w_{corroded} / w_{control}$			
w/c	*Cover*	*%*	*Icorr*	T_{init}	T_{crack}	T_{init}	T_{crack}	*50*	*75*	*100*	*125*
	mm	*conc.*	$\mu A/cm^2$	*years*	*years*	*years*	*years*	*years*	*years*	*years*	*years*
0.45	30	0.08	0.2	110	126	195	217	1.00	1.00	1.00	1.00
			0.6	110	115	195	202	1.00	1.00	1.00	1.00
		0.12	0.2	24	41	43	65	0.99	0.94	0.89	0.84
			0.6	24	30	43	51	0.96	0.47	0.00	0.00
	50	0.08	0.2	304	332	438	471	1.00	1.00	1.00	1.00
			0.6	304	313	438	449	1.00	1.00	1.00	1.00
		0.12	0.2	68	95	98	130	1.00	1.00	1.00	0.95
			0.6	68	77	98	109	1.00	1.00	0.99	0.55
0.55	30	0.08	0.2	55	72	99	120	1.00	1.00	1.00	0.95
			0.6	55	61	99	106	1.00	1.00	0.99	0.51
		0.12	0.2	12	29	22	44	0.94	0.90	0.85	0.80
			0.6	12	18	22	29	0.84	0.00	0.00	0.00
	50	0.08	0.2	154	181	222	254	1.00	1.00	1.00	1.00
			0.6	154	163	222	233	1.00	1.00	1.00	1.00
		0.12	0.2	34	62	49	82	1.00	0.95	0.90	0.86
			0.6	34	43	49	60	1.00	0.86	0.00	0.00

8.3 Detailing issues

Detailing issues can make a difference to the way that a deteriorating structure performs. Several of these issues are discussed in this section.

8.3.1 Curtailment

BS 8110[69] clause 3.12.10.2 allows 50% of the reinforcement required to resist mid-span bending to be curtailed before a simple support. The amount of steel that is saved is negligible. However, if the beam is framing in to a column then 50% less reinforcement may ease any congestion at the beam-column junction. The effects of carrying all of the reinforcement through to the support are shown in Figure 8-3.

Despite doubling the amount of tension reinforcement resisting shear, only around 10% extra shear capacity is gained and the capacity diminishes at the same time and rate as with curtailed reinforcement. For a given section, BS 8110 predicts the increase in shear capacity to be proportional to the cube root of the amount of tension reinforcement. Shear links are a more effective way of increasing the shear capacity. It would appear that there is more benefit to be gained in continuing the tension reinforcement in members with no shear link reinforcement. This would lead to a proportionally higher initial shear capacity than when links are present.

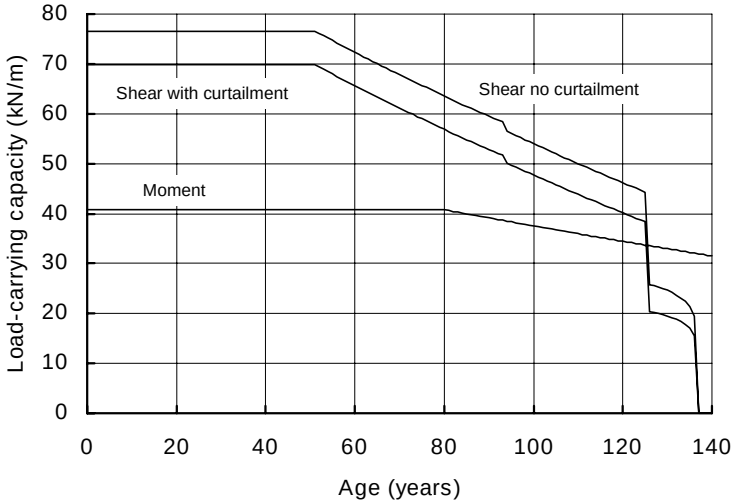

Figure 8-3: The effects of curtailment at simple supports on the load-carrying capacity of corrosion-damaged concrete beams

8.3.2 Bar size

The designer has to provide sufficient area of reinforcement to resist the applied loads. It is up to the designer how that area is to be provided. Issues such as buildability and standardisation are likely to dictate that choice. However, it is worth considering how those choices affect the

residual load-carrying capacity of corroded members. The effects of using 6T20 as the tension reinforcement instead of the default 4T25 are shown in Figure 8-4.

Although the nominal areas are near identical, using different bar arrangements does have an effect once corrosion has started. As corrosion is assumed to consume the whole circumference of a bar equally, a 100 μm radius loss on a 20 mm diameter bar will result in a more significant section loss than on a 25 mm diameter bar. Hence the beam with 6T20 is losing moment capacity faster than the default beam with 4T25. However, the 6T20 will crack later as, for a given cover, they have a higher c/D ratio. Loss of bond strength is assumed to be proportional to the area of bar lost due to corrosion. This means that a T20 bar has to have a larger radius loss to achieve the same corroded area as a T25. For the same corrosion rate this implies that the rate of bond strength loss is smaller. This implies that if bond is a concern, a large number of smaller bars is preferable to a small number of larger bars.

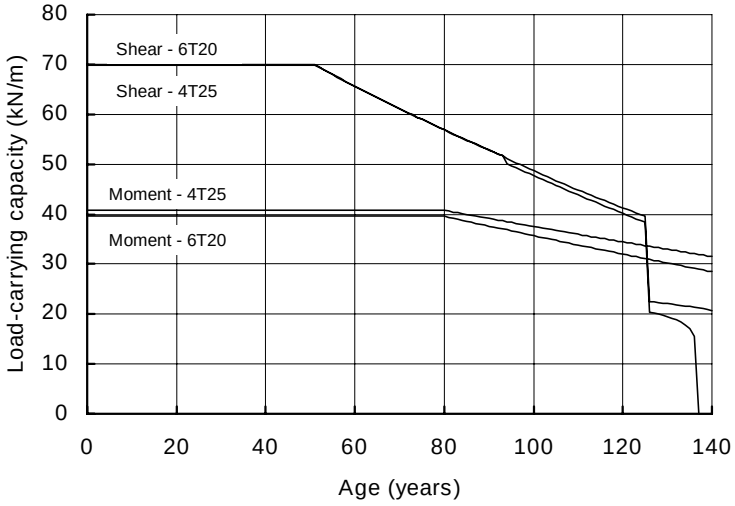

Figure 8-4: The effects of different tension reinforcement bar diameters on the load-carrying capacity of corrosion-damaged concrete beams

8.3.3 Link size and spacing

As discussed in the previous section, the designer can decide the reinforcement arrangement. The effects of two link arrangements, T8 at 125 mm centres and the default T10 at 200 mm centres, on the load-carrying capacity are shown in Figure 8-5.

The loss in shear strength of the T8 is somewhat greater than that of the T10. Assuming that all of the links are corroding at the same rate, the effect of a given radius loss is greater on an 8 mm diameter bar than on a 10 mm bar. In the case of shear links, section loss is likely to be more important than bond loss as anchorage is provided by the geometry of the links.

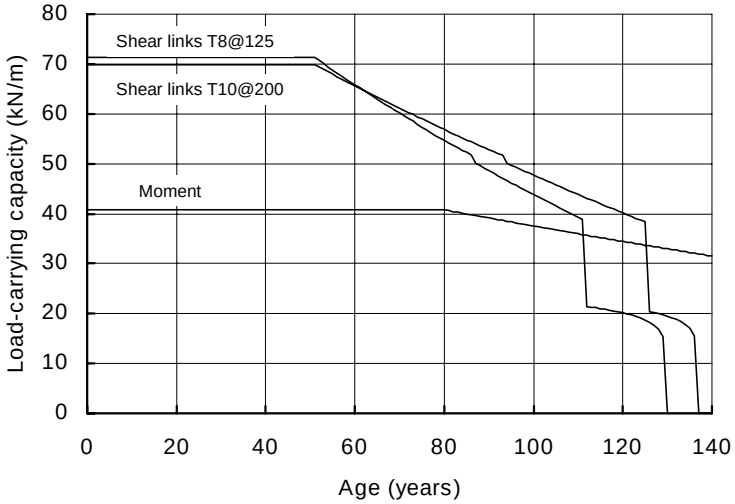

Figure 8-5: The effects of varying link size and spacing on the load-carrying capacity of corrosion-damaged concrete beams

8.3.4 Minimum shear link requirements

As discussed in Sections 4.5 and 6.3.2, BS 8110[69] requires a minimum amount of shear link reinforcement corresponding to $(A_{sv}\ f_{yv}) / (\gamma_s\ b_v\ s_v) = 0.4$, whilst BD 44/95[73] only requires 0.2. If 0.2 has been justified for BD 44/95 then it would seem reasonable that it should be applicable for use with BS 8110. The effects of the two code requirements for minimum links on load-carrying capacity are shown in Figure 8-6.

As discussed in Section 4.5 a bond enhancement of only $0.5 / \gamma_{mb}$ N/mm^2 can be justified with a minimum link value of 0.2 compared to $1.0 / \gamma_{mb}$ N/mm^2 for the BS 8110 minimum of 0.4. Even with this smaller bond enhancement, the beneficial effects of having the link reinforcement active for longer can be seen clearly in Figure 8-6. The links contribute to the shear strength in two ways: by enhancing the bond strength of the tension reinforcement for longer and by carrying shear for longer. Tests should be carried out to demonstrate that corroded links are still effective at the 0.2 level such that this level can be used for corroded members.

Figure 8-6: The effect of varying the requirement for the minimum amount of shear links on the load-carrying capacity of corrosion-damaged concrete beams

8.3.5 Other detailing issues

Not all members are detailed in the simplified manner of the beam shown in Figure 8-1. The geometry of some structures can dictate detailing, whilst some methods of detailing are no longer used. Several of these issues are considered qualitatively.

Wide beams are popular as a means of reducing overall depth. Instead of having only two vertical legs of links, one on each of the side faces they have a number of vertical legs distributed throughout the breadth of the beam. This means that only the two outer vertical legs are exposed directly to chlorides. Whilst the horizontal legs on the top and bottom faces may be exposed to chlorides, it is only the vertical legs that are required to resist shear. Provided the horizontal legs still provide anchorage to the vertical legs, any reduction in shear capacity is likely to be small. A means of providing shear resistance in many older structures was by the use of bent-up bars. These were typically bent up at 45° to intersect the shear failure plane. Their use in the UK is rare now as they have buildability problems. However, they are found regularly in assessments of older structures. The bent-up bars were traditionally placed in the middle of the longitudinal bars. Hence, the bar section resisting shear is away from the exposed faces and protected to some extent from the source of chlorides. Provided the horizontal legs still provide anchorage to the

inclined legs, any reduction in shear capacity is likely to be small.

The Author[122, 123] has suggested that other aspects of structural detailing which enhance the performance of deteriorated structures include:

(i) Adequate anchorage and lap lengths.
(ii) Details that avoid or relieve stress concentrations.
(iii) Tie reinforcement to prevent progressive collapse.
(iv) Details which are largely protected from the source of deterioration.
(v) Details which retain ductility.
(vi) Details which are easy to construct (as congested reinforcement can lead to poor compaction).

Whilst the previous examples were beneficial, there are other examples where the detailing is detrimental to the load-carrying capacity. Wallbank[8] singled out piers and abutments as the bridge elements with the most severe exposure. This was primarily due to leaking movement joints affecting the tops of piers and abutments, and salt spray from passing vehicles affecting the base of piers. There are a number of possible reasons for poor performance of members such as these. These include plastic settlement cracking at the pier tops due to congested reinforcement in tall members, cold joints, low quality kickers and lapped reinforcement (this reduces bar spacing and can lead to poor compaction). The problem is compounded by the fact that the areas where chlorides can gain access are also the most highly stressed. The bursting stresses under the bearings are particularly high, whilst the highest bending moments and shears will occur at the base.

8.4 Location of corrosion

Examination of the figures showing reductions in load-carrying capacity with time in the previous sections of this Chapter indicates that shear is more sensitive to corrosion than bending. This is largely because the shear links are closer to the surface than the bending reinforcement, and they also tend to be smaller diameter bars. Shear links start corroding earlier than the bending reinforcement and a given radius loss leads to larger relative reductions in section. Corrosion is

more likely to have significant effects if it occurs in locations where shear is critical. However, in continuous members and cantilevers critical shear and moment locations coincide at supports.

Not all members have shear links in them. The effects of corrosion on members resisting shear solely by the tension reinforcement is shown in Figure 8-7, where the shear links are removed from the default beam. Both moment and shear capacities start to reduce when the tension reinforcement starts to corrode. When the cover to the tension reinforcement cracks, the shear capacity starts to reduce at a faster rate than the moment capacity due to the effects of bond reduction. As the bond strength is reduced significantly, the shear capacity tails off.

Figure 8-7: The effects of omitting shear links on the load-carrying capacity of corrosion-damaged concrete beams

8.5 Criteria for repair

It was stated earlier in this Chapter that some researchers have proposed a section loss of 100 μm as a suitable limit for determining the end of the service life and thus the time for repair. Figure 8-8 shows how section losses on the shear links and the main tension reinforcement correspond to load-carrying capacity for the default beam.

The main tension reinforcement has an extra 10 mm of cover compared with the shear links and, hence, starts to corrode later than the links. Whilst the main tension reinforcement requires a lower percentage section loss for it to crack the concrete cover than the shear links do, this

corresponds to a higher radius loss. By the time that the main bars start corroding about 13 kN/m of shear load-carrying capacity has been lost, with the links having already lost around 130 μm. A loss of 100 μm on the shear links corresponds to a reduction in shear load-carrying capacity of around 10 kN/m (14%). A 100 μm loss on the main bars correspond to a 22 kN/m (33%) reduction in shear load-carrying capacity but only 3 kN/m (9%) reduction in moment load-carrying capacity.

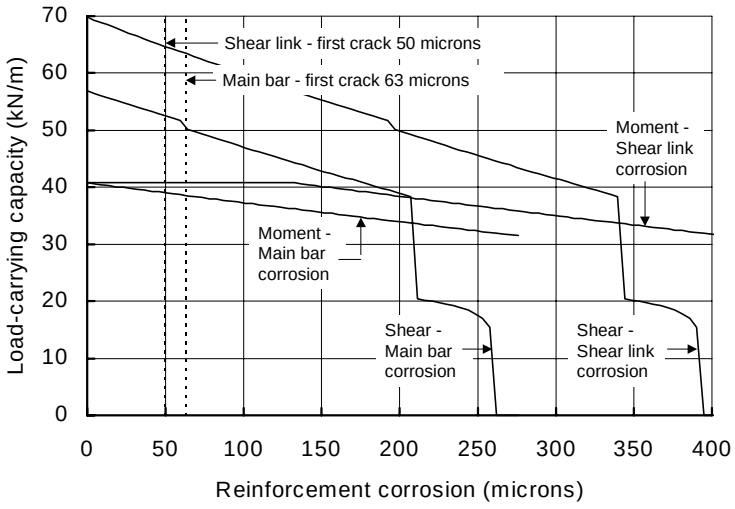

Figure 8-8: The relationship between link and main tension reinforcement section loss and load-carrying capacity for the default beam

It is difficult to make a judgement about the effect of main bar section loss from the default beam as the effects of the shear links dominate. The default beam was thus re-analysed without any shear links. The results are shown in Figure 8-9. In this case section losses of 100 μm in the main tension bars resulted in a loss of shear load-carrying capacity of 1.5 kN/m (around 5%) and a loss in moment load-carrying capacity of 3.5 kN/m (around 9%).

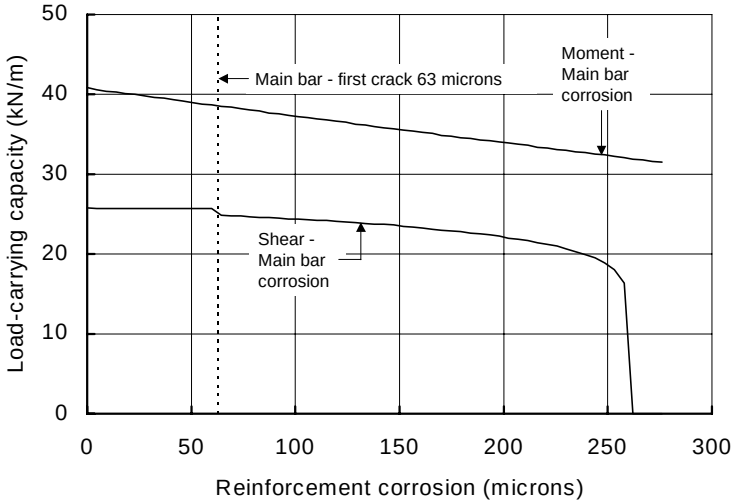

Figure 8-9: The relationship between link and main tension reinforcement section loss and load-carrying capacity for the default beam with no shear links

The implications of these reductions in load-carrying capacity will vary depending on the individual situation. When a structure is assessed using the IStructE assessment guide[72] it may be possible to reduce some of the BS 8110[69] partial safety factors for load and resistance. This is because many of the unknowns present during the design have been eliminated by the structure having been built, inspected and measured. As such, a slightly lower load-carrying capacity, such as that associated with 100 μm losses on the main tension bars where no shear links are present, may well be compatible with the assessment requirements. The larger reductions in load-carrying capacity associated with 100 μm losses on the main tension bars when shear links are present are unlikely to be acceptable. The potential for spalling has also to be considered. In many cases this may be the limiting criterion. However, reliable spalling models are required.

This implies that is not possible to establish general limiting criteria for all cases. Each structure needs to be assessed individually and a judgement made. However, with the spreadsheet *BEAMCOL_CORR* the technology is now available to assess a number of scenarios very quickly.

This does not really help the code writer very much, particularly those who need to develop general specifications. In such cases it would seem that the 100 μm section loss criteria is reasonable providing that it is applied to the bar nearest the surface and spalling does not predominate.

8.6 Implications for real structures

Laboratory tests give an understanding of the possible effects of corrosion on the basic structural mechanisms: bending, bond and shear. However, to get results in viable time scales the corrosion process has to be accelerated, often to several orders of magnitude greater than occurs in practice. There are several points that have to be borne in mind when relating these laboratory tests to structures; otherwise a pessimistic view may result. In particular:

(i) The lack of quality experimental data in the public domain.
(ii) Not every member will corrode.
(iii) Not every bar in a member will corrode.
(iv) Rust staining provides warning in cases where general corrosion is present.
(v) Most structures have a degree of redundancy, with alternative load-paths.

Much of the preceding sections were based on the behaviour of small isolated laboratory specimens. This behaviour has then to be translated to the behaviour in structures. Some of this translation is achieved by revising existing rules in Codes of Practice to incorporate the effects of corrosion. However, there are several other points that need to be considered in undertaking this translation. Some of the points are quantitative, whilst others are qualitative and will serve to give the assessing engineer increased confidence in their assessment due to the presence of 'hidden' strength and redundancy.

(i) Single-member behaviour is unusual in real structures. Most members are monolithic with other members, and load would be shared. Failure would require the collapse of an interconnected system rather than one member. Some recent shear tests on beam and slab bridge decks (with no corrosion) at Cambridge University (Ibell et al[124]) have shown that at failure the load is shared between adjacent members and is considerably higher than that predicted to be carried by a single member.
(ii) Tests carried out by Jackson[125] show that slabs are largely unaffected by localised deterioration. Tests have been carried out on half-scale bridge decks to simulate the effects of corrosion damage localised in a small area and the overall performance was not

impaired.

(iii) The concern is primarily where there are no alternative load paths.

(iv) The main requirement for bond strength is for the anchorage of reinforcement at supports. Bond is enhanced at supports due to the force from support reactions; this is not catered for explicitly in BS 8110.

(v) Links are present in most beams. This will help to maintain bond strength unless only a small number are present and/or those that are present are heavily corroded.

(vi) Laps will be present in longer members. Some of the assumptions regarding tied arch behaviour and flexure are no longer applicable if the reinforcement is unable to transmit forces at laps in the span.

8.7 Conclusions

The following conclusions can be drawn from the work reported in this Chapter:

1. The concrete durability provisions in BS 8110 appear to be adequate.

2. The decision of the UK Highways Agency to make the concrete durability provisions in BD 57 more onerous than those in BS 5400 for some concrete appears to be justified.

3. Both the times to cracking and load-carrying capacity are sensitive to small variations in the concrete durability parameters. It is thus imperative to achieve the relevant code specification or the required design life may not be achieved.

4. The surface chloride level appeared to be the most significant of the concrete durability parameters. This has serious implications for maintenance in that increasing the surface chloride level due to leaks or poor drainage could significantly reduce the service life.

5. Small variations in cover to the reinforcement, typical of those found on sites, can significantly reduce the service life.

6. The significance of the corrosion rate appeared to increase with the length of service life that was required in the propagation period.

7. Curtailing 50% of the tension reinforcement before the support appeared to cause no reduction in the service life of members with links. However, if the bars had not been curtailed the shear load-carrying capacity would have been a little higher at all points up to collapse.

8. Using a larger number of smaller diameter tension bars instead of a smaller number of larger bars makes little difference to the load-carrying capacity until the bond strength is solely dependent on the tension bars without links. At this point a smaller reduction in bond strength is predicted for a given corrosion (expressed as radius loss) in smaller bars and the load-carrying capacity is maintained longer.

9. Using a larger number of smaller diameter shear links instead of a smaller number of larger links is detrimental to the shear load-carrying capacity. For a given corrosion (expressed as radius loss) the section loss in smaller bars is larger.

10. The relative merits of bar size vary depending on which load-carrying mechanism is critical. If bond is critical then smaller bars lose their bond strength at a slower rate for a given corrosion rate. If the tensile strength of the bar is critical then larger bars lose their strength at a slower rate for a given corrosion rate.

11. Reducing the BS 8110 criteria for minimum links from 0.4 to the BD 44/95 value of 0.2 would allow the links to remain active for longer and thus extend the residual service life. Further tests are required, however, to justify this.

12. Well detailed members, and those where the critical bars and locations are protected from the environment are likely to perform better than other members.

13. The critical locations for corrosion are likely to be in shear critical regions.

14. It is difficult to specify general criteria for repair or end of the service life, as this will vary depending on the individual structure. However, the spreadsheet *BEAMCOL_CORR* does provide a means for establishing criteria for individual structures.

15. The criterion that suggests that the end of the service life is reached when 100 μm of the bar radius is lost due to corrosion leads to reductions in load-carrying capacity of less than 10% for the default beam considered here. This will vary depending on the bar sizes used in a member.

16. In some structures the effects of spalling may be the limiting criteria and should be considered in addition to reductions in load-carrying capacity.

17. The implications for real structures are perhaps not as onerous as the parameter studies may suggest. The main reasons for this are likely to be that not all bars tend to corrode in all members, and single members are unusual with most members being connected to others (thus benefiting from redundancy).

18. The effects of variability are such that single calculations are not adequate, and sensitivity analyses will need to be performed within a credible range of variables. Spreadsheets offer an ideal way to assess the effects of variability.

9 CONCLUSIONS

The following conclusions can be drawn from the work carried out in this Thesis. Only the key conclusions are included in this Chapter. A full set of conclusions is included at the end of each Chapter.

9.1 General conclusions

1. It is possible to model the structural effects of corrosion in relatively simple ways that are, essentially, extensions and modifications to current practice.

2. There are insufficient quality data in the public domain to produce a comprehensive and validated code of practice for assessing corrosion-damaged concrete structures. However, the material contained in this Thesis provides a first step in achieving such a code of practice.

3. Procedures are implemented for linking the material and structural effects of corrosion to give estimates of the residual load-carrying capacity of reinforced concrete structures.

4. The assessment of corrosion-damaged concrete structures is not an exact science. Each situation is likely to be unique, and requires engineering judgement to apply the procedures developed here to that situation.

5. There is considerable variability and uncertainty in the input parameters to a service life assessment. As such, sensitivity analyses should be carried out to obtain a feel for the consequences of potential variations. A spreadsheet *BEAMCOL_CORR* has been developed to carry out such analyses.

6. Whilst laboratory tests can give an understanding of the effects of deterioration on the basic load-carrying mechanisms such as bending, bond and shear, interpretation is required to translate this technology into real structural performance.

7. The principal differences between structural elements in the laboratory and real structures are that not all members or bars will corrode in real structures, and single member behaviour tends not to be present in real structures where most members tend to be monolithic and have alternative load-paths.

8. Further test data are required. In particular, data are required on the effects of corrosion on bond, shear and ductility. Tests on members from deteriorated structures would be particularly useful.

9.2 Cracking

9. The amount of corrosion observed to cause cracking is substantially greater than the amount of radial expansion theoretically required to induce cracking. It is likely that the remainder of the rust product over and above that theoretically required to induce cracking will be accommodated in the concrete pore structure surrounding the bar.

10. A theory has been derived to estimate the amount of corrosion product that is accommodated within the pore structure. The most significant variable in determining both the amount of corrosion product accommodated in the concrete pore structure and the amount of corrosion to cause cracking is the cover to bar diameter (c/D) ratio.

11. An estimate of the amount of corrosion required to cause cracking, expressed as a percentage of the original bar area, can be obtained by halving the c/D ratio.

12. A simplified theory has been derived to estimate the amount of corrosion required to cause the corner concrete cover to spall due to corrosion. This theory indicated that corrosion over short lengths is more critical for spalling as the length of cover concrete is stiffer and will be able to absorb less corrosion-induced deflection.

13. The cracking and spalling theories can be used together to provide an estimate of the amount of in situ corrosion that has taken place in concrete structures cracked due to corrosion.

9.3 Bond

14. The corroded bond strength appears to increase with increasing c/D ratio and concrete tensile strength. The corroded bond strength of plain and ribbed bars without links can be related to the Tepfers bond strength by using a variable that is a function of the area of steel lost due to corrosion.

15. The corroded bond strength of ribbed bars is enhanced due to the presence of links. The enhancement appears to be more significant at lower levels of link reinforcement. A bond enhancement of 1.0 N/mm^2 has been extrapolated from the test data for the point where the minimum amount of links, as specified in BS 8110, is present.

16. It is not possible to make recommendations for assessing the bond strength of ribbed bars with links when the level of link reinforcement is less than the minimum amount required in BS 8110. Until more experimental data become available, ribbed bars with links will have to be treated as ribbed bars without links when the link area falls below the minimum amount.

9.4 Flexural strength

17. The flexural load-carrying capacity of singly-reinforced corroded beams can be estimated by reducing the area of reinforcement alone (to allow for corrosion including pitting) provided that premature failure due to bar fracture or a change in failure mechanism does not occur.

18. When pitting was present the ratio of maximum to average corrosion was found to increase with increasing corrosion. This manifested itself as an apparent reduction in yield stress.

19. Some beams can fail prematurely due to bar fracture, bond or shear.

20. Corrosion can reduce both the elongation at maximum load and the ratio of yield to

ultimate strength of the reinforcement. These reductions can lead to premature fracture of the bar before yield is reached. There are no general relationships for ascertaining the reduction in either the elongation at maximum load or the ratio of ultimate to yield strength of a bar due to corrosion.

21. When reinforcement in the compression zone corrodes, a better fit to the experimental data is achieved by considering the effects of concrete spalling within the compression zone. Ignoring the effects of spalling leads to an overestimate of the flexural load-carrying capacity.

9.5 Shear strength

22. The empirical nature of the BS 8110 procedures for calculating shear strength makes it difficult to identify where and how modifications are to be made to reflect the effects of corrosion.

23. The behaviour of beams with plain and ribbed bars appears to be different, with significant increases in shear load-carrying capacity above that of the uncorroded beams occurring in the beams with corroded plain bars.

24. The increase in shear load-carrying capacity of beams with corroded plain bars is explained using the model of tied arch behaviour that occurs in the presence of low bond strength. A numerical procedure is presented, but needs validation against further test data.

25. The effects of corrosion can be incorporated in the empirical shear rules of BS 8110 by calculating an effective area of tension reinforcement. The primary variables in the formula for effective area of tension reinforcement are c/D ratio and the ratio of corroded to BS 8110 bond strength.

26. Shear links have beneficial effects on both the bond and shear strength of corroded members. However, due to their location, links are prone to significant corrosion. It is

not possible to ascertain whether shear links contribute to the shear resistance of corroded members when the proportion of links is below the minimum level specified in BS 8110.

27. The V_c component (calculated using the expression for the effective area of tension reinforcement) also appears to be appropriate for use with members containing links.

28. BS 8110, with the modifications proposed in Chapter 6, gives similar means and coefficients of variation for the test/predicted shear load-carrying capacities of both control and corroded beams. This suggests that for the beams considered here the effects of corrosion are catered for in the proposed modifications. The modifications give conservative predictions in the majority of cases.

29. EC 2 without any modifications gives the best mean test/predicted shear load-carrying capacity ratios for beams without links. It does so at the expense of a high coefficient of variation. When links are included, EC 2 tends to overestimate the shear capacity of corroded beams. This suggests that modifications are necessary to incorporate the effects of corrosion.

30. The Modified Compression Field Theory as implemented in CSA A23.3 gives adequate predictions for members with and without links. It appears better able to cope with low level of link reinforcement. However, it may require some modifications to reduce the variability of the predictions when no links are present.

9.6 Column behaviour

31. The whole of the cover region outside the links should be ignored in calculating the axial load-carrying capacity of columns with corroded reinforcement.

32. Breaking of links and buckling of the compression reinforcement appears to be a post-failure phenomenon and, as such, should be ignored in strength calculations unless broken links are observed before loading is applied.

33. The methods developed for flexural and axial load-carrying capacity can be used together to create M-N interaction diagrams which predict adequately the failure of corrosion-damaged concrete columns subject to moments about one axis.

34. The BS 8110 method of using an increased moment about one axis to represent the effects of biaxial bending gives adequate predictions when used with the M-N interaction diagram for corrosion-damaged concrete columns.

9.7 Implications for design and assessment

35. The concrete durability provisions in BS 8110 appear to be adequate.

36. The decision of the UK Highways Agency to make the concrete durability provisions in BD 57 more onerous than those in BS 5400 for some concrete appears to be justified.

37. Both the times to cracking and load-carrying capacity are sensitive to small variations in the concrete durability parameters.

38. The surface chloride level appeared to be the most significant of the concrete durability parameters. This has serious implications for maintenance in that increasing the surface chloride level due to leaks or poor drainage could significantly reduce the service life.

39. Small variations in cover to the reinforcement, typical of those found on sites, can significantly reduce the service life.

40. The significance of the corrosion rate appeared to increase with the length of the service life that was required in the propagation period.

41. Curtailing 50% of the tension reinforcement before the support appeared to cause no reduction in the service life of members with links. However, if the bars had not been curtailed the shear load-carrying capacity would have been a little higher at all points up to collapse.

42. The relative merits of bar size vary depending on which load-carrying mechanism is critical. If bond is critical then smaller bars lose their bond strength at a slower rate for a given corrosion rate. If the tensile strength of the bar is critical such as for bending or in the case of shear links then larger bars lose their strength at a slower rate for a given corrosion rate.

43. Reducing the BS 8110 criteria for minimum links from 0.4 to the BD 44/95 value of 0.2 allows the links to remain active for longer and thus extends the residual service life. However, further tests are required to justify this.

44. Well detailed members, and those where the critical bars and locations are protected from the environment are likely to perform better than other members.

45. The critical location for corrosion is in shear critical regions.

46. It is difficult to specify general criteria for repair or end of service life, as this will vary depending on the individual structure. However, the spreadsheet *BEAMCOL_CORR* does provide a means for establishing criteria for individual structures.

47. The criterion that suggests that the end of the service life is reached when 100 μm of the bar radius is lost due to corrosion leads to reductions in load-carrying capacity of less than 10% for the default beam considered here. This will vary depending on the bar sizes used in a member.

48. In some structures the effects of spalling may be the limiting criteria and should also be considered in addition to reductions in load-carrying capacity.

49. The implications for real structures are perhaps not as onerous as the parameter studies may suggest. The main reasons for this are likely to be that not all bars tend to corrode in all members, and single members are unusual with most members being connected to

others and thus benefiting from redundancy.

50. The effects of variability are such that single calculations are not adequate, and sensitivity analyses will need to be performed within a credible range of variables. Spreadsheets offer an ideal way to assess the effects of variability. Such a spreadsheet, *BEAMCOL_CORR*, has been developed as part of this Thesis.

10 RECOMMENDATIONS

The following recommendations are based on the work carried out for this Thesis.

10.1 Recommendations resulting from this work

1. Once validated against further test data, the procedures developed here should be considered for translation into a Code of Practice for the assessment of corrosion-damaged concrete structures.

2. The validated procedures could be used in combination with a sensitivity analysis to obtain estimates of possible reductions in load-carrying capacity with time.

3. Spreadsheet solutions should be used in order to carry out such sensitivity analyses.

10.2 Recommendations for further work

1. Test and analytical work are required to develop a procedure for predicting the onset and extent of spalling. This would need to be validated against the performance of real structures.

2. Tests are required to establish the effects of corrosion on bond in members with varying levels of link corrosion in order to establish at what amount of corrosion the links cease to contribute to enhancing the bond strength of the longitudinal bars.

3. Tests are required to establish the effects of corrosion on the ductility of members.

4. Tests are required to establish a general theory for the shear strength of members with corroded plain bars.

5. Tests are required to ascertain the effects of corrosion on the punching shear strength of slabs.

6. Tests on members from corroded structures would prove useful in calibrating assessment models, and in relating laboratory behaviour to that of real structures.

7. A consistent methodology is required for incorporating test data into Codes of Practice.

8. Since many of the assessment procedures presented in this Thesis are only based on one set of data further test and analytical work are required to validate the concepts and details proposed here.

11 REFERENCES

1 BUILDING RESEARCH ESTABLISHMENT: 'Concrete corrosion – tackling this £550m a year problem', *News release*, 4th December 1998.

2 HOBBS, D. W.: 'Chloride ingress and chloride-induced corrosion in reinforced concrete members', *Corrosion of reinforcement in concrete construction*, Ed. C. L. Page, P. B. Bamforth and J. W. Figg, Special Publication 183, The Royal Society of Chemistry, 1996, pp. 124-135.

3 YEUNG, H.W.: 'Canopy and balcony collapses – Lessons from the past', *Safety in Buildings*, Hong Kong Institution of Engineers Materials Division, Hong Kong Exhibition and Conference Centre, 16 March 1999.

4 CROPPER, D., JONES, A. K. and ROBERTS, M. B.: 'A risk based maintenance strategy for the Midlands links motorway viaducts', *The Management of Highway Structures*, ICE, 22-23 June 1998.

5 TUUTTI, K.: *Corrosion of steel in concrete*, Swedish Cement and Concrete Research Institute, Report 4-82, 1982, pp. 469.

6 BROOMFIELD, J. P.: *Corrosion of steel in concrete: Understanding, investigation and repair*, E & F N Spon, London, 1997, pp. 240.

7 BEEBY, A. W.: *Concrete in the oceans – Cracking and corrosion*, Technical Report 1, CIRIA/UEG – Cement and Concrete Association – Department of Energy, C&CA Publication 15.286, 1978, pp. 77.

8 WALLBANK, E. J.: *The performance of concrete in bridges – A survey of 200 highway bridges*, HMSO, London, April 1989.

9 THEOPHILUS, J.: 'Problems with concrete, why they occur. Corrosion of steel in

concrete', source unknown.

10 KROPP, J., HILSDORF, H. K., GRUBE, H., ANDRADE, C. and NILSSON, L. O.: 'Transport mechanisms and definitions', *Performance Criteria for Concrete Durability,* E & F N Spon, London, 1995, pp. 4-14.

11 PARROTT, L. J.: *A review of carbonation in reinforced concrete,* BRE/C&CA Report C1, July 1987, pp. 126.

12 HOBBS, D. W. and MATTHEWS, J. D.: 'Minimum requirements for concrete to resist chloride-induced corrosion', Chapter 3, *Minimum requirements for durable concrete: Carbonation- and chloride-induced corrosion, freeze-thaw attack and chemical attack,* Edited by D. W. Hobbs, British Cement Association, 1998, pp. 43-89.

13 WEBSTER, M. P.: *CHLORPRO – A spreadsheet for analysing measured chloride profiles,* British Cement Association, unpublished, 1999.

14 BRITISH STANDARDS INSTITUTION: *Concrete – performance, production and conformity,* Pr EN 206, Draft for public comment, 1997.

15 FAGERLUND, G. and HEDENBLAD, G.: *Calculation of the moisture-time fields in concrete,* Deliverable 12.1, BRITE-EURAM Project BREU-CT92-0591, The residual service life of concrete structures, Lund, March 1993.

16 RODRIGUEZ, J., ORTEGA, L. M., GARCIA, A. M., JOHANNSON, L. and PETTERSON, K.: 'On-site corrosion measurements in concrete structures', *Construction Repair*, November/December 1995, pp. 27-30.

17 ANDRADE, C. and ALONSO, C.: 'Corrosion rate monitoring in the laboratory and on site', *Construction and Building Materials,* Vol.10, No.5, 1996, pp. 315-328.

18 ANDRADE, C: Private communication, May 1998.

19 GRANTHAM, M. G., GRAY, M. J. and BROOMFIELD, J. P.: 'Chloride diffusion modelling and corrosion rate data for lifetime prediction in marine, highway and car parking structures', *Structural faults and repairs*, Edinburgh, 1997, pp. 275-284

20 BAMFORTH, P. B.: 'Guidance on the selection of measures for enhancing reinforced concrete durability', *Report for DoE PiT Project CI 39/3/376 (cc 967)*, Draft Report, November 1998, pp. 129 plus Appendices.

21 ATKINS, C. P., ROBERTS, M. B., LANE, I. R. and GOWER, M. R.: 'Deterioration modelling to determine the residual life of reinforced concrete structures', *BCA Conference Concrete car parks - Design and maintenance issues*, London, 29th September 1997, pp. 9.

22 ANDRADE, C., ALONSO, C. and MOLINA, F. J.: 'Cover cracking as a function of bar corrosion: Part I - Experimental test', *Materials and structures*, 26, 1993, pp. 453-464.

23 ANDRADE, C., ALONSO, C., GARCIA, D. and RODRIGUEZ, J.: 'Remaining lifetime of reinforced concrete structures: Effect of corrosion on the mechanical properties of the steel', *Life prediction of corrodible structures*, NACE, Cambridge, 23-26 September 1991, pp. 12/1-12/11.

24 BRITISH STANDARDS INSTITUTION: *Specification for carbon steel bars for the reinforcement of concrete*, BS 4449, 1997.

25 ALONSO, C., ANDRADE, C., RODRIGUEZ, J and DIEZ, J. M.: 'Factors controlling cracking of concrete affected by reinforcement corrosion', *Materials and Structures*, Vol. 31, August-September 1998, pp. 435-441.

26 CABRERA, J. G.: 'Deterioration of concrete due to reinforcement steel corrosion', *Cement and Concrete Composites*, 18, 1996, pp. 47-59.

27 LIU, Y.: *Modelling the time-to-corrosion cracking of the cover concrete in chloride contaminated reinforced concrete structures*, PhD, Virginia Tech, October 1996, pp. 117.

28 MORINAGA, S.: 'Prediction of Service Lives of Reinforced Concrete Buildings Based on Rate of Corrosion of Reinforcing Steel', *Special Report of Institute of Technology, Shimizu Corporation*, No 23, June 1988, pp. 82.

29 BAZANT, Z. P.: 'Physical model for steel corrosion in concrete sea structures – Application', *Journal of the Structural Division*, Proceedings of the American Society of Civil Engineers Vol. 105, ST6, June 1979, pp. 1155-1166.

30 CADY, P. D. and WEYERS, R. E.: 'Deterioration rates of concrete bridge decks', *American Society of Civil Engineers, Journal of the Transportation Division*, Vol. 110, No. 1, January 1984, pp. 34-44.

31 WEYERS, R. E.: 'Service life model for concrete structures in chloride laden environments', *ACI Materials Journal*, Vol. 95, No. 4, July-August 1998, pp. 445-453.

32 WEYERS, R. E.: Private Communication, November 1998.

33 MOLINA, F. J., ANDRADE, C. and ALONSO, C.: 'Cover cracking as a function of bar corrosion: Part II - Numerical model', *Materials and structures*, 26, 1993, pp. 532-548.

34 CHAN, A.H.C., DU, Y.G. and CLARK, L.A.: 'Finite Element Analysis of Expansive Effect of Steel Corrosion', *Civil Comp Ltd*, 1996, pp. 143-512.

35 SAIFULLAH, M.: *Effect of reinforcement corrosion on bond strength in reinforced*

concrete, PhD, University of Birmingham, April 1994, pp. 258.

36 DAGHER H. J. and KULENDRAN S.: 'Finite Element Modelling of Corrosion Damage in Concrete', *ACI Structural Journal*, Vol. 89, November-December 1992, pp. 699-708.

37 UEDA, T., SATO, Y., KAKUTA, Y. and KAMEYA, H.: 'Analytical study of concrete cover cracking due to reinforcement corrosion', *Concrete in severe environments*, CONSEC '98, Norway, E & FN Spon, pp. 678-687.

38 AL-SULAIMANI, G. J., KALEEMULLAH, M., BASUNBAL, I. A. and RASHEEDUZZAFAR: 'Influence of corrosion and cracking on bond behaviour and strength of reinforced concrete members', *ACI Structural Journal*, Vol. 87, No. 2, March-April 1990, pp. 220-231.

39 ALMUSALLAM, A. A., AL-GAHTANI, A. S., AZIZ, A. R. and RASHEEDUZZAFAR: 'Effect of reinforcement corrosion on bond', *Construction and Building Materials.* Vol. 10, No. 2., 1996, pp. 123-129.

40 CABRERA, J.G. and GHODDOUSSI, P.: 'The effect of reinforcement corrosion on the strength of the steel/concrete – bond', *Proceedings of the International conference on Bond in concrete*, Riga, Latvia, 1992, pp. 10/11-10/24.

41 CLARK, L. A. and SAIFULLAH, M.: 'Effect of corrosion on reinforcement bond strength', *Structural Faults and Repairs*, 1993, Vol. 3, pp. 113-119.

42 SAIFULLAH, M. and CLARK, L. A.: 'Effect of corrosion rate on the bond strength of corroded reinforcement', *Corrosion and corrosion protection of steel in concrete*, Proceedings of an International Conference, Sheffield University, 24-28 July 1994, pp. 591-602.

43 CORONELLI, D.: 'Bond of corroded bars in confined concrete: Test results and

mechanical modelling', *Studi E Recherche*, Vol. 18, 1997, pp. 187-211.

44 LIN, C. Y.: 'Bond deterioration due to corrosion of reinforcing steel', *Performance of Concrete in the Marine Environment*, ACI SP-95, 1980, pp. 255-269.

45 RODRIGUEZ, J., ORTEGA, L. M. and CASAL, J.: 'Corrosion of reinforcing bars and service life of reinforced concrete structures: Corrosion and bond deterioration', *International Conference on Concrete Across Borders*, Odense, Denmark, 1994, Vol. II, pp. 315-326.

46 CHANA, P. S.: 'A test method to establish realistic bond stresses', *Magazine of Concrete Research*, Vol. 42, No. 15, June 1990, pp. 83-90.

47 TEPFERS, R.: 'Cracking of concrete cover along anchored deformed reinforcing bars', *Magazine of Concrete Research*, Vol. 31, No. 106, March 1979, pp. 3-12.

48 REYNOLDS G. C.: *Bond strength of deformed bars in tension*, Technical Report 548, Cement and Concrete Association, Slough, 1982, 23 pages.

49 RODRIGUEZ, J. and ORTEGA, L.M.: *Assessment of deterioration and structural implications – RC structures with corroded bars*, BRITE-EURAM Project Workshop, Imperial College, 4-5 April 1995.

50 BALDWIN, M.: 'The assessment of reinforcing bars with inadequate anchorage', *Magazine of Concrete Research*, 47, No. 171, June 1995, pp. 895-102.

51 SAKAMOTO, N. and IWASAKI, N.: 'Influence of sodium chloride on the concrete/steel and galvanised steel bond', *Bond in Concrete*, Edited by P. Bartos, Applied Science Publishers, London, 1982, pp. 239-249.

52 MASLEHUDDIN, M., ALLAM, I. M., AL-SULAIMANI, G. J., AL-MANA, A. I. and ABDULJAUWAD, S. N.: 'Effect of rusting of reinforcing steel on its mechanical properties and bond with concrete', *ACI Materials Journal*, Vol. 87, No. 5, September-October 1990, pp. 496-502.

53 ALMUSALLAM, A. A., AL-GAHTANI, A. S., AZIZ, A. R., DAKHIL, F. H. and RASHEEDUZZAFAR: 'Effect of reinforcement corrosion on flexural behaviour of concrete slabs', *ASCE Journal of materials in Civil Engineering*, Vol. 9, No. 3, August 1996, pp. 123-127.

54 HUANG, R. and YANG, C. C.: 'Condition Assessment of Reinforced Concrete Beams Relative to Reinforcement Corrosion', *Cement and Concrete Composites*, 19, 1997, pp. 131-137.

55 KAWAMURA, A., MARUYAMA, K., YOSHIDA, S. and MASUDA, T. 'Residual capacity of concrete beams damaged by salt attack', *Concrete under severe conditions: Environment and loading*, E & F N Spon, 1995, pp. 1448-1457.

56 MARUYAMA, K. and SHIMOMURA, T.: 'Effect of rebar corrosion on the structural capacity of concrete structures', *Concrete in severe environments*, CONSEC '98, Norway, E & FN Spon, pp. 364-371.

57 LEE, H. S., NOGUCHI, T, and TOMOSAWA, F.: 'FEM analysis for structural performance of deteriorated RC structures due to rebar corrosion', *Concrete under severe conditions: Environment and loading*, CONSEC '98, E & F N Spon, 1998, pp. 327-336.

58 OKADA, K., KOBAYASHI, K., and MIYAGAWA, T.: 'Influence of longitudinal cracking due to reinforcement corrosion on characteristics of reinforced concrete members', ACI *Structural Journal*, March-April 1988, pp. 134-140.

59 BRITISH STANDARDS INSTITUTION: *Eurocode 2: Design of concrete structures. Part 1: General rules and rules for buildings*, ENV 1992-1-1, 1991.

60 TACHIBANA, Y., MAEDA, K., KAJIKAWA, Y, and KAWAMURA, M.: 'Mechanical behaviour of RC beams damaged by corrosion of reinforcement', *Third international symposium on corrosion of reinforcement in concrete construction*, 21-24 May 1990, pp. 178-187.

61 TING, S.-C. and NOWAK, A. S.: 'Effect of reinforcing steel area loss on flexural behaviour of reinforced concrete beams', *ACI Structural Journal*, Vol. 88, No. 3, June 1988, pp. 309-314.

62 UOMOTO, T., TSUJI, K. and KAKIZAWA, T.: 'Deterioration mechanism of concrete structures caused by corrosion of reinforcing bars', *Transactions of the Japan Concrete Institute*, Vol. 6, 1984, pp. 163-170.

63 UOMOTO, T. and MISRA, S.: 'Behaviour of concrete beams and columns in marine environment when corrosion of reinforcing bars takes place', *Concrete in marine environments*, ACI SP 109-6, 1990, pp. 127-146.

64 DALY, A. F.: *Effects of accelerated corrosion on the flexural strength of small scale beams*, TRL Research Report PR/CE/15/94, Crowthorne, Unpublished, 1994.

65 HIGHWAYS AGENCY: *The assessment of concrete highway bridges and structures*, Departmental Standard BD 44/90, 1990.

66 DALY, A. F.: *Effects of accelerated corrosion on the shear behaviour of small scale beams*, TRL Research Report PR/CE/97/95, Crowthorne, Unpublished, 1995.

67 KONG, F. K. and EVANS, R. H.: *Reinforced and prestressed concrete*, Van Nostrand Reinhold, 3rd Edition, 1987, pp. 71-75.

68 RODRIGUEZ, J., ORTEGA, L. M. and CASAL, J.: 'Load carrying capacity of concrete columns with corroded reinforcement', *Fourth international symposium on the corrosion of reinforcement in concrete structures*, Cambridge, UK, 1996, pp. 220-230.

69 BRITISH STANDARDS INSTITUTION: *Structural use of concrete - Part 1: Code of practice for design and construction*, BS 8110: Part 1: 1997.

70 BRITISH STANDARDS INSTITUTION: *Structural use of concrete - Part 2: Code of practice for special circumstances*, BS 8110: Part 2: 1985, 1989.

71 WEBSTER, M. P. and SOMERVILLE, G.: 'The assessment of deteriorating concrete bridges', *Concrete under severe conditions: Environment and loading*, CONSEC '98, E & F N Spon, 1998, pp. 698-707.

72 INSTITUTION OF STRUCTURAL ENGINEERS: *Appraisal of existing structures*, London, 2nd Edition, October 1996.

73 HIGHWAYS AGENCY: *The assessment of concrete highway bridges and structures*, Departmental Standard BD 44/95, 1995.

74 HIGHWAYS AGENCY: *The use of Departmental Standard BD 44/90 for the assessment of highway bridges and structures*, Departmental Advice Note BA 44/90, 1990.

75 HIGHWAYS AGENCY: *The assessment of highway bridges and structures*, Departmental Standard BD 21/93, 1993.

76 HIGHWAYS AGENCY: *The assessment of highway bridges and structures*, Departmental Advice Note BA 16/93, 1993

77 HIGHWAYS AGENCY: *The assessment of concrete structures affected by steel corrosion*, Departmental Advice Note BA 51/95, 1996.

78 ROCHESTER, T. A.: 'Trunk road bridges - current needs for design and assessment', *International Symposium on The Safety of Bridges*, Institution of Civil Engineers, 4-5 July 1996.

79 INSTITUTION OF CIVIL ENGINEERS: *International Symposium on the Safety of Bridges*, London, 4-5 July 1996.

80 INSTITUTION OF CIVIL ENGINEERS: *The Management of Highway Structures*, London, 22-23 June 1998.

81 HIGHWAYS AGENCY: *The Management of sub-standard highway structures*, Departmental Advice Note BA 79/98, 1998.

82 CANADIAN STANDARDS ASSOCIATION: *Existing bridge evaluation, Supplement No. 1 to CAN/CSA-S6-88*, 1990.

83 CANADIAN STANDARDS ASSOCIATION: *Design of highway bridges*, CAN/CSA-S6-88, 1988.

84 COMITE EURO-INTERNATIONAL DU BETON: *Strategies for testing and assessment of concrete structures – Guidance Report*, Lausanne, Bulletin 243, May 1998.

85 TIMOSHENKO, S. P. and GOODIER, J. N.: *Theory of elasticity*, McGraw-Hill, Third edition, 1970, pp. 567.

86 RAPHAEL, J. M.: 'Tensile strength of concrete', *ACI Journal*, March-April 1984, pp. 158-165.

87 TAYLOR, H. P. J.: *Investigation of the forces carried across cracks in reinforced concrete beams by interlock of aggregate,* Cement and Concrete Association, Technical Report 447, November 1970, pp. 22.

88 CASE, J.: *The strength of materials*, Edward Arnold & Co., Third Edition, 1938, pp. 602.

89 NAVARATNARAJAH, V. and SPEARE, P. R. S.: 'An experimental study of the effects of lateral pressure on the transfer bond of reinforcing bars with variable cover', *Proceedings of the Institution of Civil Engineers*, Part 2, 81, December 1986, pp. 697-715.

90 ROBINS, P. J. and STANDISH, I. G.: 'The influence of lateral pressure on anchorage bond', *Magazine of Concrete Research*, Vol. 36, No. 129, December 1994, pp. 195-202.

91 ROWE, R. E., SOMERVILLE, G., BEEBY, A. W., MENZIES, J. B., FORREST, J. C. M., HARRISON, T. A., MOORE, J. F. A., NEWMAN, K., TAYLOR, H. P. J., THRELFALL, A. J. and WHITTLE, R.: *Handbook to BS 8110: 1985: Structural Use of Concrete,* Palladian Publications Ltd, London, 1987, pp. 206.

92 ANDRADE, C.: Private communication, April 1999.

93 WILLIAMSON, S. J.: Private communication, March 1999.

94 TASSIOS, T. P.: *Background document for Chapter 2 – Part 1.3 Eurocode 8, May 1993 Specific rules for concrete structures*, National Technical University of Athens, Undated.

95 CLARK, L. A.: Private communication, 1997

96 DU, Y.: Private communication, 1999.

97 BRITISH STANDARDS INSTITUTION: *Steel, concrete and composite bridges. Part 4. Code of practice for design of concrete bridges*, BS 5400: Part 4, 1990.

98 REGAN, P. E.: 'Research on shear: a benefit to humanity or a waste of time?', *Structural Engineer*, Vol. 71, No. 19, 5 October, 1993, pp. 337-347.

99 TAYLOR, H. P. J.: 'The fundamental behaviour of reinforced concrete beams in bending and shear', *Shear in reinforced concrete*, ACI SP-42, American Concrete Institute, 1974, pp 43-77.

100 CLARK, L. A., BALDWIN, M. I. and GUO, M.: 'Assessment of concrete bridges with inadequately anchored reinforcement', *Bridge Management 3*, E & F N Spon, 1996, pp.225-232.

101 CHANA, P. S.: 'Analytical and experimental studies of shear failures in reinforced concrete beams', *Proceedings of the Institution of Civil Engineers*, Part 2, 85, December 1988, pp. 609-628.

102 CHANA, P. S.: 'Investigation of the mechanism of shear failure of reinforced concrete beams', *Magazine of Concrete Research*, Vol. 39, No. 141, December 1987, pp. 196-204.

103 TAYLOR, H. P. J.: *Investigation of the dowel forces carried by the tensile steel in reinforced concrete beams*, Cement and Concrete Association, Technical Report 431, November 1969, 24 pages.

104 CANADIAN STANDARDS ASSOCIATION: *Design of concrete structure: Structures (Design)*, A23.3, December 1994, pp. 199.

105 VECCHIO, F. J. and COLLINS, M. P.: 'The modified compression field theory for reinforced concrete elements subjected to shear', *ACI Journal*, March-April 1986, pp. 219-231.

106 COLLINS, M. P., MITCHELL, D., ADEBAR, P. and VECCHIO, F. J.: 'A General shear design method', *ACI Structural Journal*, January-February 1996, pp.36-45.

107 ADEBAR, P. and COLLINS, M. P.: 'Shear strength of members without transverse reinforcement', *Canadian Journal of Civil Engineering*, 23, 1996, pp. 30-41.

108 BEEBY, A. W., NARAYANAN, R. S., WHITTLE, R. and THRELFALL, A. J.: *Worked examples for the design of concrete buildings. Based on BSI publication DD ENV 1992-1-1*, Publication 43.505, British Cement Association, 1994.

109 NIELSEN, M. P.: *Limit analysis and plastic theory*, Prentice Hall, 1984, pp. 212-214.

110 LEONHARDT, F, and WALTHER, R.: *The Stuttgart shear tests, 1961*, Cement and Concrete Association, Translation CJ.111, 1964, 134 pp.

111 SWAMY, R. N., ANDRIOPOULOS, A. and ADEPEGBA, D.: 'Arch action and bond in concrete shear failures', *Proceedings of the ASCE Journal of the Structural Division*, Vol. 96, ST6, June 1970, pp. 1069-1091.

112 KANI, G. N. J.: 'The riddle of shear failure and its solution', *Journal of the American Concrete Institute*, 61, No. 4, April 1964, pp. 441-467.

113 CAIRNS, J.: 'Strength in shear of concrete beams with exposed reinforcement', *Proceedings of the Institution of Civil Engineers, Structures and Buildings*, Vol. 110, May 1995, pp. 176-185.

114 LORENTSEN, M.: 'Shear and bond in prestressed concrete beams without shear reinforcement' *Hadlingar Nr 47*, Statens Råd för Byggnadsforskning, Stockholm, 1964, pp. 195.

115 BAZANT, Z. P. and KIM, J.-K.: 'Size effect in shear failure of longitudinally reinforced beams', *ACI Journal*, September-October 1984, pp. 456-468.

116 BRITISH STANDARDS INSTITUTION: *The structural use of concrete. Part 1: Design, materials and workmanship*, CP 110: Part 1, 1972.

117 BEEBY, A. W.: *The design of sections for flexure and axial load according to CP 110*, Development Report 2, Cement and Concrete Association, December 1978, pp. 31.

118 HIGHWAYS AGENCY: *Design for durability*, Departmental Standard, BD 57/95, 1995.

119 BUNGEY, J. H. and MILLARD, S. G.: *Testing of concrete in structures*, Third edition, Blackie Academic and Professional, 1996.

120 CLARK, L. A., SHAMMAS-TOMA, M. G. K., SEYMOUR, D. E., PALLETT, P. F. and MARSH, B. K.: 'How can we get the cover we need?', *Structural Engineer*, Volume 75, No. 17, 2 September 1997, pp 289-296.

121 WEBSTER, M. P.: *Relating quality to whole life costing*, Final Report, DETR Partners in Technology Project CI 38/13/23 (cc1401), September 1998.

122 WEBSTER, M. P.: 'The influence of design concept and detailing on the response of concrete structures to deterioration', *Concrete Communication Conference*, Chilwell Manor, Southampton, July 1998, pp. 137-149.

123 WEBSTER, M. P.: *The impact of deterioration on the safety of concrete structures*, Final Report, DETR Partners in Technology Project CI 38/13/20 (cc1030), July 1998.

124 IBELL, T. J., MORLEY, C. T. and MIDDLETON, C. R.: 'Shear assessment of concrete beam-and-slab bridges', *Proceedings of the Institution of Civil Engineers, Structures and Buildings*, Vol.128, No.3, August 1998, pp. 264-273.

125 JACKSON, P. A.: 'The effect of local corrosion on the life of bridge deck slabs', *The life of structures: Physical testing*, Edited by Garas, F. K. Clarke, J. L. and Armer, G. S. T., Butterworths, London, 1989, pp. 360-367.

APPENDIX A

Procedures for assessing corrosion-damaged concrete structures

APPENDIX A

PROCEDURES FOR ASSESSING CORROSION-DAMAGED CONCRETE STRUCTURES

A1 Introduction

In order to ascertain the impact of deterioration on the safety of concrete structures, the influence of deterioration has to be considered over the whole life of the structure. To do this, new procedures have been developed for modelling the effects of both material and structural deterioration, and are described in the main body of this Thesis.

The methods described in Chapters 3 to 7 are combined in this Appendix to give an estimate of the reduction in load-carrying capacity with time for corrosion-damaged concrete structures in a chloride environment. The approach described in this Appendix is based on procedures which are amenable to hand calculation. For ease of use these procedures are implemented in the spreadsheet *BEAMCOL_CORR*. A typical printout from this spreadsheet is included in Appendix B.

A2 Estimating the initiation period

The assumption is made that corrosion initiates when the chloride content in the concrete reaches the critical level at the reinforcement. The time to initiation is calculated for each reinforcement bar, or group of bars, using Fick's 2nd law rearranged to make time the subject of the calculation:

$$T_{init} = \left[\frac{x}{2erfc^{-1}\left[\frac{C_{crit} - C_i}{C_s - C_i} \right]} \right]^2 D_{ce} \qquad \text{… (A2-1)}$$

where: C_{crit} = critical total chloride threshold level (% by mass of concrete)

C_i = initial total chloride content in the concrete i.e. from sea dredged aggregate or calcium chloride accelerator (% by mass of concrete)

C_s = total chloride content at the surface (% by mass of concrete)

D_{ce} = effective chloride diffusion co-efficient (m^2/s)

T_{init} = initiation period (years)

$erfc^{-1}$ = inverse error function complement $(1 - erf)^{-1}$

x = depth below the exposed surface to the point being considered (m)

The effective diffusion co-efficient, D_{ce}, is given by the following equations for XS3 marine exposure and XD3 de-icing salt exposure respectively:

$$D_{ce} = 0.04\,(1166^{\,w/c})\,x\,10^{-12} \quad (m^2/s) \qquad \textbf{… (A2-2)}$$

$$D_{ce} = 0.06\,(906^{\,w/c})\,x\,10^{-12} \quad (m^2/s) \qquad \textbf{… (A2-3)}$$

Default values for the surface chloride level, C_s, and the critical chloride threshold, C_{crit}, are given in Table A2-1 for XS3 marine exposure and XD3 de-icing salt exposure.

Table A2-1: Default values of C_s and C_{crit} for XS3 and XD3 exposure classes

Exposure condition	C_s *(% by mass of concrete)*	C_{crit} *(% by mass of concrete)*
XS3 – Tidal, splash and spray zones	0.4	0.2
XD3 – Cyclic wet and dry	0.1*	0.06

* For D_{ce} values of $1x10^{-12}$ m^2/s or higher take C_s as 0.1%. For D_{ce} values less than $1x10^{-12}$ m^2/s increase C_s.

A3 Corrosion rate

The corrosion rates in Figure A3-1 can be used to calculate the cumulative corrosion with time. For instance, a characteristic (95%) value of, say, 1.5 μA/cm^2 could be used. Alternatively, if in situ values are available they could be used instead. The corrosion is expressed as a radius loss, and also converted into percentage corrosion and corroded area lost for later use. Faraday's law can be used to convert the corrosion rate into a radius loss (in μm) using the following expression:

$$\delta_{corr} = 11.6 I_{corr} \qquad \text{… (A3-1)}$$

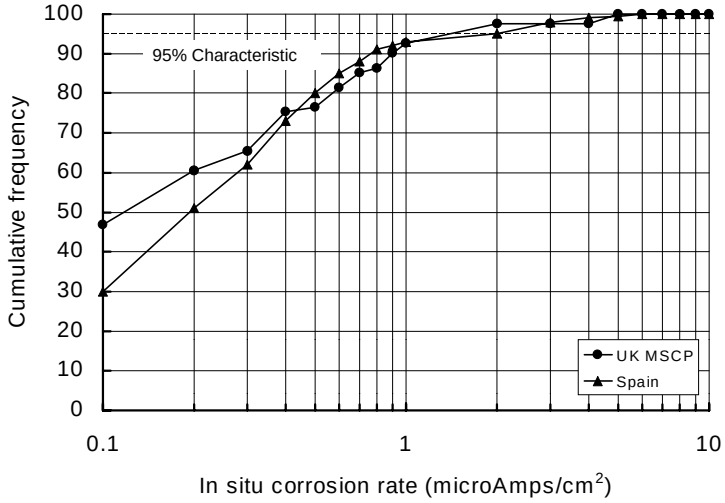

Figure A3-1: In situ chloride-induced corrosion rates measured in UK and Spanish structures

A4 Estimated time to cracking

The percentage corrosion to cause cracking can be estimated from the following equation:

$$\Delta_{cr} = \frac{c}{2D} \qquad \text{… (A4-1)}$$

Δ_{cr} can then be converted into the bar radius loss δ_{cr}:

$$\delta_{cr} = \frac{D}{2} - \sqrt{\frac{D^2}{4}\left(1 - \frac{\Delta_{cr}}{100}\right)} \approx 1.25c \qquad \textbf{… (A4-2)}$$

The time to cracking is thus given by:

$$t_{cr} = \frac{1000\delta_{cr}}{11.6I_{corr}} \qquad \textbf{… (A4-3)}$$

where: c = concrete cover to bar (mm)

D = bar diameter (mm)

I_{corr} = corrosion rate ($\mu A/cm^2$)

δ_{cr} = bar radial loss required for corrosion-induced cracking (μm)

Δ_{cr} = bar section loss required for corrosion-induced cracking (%)

A5 Reinforcement bar diameters after corrosion

Based on the corrosion rate established in Section A3, the residual bar diameters are calculated for each bar. Chlorides can induce pitting corrosion of around 4 to 8 times larger than general corrosion. An average pitting factor of 6 could be assumed for initial calculations. Subsequent checks on the sensitivity of the member to larger pitting factors should be carried out. The pitting factor should be applied to those load-carrying mechanisms where the strain is localised such as the tension reinforcement under bending, and the shear links. General corrosion should be applied to those mechanisms that develop strength over a length of bar, such as bond and the tension reinforcement in shear.

A6 Bond strength of ribbed bars with no links

General corrosion is used in this calculation, not pitting corrosion, as the effects are averaged over the bonded length. The characteristic corroded bond strength is given by:

$$f_b = (0.31 - 0.015Acorr)\left(0.5 + \frac{c}{D}\right)f_{ct} \qquad \textbf{… (A6-1)}$$

where: f_b = the corroded bond strength (N/mm^2)
Acorr = area of the of bar corroded (mm^2)
c/D = the cover to bar diameter ratio
f_{ct} = the concrete tensile strength (N/mm^2)

A7 Bond strength enhancement due to links

If the minimum amount of links is still present then the allowable corroded bond strength calculated in Section A6 can be enhanced by 1.0 / γ_{mb} N/mm^2. The requirement for minimum links is given by:

$$\frac{A_{sv}(f_{yv}/\gamma_{ms})}{b_v s_v} \geq 0.4 \qquad \text{… (A7-1)}$$

where: A_{sv} = cross-sectional area of all the legs of the links (mm^2)
b_v = width of the section (mm)
d = effective depth to the tension reinforcement (mm)
f_{yv} = characteristic strength of the shear reinforcement (N/mm^2)
s_v = spacing of the links along the member (mm)
γ_{mv} = the partial safety factor for shear

The value of 0.4 is specified in BS 8110. If the BD 44/95 value of 0.2 is to be taken, then the corroded bond strength should only be enhanced by 0.5 / γ_{mb} N/mm^2. These levels of enhancement are likely to be conservative when there is little link corrosion.

If the residual area of links is below the minimum level then the longitudinal bars should be treated as if no links were present and no enhancement should be applied to the bond strength calculated in Section A6.

The allowable bond strength should be used to obtain the effective area of tension reinforcement for use in shear calculations, and for checks on laps and curtailment in areas of concern. The bond calculations need only be carried out when the concrete surrounding the bar in question has

cracked. Prior to cracking there is a potential for bond enhancement due to corrosion. This is ignored, and the uncorroded bond strength from the following formula, on which BS 8110 Table 3.26 is based, should be used:

$$f_{bu} = \frac{0.28}{\gamma_{mb}}\left(0.5 + \frac{c}{D}\right)\sqrt{f_{cu}} \qquad \textbf{… (A7-2)}$$

where: c = concrete cover to bar (mm)

D = bar diameter (mm)

f_{bu} = ultimate bond stress (N/mm^2)

f_{cu} = concrete cube strength (N/mm^2)

γ_{mb} = partial safety factor for bond strength

When nominal transverse (shear link) reinforcement is present, then an extra term, $(0.28 \sqrt{f_{cu}})/\gamma_{mb}$ is added to the basic equation.

Using this equation allows the beneficial effects of c/D ratios in excess of 1 to be applied. This avoids the anomaly of a bar with cracked cover but little corrosion having a higher estimated bond strength than when it was uncorroded.

A8 Bending strength

The bending moment capacity is calculated either by using re-arranged BS 8110 formulae for simple members or a strain compatibility approach for more complex members. The pitted reinforcement areas are used. The bending capacity is translated into a load-carrying capacity based on the loading and member geometry.

If spalling is likely to occur along the line of the compression reinforcement, then two extra effects may need to be considered:

(i) Loss of concrete section

If spalling of cover is considered to reduce the compression zone significantly then this reduction should be included in the calculation by assuming that rectangular sections of concrete are lost to the centre-line of the compression bars under consideration as shown in Figure A8-1. A strain compatibility approach would need to be used due to the complexity of the geometry. This check is likely to be most relevant in smaller members.

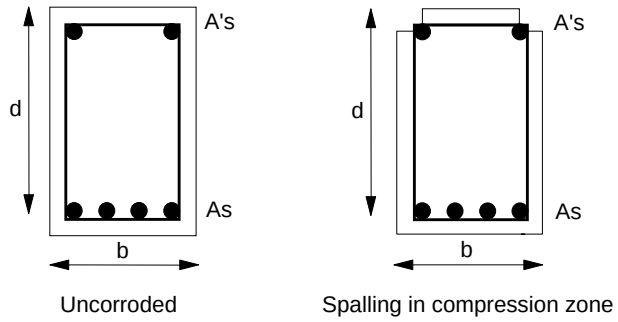

Figure A8-1: The effects of spalling in the compression zone of reinforced concrete beams

(ii) Compression reinforcement buckling

If the cover concrete spalls along the line of the compression reinforcement, restraint will be lost and there is a possibility that the reinforcement may buckle in compression before it can yield. The limiting buckling stress, σ_{cr}, is given by the following equation. If this is lower than the yield stress, then it should be used in the calculations instead of the yield stress.

$$\sigma_{cr} = \frac{\pi^2 E D^2}{16(ks_v)^2} \qquad \textbf{… (A8-1)}$$

where: E = elastic modulus of the reinforcement (N/mm^2)

D = diameter of the compression reinforcement after corrosion (mm)

k = 1.0 when sufficient restraint is provided

= 1.5 when sufficient restraint is provided at first and third links, but less than sufficient restraint is provided at the second link

= 2.0 when sufficient restraint is provided at first and third links, but no

restraint is provided at the second link

s_v = spacing between adjacent link reinforcement (mm)

σ_{cr} = critical buckling stress (N/mm^2)

A9 Shear strength

The BS 8110 formula is used as shown:

$$V = \left[\frac{0.79}{\gamma_{mv}}\right]\left[\frac{400}{d}\right]^{1/4}\left[\frac{100\,A_{s.eff}}{b_w d}\right]^{1/3}\left[\frac{f_{cu}}{25}\right]^{1/3} b_w d + \left[\frac{f_{yv}}{\gamma_{ms}}\right]\frac{A_{sv}\,d}{s_v} \qquad \textbf{… (A9-1)}$$

where: $A_{s.eff}$ = area of effectively anchored longitudinal tensile reinforcement (mm^2)

A_{sv} = net corroded cross-sectional area of all the legs of the links considering pitting (mm^2)

b_w = width of the section (mm)

d = effective depth to the tension reinforcement (mm)

f_{cu} = characteristic concrete cube strength (N/mm^2)

f_{yv} = characteristic strength of the shear reinforcement (N/mm^2)

s_v = spacing of the links along the member (mm)

V = ultimate shear load-carrying capacity (N)

γ_{mv} = partial safety factor for shear strength

γ_{ms} = partial safety factor for strength of reinforcement

The shear capacity is translated into a load-carrying capacity based on the loading and member geometry.

The area of effectively anchored tension reinforcement is calculated using the following expression:

$$\frac{A_{s.eff}}{A_{s.nom}} = 0.8\left[\frac{c}{D}\right]^{0.3}\left[\frac{f_{b.corr}}{f_{b.8110}}\right]^{0.3} \qquad \textbf{… (A9-2)}$$

where: $A_{s.eff}$ = effective area of the corroded tension reinforcement (mm^2)

$A_{s.nom}$ = nominal area of the uncorroded tension reinforcement (mm^2)

c = vertical cover to the tension reinforcement (mm)

D = nominal diameter of the uncorroded tension reinforcement (mm)

$f_{b.corr}$ = corroded bond strength of the tension reinforcement (N/mm^2)

$f_{b.8110}$ = bond strength of the tension reinforcement calculated in accordance with BS 8110 (N/mm^2)

The links are only considered effective in shear if the following equation is satisfied. If not, the member is treated as if it contained no shear reinforcement.

$$\frac{A_{sv}(f_{yv}/\gamma_{ms})}{b_v s_v} \geq 0.4 \qquad \textbf{… (A9-3)}$$

The value of 0.4 is the one specified in BS 8110. BD 44/95 allows a value of 0.2 to be taken. However, the values used for shear and bond should be the same.

There must be sufficient effective longitudinal reinforcement to ensure that the links are effective in a 45° truss. The limiting shear capacity can be calculated on the basis of the following equation when links are present:

$$V = 2\left[F_b - \frac{M}{z}\right] \qquad \textbf{… (A9-4)}$$

where: F_b = tensile force that can be generated in the corroded reinforcement over the anchorage length (kN)

M = ultimate moment co-existent with V (kNm)

V = ultimate allowable shear force that can co-exist with M (kN)

z = lever arm for bending, and may be taken as 0.9 d (m)

A10 Reduction in load-carrying capacity with time

The minimum of the bending and shear capacities dictates the maximum load-carrying capacity at any one time.

A11 Column load-carrying capacity

From the limited test data available, the proposals in this section would appear to be applicable to the three types of column considered in the following section. The concrete area outside the link reinforcement should be excluded in the assessment of the column load-carrying capacity, as there is a significant chance that this concrete will spall and delaminate before the ultimate load is reached. If broken links are observed then the possibility of buckling in the longitudinal bars should be checked using the procedure described in Section A8.

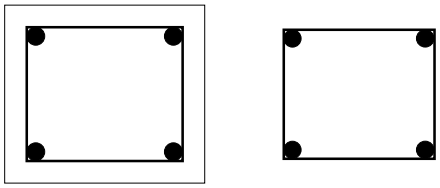

Figure A11-1: The effects of spalling on reinforced concrete column cross-sections

A11.1 Column with primarily axial loads (and nominal moments)

The axial load-carrying capacity is given by:

$$N = \frac{0.67\, f_{cu} A_c}{\gamma_{mc}} + \frac{f_y A_{sc}}{\gamma_{ms}} \qquad \text{… (A11-1)}$$

where: A_c = area of concrete excluding the cover concrete

A_{sc} = area of reinforcement (mm^2)

f_{cu} = concrete compressive cube strength (N/mm^2)

f_y = reinforcement yield stress (N/mm^2)

N = ultimate axial strength (N)

γ_m = partial safety factor for concrete

γ_s = partial safety factor for reinforcement

If nominal moments are present, then the axial load-carrying capacity should be taken as 90% of this value.

A11.2 Significant moments bent about one axis only.

The procedures outlined in Section A8 for flexure are used in combination with a net concrete area that ignores the cover concrete. A moment – axial load (M-N) interaction diagram can be produced.

A11.3 Significant moments bent about two axes.

For symmetrical sections, the procedures outlined in Section A8 for flexure are used in combination with a net concrete area that ignores the cover concrete. Biaxial bending is catered for by increasing the moment about one axis and then checking for the increased moment using the procedure for columns bent about one axis. Either the moment about the x or the y-axis is enhanced depending on the relative magnitude of the two moments. The enhanced moments are calculated using the following equations:

When:

$$\frac{M_x}{h'} \geq \frac{M_y}{b'} \qquad \textbf{… (A11-2)}$$

$$M_x' = M_x + \beta \frac{h'}{b'} M_y \qquad \textbf{… (A11-3)}$$

and when:

$$\frac{M_x}{h'} < \frac{M_y}{b'} \qquad \text{… (A11-4)}$$

$$M_y' = M_y + \beta \frac{b'}{h'} M_x \qquad \text{… (A11-5)}$$

where: b’ = effective depth to the reinforcement taken perpendicular to the y-axis (mm)

h’ = effective depth to the reinforcement taken perpendicular to the x-axis (mm)

M_x = applied moment about the x-axis (kNm)

M_x’ = increased moment about the x-axis (kNm)

M_y = applied moment about the y-axis (kNm)

M_y’ = increased moment about the y-axis (kNm)

β = a coefficient which is a function of N/bhf_{cu}

A12 Implementation

These procedures are implemented in the spreadsheet *BEAMCOL_CORR*. A typical print out from this spreadsheet is included in Appendix B.

Whilst the procedures are suitable for hand calculation, it is more convenient to implement them in a spreadsheet. In *BEAMCOL_CORR* the procedures are repeated for a number of ages up to 150 years. Graphical and tabular output are provided so that an assessment can be made of the implications of deterioration with time.

The spreadsheet has been written for the assessment of sections. A variety of support conditions can be allowed for simply by altering the moment and shear coefficients.

APPENDIX B

Spreadsheet *BEAMCOL_CORR*

Project	The assessment of corrosion-damaged concrete structures	**British Cement Association**	
Client	University of Birmingham	Made by	Date / Page
Structure	Parameter study	MPW	23-Jul-00 / 1
Location	Default beam Level 0 - from grid ref A1 to grid ref A2	Checked	Revision / Job No
	Structural assessment of corrosion-damaged concrete structures to BS 81110 (modified) © 2000 MPW		Final / PhD

Section and Material Details

Location Level 0 From grid ref A1 to grid ref A2

Age 140 years

Mix details

w/c	0.5	
Cement content	350	kg/m^3
Density	2350	kg/m^3
Multiplier	6.71	

Exposure

Exposure d

Marine m

De-icing d

Chloride constants

Cl threshold	0.40	% by wt of cement
Dce	1.81E-12	m^2/sec
Cs	0.67	% by wt of cement

Corrosion

Icorr.conc	0.4	µA/cm^2
Icorr.conc	4.600	µm / year
Icorr.exp	100	µm / year

Exposure conditions and constants

Exposure conditions	a	b	Dce m^2/sec	Cs % conc	Cs % cem	Ccrit % conc	Ccrit % cem
Marine	0.04	1166	1.37E-12	0.4	2.69	0.2	1.34
De-icing salt	0.06	906	1.81E-12	0.1	0.67	0.06	0.40

Section Properties

		As built	Loss	Effective	
Top flange width	b.tf	0	0	0	mm
Top flange depth	h.tf	0	0	0	mm
Web width	bw	300	0	300	mm
Web depth	dw	500	0	500	mm
Bottom flange width	b.bf	0	0	0	mm
Bottom flange depth	h.bf	0	0	0	mm
Section depth	h	500	0	500	mm

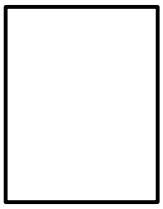

Concrete Details

Cube strength	fcu	45.0	N/mm²
Tensile strength	fct	3.3	N/mm²
Gamma.c	γc	1.5	
Limiting strain	εcu	0.0035	
Elastic modulus	Ec	33.5	kN/mm²
Creep factor	ϕ	2	

Member

Span L 8 m

Column depth h 300 mm

Reinforcement Details

Gamma.s	γs	1.05	
Gamma.bond	γbond	1.4	
Anchorage length	nD.req	12	bar diameters
Rebar yield params	a	1	
fycorr / fy = a - b.corr	b	0	
Bond parameters	a	0.31	fb = (a - b Acorr) (0.5 + c / D) fct
	b	0.0153	
No. bars	nrebar	2	

Loading

Bending moment = 0.125 w.L^2

Shear force = 0.5 w.L

Calculate V at 1 d from column face

Shear span av 1500 mm

Layer	Cover Horiz mm	Cover Vert mm	Depth to bar - mm	No bars	Effective in shear	Anchorage mm	fy N/mm²	E kN/mm²	Nom dia mm	Radius loss mm	Pitting factor	Icorr µm / year
1	50	50	58.0	2	2	192	460	200	16	0.28	6	4.6
2	50	50	437.5	4	2	300	460	200	25	0.28	6	4.6
3	0	0	0.0	0	0	0	0	0	0	0.00	0	0
4	0	0	0.0	0	0	0	0	0	0	0.00	0	0
5	0	0	0.0	0	0	0	0	0	0	0.00	0	0
6	0	0	0.0	0	0	0	0	0	0	0.00	0	0
7	0	0	0.0	0	0	0	0	0	0	0.00	0	0
8	0	0	0.0	0	0	0	0	0	0	0.00	0	0
9	0	0	0.0	0	0	0	0	0	0	0.00	0	0

Shear links at supports

Nominal bar diameter	Dsv	10	mm
Loss	sv.radloss	0.41	mm
Pitting factor		6	
Corrosion rate	Icorr	4.6	µm / year
No. legs	nvleg	2	
Spacing	sv	200	mm
Cover		40	mm
Yield strength	fyv	460	N/mm²
(Asv.fyv / γs.bv.sv).min		0.4	
Bond with min links	fb.link	1.0	N/mm²
Gamma.s	γs	1.05	
Gamma.shear	γsv	1.25	

Links at mid-span

Nominal bar diameter	Dsm	10	mm
Loss	Dsm.radloss	0.41	mm
Pitting factor		6	
Corrosion rate	Icorr	4.6	µm / year
No. legs	nmleg	2	
Spacing	sm	200	mm
Cover		40	mm
Yield strength	fym	460	N/mm²
(Asm.fy / γs.bv.sm).min		0.4	

Summary of whole life calculations

Section properties

	Concrete section		Combined section: Short-term		Combined section: Long-term	
	A	Ixx	A	Ixx	A	Ixx
	mm^2	$mm^4 \times 10^6$	mm^2	$mm^4 \times 10^6$	mm^2	$mm^4 \times 10^6$
Uncorroded	150000	3125	161759	3529	190009	1291
Corroded	150000	3125	161197	3510	188097	1476

Reinforcement

					General				Pitting				
Layer	Bars effective in Bending	Bars effective in Shear	Nom dia (mm)	As.nom (mm^2)	Dia (mm)	As.corr (mm^2)	Corr (%)	Acorr (mm^2)	Dia (mm)	As.corr (mm^2)	Corr (%)	Acorr (mm^2)	fy.corr (N/mm^2)
1	2	2	16	201	15.448	187	6.78	13.6	12.688	126	37.1	74.6	460
2	4	2	25	491	24.448	469	4.37	21.4	21.688	369	24.7	121.4	460
3	0	0	0	0	0.000	0	0.00	0.0	0.000	0	0.0	0.0	0
4	0	0	0	0	0.000	0	0.00	0.0	0.000	0	0.0	0.0	0
5	0	0	0	0	0.000	0	0.00	0.0	0.000	0	0.0	0.0	0
6	0	0	0	0	0.000	0	0.00	0.0	0.000	0	0.0	0.0	0
7	0	0	0	0	0.000	0	0.00	0.0	0.000	0	0.0	0.0	0
8	0	0	0	0	0.000	0	0.00	0.0	0.000	0	0.0	0.0	0
9	0	0	0	0	0.000	0	0.00	0.0	0.000	0	0.0	0.0	0
Links @ support			10	79	9.181	66	15.71	12.3	5.087	20	74.1	58.2	460
Links @ mid-span			10	79	9.181	66	15.71	12.3	5.087	20	74.1	58.2	460

	Cover				Time to		
Layer	Horiz (mm)	Vert (mm)	Minimum (mm)	c / D	Initiation (years)	Cracking (years)	Spalling (years)
1	50	50	50	3.1	80	94	131
2	50	50	50	2.0	80	94	127
3	0	0	0	0.0	0	0	0
4	0	0	0	0.0	0	0	0
5	0	0	0	0.0	0	0	0
6	0	0	0	0.0	0	0	0
7	0	0	0	0.0	0	0	0
8	0	0	0	0.0	0	0	0
9	0	0	0	0.0	0	0	0
Links @ support				4.0	51	62	0
Links @ mid-span				4.0	51	62	0

Load-carrying capacity to BS 8110

N	0.0 kN
M	251.9 kNm
Vc	0.0 kN
Vs	0.0 kN
V	0.0 kN

Limitations to shear force due to bond deterioration

Vmax 0.0 kN

Column load cases

	Required		Provided		
Load case	M kN	N kNm	M kN	N kNm	Pass or fail
1	200	250	321	250	Pass
2	300	475	341	475	Pass
3	350	700	352	700	Pass
4	175	3750	-76	3750	Fail
5	275	3300	11	3300	Fail
6					
7					
8					
9					
10					

Section Properties - Sheet 1 of 2

Concrete section properties - uncorroded

	b mm	h mm	Centroid mm	Area mm^2	y-y.bar mm	I.own_axis $mm^4 \times 10^6$	I.offset $mm^4 \times 10^6$	Ixx $mm^4 \times 10^6$
Top flange	0	0	0	0	-250	0	0	0
Web	300	500	250	150000	0	3125	0	3125
Bot flange	0	0	500	0	250	0	0	0
Overall		500	250	150000				3125

Concrete section properties - corroded

	b mm	h mm	Centroid mm	Area mm^2	y-y.bar mm	I.own_axis $mm^4 \times 10^6$	I.offset $mm^4 \times 10^6$	Ixx $mm^4 \times 10^6$
Top flange	0	0	0	0	-250	0	0	0
Web	300	500	250	150000	0	3125	0	3125
Bot flange	0	0	500	0	250	0	0	0
Overall		500	250	150000				3125

Composite section properties - uncorroded

	Centroid mm	Area mm^2	Modular ratio, m	m.Area mm^2	y-y.bar mm	I.own_axis $mm^4 \times 10^6$	I.offset $mm^4 \times 10^6$	Ixx $mm^4 \times 10^6$
Top flange	0	0	1.00	0	-258.9	0	0.00	0
Web	250	150000	1.00	150000	-8.9	3125	11.99	3137
Bot flange	500	0	1.00	0	241.1	0	0.00	0
Layer 1	58	402	4.97	1999	-200.9	0.013	80.71	81
Layer 2	437.5	1963	4.97	9760	178.6	0.153	311.19	311
Layer 3	0	0	-1.00	0	-258.9	0.000	0.00	0
Layer 4	0	0	-1.00	0	-258.9	0.000	0.00	0
Layer 5	0	0	-1.00	0	-258.9	0.000	0.00	0
Layer 6	0	0	-1.00	0	-258.9	0.000	0.00	0
Layer 7	0	0	-1.00	0	-258.9	0.000	0.00	0
Layer 8	0	0	-1.00	0	-258.9	0.000	0.00	0
Layer 9	0	0	-1.00	0	-258.9	0.000	0.00	0
Overall	258.9			161759				3529

Composite section properties - corroded

	Centroid mm	Area mm^2	Modular ratio, m	m.Area mm^2	y-y.bar mm	I.own_axis $mm^4 \times 10^6$	I.offset $mm^4 \times 10^6$	Ixx $mm^4 \times 10^6$
Top flange	0	0	1.00	0	-258.6	3125	0.00	3125
Web	250	150000	1.00	150000	-8.6	0	11.19	11
Bot flange	500	0	1.00	0	241.4	0	0.00	0
Layer 1	58	375	4.97	1863	-200.6	0.013	75.01	75
Layer 2	437.5	1878	4.97	9334	178.9	0.153	298.61	299
Layer 3	0	0	-1.00	0	-258.6	0.000	0.00	0
Layer 4	0	0	-1.00	0	-258.6	0.000	0.00	0
Layer 5	0	0	-1.00	0	-258.6	0.000	0.00	0
Layer 6	0	0	-1.00	0	-258.6	0.000	0.00	0
Layer 7	0	0	-1.00	0	-258.6	0.000	0.00	0
Layer 8	0	0	-1.00	0	-258.6	0.000	0.00	0
Layer 9	0	0	-1.00	0	-258.6	0.000	0.00	0
Overall	258.6			161197				3510

Section Properties - Sheet 2 of 2

Composite section properties - uncorroded - long term

	Centroid mm	Area mm^2	Modular ratio, m	m.Area mm^2	y-y.bar mm	I.own_axis $mm^4 \times 10^6$	I.offset $mm^4 \times 10^6$	Ixx $mm^4 \times 10^6$
Top flange	0	0	1.00	0	-275.9	0	0.00	0
Web	250	150000	1.00	150000	-25.9	0	100.60	101
Bot flange	500	0	1.00	0	224.1	0	0.00	0
Layer 1	58	402	16.91	6801	-217.9	0.013	322.90	323
Layer 2	437.5	1963	16.91	33208	161.6	0.153	867.24	867
Layer 3	0	0	-1.00	0	-275.9	0.000	0.00	0
Layer 4	0	0	-1.00	0	-275.9	0.000	0.00	0
Layer 5	0	0	-1.00	0	-275.9	0.000	0.00	0
Layer 6	0	0	-1.00	0	-275.9	0.000	0.00	0
Layer 7	0	0	-1.00	0	-275.9	0.000	0.00	0
Layer 8	0	0	-1.00	0	-275.9	0.000	0.00	0
Layer 9	0	0	-1.00	0	-275.9	0.000	0.00	0
Overall	275.9			190009				1291

Composite section properties - corroded - long term

	Centroid mm	Area mm^2	Modular ratio, m	m.Area mm^2	y-y.bar mm	I.own_axis $mm^4 \times 10^6$	I.offset $mm^4 \times 10^6$	Ixx $mm^4 \times 10^6$
Top flange	0	0	1.00	0	-279.0	0	0.00	0
Web	250	150000	1.00	150000	-29.0	0	126.01	126
Bot flange	500	0	1.00	0	221.0	0	0.00	0
Layer 1	58	375	16.91	6340	-221.0	0.013	309.60	310
Layer 2	460	1878	16.91	31757	181.0	0.153	1040.59	1041
Layer 3	0.4	0	-1.00	0	-278.6	0.000	0.00	0
Layer 4	1	0	-1.00	0	-278.0	0.000	0.00	0
Layer 5	1.05	0	-1.00	0	-277.9	0.000	0.00	0
Layer 6	1.25	0	-1.00	0	-277.7	0.000	0.00	0
Layer 7	0	0	-1.00	0	-279.0	0.000	0.00	0
Layer 8	0	0	-1.00	0	-279.0	0.000	0.00	0
Layer 9	0	0	-1.00	0	-279.0	0.000	0.00	0
Overall	279.0			188097				1476

Project	The assessment of corrosion-damaged concrete structures	British Cement Association		
Client	University of Birmingham	Made by	Date	Page
Structure	Parameter study	MPW	24-Jul-00	4A
Location	Default beam, Level 0 - from grid ref A1 to grid ref A2	Checked	Revision	Job No
	Structural assessment of corrosion-damaged concrete structures to BS 81110 (modified) © 2000 MPW		Final	PhD

Durability, cracking and spalling - Sheet 1 of 2

Spalling

fcu	45.0	N/mm^2	Ec.eff	11165	kN/mm^2	sin 45	0.707
ft.flex	4.8	N/mm^2	FoS	1		cos 45	0.707
ft.shear	1.2	N/mm^2	ϕ	45	degrees		

Layer				Length of crack (mm) 250	500	750	1000	1250	1500	1750	2000	Ave t.spall (years)
1												
Horiz cover (mm)	50	self wt	N/mm	0.058	0.058	0.058	0.058	0.058	0.058	0.058	0.058	
Vert cover (mm)	50	σ.flex.all	N/mm^2	4.75	4.71	4.64	4.53	4.41	4.25	4.06	3.84	
x (mm)	25	σ.shear.all	N/mm^2	1.19	1.18	1.18	1.17	1.17	1.16	1.16	1.16	
y (mm)	25	Mcorr	Nm	69976	69341	68282	66799	64893	62564	59811	56635	
Ixx (mm4)	520833.3	w.corr.flex	N/mm	13.44	3.33	1.46	0.80	0.50	0.33	0.23	0.17	
Iyy (mm4)	520833.3	vsw	N/mm^2	0.004	0.009	0.013	0.017	0.022	0.026	0.030	0.035	
θNA (rads)	0.785398	Vcorr	N	1981	1978	1976	1973	1970	1968	1965	1962	
Ina	520833.3	w.corr.shr	N/mm	15.85	7.91	5.27	3.95	3.15	2.62	2.25	1.96	
Dia (mm)	16	w.corr	N/mm	13.44	3.33	1.46	0.80	0.50	0.33	0.23	0.17	
dr.pore (μm)	138	delta.mid	mm	24	93	206	359	545	756	984	1217	
rad.loss/year (μm)	4.6	dr.spall	mm	57	81	121	175	240	315	395	477	
		t.spall	years	12.3	17.7	26.3	38.0	52.2	68.4	85.9	103.7	50.6
2												
Horiz cover (mm)	50	self wt	N/mm	0.058	0.058	0.058	0.058	0.058	0.058	0.058	0.058	
Vert cover (mm)	50	σ.flex.all	N/mm^2	4.75	4.71	4.64	4.53	4.41	4.25	4.06	3.84	
x (mm)	25	σ.shear.all	N/mm^2	1.19	1.18	1.18	1.17	1.17	1.16	1.16	1.16	
y (mm)	25	Mcorr	Nm	69976	69341	68282	66799	64893	62564	59811	56635	
Ixx (mm4)	520833.3	w.corr.flex	N/mm	13.44	3.33	1.46	0.80	0.50	0.33	0.23	0.17	
Iyy (mm4)	520833.3	vsw	N/mm^2	0.004	0.009	0.013	0.017	0.022	0.026	0.030	0.035	
θNA (rads)	0.785398	Vcorr	N	1981	1978	1976	1973	1970	1968	1965	1962	
Ina	520833.3	w.corr.shr	N/mm	15.85	7.91	5.27	3.95	3.15	2.62	2.25	1.96	
Dia (mm)	25	w.corr	N/mm	13.44	3.33	1.46	0.80	0.50	0.33	0.23	0.17	
dr.pore (μm)	88	delta.mid	mm	24	93	206	359	545	756	984	1217	
rad.loss/year (μm)	4.6	dr.spall	mm	39	64	104	157	223	297	378	460	
		t.spall	years	8.5	13.9	22.5	34.2	48.4	64.6	82.1	99.9	46.8
3												
Horiz cover (mm)	0	self wt	N/mm	0.000	0.000	0.000	0.000	0.000	0.000	0.000	0.000	
Vert cover (mm)	0	σ.flex.all	N/mm^2	#DIV/0!	#DIV/0!	#DIV/0!	#DIV/0!	#DIV/0!	#DIV/0!	#DIV/0!	#DIV/0!	
x (mm)	0	σ.shear.all	N/mm^2	#DIV/0!	#DIV/0!	#DIV/0!	#DIV/0!	#DIV/0!	#DIV/0!	#DIV/0!	#DIV/0!	
y (mm)	0	Mcorr	Nm	#DIV/0!	#DIV/0!	#DIV/0!	#DIV/0!	#DIV/0!	#DIV/0!	#DIV/0!	#DIV/0!	
Ixx (mm4)	0	w.corr.flex	N/mm	#DIV/0!	#DIV/0!	#DIV/0!	#DIV/0!	#DIV/0!	#DIV/0!	#DIV/0!	#DIV/0!	
Iyy (mm4)	0	vsw	N/mm^2	#DIV/0!	#DIV/0!	#DIV/0!	#DIV/0!	#DIV/0!	#DIV/0!	#DIV/0!	#DIV/0!	
θNA (rads)	0	Vcorr	N	#VALUE!	#VALUE!	#VALUE!	#VALUE!	#VALUE!	#VALUE!	#VALUE!	#VALUE!	
Ina	0	w.corr.shr	N/mm	#VALUE!	#VALUE!	#VALUE!	#VALUE!	#VALUE!	#VALUE!	#VALUE!	#VALUE!	
Dia (mm)	0	w.corr	N/mm	#DIV/0!	#DIV/0!	#DIV/0!	#DIV/0!	#DIV/0!	#DIV/0!	#DIV/0!	#DIV/0!	
dr.pore (μm)	0	delta.mid	mm	#DIV/0!	#DIV/0!	#DIV/0!	#DIV/0!	#DIV/0!	#DIV/0!	#DIV/0!	#DIV/0!	
rad.loss/year (μm)	0	dr.spall	mm	#DIV/0!	#DIV/0!	#DIV/0!	#DIV/0!	#DIV/0!	#DIV/0!	#DIV/0!	#DIV/0!	
		t.spall	years	#DIV/0!	#DIV/0!	#DIV/0!	#DIV/0!	#DIV/0!	#DIV/0!	#DIV/0!	#DIV/0!	#DIV/0!
4												
Horiz cover (mm)	0	self wt	N/mm	0.000	0.000	0.000	0.000	0.000	0.000	0.000	0.000	
Vert cover (mm)	0	σ.flex.all	N/mm^2	#DIV/0!	#DIV/0!	#DIV/0!	#DIV/0!	#DIV/0!	#DIV/0!	#DIV/0!	#DIV/0!	
x (mm)	0	σ.shear.all	N/mm^2	#DIV/0!	#DIV/0!	#DIV/0!	#DIV/0!	#DIV/0!	#DIV/0!	#DIV/0!	#DIV/0!	
y (mm)	0	Mcorr	Nm	#DIV/0!	#DIV/0!	#DIV/0!	#DIV/0!	#DIV/0!	#DIV/0!	#DIV/0!	#DIV/0!	
Ixx (mm4)	0	w.corr.flex	N/mm	#DIV/0!	#DIV/0!	#DIV/0!	#DIV/0!	#DIV/0!	#DIV/0!	#DIV/0!	#DIV/0!	
Iyy (mm4)	0	vsw	N/mm^2	#DIV/0!	#DIV/0!	#DIV/0!	#DIV/0!	#DIV/0!	#DIV/0!	#DIV/0!	#DIV/0!	
θNA (rads)	0	Vcorr	N	#VALUE!	#VALUE!	#VALUE!	#VALUE!	#VALUE!	#VALUE!	#VALUE!	#VALUE!	
Ina	0	w.corr.shr	N/mm	#VALUE!	#VALUE!	#VALUE!	#VALUE!	#VALUE!	#VALUE!	#VALUE!	#VALUE!	
Dia (mm)	0	w.corr	N/mm	#DIV/0!	#DIV/0!	#DIV/0!	#DIV/0!	#DIV/0!	#DIV/0!	#DIV/0!	#DIV/0!	
dr.pore (μm)	0	delta.mid	mm	#DIV/0!	#DIV/0!	#DIV/0!	#DIV/0!	#DIV/0!	#DIV/0!	#DIV/0!	#DIV/0!	
rad.loss/year (μm)	0	dr.spall	mm	#DIV/0!	#DIV/0!	#DIV/0!	#DIV/0!	#DIV/0!	#DIV/0!	#DIV/0!	#DIV/0!	
		t.spall	years	#DIV/0!	#DIV/0!	#DIV/0!	#DIV/0!	#DIV/0!	#DIV/0!	#DIV/0!	#DIV/0!	#DIV/0!
5												
Horiz cover (mm)	0	self wt	N/mm	0.000	0.000	0.000	0.000	0.000	0.000	0.000	0.000	
Vert cover (mm)	0	σ.flex.all	N/mm^2	#DIV/0!	#DIV/0!	#DIV/0!	#DIV/0!	#DIV/0!	#DIV/0!	#DIV/0!	#DIV/0!	
x (mm)	0	σ.shear.all	N/mm^2	#DIV/0!	#DIV/0!	#DIV/0!	#DIV/0!	#DIV/0!	#DIV/0!	#DIV/0!	#DIV/0!	
y (mm)	0	Mcorr	Nm	#DIV/0!	#DIV/0!	#DIV/0!	#DIV/0!	#DIV/0!	#DIV/0!	#DIV/0!	#DIV/0!	
Ixx (mm4)	0	w.corr.flex	N/mm	#DIV/0!	#DIV/0!	#DIV/0!	#DIV/0!	#DIV/0!	#DIV/0!	#DIV/0!	#DIV/0!	
Iyy (mm4)	0	vsw	N/mm^2	#DIV/0!	#DIV/0!	#DIV/0!	#DIV/0!	#DIV/0!	#DIV/0!	#DIV/0!	#DIV/0!	
θNA (rads)	0	Vcorr	N	#VALUE!	#VALUE!	#VALUE!	#VALUE!	#VALUE!	#VALUE!	#VALUE!	#VALUE!	
Ina	0	w.corr.shr	N/mm	#VALUE!	#VALUE!	#VALUE!	#VALUE!	#VALUE!	#VALUE!	#VALUE!	#VALUE!	
Dia (mm)	0	w.corr	N/mm	#DIV/0!	#DIV/0!	#DIV/0!	#DIV/0!	#DIV/0!	#DIV/0!	#DIV/0!	#DIV/0!	
dr.pore (μm)	0	delta.mid	mm	#DIV/0!	#DIV/0!	#DIV/0!	#DIV/0!	#DIV/0!	#DIV/0!	#DIV/0!	#DIV/0!	
rad.loss/year (μm)	0	dr.spall	mm	#DIV/0!	#DIV/0!	#DIV/0!	#DIV/0!	#DIV/0!	#DIV/0!	#DIV/0!	#DIV/0!	
		t.spall	years	#DIV/0!	#DIV/0!	#DIV/0!	#DIV/0!	#DIV/0!	#DIV/0!	#DIV/0!	#DIV/0!	#DIV/0!

Project	The assessment of corrosion-damaged concrete structures	British Cement Association		
Client	University of Birmingham	Made by	Date	Page
Structure	Parameter study	MPW	24-Jul-00	4B
Location	Default beam, Level 0 - from grid ref A1 to grid ref A2	Checked	Revision	Job No
	Structural assessment of corrosion-damaged concrete structures to BS 81110 (modified) © 2000 MPW		Final	PhD

Durability, cracking and spalling - Sheet 2 of 2

Layer				Length of crack (mm) 250	500	750	1000	1250	1500	1750	2000	Ave t.spall (years)
6												
Horiz cover (mm)	0	self wt	N/mm	0.000	0.000	0.000	0.000	0.000	0.000	0.000	0.000	
Vert cover (mm)	0	σ.flex.all	N/mm^2	#DIV/0!	#DIV/0!	#DIV/0!	#DIV/0!	#DIV/0!	#DIV/0!	#DIV/0!	#DIV/0!	
x (mm)	0	σ.shear.all	N/mm^2	#DIV/0!	#DIV/0!	#DIV/0!	#DIV/0!	#DIV/0!	#DIV/0!	#DIV/0!	#DIV/0!	
y (mm)	0	Mcorr	Nm	#DIV/0!	#DIV/0!	#DIV/0!	#DIV/0!	#DIV/0!	#DIV/0!	#DIV/0!	#DIV/0!	
Ixx (mm4)	0	w.corr.flex	N/mm	#DIV/0!	#DIV/0!	#DIV/0!	#DIV/0!	#DIV/0!	#DIV/0!	#DIV/0!	#DIV/0!	
Iyy (mm4)	0	vsw	N/mm^2	#DIV/0!	#DIV/0!	#DIV/0!	#DIV/0!	#DIV/0!	#DIV/0!	#DIV/0!	#DIV/0!	
θNA (rads)	0	Vcorr	N	#VALUE!	#VALUE!	#VALUE!	#VALUE!	#VALUE!	#VALUE!	#VALUE!	#VALUE!	
Ina	0	w.corr.shr	N/mm	#VALUE!	#VALUE!	#VALUE!	#VALUE!	#VALUE!	#VALUE!	#VALUE!	#VALUE!	
Dia (mm)	0	w.corr	N/mm	#DIV/0!	#DIV/0!	#DIV/0!	#DIV/0!	#DIV/0!	#DIV/0!	#DIV/0!	#DIV/0!	
dr.pore (μm)	0	delta.mid	mm	#DIV/0!	#DIV/0!	#DIV/0!	#DIV/0!	#DIV/0!	#DIV/0!	#DIV/0!	#DIV/0!	
rad.loss/year (μm)	0	dr.spall	mm	#DIV/0!	#DIV/0!	#DIV/0!	#DIV/0!	#DIV/0!	#DIV/0!	#DIV/0!	#DIV/0!	
		t.spall	years	#DIV/0!	#DIV/0!	#DIV/0!	#DIV/0!	#DIV/0!	#DIV/0!	#DIV/0!	#DIV/0!	#DIV/0!
7												
Horiz cover (mm)	0	self wt	N/mm	0.000	0.000	0.000	0.000	0.000	0.000	0.000	0.000	
Vert cover (mm)	0	σ.flex.all	N/mm^2	#DIV/0!	#DIV/0!	#DIV/0!	#DIV/0!	#DIV/0!	#DIV/0!	#DIV/0!	#DIV/0!	
x (mm)	0	σ.shear.all	N/mm^2	#DIV/0!	#DIV/0!	#DIV/0!	#DIV/0!	#DIV/0!	#DIV/0!	#DIV/0!	#DIV/0!	
y (mm)	0	Mcorr	Nm	#DIV/0!	#DIV/0!	#DIV/0!	#DIV/0!	#DIV/0!	#DIV/0!	#DIV/0!	#DIV/0!	
Ixx (mm4)	0	w.corr.flex	N/mm	#DIV/0!	#DIV/0!	#DIV/0!	#DIV/0!	#DIV/0!	#DIV/0!	#DIV/0!	#DIV/0!	
Iyy (mm4)	0	vsw	N/mm^2	#DIV/0!	#DIV/0!	#DIV/0!	#DIV/0!	#DIV/0!	#DIV/0!	#DIV/0!	#DIV/0!	
θNA (rads)	0	Vcorr	N	#VALUE!	#VALUE!	#VALUE!	#VALUE!	#VALUE!	#VALUE!	#VALUE!	#VALUE!	
Ina	0	w.corr.shr	N/mm	#VALUE!	#VALUE!	#VALUE!	#VALUE!	#VALUE!	#VALUE!	#VALUE!	#VALUE!	
Dia (mm)	0	w.corr	N/mm	#DIV/0!	#DIV/0!	#DIV/0!	#DIV/0!	#DIV/0!	#DIV/0!	#DIV/0!	#DIV/0!	
dr.pore (μm)	0	delta.mid	mm	#DIV/0!	#DIV/0!	#DIV/0!	#DIV/0!	#DIV/0!	#DIV/0!	#DIV/0!	#DIV/0!	
rad.loss/year (μm)	0	dr.spall	mm	#DIV/0!	#DIV/0!	#DIV/0!	#DIV/0!	#DIV/0!	#DIV/0!	#DIV/0!	#DIV/0!	
		t.spall	years	#DIV/0!	#DIV/0!	#DIV/0!	#DIV/0!	#DIV/0!	#DIV/0!	#DIV/0!	#DIV/0!	#DIV/0!
8												
Horiz cover (mm)	0	self wt	N/mm	0.000	0.000	0.000	0.000	0.000	0.000	0.000	0.000	
Vert cover (mm)	0	σ.flex.all	N/mm^2	#DIV/0!	#DIV/0!	#DIV/0!	#DIV/0!	#DIV/0!	#DIV/0!	#DIV/0!	#DIV/0!	
x (mm)	0	σ.shear.all	N/mm^2	#DIV/0!	#DIV/0!	#DIV/0!	#DIV/0!	#DIV/0!	#DIV/0!	#DIV/0!	#DIV/0!	
y (mm)	0	Mcorr	Nm	#DIV/0!	#DIV/0!	#DIV/0!	#DIV/0!	#DIV/0!	#DIV/0!	#DIV/0!	#DIV/0!	
Ixx (mm4)	0	w.corr.flex	N/mm	#DIV/0!	#DIV/0!	#DIV/0!	#DIV/0!	#DIV/0!	#DIV/0!	#DIV/0!	#DIV/0!	
Iyy (mm4)	0	vsw	N/mm^2	#DIV/0!	#DIV/0!	#DIV/0!	#DIV/0!	#DIV/0!	#DIV/0!	#DIV/0!	#DIV/0!	
θNA (rads)	0	Vcorr	N	#VALUE!	#VALUE!	#VALUE!	#VALUE!	#VALUE!	#VALUE!	#VALUE!	#VALUE!	
Ina	0	w.corr.shr	N/mm	#VALUE!	#VALUE!	#VALUE!	#VALUE!	#VALUE!	#VALUE!	#VALUE!	#VALUE!	
Dia (mm)	0	w.corr	N/mm	#DIV/0!	#DIV/0!	#DIV/0!	#DIV/0!	#DIV/0!	#DIV/0!	#DIV/0!	#DIV/0!	
dr.pore (μm)	0	delta.mid	mm	#DIV/0!	#DIV/0!	#DIV/0!	#DIV/0!	#DIV/0!	#DIV/0!	#DIV/0!	#DIV/0!	
rad.loss/year (μm)	0	dr.spall	mm	#DIV/0!	#DIV/0!	#DIV/0!	#DIV/0!	#DIV/0!	#DIV/0!	#DIV/0!	#DIV/0!	
		t.spall	years	#DIV/0!	#DIV/0!	#DIV/0!	#DIV/0!	#DIV/0!	#DIV/0!	#DIV/0!	#DIV/0!	#DIV/0!
9												
Horiz cover (mm)	0	self wt	N/mm	0.000	0.000	0.000	0.000	0.000	0.000	0.000	0.000	
Vert cover (mm)	0	σ.flex.all	N/mm^2	#DIV/0!	#DIV/0!	#DIV/0!	#DIV/0!	#DIV/0!	#DIV/0!	#DIV/0!	#DIV/0!	
x (mm)	0	σ.shear.all	N/mm^2	#DIV/0!	#DIV/0!	#DIV/0!	#DIV/0!	#DIV/0!	#DIV/0!	#DIV/0!	#DIV/0!	
y (mm)	0	Mcorr	Nm	#DIV/0!	#DIV/0!	#DIV/0!	#DIV/0!	#DIV/0!	#DIV/0!	#DIV/0!	#DIV/0!	
Ixx (mm4)	0	w.corr.flex	N/mm	#DIV/0!	#DIV/0!	#DIV/0!	#DIV/0!	#DIV/0!	#DIV/0!	#DIV/0!	#DIV/0!	
Iyy (mm4)	0	vsw	N/mm^2	#DIV/0!	#DIV/0!	#DIV/0!	#DIV/0!	#DIV/0!	#DIV/0!	#DIV/0!	#DIV/0!	
θNA (rads)	0	Vcorr	N	#VALUE!	#VALUE!	#VALUE!	#VALUE!	#VALUE!	#VALUE!	#VALUE!	#VALUE!	
Ina	0	w.corr.shr	N/mm	#VALUE!	#VALUE!	#VALUE!	#VALUE!	#VALUE!	#VALUE!	#VALUE!	#VALUE!	
Dia (mm)	0	w.corr	N/mm	#DIV/0!	#DIV/0!	#DIV/0!	#DIV/0!	#DIV/0!	#DIV/0!	#DIV/0!	#DIV/0!	
dr.pore (μm)	0	delta.mid	mm	#DIV/0!	#DIV/0!	#DIV/0!	#DIV/0!	#DIV/0!	#DIV/0!	#DIV/0!	#DIV/0!	
rad.loss/year (μm)	0	dr.spall	mm	#DIV/0!	#DIV/0!	#DIV/0!	#DIV/0!	#DIV/0!	#DIV/0!	#DIV/0!	#DIV/0!	
		t.spall	years	#DIV/0!	#DIV/0!	#DIV/0!	#DIV/0!	#DIV/0!	#DIV/0!	#DIV/0!	#DIV/0!	#DIV/0!

Initiation and propagation periods

Level	Cover (mm)	Diameter (mm)	c / D	Corrosion to cause cracking (%)	(mm)	Icorr (mm / year)	Overall time to Initiation (years)	Cracking (years)	Spalling (years)
1	50	16	3.1	1.56	0.063	0.0046	80	94	131
2	50	25	2.0	1.00	0.063	0.0046	80	94	127
3	0	0	0.0	0.00	0.000	0.0000	0	0	0
4	0	0	0.0	0.00	0.000	0.0000	0	0	0
5	0	0	0.0	0.00	0.000	0.0000	0	0	0
6	0	0	0.0	0.00	0.000	0.0000	0	0	0
7	0	0	0.0	0.00	0.000	0.0000	0	0	0
8	0	0	0.0	0.00	0.000	0.0000	0	0	0
9	0	0	0.0	0.00	0.000	0.0000	0	0	0
						Min rebar	80	94	127
Links @ support	40	10	4.0	2.00	0.050	0.0046	51	62	
Links @ mid-span	40	10	4.0	2.00	0.050	0.0046	51	62	
						Min links	51	62	
						Min all	51	62	

Flexural capacity in accordance with BS 8110 (modified)

Limiting reinforcement stresses and strains

Layer	E (kN/mm²)	Limiting stress: Tension (N/mm²)	Buckling (N/mm²)	Compress (N/mm²)	Buckled	Limiting strain: Tension (N/mm²)	Compress (N/mm²)
1	200	-438	473	438	no	-0.0022	0.0022
2	200	-438	1382	438	no	-0.0022	0.0022
3	0	0	0	0	no	0.0000	0.0000
4	0	0	0	0	no	0.0000	0.0000
5	0	0	0	0	no	0.0000	0.0000
6	0	0	0	0	no	0.0000	0.0000
7	0	0	0	0	no	0.0000	0.0000
8	0	0	0	0	no	0.0000	0.0000
9	0	0	0	0	no	0.0000	0.0000

Links

Dsm	5.09	mm
No. legs	2	
Asm	41	mm
fym	460	N/mm²
Sm	200	mm
Asm.fym	19	kN
fyc.max	748	kN
γs	1.05	
k	1	
No. bars	0	
buckled		

Reinforcement

Layer	Diameter (mm)	As.corr (mm2)	No. bars	fy.corr (MPa)	Depth (mm)	ecc. (mm)	Location Strain	Stress (N/mm²)	Yielded	Force (kN)	Moment (kNm)
Top face					0		0.0035				
1	12.69	126	2	460	58	-192	0.0016	312	no	79	-15
2	21.69	369	4	460	437.5	187.5	-0.0111	-438	yes	-647	-121
3	0.00	0	0	0	0	-250	0.0000	0	no	0	0
4	0.00	0	0	0	0	-250	0.0000	0	no	0	0
5	0.00	0	0	0	0	-250	0.0000	0	no	0	0
6	0.00	0	0	0	0	-250	0.0000	0	no	0	0
7	0.00	0	0	0	0	-250	0.0000	0	no	0	0
8	0.00	0	0	0	0	-250	0.0000	0	no	0	0
9	0.00	0	0	0	0	-250	0.0000	0	no	0	0
Bottom face					500		-0.0132		Total	-568	-137

Concrete

	b (mm)	h (mm)	Top face (mm)	Bot face (mm)	hc (mm)	A (mm²)	y (mm)	ecc (mm)	F (kN)	M (kNm)
Top flange	0	0	0	0	0.0	0	0.0	-250.0	0	0
Web	300	500	0	500	94.3	28277	47.1	-202.9	568	-115
Bot flange	0	0	500	500	0.0	0	500.0	250.0	0	0
Total		500				28277			568	-115

Equilibrium

N.required 0 kN Compression +ve

	N kN	**M kNm**
Concrete	568	115
Steel	-568	-137
Total	**0**	**252**

x 104.7 mm

dc 94.3 mm

Bond strength in accordance with BS 8110 (modified)

Tension reinforcement effective in shear

Layer	D (mm)	c / D	Uncorroded As.nom (mm²)	fb.bar (N/mm²)	fb.total (N/mm²)	lb.req (mm)	Fs.req (kN)
1	16	3.13	402	1.88	3.35	0	0.0
2	25	2.00	982	1.88	3.35	300	158.1
3	0	0.00	0	1.88	3.35	0	0.0
4	0	0.00	0	1.88	3.35	0	0.0
5	0	0.00	0	1.88	3.35	0	0.0
6	0	0.00	0	1.88	3.35	0	0.0
7	0	0.00	0	1.88	3.35	0	0.0
8	0	0.00	0	1.88	3.35	0	0.0
9	0	0.00	0	1.88	3.35	0	0.0
Total							158.1

Layer	D (mm)	Corroded Acorr (mm²)	Cover cracked	fb.bar (N/mm²)	fb.total (N/mm²)	fb.corr / fb.8110	lb.prov (mm)	Fs.prov (kN)	As.eff (mm²)
1	15.4	13.6	yes	0.87	0.87	0.26	192	16	0
2	24.4	21.4	yes	0.00	0.00	0.00	300	0	0
3	0.0	0.0	no	1.88	1.88	1.00	0	0	0
4	0.0	0.0	no	1.88	1.88	1.00	0	0	0
5	0.0	0.0	no	1.88	1.88	1.00	0	0	0
6	0.0	0.0	no	1.88	1.88	1.00	0	0	0
7	0.0	0.0	no	1.88	1.88	1.00	0	0	0
8	0.0	0.0	no	1.88	1.88	1.00	0	0	0
9	0.0	0.0	no	1.88	1.88	1.00	0	0	0
Total								16	0

Basic data

Effective breadth	300	mm
fcu	45	N/mm²
fct	3	N/mm²
No. diameters	12	
γbond	1.4	

Bond parameters

a	0.31
b	0.0153

fb = (a - b Acorr) (0.5 + c / D) fct

Uncorroded links

D	10	mm
No. legs	2	
Asv	157	mm²
fyv	460	N/mm²
sv	200	mm
γs	1.05	
(Asv.fyv / γs.bv.sv)	0.4	min
Nominal Asv	55	mm²
Nominal exceeded	yes	
fb.link	1.48	N/mm²

Corroded links

Dsv.eff	5.09	mm
No. legs	2	
Asv	41	mm²
fyv	460	N/mm²
sv	200	mm
γs	1.05	
(Asv.fyv / γs.bv.sv)	0.4	min
Nominal Asv	55	mm²
Nominal exceeded	no	
fb.link	0.71	N/mm²

Shear capacity in accordance with BS 8110 (modified)

Tension reinforcement available to resist shear

Layer	Depth (mm)	Force (kN)	D (mm)	As.corr (mm²)	Cover cracked	fb (N/mm²)	As.eff (mm²)	Fs.prov (kN)	Fs.enhance (kN)
1	58	0	15.448	253	yes	0.87	0	0	0
2	437.5	-324	24.448	739	yes	0.00	0	0	0
3	0	0	0.000	0	no	1.88	0	0	0
4	0	0	0.000	0	no	1.88	0	0	0
5	0	0	0.000	0	no	1.88	0	0	0
6	0	0	0.000	0	no	1.88	0	0	0
7	0	0	0.000	0	no	1.88	0	0	0
8	0	0	0.000	0	no	1.88	0	0	0
9	0	0	0.000	0	no	1.88	0	0	0
Total		-324					0	0	0

Effective depth	438	mm	Effective breadth	300	mm
Shear span	1500	mm	Column depth	300	mm
av / d	3.4				

Table 3.9 - Concrete contribution - Vc

fcu	45	N/mm²
As.eff	0	mm²
100As.eff/bd	0.00	%
400/d	1.00	
fcu/25	1.60	N/mm²
av / d	3.00	
vc	0.00	N/mm²
Vc	0.0	kN

Table 3.8 - Steel contribution - Vs

Dsv.eff	5.087	
No legs	2	
Asv	41	mm²
fyv	460	N/mm²
fyv.corr	460	N/mm²
sv	200	mm
γs	1.05	
(Asv.fyv / γs.bv.sv)	0.4	min
Nominal Asv	55	mm²
Nominal exceeded	no	
vs	0.00	N/mm²
Vs	0.0	kN

3.4.5.2 - Maximum shear capacity

vmax	5.37	N/mm2
Vmax	704	kN

Shear Capacity - V = Vc + Vs

v	0.00	N/mm2
V	**0**	kN

Enhancement to anchorage bond

Support reaction	0.0	kN
Transverse pressure	0.00	N/mm²
Enhancement	1.00	

Anchorage bond

Mrequired	0	kNm
z	393.8	mm
T.moment	0.0	kN
T.allowable	0.0	kN
T.shear	0.0	kN
V.allow	0.0	kN

Note:
(i) Anchorage bond is checked at the supports.
(ii) Anchorage enhancement is calculated in accordance with EC 2

Moment-Axial force Interaction

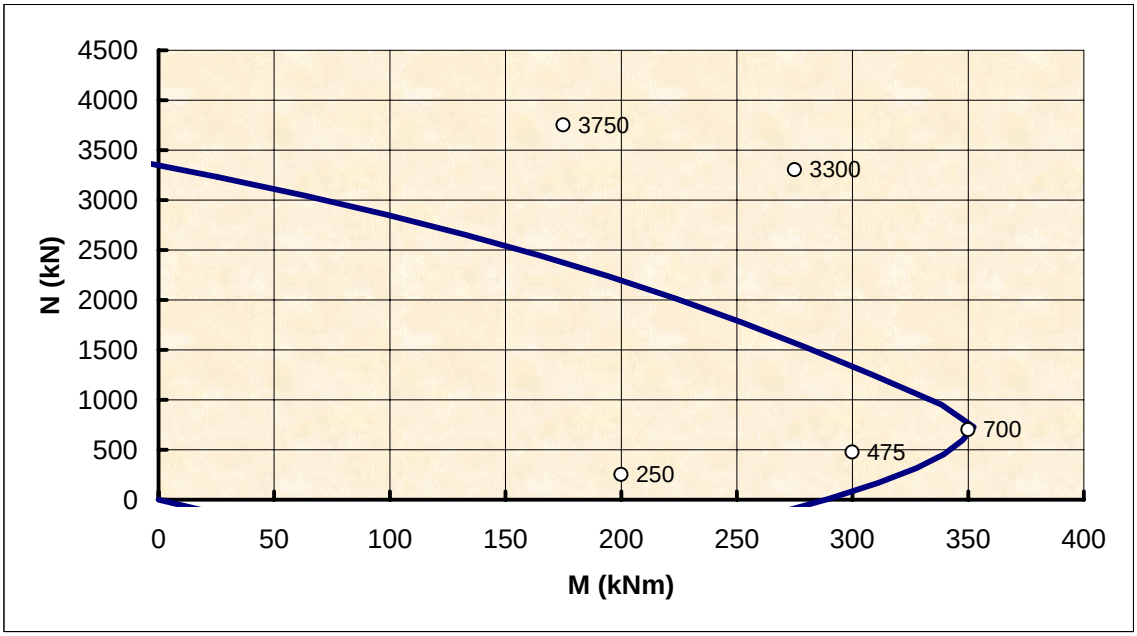

Load cases 5

Load case	Required M kN	Required N kNm	Provided M kN	Provided N kNm	Pass or fail
1	200	250	321	250	Pass
2	300	475	341	475	Pass
3	350	700	352	700	Pass
4	175	3750	-76	3750	Fail
5	275	3300	11	3300	Fail
6					
7					
8					
9					
10					

Project	The assessment of corrosion-damaged concrete structures	British Cement Association	
Client	University of Birmingham	Made by: MPW	Date: 24-Jul-00	Page: 9
Structure	Parameter study	Checked:	Revision: Final	Job No: PhD
Location	Default beam, Level 0 - from grid ref A1 to grid ref A2			

Structural assessment of corrosion-damaged concrete structures to BS 81110 (modified)

Whole life load-carrying capacity

Member

Span	8	m
Column width	300	mm

No. years 140

Loading

Bending moment =	0.125	w.L^2
Shear force =	0.5	w.L
Calculate V at	1	d from column face

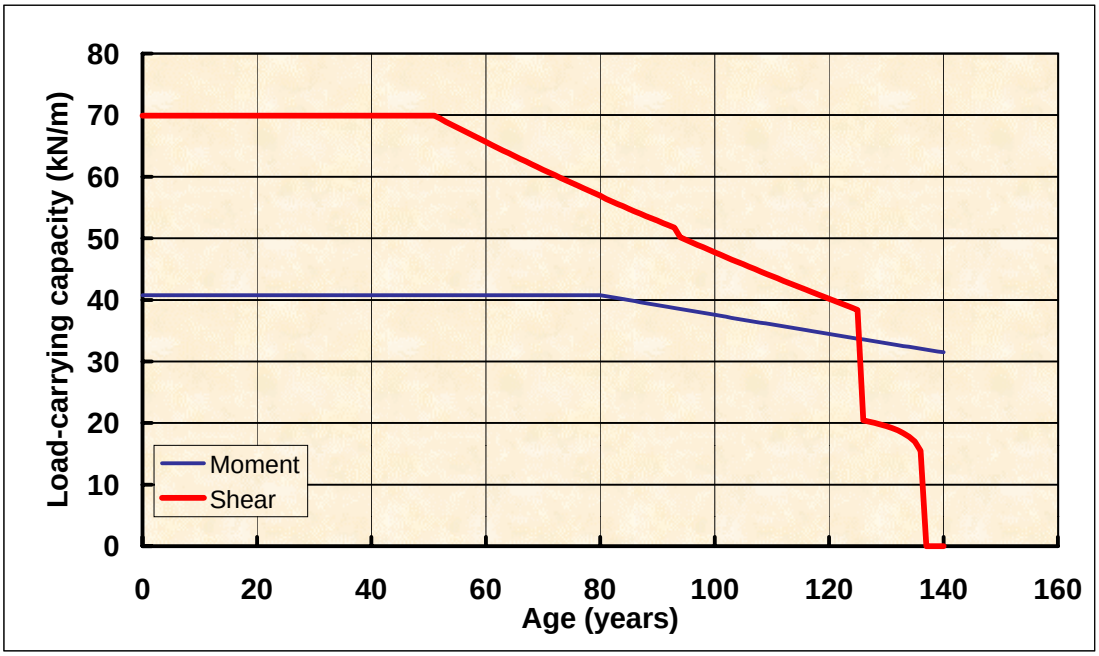

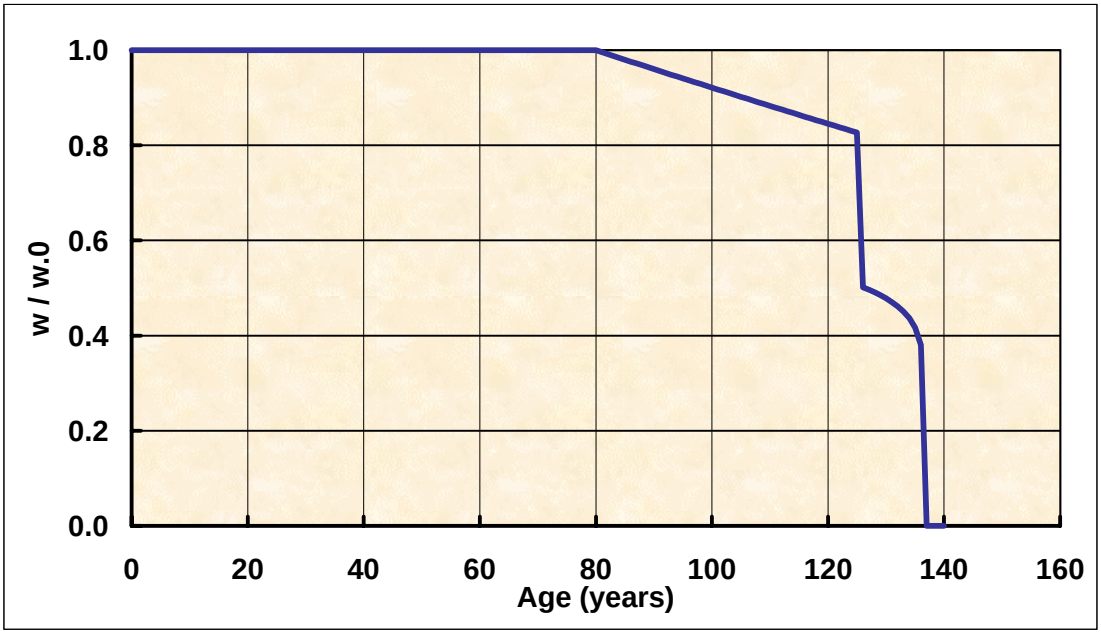

Project	The assessment of corrosion-damaged concrete structures	British Cement Association	
Client	University of Birmingham	Made by: MPW	Date: 24-Jul-00 / Page: 10A
Structure	Parameter study	Checked	Revision: Final / Job No: PhD
Location	Default beam, Level 0 - from grid ref A1 to grid ref A2		

Structural assessment of corrosion-damaged concrete structures to BS 81110 (modified)

Parameter study - De-icing salt exposure - Sheet 1 of 2

Defaults

				Control		Corroded	
					w (kN/m)		w (kN/m)
w/c	0.5						
c	350	kg/m^3					
fcu	45	N/mm^2					
Cover	40	mm	M kNm	310.6	38.8	185.5	23.2
Cs	0.1	% by wt of concrete	V kN	233.8	68.5	0.0	0.0
Crit	0.06	% by wt of concrete	B kN				
Icorr	0.4	µA/cm^2	Min		38.8		0.0
Pit factor	6						

Member

Span 8 m
Column width 300 mm

Loading

Bending moment = 0.125 w.L^2
Shear force = 0.5 w.L
Calculate V at 1 d from column face

= default value

Concrete grade

			Links		Main		w.corroded / w.control			
w/c	fcu MPa	cem kg/m3	Ti years	Tcrack years	Ti years	Tcrack years	50 years	75 years	100 years	125 years
0.4	55	425	101	112	158	172	1.00	1.00	1.00	1.00
0.45	50	400	72	83	112	126	1.00	1.00	1.00	0.95
0.5	45	350	51	62	80	94	1.00	1.00	0.92	0.83
0.55	40	325	36	47	57	71	1.00	0.93	0.83	0.00
0.6	35	300	26	37	40	54	0.96	0.87	0.78	0.00
0.65	30	275	18	29	29	42	0.92	0.83	0.00	0.00
0.7	25	250	13	24	20	34	0.90	0.81	0.00	0.00

	Links		Main		w.corroded / w.control			
Cover mm	Ti years	Tcrack years	Ti years	Tcrack years	50 years	75 years	100 years	125 years
10	3	6	13	18	0.85	0.76	0.00	0.00
15	7	11	20	27	0.88	0.79	0.00	0.00
20	13	18	29	37	0.92	0.82	0.00	0.00
25	20	27	39	49	0.96	0.86	0.00	0.00
30	29	37	51	62	1.00	0.91	0.81	0.00
35	39	49	65	77	1.00	0.96	0.86	0.00
40	51	62	80	94	1.00	1.00	0.92	0.83
45	65	77	97	112	1.00	1.00	0.99	0.89
50	80	94	115	132	1.00	1.00	1.00	0.96
55	97	112	135	153	1.00	1.00	1.00	1.00
60	115	132	157	176	1.00	1.00	1.00	1.00
65	135	153	180	200	1.00	1.00	1.00	1.00
70	157	176	205	227	1.00	1.00	1.00	1.00
75	180	201	231	254	1.00	1.00	1.00	1.00

	Links		Main		w.corroded / w.control			
Cs %	Ti years	Tcrack years	Ti years	Tcrack years	50 years	75 years	100 years	125 years
0.05	194	205	303	316	1.00	1.00	1.00	1.00
0.075	219	230	342	355	1.00	1.00	1.00	1.00
0.1	51	62	80	94	1.00	1.00	0.92	0.83
0.125	28	39	44	58	0.98	0.88	0.79	0.00
0.15	20	31	31	45	0.92	0.83	0.00	0.00
0.175	16	27	24	38	0.90	0.81	0.00	0.00
0.2	13	24	20	34	0.88	0.79	0.00	0.00

	Links		Main		w.corroded / w.control			
Ccrit %	Ti years	Tcrack years	Ti years	Tcrack years	50 years	75 years	100 years	125 years
0.01	5	16	8	22	0.84	0.75	0.00	0.00
0.02	9	19	13	27	0.86	0.77	0.00	0.00
0.03	13	24	20	34	0.88	0.79	0.00	0.00
0.04	20	31	31	45	0.92	0.83	0.00	0.00
0.05	31	42	48	62	0.99	0.90	0.80	0.00
0.06	51	62	80	94	1.00	1.00	0.92	0.83
0.07	95	106	148	162	1.00	1.00	1.00	1.00
0.08	219	230	342	355	1.00	1.00	1.00	1.00

Parameter study - De-icing salt exposure - Sheet 2 of 2

	Links		Main					
Icorr	Ti	Tcrack	Ti	Tcrack	w.corroded / w.control			
µA/cm²	years	years	years	years	50 years	75 years	100 years	125 years
0.01	51	488	80	625	1.00	1.00	1.00	1.00
0.1	51	95	80	134	1.00	1.00	0.98	0.96
0.25	51	69	80	102	1.00	1.00	0.95	0.89
0.4	51	62	80	94	1.00	1.00	0.92	0.83
0.5	51	60	80	91	1.00	1.00	0.90	0.36
0.75	51	57	80	87	1.00	1.00	0.53	0.00
1	51	56	80	85	1.00	1.00	0.48	0.00
1.25	51	55	80	84	1.00	0.63	0.00	0.00
1.5	51	54	80	84	1.00	0.63	0.00	0.00
1.75	51	54	80	83	1.00	0.63	0.00	0.00
2	51	53	80	83	1.00	0.63	0.00	0.00
2.5	51	53	80	82	1.00	0.63	0.00	0.00
5	51	52	80	81	1.00	0.63	0.00	0.00
10	51	52	80	81	1.00	0.63	0.00	0.00

	Links		Main					
Pitting	Ti	Tcrack	Ti	Tcrack	w.corroded / w.control			
factor	years	years	years	years	50 years	75 years	100 years	125 years
1	51	62	80	94	1.00	1.00	0.99	0.97
2	51	62	80	94	1.00	1.00	0.97	0.94
3	51	62	80	94	1.00	1.00	0.96	0.91
4	51	62	80	94	1.00	1.00	0.95	0.88
5	51	62	80	94	1.00	1.00	0.93	0.85
6	51	62	80	94	1.00	1.00	0.92	0.83
7	51	62	80	94	1.00	1.00	0.91	0.51
8	51	62	80	94	1.00	1.00	0.90	0.51
9	51	62	80	94	1.00	1.00	0.88	0.51
10	51	62	80	94	1.00	1.00	0.57	0.51

Parameter interaction

	Min	Max	fcu Min	fcu Max	Cement content Min	Cement content Max
w/c	0.45	0.55	50	40	400	325
Cover	30	50				
Cs	0.08	0.12				
Icorr	0.20	0.60				

				Links		Main					
w/c	Cover	Cs	Icorr	Ti	Tcrack	Ti	Tcrack	w.corroded / w.control			
	mm	% conc	µA/cm2	years	years	years	years	50 years	75 years	100 years	125 years
0.45	30	0.08	0.2	110	126	195	217	1.00	1.00	1.00	1.00
			0.6	110	115	195	202	1.00	1.00	1.00	1.00
		0.12	0.2	24	41	43	65	0.99	0.94	0.89	0.84
			0.6	24	30	43	51	0.96	0.46	0.00	0.00
	50	0.08	0.2	304	332	438	471	1.00	1.00	1.00	1.00
			0.6	304	313	438	449	1.00	1.00	1.00	1.00
		0.12	0.2	68	95	98	130	1.00	1.00	1.00	0.95
			0.6	68	77	98	109	1.00	1.00	0.99	0.54
0.55	30	0.08	0.2	55	72	99	120	1.00	1.00	1.00	0.95
			0.6	55	61	99	106	1.00	1.00	0.99	0.50
		0.12	0.2	12	29	22	44	0.95	0.90	0.85	0.80
			0.6	12	18	22	29	0.84	0.00	0.00	0.00
	50	0.08	0.2	154	181	222	254	1.00	1.00	1.00	1.00
			0.6	154	163	222	233	1.00	1.00	1.00	1.00
		0.12	0.2	34	62	49	82	1.00	0.95	0.90	0.86
			0.6	34	43	49	60	1.00	0.85	0.00	0.00